Southwest Pacific Paleoceanography During the Late Holocene

3000 years of ocean circulation and marine biogeochemistry reconstructed from New Zealand deep-sea black corals

By

Nicholas Thomas Hitt

A thesis
Submitted to the Victoria University of Wellington in
fulfillment of the requirements for the degree of
Doctor of Philosophy in Geology

Victoria University of Wellington (2021)

To Aotearoa

and those unwavering, mysterious creatures that call the deep sea 'home'

Black Corals

Acknowledgements:

First, I'd like to thank the Faculty of Graduate Research, who, by giving me a 100,000 word limit for my thesis, allows me to properly thank those people who contributed to this research, help me reach this career milestone and (most importantly) keep my sanity.

I will forever be grateful for the support of my supervisors Dan Sinclair, Stewart Fallon, Helen Neil, and Aimée Komugabe-Dixson. Together, they provided a diverse perspective on a wide variety of topics and helped guide me to my greatest academic achievement (so far!). I thank Dan for his great vision. Dan had this huge vision for what this project could become – but it was clear that I needed to put in the work in order for us to get there. Dan gave me all the tools, support (and most importantly) the patience I needed to get there. A big thank you to Stewart for giving me one of the most rewarding academic experiences I've had thus far. This work would not be possible without the freedom and guidance Stewart gave me in his lab. Beyond that, Stewart has always down for a chat about anything – science, basketball, music, life, whatever. Those are crucial when you're staying late in the radiocarbon lab! For Helen's part, I've been so inspired by the sheer superhuman strength she demonstrates in her role as NIWA General Manager. As a baby graduate student, it reminds me how lucky I was to simply focus on what I love to do; research! Helen taught me some of the most important professional lessons I've had to date, and for that I will be forever thankful. Lastly, I'd like to thank Aimée for giving me the confidence to do this work. Aimée was my predecessor – much of this work comes from the seeds she planted with her PhD thesis and 2016 paper. Her encouragement during our first meeting back in 2017 gave me the confidence to leave no stone unturned and take this scientific dream as far as I could. I know that Dan, Stewart, Helen and Aimée will all continue to be excellent mentors in the years to come, but perhaps what's more important is that I know that our friendship has only just started.

This work would not have been possible without the many academic supporters and mentors I've had throughout this journey. To Di Tracey - my academic auntie – thanks for being such a great teacher of all things black coral, teaching me the ins and outs of NIWA, and introducing me to the deep-sea coral community. To Drew Lorrey and Helen Bostock – it was so inspiring to see senior academics, who I respect greatly, take an interest in my work. Our chats and dinners got me so motivated to get this done and your scientific perspectives were invaluable

to this thesis. I'm so thankful to call y'all friends and colleagues! Chazz Marriot, thanks for just being you man. You're a jack of all trades deep-sea coral guru and who always has some great yarns. And lastly, a big thank you to my friends at the NIWA Invertebrate Collection and Stable Isotope Lab. This work would definitely have not happened without the assistance of Sadie Mills, Diana McPherson, Sarah Bury, Amandine Sabadel, Josette Delgado, and Julie Brown.

Frankly, I wouldn't be here without the support and patience of two mentors I have a great deal of respect for. In 2014, I was a depressed, lowly undergraduate student at Georgia Tech looking for my purpose. I found one in Kim Cobb's paleoclimate lab. She took me in and gave Hussein Sayani the arduous task of being my day to day mentor. Together, they gave me all the tools I needed to not only learn how to be a paleoclimatologist, but also become a confident person. I wasn't the best undergrad student when I started – my priorities weren't in the right place. Yet, they showed extreme patience with me when perhaps they shouldn't have. I wouldn't be here without that patience. I often tell people I went to the Kim Cobb school of hard knocks where you either sink or swim in her world of paleoclimate. Hussein taught me how to be independent, self-reliant and ultimately, how to swim in the Cobb lab! Some quit before they learn those lessons from the Cobb lab experience and I'm so thankful for having Hussein teach them to me. I wouldn't be finishing my PhD on time without Hussein's sass-filled lessons, his mentorship, and most importantly, his great patience during my early science days. Kim and Hussein – thank you for giving me my start and sticking with me when a lot of people wouldn't have. Is it true that you never really leave the Cobb lab?

Just a quick shout out to my Crossfit Central Wellington whānau. Earning a PhD requires you to handle copious - seemingly never ending - amounts of stress. CCW gave me a space where I could forget everything else in the world, release all that stress, and focus on working on myself in the company of some of exceptional people. I learned at CCW that I could take any negative energy and turn it into something positive. That mindset extends to this thesis. So, to all the coaches and athletes at CCW, thanks for the love, support and daily reminder to **Build. Improve. Achieve.** I couldn't have done this without y'all. #lunchtimelemers4life! Right Te?

I am most grateful for my two biggest cheerleaders, my parents - Matt and Jennifer. Dad, we don't see eye to eye on much anymore (probably because I'm smarter than you now but just as stubborn) – but I'll admit that I couldn't have done this without your support. You've always told me how it is. Sometimes I didn't and still don't want to hear that, but I always need that

perspective. I think that's what separates you from many people who nowadays hide behind excuses. When I was a kid, you set the tone for what a relentless pursuit to succeed looks like. I've always looked up to that. Thanks for teaching me to never give up, to never let someone else's opinion define me, to never make excuses, and, when all else fails, **get mad**. Mom, there's not enough words in the dictionary to accurately illustrate how lucky and thankful I am to have you as my mother. You've always been there for me, day and night, when I'm happy or sad. You and Dad set the tone growing up for what hard work and good parenting looks like. I still tell people about your workout regimen before getting us kids up for school – they all think you were crazy. What that taught me was if there was something I wanted to change or do in my life, then I need to just suck it up and do it. Perhaps more importantly, you taught me how to love myself; that's the best lesson a mom can teach her son. Thanks for prepping me for the real world and supporting me guys, y'all are the best parents a liberal academic like myself could ask for.

To my grandparents, Noni and Pop Pop. You two have always been my moral compass and always provided a space where I can learn who I am and grow into my own person. I've always taken something from Noni's religious teachings (she is a saint!) and the many Canada trips Pop Pop and I went on. You guys always gave me a place where I could clear my head, dream about the future and think about the things that really matter. Pop Pop, you've been my best friend since I was born – dressing me in camo and giving me a Budweiser right out the womb! During this journey I've never hesitated to reach out and talk to you about things that I couldn't talk to anyone else about. Thanks for taking on the job of being my secret keeper, my best friend and giving me the (many) kicks in the ass I needed to realize my full potential.

I have 5 siblings; 3 brothers: Andrew, Ryan and Christian; and 2 sisters: Ashley and Noelle. They have given me everything I could've asked for as a brother. My older brother Andrew is my rock. He's always been there, even when he isn't physically, and I couldn't have done this without his patient ear and drunken raps. My younger brothers Ryan and Christian are really two of the best motivators I've ever had. They are incredibly smart and tough; they just never give up. They pushed me hard growing up, which gave me my love for competing with others and myself. I needed that internal motivation to finish this thesis. My two twin sisters Ashley and Noelle have been my light since they were born. They gave me hope during the darkest times of my PhD. VUW told me going in that this experience would be a rollercoaster - and man it was. The highs were high, and the lows were low, but my sisters were always there to

pick me up and support me when things got tough. You girls were and always will be a source of inspiration. Above all, I will be forever thankful for the love and support that my siblings gave me. I'm so blessed to have them, and I wouldn't trade any of 'em for the world.

I wouldn't be where I am without the support of all my friends. The people I've connected with here in Wellington have taught me so much! Y'all took in a cocky American and showed me how to be a kiwi and call Aotearoa my home. I'll always be thankful for that. A special shoutout to my extended Kiwi family – Dave (RIP) and Anita Bailey. Thank you for welcoming me into your Auckland home and checking in on me when nobody else did. I know you're watching from upstairs Dave – god speed my friend – we'll share some more Lion Reds someday! To my ATL squad - Yasir, George, Panda, and Hunter – y'all are some real ones. We don't get to see each other often anymore, but when we do it's like nothing's changed. Thanks for always taking an interest in my research and supporting me from afar. KC – you've been a great friend since we met when I was 16. We first bonded over our mutual love for the ocean and since then we've talked every day for years. I can't imagine what it would be like to not have you bugging me about Tom Brady and the Pats. And lastly, to my best friends from Baltimore – Sean, Maks and my older brother Andrew – it's been nearly a decade since we've all lived in the same city and I feel like our group couldn't be stronger. Maks – thanks for the late-night chats about everything and everything (the world would be a better place if it listened to us, right?); Sean – you've been my best bro since we were just teenagers. You've always been there for me when I needed you most and quite frankly, I don't know where I'd be without your love, support, and brutally blunt honesty. You're my guy – thanks bro. And Andrew – well you already know it, but I'll say it again – I've only got one older brother - thanks for being the best one I could've asked for – even if Bucksworth drive me nuts sometimes when he comes out his cave.

Funding for this thesis work was provided by the New Zealand Royal Society Marsden Fund Grant No. NIWA1602 awarded to Helen L. Neil, Daniel J. Sinclair, Stewart J. Fallon and Aimée Komugabe-Dixson.

"Nothing in this world is worth having or worth doing unless it means pain, effort and difficulty. We get one chance in life to do whatever we are going to do and leave whatever legacy we make."

GET AFTER IT. LEAVE YOUR LEGACY.

VITA

2014-2017	Teaching Assistant, Earth and Atmospheric Sciences, Georgia Institute of Technology
2014-2017	Research Associate, Earth and Atmospheric Sciences, Georgia Institute of Technology
2016	B.S. in Earth and Atmospheric Sciences, Georgia Institute of Technology
2017-2020	Graduate Research Assistant, Victoria University of Wellington, School of Geography, Earth and Environmental Science
	Graduate Research Assistant, National Institute of Water and Atmosphere

Publications

Tracey, D., Marriot, P., Bostock, H., Bilewitch, J., Komugabe-Dixson, A., **Hitt, N.** "Coral Biology" In: The State of Knowledge of Deep-Sea Corals in the New Zealand Region, eds. Tracey D., Hjorvarsdottir, F. (2019). 140p.

Sayani, H.R., K.M. Cobb, K.L. Delong, **N. T. Hitt**, and E.R.M. Druffel. (2019) Intercolony $\delta^{18}O$ and Sr/Ca variability among *Porites* corals from Palmyra Atoll: Towards more robust coral-based estimates of climate. *Geochemistry, Geophysics, Geosystems*. doi:10.1029/2019GC008420

Hitt, N. T., Sinclair, D. J., Neil, H.L., Fallon, S. J., Tracey, D., Komugabe-Dixson, A., Marriot, P. Growth and Longevity of New Zealand Black Corals. *Deep-Sea Research I* (2020)

Marriott, P. M., Tracey, D.M., Bostock, H. C., **Hitt, N. T.**, Fallon, S. F., Ageing deep-sea black coral Bathypathes Patula *Frontiers in Marine Science* (2020)

Hitt, N. T., Sayani, H. R., Atwood, A. R., Grothe, P. R., Maupin, C., Lu, Y., Cheng, H., Edwards, R. L., Cobb, K. M. Central tropical Pacific warming and freshening in the 20th century: New insights from a coral ensemble approach. (Submitted to *Geophysical Research Letters*)

Hitt, N.T., Sinclair, D. J., Neil, H.L., Fallon, S. J., Komugabe-Dixson, A., Hellstrom, J. Highly Variable South Pacific Gyre Strength over the Late Holocene (In review for *Proceedings of the National Academy of Sciences*)

Hitt, N.T., Sinclair, D. J., Fallon, S. J., Komugabe-Dixson, A., Neil, H.L., Bury, S., Brown, J., Delgado, J., Hellstrom, J. SOI-Driven variability in last millennium southwest Pacific nitrogen fixation and upwelling rates (In Prep for *Geophysical Research Letters*)

Hitt, N.T., Sinclair, D. J., Fallon, S. J., Komugabe-Dixson, A., Neil, H.L., Bury, S., Sabadel, A., Brown, J., Delgado, J., Hellstrom, J. Anthropogenically relevant change in southwest Pacific phytoplankton community structure over the last millennium (In Prep for *Science Advances*)

Hitt, N.T., Sinclair, D. J., Fallon, S. J., Komugabe-Dixson, A., Neil, H.L., Bury, S., Sabadel, A., Brown, J., Delgado, J., Hellstrom, J. A millennium-long expansion and intensification of the South Pacific Gyre during the late Holocene (In Prep for *Nature Geoscience*)

Abstract:

The global climate results from interactions between the ocean and atmosphere. Ocean gyres are perhaps one of the most significant interactions; they regulate temperature, salinity and nutrient flow across the ocean basins. Gyres transport warm, tropical waters to higher latitudes and cold waters to lower latitudes and act as the dominant heat-transport mechanism in the Earth's climate system. They also influence spatial patterns in marine primary production by distributing nutrients between the equator and poles. However, gyre circulation in the subtropics has been strengthening, leading to marine heat waves, changing biogeochemistry and reducing primary production since the early 1900s. These changes are often interpreted as a consequence of anthropogenic climate change. However, ocean circulation and primary production can exhibit natural variations on a variety of timescales. Could these recent changes be a part of a long-term natural cycle or a product of anthropogenic change?

This research aims to reconstruct South Pacific Gyre (SPG) circulation and biogeochemistry using a suite of New Zealand black corals. The primary research goal is determining if there is a precedent for the ocean changes observed over the instrumental period. Black corals are an ideal paleoceanographic archive for this work; they provide high-resolution, multi-millennial records of biogeochemistry and ocean circulation within their skeletons, derived using radiocarbon (^{14}C) and stable isotopes ($\delta^{13}C$ and $\delta^{15}N$). In this thesis, I show that late Holocene SPG strength has been highly variable and the relationship between circulation and biogeochemistry is timescale dependent.

The black coral radiocarbon records suggest late Holocene SPG circulation has been controlled by westerly wind strength. Our records show the SPG exhibits natural variability on multi-centennial and millennial timescales that corresponds to the variability within the Southern Annular Mode (SAM) and the El Niño-Southern Oscillation (ENSO). The black coral circulation record shows that the modern gyre circulation is not without precedent over the last 3000 years.

The black coral $\delta^{13}C$ and $\delta^{15}N$ records show significant variability on multi-decadal to multi-centennial timescales. Multi-centennial variability in black coral $\delta^{13}C$ and $\delta^{15}N$ appears to be driven by sea surface temperature (SST), nitrogen fixation rates and wind-driven upwelling and is possibly forced by the mean state of the Southern Oscillation Index and ocean circulation strength. A trend in black coral $\delta^{13}C$ over the last 1500 years also suggests a shift in

phytoplankton community structure towards larger and faster growing phytoplankton. These records also reveal a shift in mean coral $\delta^{13}C$ and $\delta^{15}N$ between the 0-2000BP and 2000-3000BP period, the latter corresponding to a period of stronger gyre circulation inferred from the radiocarbon records.

This work shows that: 1) New Zealand's black corals are a promising archive for studying paleoceanography; they can extend instrumental ocean records and fill the gap between traditional southwest Pacific paleoceanographic proxy records (tropical corals, sediment cores); 2) SPG circulation has been highly variable over the last 3000 years; circulation is controlled by atmospheric patterns (e.g. SAM) on multi-centennial to millennial timescales; 3) Gyre circulation is only one of many forcing factors on southwest Pacific primary production and marine biogeochemistry; comparisons between the ΔR, $\delta^{13}C$ and $\delta^{15}N$ proxies show that variations in SPG biogeochemical patterns and productivity are likely driven by local dynamics such as phytoplankton community structure, SST, upwelling *and* gyre circulation. Finally, this research demonstrates the key role that a distributed set of deep-sea coral paleoceanographic reconstructions could play in characterizing the dynamical variability in southwest Pacific Ocean circulation, biogeochemistry and primary production. This information is critical for detecting and attributing past and future anthropogenic impacts on the southwest Pacific Ocean.

Table of Contents

Table of Figures

Chapter 1

An introduction to Pacific Ocean climatology and black corals

1.1 Significance and Overview

The oceans maintain global temperatures and marine ecosystems by carrying warm waters from the tropics to the poles in a series of massive ocean gyres (Munk, 1950; Roemmich et al., 2007; Trujillo et al., 2011; Roemmich et al., 2016). These gyres have a profound impact on marine life by controlling not just heat but also nutrients (Sarmiento et al., 2006; Trujillo et al., 2011). Gyre currents drive upwelling patterns that circulate nutrient poor-waters to high latitudes and nutrient rich sub-polar waters to low latitudes (Sarmiento et al., 2006; Trujillo et al., 2011).

There is no doubt that anthropogenic greenhouse warming has impacted the global oceans. Since the early 20th century, ocean gyres have been increasing in strength and expanding towards the North and South Poles (Roemmich et al., 2007; Wu et al., 2012; Hoegh-Guldberg et al., 2014; Roemmich et al., 2016; Shears et al., 2017; Yang et al., 2020). Gyre water transport has been enhanced along western gyre margins, which has led to increased warming in the western ocean basins that exceeds the globally averaged surface warming rate by more than 1.5°C (Wu et al., 2012; Shears et al., 2017). The fact that all western subtropical ocean currents have responded similarly suggests a globally synchronous change in ocean circulation, where stronger circulation is pushing warmer waters to higher latitudes.

Because the gyres affect nutrient transport, recent changes have the potential to significantly impact marine ecosystems across the globe (Sarmiento et al., 2006; Polovina et al., 2008; Trujillo et al., 2011; Hoegh-Guldberg et al., 2014). Since the late 1980s, the expansion of ocean gyres has pushed warm water marine organisms poleward and caused foreign species to impinge on mid-high latitude ecosystems (Poloczanska et al., 2007; Polovina et al., 2008; Poloczanska et al., 2013; Poloczanska et al., 2016). Moreover, gyre expansion has altered macronutrient distributions in the oceans and reduced primary production across the globe (Gregg et al., 2003; Polovina et al., 2008; Boyce et al., 2010; Moore et al., 2013).

Modern changes to the gyres are unequivocal. However, ocean gyre strength has also exhibited significant natural variability *in the past* (Bostock et al., 2015; Komugabe-Dixson et al., 2016; Zheng et al., 2016; Seo et al., 2018). Attributing the recently observed gyre intensification to global warming therefore requires separating natural gyre variability from anthropogenic forcing. In other words: How can we be certain that the recent gyre intensification is indeed driven by anthropogenic climate change and not part of a natural ocean cycle?

Resolving this question requires oceanographic records which can quantify natural baseline ocean variability. Since ocean gyres change on interannual, decadal and millennial timescales (Isoguchi et al., 2006; Bostock et al., 2015; Komugabe-Dixson et al., 2016; Roemmich et al., 2016; Oliver et al., 2018) we need – at a minimum - decadally resolved records spanning multiple centuries to ascertain the significance of the recent gyre intensification and changes to marine biology and biogeochemistry. Unfortunately, quality instrumental ocean records are largely limited to the satellite era beginning in 1979 (Deser et al., 2010; Henson et al., 2010; Beaulieu et al., 2013; Henson et al., 2016). Paleoceanographic proxy records, such as ocean sediments or tropical corals are traditionally used to fill these gaps (Ruddiman et al., 1981; Fairbanks et al., 1997; Bostock et al., 2015). However, these records are often too low-resolution or are too short in length to provide insights into recent 20th century ocean changes. This creates a considerable gap in the understanding of how high-frequency ocean changes operate on long timescales.

In a recent study, Komugabe-Dixson et al. (2016) produced a 4500 year record of paleoceanographic circulation from the south Tasman Sea. The study showed that South Pacific Gyre (SPG) circulation strength is highly variable over the mid to late Holocene. The record found a period of stronger subtropical SPG circulation from 2000-3000BP reminiscent of changes over the last few decades. However, the authors note that more records are needed from contrasting subtropical currents to assess the validity of their claim.

In this thesis I use New Zealand black corals to reconstruct late Holocene ocean conditions and evaluate how recent ocean changes (e.g. gyre intensification) compare to those in the past. Black corals are a unique paleoceanographic archive. Paleoceanographic dynamics can be reconstructed from these corals at multi-decadal timescales using the geochemical composition of their skeleton (Prouty et al., 2014; Robinson et al., 2014; Prouty et al., 2015; Komugabe-Dixson et al., 2016). Furthermore, these corals have shown extreme longevity on the order of several millennia (Prouty et al., 2014; Robinson et al., 2014; Prouty et al., 2015; Komugabe-Dixson et al., 2016; Hitt et al., 2020). Records extracted from black corals therefore have the potential to elucidate millennial-scale ocean cycles.

New Zealand is an ideal location for investigating the contribution of natural and anthropogenic forcing to 20th century ocean changes. New Zealand marks the boundary between warm, oligotrophic, subtropical ocean currents and cool, nutrient rich, subpolar ocean currents

(Bradford-Grieve et al., 1999; Murphy et al., 2001; Chiswell et al., 2013; Ellwood et al., 2013; Chiswell et al., 2015). New Zealand's surrounding seas are therefore well suited for studying how circulation changes impact nutrient distributions and marine life. Moreover, New Zealand's surrounding waters have experienced some of the most extreme ocean changes of any region in the modern record. Ocean warming around New Zealand is 4x greater than the global average and has seen decrease in marine biodiversity due to gyre acceleration (Roemmich et al., 2007; Johnson et al., 2011; Wu et al., 2012; Roemmich et al., 2016). The large magnitude of these changes works to the benefit of investigating natural and anthropogenic contributions; it suggests that the New Zealand's circulation and marine biology is very sensitive to either external forcing or natural ocean-climate variability. Significant variations in ocean conditions should therefore be easily distinguishable in a paleo-record.

In this thesis I 1) define the length and resolution of records that could potentially be extracted from New Zealand corals by measuring longevity 2) present the first ever sub-centennially resolved records of ocean circulation for the New Zealand region by constructing a marine radiocarbon reservoir age record (ΔR) spanning the last 3000 years and 3) evaluate the effect of paleo gyre circulation on nutrient distributions and marine life by reconstructing 3000 years southwest Pacific stable isotopes ($\delta^{13}C$ and $\delta^{15}N$) at a decadal-centennial resolution.

This thesis is structured to assess five major objectives; each addressed in a specific chapter. In Section 1.2, I present a breakdown of each chapter and its objective. In Section 1.3, I present a general background on southern hemisphere and New Zealand climatology and oceanography, deep-sea black coral paleoceanographic proxies, and late Holocene paleoceanography for the southwest Pacific. In Section 1.4, I examine the broader context of this research.

1.2 Research Objectives

1.2.1 Chapter 1: An introduction to black corals and southwest Pacific oceanography

Objective 1: Provide an in-depth review on the current state of knowledge of 1) southern hemisphere climate and oceanography; 2) New Zealand climate and oceanography; 3) previous late Holocene paleoceanographic work in the southwest Pacific; 4) black coral paleoceanographic proxies.

Chapter 1 (this chapter) includes a literature review covering southern hemisphere and New Zealand climate, oceanography, and previous paleoclimate work. I first explore the connection between the ocean and atmosphere with a focus on major climate and ocean phenomena such as the westerly wind belt, ocean gyre circulation, the Southern Annular Mode and El Niño-Southern Oscillation. I then explain how thesis modes of variability affect the local New Zealand climate and oceanography, and I discuss their variability over recent decades. After this, I compare recent changes against previous paleoclimate work and highlight the areas where more work is necessary to better understand how current climate and ocean changes relate to natural climate variability.

Here I also provide a brief review of the current black coral paleoceanographic proxy literature, covering topics such as black coral physiology, the marine radiocarbon reservoir age paleo-circulation proxy, and the stable carbon and nitrogen isotope paleo-nutrient and paleo-productivity proxies. Each of these topics are described in depth in the subsequent chapters (Chapter 2, Chapter 3 and Chapter 4), and therefore the description in Chapter 1 is a general overview.

1.2.2 Chapter 2: Age and Growth Rates of New Zealand Black Corals

Objective 2: Evaluate the lifespans and growth rates of New Zealand's long-lived black corals to determine their potential for paleoceonographic applications.

Using New Zealand black corals to reconstruct paleoceanographic conditions first requires a constraint on coral age and growth rate. Determining coral age establishes what paleo intervals can be reconstructed, while calculating growth rate provides estimates on the resolution of geochemical data which can be extracted. These metrics assist in screening corals suitable for reconstructing paleoceanographic conditions. Coral age estimates also provide ecological

information on coral vulnerability to ecosystem disturbances such as fishing practices and geological events (e.g. earthquakes).

I determine the lifespans of seven New Zealand black coral colonies in this chapter and compare longevity and growth rate to other black coral growth studies. Previous work in other parts of the global oceans show that some black coral species can live for millennia. I find that New Zealand's black corals exhibit similar longevity to other Pacific black corals. This supports previous work suggesting black corals are highly vulnerable to ecosystem disturbances. I show that these seven coral colonies provide complete coverage of the last 3000 years and can be used to reconstruct a continuous record of New Zealand's late Holocene ocean conditions at the locations they are collected from.

This chapter is published in the journal *Deep-Sea Research I* as a collaborative work between myself, Daniel Sinclair, Helen Neil, Stewart Fallon, Di Tracey, Aimée Komugabe-Dixson and Peter Marriott. I selected all coral samples, subsampled each coral, prepared radiocarbon dating material, prepared radiocarbon samples, and analyzed radiocarbon dating results. Stewart Fallon measured all radiocarbon samples. Peter Marriot oversaw subsampling corals. I wrote the manuscript with the assistance of all coauthors.

1.2.3 Chapter 3: Highly Variable South Pacific Gyre Strength during the Late Holocene

Objective 3: Reconstruct a 3000 year record of southwest Pacific gyre strength.

A baseline record of variations in South Pacific Gyre strength is needed to place modern gyre changes into a longer-term context of natural ocean variability. In this chapter I present a reconstruction of gyre strength using marine radiocarbon reservoir age (ΔR) in black corals.

Black coral ΔR is a sensitive tracer of ocean circulation; it reflects the balance of subtropical and subpolar waters at a single location. I connect ΔR variations to the Southern Annular Mode (SAM) which is the most significant mode of seasonal to decadal atmospheric variability in the mid to high latitudes of the southern hemisphere. The coupling between ΔR and paleo-SAM shows that variations in gyre strength and atmospheric circulation were synchronous over the last millennium. This suggests the recent intensification of the gyre could be an expression of natural coupled ocean-atmosphere variability. As a minimum, it suggests modern gyre changes driven by the SAM are not unprecedented over the last millennium.

Co-variations in ΔR and SAM correspond to 1) centennial changes in atmospheric regime type over New Zealand and 2) a change in New Zealand's mean temperature over the last millennium. I show that coupled ocean-atmosphere change is responsible for significant variations in New Zealand climate. New Zealand's climate changes over the last millennium are then compared to climate changes over recent decades.

I reconstruct SAM conditions over the 2000-3000BP period by calibrating last millennium ΔR with the paleo-SAM index over the last 1000 years and applying it to a ΔR record over the 2000-3000BP interval. The ΔR-based SAM reconstruction is evaluated as a reliable indicator of SAM mean state conditions over the 2000-3000BP period by comparing the SAM reconstruction to other atmospheric circulation proxies from Patagonia. I show that ocean and atmospheric circulation patterns are coupled for most of the late Holocene, but the coupled relationship is likely nonstationary. This result suggests that there may be additional climatic variables affecting the gyre and atmospheric circulation relationship that have not been resolved using instrumental data or paleo data. Unfortunately, my reconstructions are unable to provide further insight into these external variables.

This chapter was submitted to the journal *Proceedings of the National Academy of Science of the United States of America* as a collaborative work between myself, Daniel Sinclair, Helen Neil, Stewart Fallon, John Hellstrom, and Aimée Komugabe-Dixson. I selected all coral samples, subsampled each coral, prepared radiocarbon and U-Th dating material, analyzed radiocarbon and U-Th dating results, created age-depth models and constructed the ΔR record. Stewart Fallon measured all radiocarbon dates and provided assistance with radiocarbon and ΔR data interpretation. John Hellstrom measured all U-Th dates and assisted with U-Th age calculations. I wrote the manuscript with the assistance of all coauthors.

1.2.4 Chapter 4: Reconstructing Southwest Pacific Ocean Productivity and Biogeochemistry Using Black Coral $\delta^{13}C$ and $\delta^{15}N$

Objective 4: Assess southwest Pacific Ocean primary productivity, biogeochemistry and nutrient dynamics over the late Holocene.

Several studies show that recent changes in the physical ocean (e.g. surface stratification, gyre circulation) are significantly affecting surface ocean biogeochemical dynamics (nutrient utilization) and marine biology (primary production). These changes are often attributed to

anthropogenic climate change and have potential for cascading effects on major ecosystems and the global climate. However, the small window of ocean observations over recent decades confounds attempts to attribute these changes to anthropogenic change or some natural ocean-climate variability. It may not be prudent to assume that recent changes in the physical ocean, marine productivity, and biogeochemistry are anthropogenically driven as these ocean properties can exhibit natural variability on anthropogenic (multi-decadal) timescales. This chapter therefore attempts to reconstruct biogeochemical dynamics as they relate to ocean gyre change by comparing black coral-based circulation reconstructions with marine biogeochemistry reconstructions constructed from stable isotopes ($\delta^{13}C$ and $\delta^{15}N$).

Coral $\delta^{13}C$ records representing the East Auckland Current (EAuC) and Subtropical Front (STF) show co-variability over the last 1500 years. I interpret this co-variability to be driven by synchronous sea surface temperature (SST) variations around New Zealand and not other factors that affect coral $\delta^{13}C$ (e.g. CO_2 and plankton community structure). I eliminate atmospheric CO_2 forcing as a cause because changes over the late Holocene are not large enough to account for the scale of $\delta^{13}C$ variability. I consider it unlikely that changes in phytoplankton community structure drive coral $\delta^{13}C$ because each coral location has a unique ecology, making synchronous community structure changes across a large geographic region improbable. SST is the only local environmental conditions that responds unilaterally to climate forcing at both sites making it the most likely driver of synchronous coral $\delta^{13}C$ variability.

Variability observed in the coral $\delta^{15}N$ records presented in this chapter likely reflect changes in the distribution of bioavailable nitrogen in different ocean current regimes around New Zealand. I see a correlation between multi-centennial coral $\delta^{15}N$ cycles and variability in the multi-centennial mean state of the Southern Oscillation Index (SOI) over the last 1500 years. This suggests that the SOI may drive variability in the spatial distribution of bioavailable nitrogen around New Zealand on multi-centennial timescales. I hypothesize this relationship results from the effects the regional atmospheric circulation arising from ENSO may have on regional sea surface temperatures and wind-driven upwelling around New Zealand.

In this chapter I compare black coral $\delta^{13}C$ and $\delta^{15}N$ records with the ΔR paleo-circulation reconstruction from Chapter 3. Black coral $\delta^{13}C$ shows a variable relationship with the ΔR paleo-circulation reconstruction over the last 3000 years. Multi-centennial variations in ΔR do not

correspond to coral $\delta^{13}C$ variability observed over the last 1500 years; however, multi-centennial ΔR variations do correspond to coral $\delta^{13}C$ variability over the 2000-3000BP period. This lends support to the idea that multi-centennial coral $\delta^{13}C$ variability may be driven by sea surface temperature changes. The coral $\delta^{15}N$ records do not show relationship with the ΔR reconstruction; ΔR variability on multi-centennial timescales does not correspond to multi-centennial variations in $\delta^{15}N$. This implies that multi-centennial changes in ocean circulation did not modulate the pattern of bioavailable nitrogen on the same timescale.

This chapter also presents evidence for a sustained change in the strength of the SPG and its biogeochemical patterns between the 0-2000BP and 2000-3000BP intervals. I show that a period of more intense gyre circulation (2000-3000BP) corresponds to a change in mean coral $\delta^{13}C$ and $\delta^{15}N$ from the Central South Pacific. We interpret this as a change in the distribution of bioavailable nitrogen, particulate organic matter $\delta^{15}N$ and phytoplankton $\delta^{13}C$. This implies that circulation, biogeochemical patterns and nutrient variability may be coupled over millennial timescales.

The content in chapter is currently being prepared as three separate manuscripts in collaboration with Daniel Sinclair, Helen Neil, Stewart Fallon, Sarah Bury, Amandine Sabadel, Josette Delgado, Julie Brown, John Hellstrom, and Aimée Komugabe-Dixson. I selected all coral $\delta^{13}C$ and $\delta^{15}N$ samples, subsampled each coral, prepared U-Th dating material, analyzed U-Th data, analyzed $\delta^{13}C$ and $\delta^{15}N$ results and constructed age-depth models. Stewart Fallon, Sarah Bury, Josette Delgado and Julie Brown all assisted in measuring coral samples for $\delta^{13}C$ and $\delta^{15}N$. John Hellstrom measured all U-Th dates and assisted with U-Th age calculations. I wrote the thesis chapter with the assistance from Dan Sinclair, Helen Neil, Sarah Bury, Amandine Sabadel, and Aimée Komugabe-Dixson.

1.2.5 Chapter 5: Project Summary, Future Directions and Future Recommendations

Objective 5: Summarize the research findings, discuss future research directions and provide future recommendations for black coral-based paleoceanographic reconstructions

Chapter 5 provides a summary of the research findings presented in this thesis. The discussion of research findings include 1) a description of black coral growth and longevity; 2) the highly variable South Pacific Gyre strength over the late Holocene; and 3) a summary of the 3000 year history of marine biogeochemistry in the Southwest Pacific Ocean.

This chapter also includes a discussion of future research directions and recommendations. Future research directions include ongoing work (post PhD) to 1) measure stable carbon and nitrogen isotopes of individual amino acids in the black corals presented in this thesis and 2) modeling variations in marine particulate organic matter nitrogen isotope values as a function of interannual climate variability using state of the art coupled ecosystem-climate models. Chapter 5 also includes recommendations for future black coral-based paleoceanographic work using the methodology and conclusions presented in Chapters 2-4. The research presented in this thesis therefore provides a methodological and paleoceonographic framework which later projects can build upon.

Note: Chapters of this thesis are published, submitted or being prepared as manuscripts for publication. This leads to some content repetition in the introduction sections of each chapter on topics such as oceanographic setting, major climate modes, and description of proxies in deep-sea corals. All chapter references are formatted to a consistent style, which may differ from the reference style of the published chapter manuscripts.

1.3 Background

In this section I review the following: 1) southern hemisphere ocean and climate, 2) the regional climatology and oceanography of New Zealand, and 3) deep-sea coral paleoceanographic proxies.

1.3.1 Southern Hemisphere Climate and Oceanography

1.3.1.1 The South Pacific Gyre (SPG)

Global climate patterns primarily result from interactions between the ocean and atmosphere (Munk, 1950; Ruddiman, 2008; Trujillo et al., 2011). The most prominent ocean-atmosphere interaction is the interplay of atmospheric winds and surface waters, which drive a series of surface-ocean gyres that affect the global distribution of temperature, salinity and nutrients (Munk, 1950; Sarmiento et al., 2006; Ruddiman, 2008; Trujillo et al., 2011).

Basin-wide atmospheric wind patterns in the tropical and subtropical Pacific Ocean are driven by a combination of the Hadley and Walker Circulation patterns and the Coriolis force. The Hadley circulation is a global scale tropical atmospheric circulation pattern where air rises near the equator, flows poleward at a height of 10-15 kilometers, descends in the subtropics at about 30˚ latitude and returns equatorward near the surface (Ruddiman, 2008; Trujillo et al., 2011; Hartmann, 2015). This circulation pattern is the main meridional atmospheric convection pattern in the tropical Pacific in both hemispheres (Hartmann, 2015). The Walker circulation is the main zonal pattern of atmospheric circulation in the equatorial regions; it describes the east-west convection pattern between the western and eastern Pacific (Bjerknes, 1969). It results from the influence of the sea surface temperature (SST) gradient across the equatorial Pacific. Warm SSTs in the western Pacific result in warm, moist, buoyant air ascending over this region. Condensation and precipitation of moisture at altitude releases latent heat. Therefore, compared to the eastern Pacific, surface air pressure is low and upper troposphere pressure is heigh. This results in a pressure gradient across the Pacific and a prevailing easterly flow near the equator (Bjerknes, 1969). The Coriolis force effects surface winds due to the Earth's rotation. The Earth's rotation causes circulation patterns (e.g. the Hadley Circulation) to deflect, which results in curved, basin-wide paths (Ruddiman, 2008; Trujillo et al., 2011; Hartmann, 2015). Together, the Hadley and Walker Circulation, and the Coriolis Force, create an anticyclonic atmospheric convection pattern of easterly winds at the equator (the trade winds) and westerly winds at the

mid-latitudes (Ruddiman, 2008; Trujillo et al., 2011; Hartmann, 2015). This drives a surface ocean gyre in the South Pacific termed the South Pacific Gyre (SPG) (Munk, 1950).

In the South Pacific, easterly trade winds created by the Coriolis force and Hadley and Walker circulations push equatorial waters to the west at the equator (e.g. the South Pacific Equatorial Current), while mid-latitude westerly winds force waters to the east. This creates the massive anticyclonic ocean circulation pattern in the South Pacific Ocean, the South Pacific Gyre (SPG) (Figure 1.1; Munk, 1950). The SPG is the largest gyre on Earth and plays a critical role regulating Pacific climate through complex air-sea interactions (e.g. El Niño-Southern Oscillation (ENSO) and the Southern Annular Mode (SAM); see sections 1.3.1.4 and 1.3.1.5).

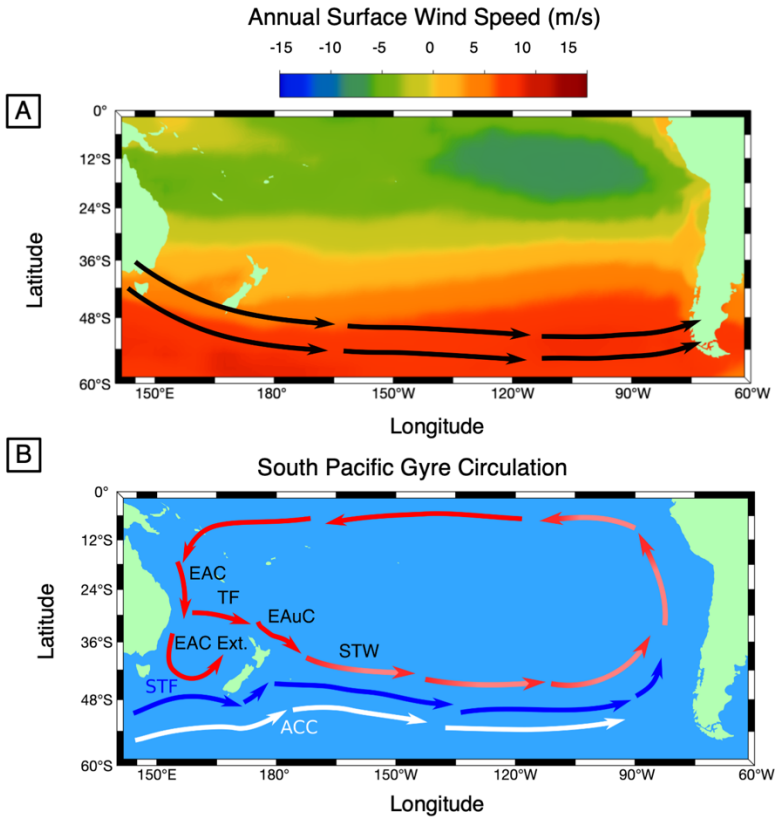

Figure 1.1: Westerly Wind and South Pacific Gyre Circulation. Panel A: Annual Mean Zonal Wind Speed (u-wind) at the ocean surface. Data source: ERAv4. Panel B: A schematic of South Pacific Gyre circulation with individual current and front names. Red arrows indicate warm, tropical water currents, blue arrows indicate temperate surface currents, white arrows indicate Antarctic and polar currents. EAC: East Australian Current, TF: Tasman Front, EAuC: East Auckland Current, EAC Ext: East Australian Current Extension, STW: Subtropical Water, STF: Subtropical Front, ACC: Antarctic Circumpolar Current.

1.3.1.2 Atmospheric Influences on the South Pacific Gyre Circulation

The circulation of the SPG is strongly influenced by several atmospheric features, such as the South Pacific Anticyclone (SPA; also referred to as the South Pacific Subtropical High; Rodwell et al. (2001); Grotjahn (2004); Zou et al. (2018); Flores-Aqueveque et al. (2020)) and South Pacific Convergence Zone (SPCZ) (Takahashi et al., 2007b; Takahashi et al., 2007a). The SPA is a large-scale, quasi-permanent high-pressure system in the mid-latitude eastern Pacific produced by the general circulation of the atmosphere (Rodwell et al., 2001; Grotjahn, 2004; Ancapichún et al., 2015; Flores-Aqueveque et al., 2020). The subsiding branch of the Hadley cell determines the location of this high surface pressure at 30˚S (Rodwell et al., 2001; Flores-Aqueveque et al., 2020). At the northern edge of this high surface pressure, air masses flow westward and, in conjunction with the Walker Circulation, produce the equatorial trade winds (Fig. 1.2 & 1.4; Rodwell et al., 2001; Takahashi et al., 2007b; Takahashi et al., 2007a; Flores-Aqueveque et al., 2020). These trade winds cause upwelling of deep water in the eastern equatorial Pacific that is advected westward. At the south edge of the SPA air masses flow eastward and are fed by the mid-latitude southern hemisphere westerly wind belt (see section 1.3.1.3 for more details on the SHWW). This high pressure regions determines the poleward boundary of tropical atmospheric circulation in the southeast Pacific, and form the southern boundary of the SPA (Cherchi et al., 2018).

Seasonally, the SPA migrates north and south with little impact to the trade winds (Rodwell et al., 2001); however, on longer timescales (e.g. interannual to millennial timescales) a migration can weaken or enhance the southeast trade winds and weaken or enhance the equatorial countercurrent (ECC) (Zou et al., 2018). Changes in trade wind intensity and location can modulate the position of 1) vertical atmospheric convection zones across the equatorial Pacific (e.g. the Intertropical Convergence Zone and South Pacific Convergence Zone; Takahashi et al. (2007b); Flores-Aqueveque et al. (2020)) and 2) the equatorial and eastern south Pacific currents (the North and South Equatorial Currents and Humboldt Current; Zou et al. (2018)). Variations in trade wind strength associated with the location of the SPA can therefore amplify or suppress precipitation and equatorial ocean circulation across the eastern and equatorial portions of the gyre (Rodwell et al., 2001; Takahashi et al., 2007b; Takahashi et al., 2007a; Ancapichún et al., 2015; Zou et al., 2018). The influences the SPA has on equatorial Pacific circulation makes the SPA a significant influence on the circulation of the SPG, as well

as basin-wide Pacific climate modes which alter ocean-atmospheric circulation patterns, such as the El Niño-Southern Oscillation (Zou et al. (2018); see section 1.3.1.5 for more details).

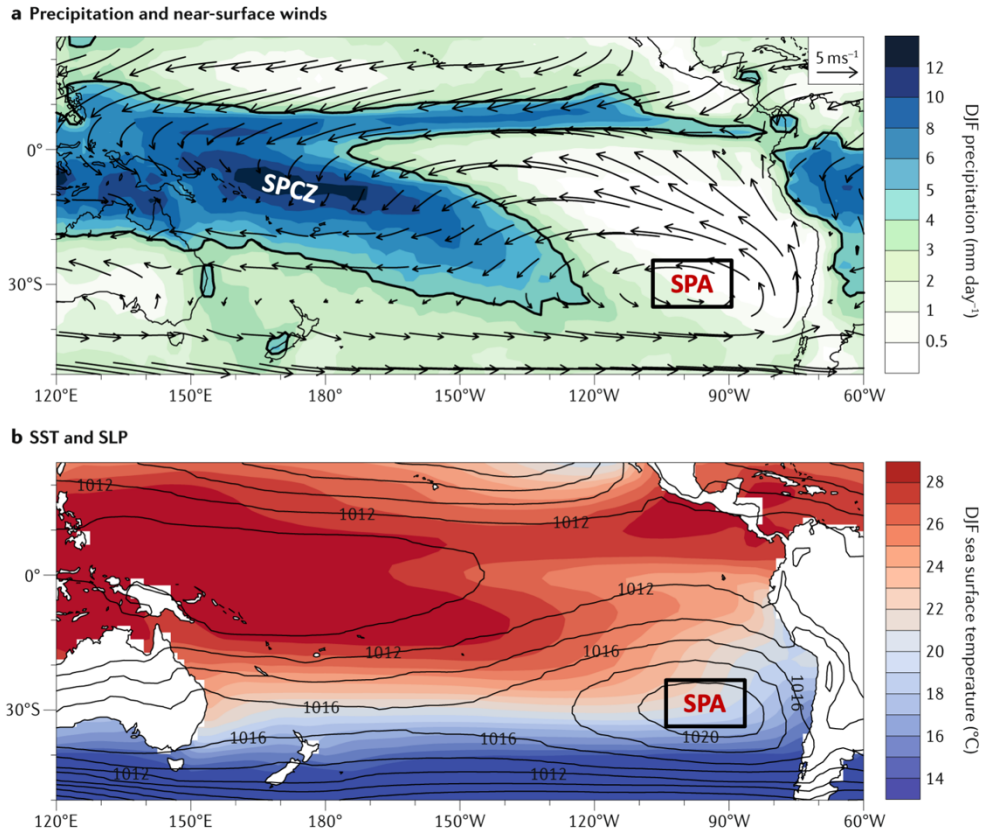

Figure 1.2: The Circulation of the South Pacific Gyre as it relates to the South Pacific Anticyclone and South Pacific Convergence Zone. Mean December–February (DJF) precipitation (shaded contours; mm day−1) and 925-hPa winds (vectors; m s−1) (panel a), and sea surface temperature (SST; shaded contours; °C) and sea-level pressure (SLP; contours; hPa) (panel b) averaged over 1980–2005. The bold 4 mm day−1 contour in panel a indicates the position of the South Pacific Convergence Zone in the South Pacific. The South Pacific Anticyclone (SPA) is identified with a black box and the South Pacific Convergence Zone is identified with bolded white text. Figure is modified from Brown et al., 2020.

Ocean and atmospheric circulation in the equatorial SPG is also affected by the South Pacific Convergence Zone (SPCZ) (Delcroix et al., 1998; Takahashi et al., 2007b; Takahashi et al., 2007a; Komugabe-Dixson et al., 2016). The SPCZ is a band of low-level convergence in the western equatorial Pacific which occurs where southeast trade winds meet the easterly flow from the eastern SPA, which produces heavy convection and rainfall (Takahashi et al., 2007b; Takahashi et al., 2007a; Brown et al., 2020). The precipitation generated by the SPA forces a salinity gradient in the ocean where waters in the western Pacific are warm and fresh and transition to warm and salty in the central Pacific (Delcroix et al., 1998; Linsley et al., 2006;

Brown et al., 2020). This region is termed the west Pacific salinity front (WPSF) which can inhibit the transport along the equatorial portion of the western south Pacific (Delcroix et al., 1991; Delcroix et al., 1998; Komugabe-Dixson et al., 2016). However, the position of the SPCZ can change on seasonal, interannual and longer timescales due to variations in atmospheric circulation patterns (Delcroix et al., 1991; Delcroix et al., 1998; Linsley et al., 2006; Brown et al., 2020), with potential effects to the strength of ocean circulation in the southwestern portion of the SPG (Komugabe-Dixson et al., 2016).

The shape and intensity of the SPG can therefore be subject to the modes of natural climate variability which influence the SPA and SPCZ. The most significant climate mode which affects these climate features is the El Niño-Southern Oscillation (ENSO). ENSO can play a role in modulating the position of the SPA and SPCZ by causing southern and northern shifts in the SPCZ and SPA on interannual timescales (Zou et al., 2018; Brown et al., 2020; Flores-Aqueveque et al., 2020). These shifts affect the circulation of the gyre, such that during a positive ENSO phase (El Niño), the SPCZ shifts north and facilitates circulation from the equatorial southwestern Pacific to the mid-latitude southwest Pacific (Delcroix et al., 1991; Delcroix et al., 1998; Komugabe-Dixson et al., 2016). This usually coincides with a southern shift in the SPA, which suppresses circulation along the eastern boundary of the SPG (Ancapichún et al., 2015; Zou et al., 2018). A further description of the influence ENSO has on the SPCZ, SPA and SPG circulation is provided in 1.3.1.6.

1.3.1.3 Modes of Variability in the Pacific Ocean Gyres

The basin wide gyres of the Pacific basin, the North Pacific Gyre (NPG) and SPG were once thought to be stable systems from an biological and physical oceanographic perspective (Karl, 1999); however, much work over recent decades shows this is not the case for the NPG (Karl, 1999; Karl et al., 2001a; Karl et al., 2001b; Di Lorenzo et al., 2008; Sherwood et al., 2013; Newman et al., 2016; Liguori et al., 2018; Liu et al., 2018; Glynn et al., 2019). In particular, the NPG exhibits a wide spectrum of natural variability on interannual to millennial timescales. For example, phytoplankton communities appear to respond on seasonal to millennial timescales in response to changes in the mean state of the Pacific ocean in the NPG (Karl et al., 1995; Karl, 1999; Karl et al., 2001b; Corno et al., 2007; Sherwood et al., 2013; McMahon et al., 2015; Glynn et al., 2019). Physical oceanographic characteristics, such as SST, salinity and thermocline height also exhibit a range of natural variability on interannual to decadal timescales in the NPG

(Di Lorenzo et al., 2008; Newman et al., 2016; Liguori et al., 2018; Liu et al., 2018). This has led to a paradigm shift in our understanding of how the subtropical systems in basin-wide gyres operate; they are indeed highly variable and not unchanging and stable as previously thought.

Much of the insight to natural variability in the NPG largely results from paleoceanographic reconstructions (Sherwood et al., 2013; McMahon et al., 2015; Glynn et al., 2019) or data from the Hawaiian Ocean Timeseries (Karl et al., 1996). Natural ocean and ecosystem variability in the NPG can therefore be established; however, the same is not true for the subtropical SPG. There is a paucity of observations in the subtropical SPG (Deser et al., 2010) relative to the NPG due to the vast size of the SPG. Therefore, while it may be reasonable to assume the SPG experiences modes of variability akin to the NPG, there is little evidence to support such a claim.

1.3.1.4 Southern Hemisphere Westerly Winds (SHWW)

The southern hemisphere westerly winds (SHWW) are an integral component of the global climate system. These westerlies are driven by the large meridional pressure gradient between 30°S and 60°S. The SHWW dominate South Pacific Ocean circulation patterns on annual to glacial timescales (Moreno et al., 2009; Lamy et al., 2010; Moreno et al., 2010; Bostock et al., 2015). On these timescales the winds can expand north, weaken and reduce ocean circulation and vice versa (Lamy et al., 2010; Kohfeld et al., 2013; Bostock et al., 2015). These variations can modulate equator-pole heat transport, the upwelling of deepwater, and marine CO_2 outgassing/ventilation (Russell et al., 2006; Toggweiler et al., 2006; Ruddiman, 2008). The strength and position of the SHWW can therefore alter global temperatures by changing the latitudinal temperature gradient and atmospheric CO_2 composition (Kushner et al., 2001; Toggweiler et al., 2006; Kohfeld et al., 2013).

1.3.1.5 The Southern Annular Mode (SAM)

On seasonal to interdecadal timescales, the largest influence on the SHWW is the Southern Annular Mode (SAM) (Thompson et al., 2000; Marshall, 2003). SAM is the leading mode of climate variability in the southern mid-latitudes and is characterized by near zonally-symmetric, anti-phased sea level pressure anomalies between the mid-latitudes (40-50°S) and Antarctica (50-70°S) (Figure 1.2; Thompson et al., 2000; Marshall, 2003). Positive SAM phases have more rising poleward motion at 60˚S and sinking motion between 40-50˚S, and correspond

to positive mid-latitude pressure anomalies and stronger westerly winds on the poleward edge of the subtropical high and in the circumpolar trough (Thompson et al., 2000; Marshall, 2003). Zonal winds strengthen at 50˚S, which increase circulation at the mid-latitudes (Fogt et al., 2006). SAM is known to vary on seasonal to decadal timescales and thought to oscillate on centennial to millennial timescales (Jones et al., 2009; Kidston et al., 2009; Abram et al., 2014; Moreno et al., 2014; Moreno et al., 2018). SAM likely plays a role in major climate shifts (e.g. the Last Glacial Maximum, Holocene climate optimum and temperature variability) by altering atmospheric CO_2 concentration and the equator-pole heat flux (Lovenduski et al., 2005; Abram et al., 2014; Moreno et al., 2018; Reynhout et al., 2019).

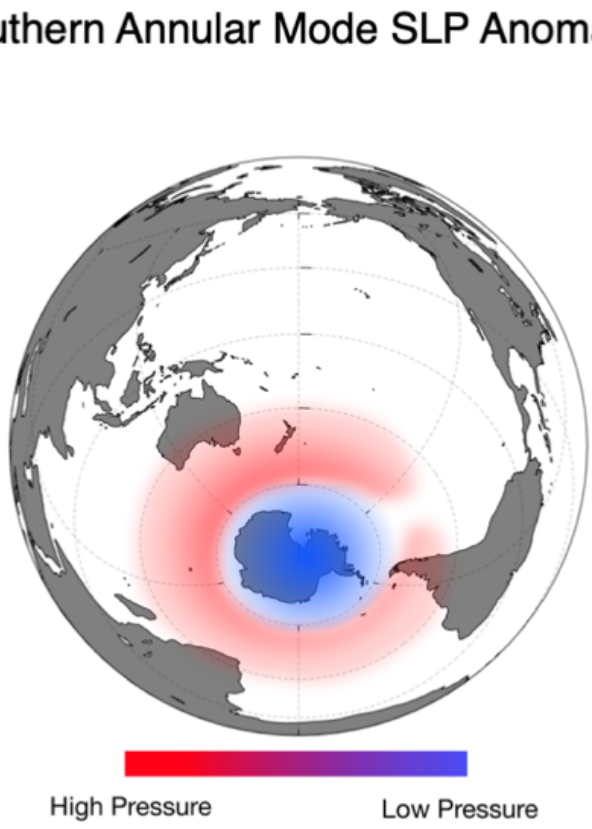

Figure 1.3: A Schematic of the Southern Annular Mode (SAM) Sea Level Pressures. A schematic of mean sea level pressure anomalies (MSLPA) for the positive phase of the Southern Annular Mode (SAM). Red indicates positive MSLPA and blue indicates negative MSLPA.

1.3.1.6 The El Niño-Southern Oscillation (ENSO)

The dominant mode of climate variability across the entire Pacific Ocean is the El Niño-Southern Oscillation (ENSO; Bjerknes, 1969; Cane et al., 1986; Sarachik et al., 2010). ENSO is a quasi-periodic variation on subdecadal timescales (2-7 years) in the coupled ocean-atmosphere

systems along the equator (Pacific Walker Circulation, sea-surface temperatures and thermocline depth) (Bjerknes, 1969; Cane et al., 1986; Sarachik et al., 2010). During the 'El Niño' phase of ENSO, a reduction in trade wind strength and westerly wind bursts causes warm sea surface temperatures from the western Pacific warm pool to propagate east (Bjerknes, 1969; Cane et al., 1986; Sarachik et al., 2010). This diminishes upwelling in the Humboldt current offshore of Peru, and increases sea surface temperatures across the central and eastern Pacific Ocean, while reducing sea surface temperatures in the west Pacific (Figure 1.3). This reduces the thermocline depth in the west but increases thermocline depth in the east (Bjerknes, 1969; Cane et al., 1986; Sarachik et al., 2010). During the La Nina phase of ENSO, the opposite occurs. Trade wind circulation increases, which promotes eastern pacific upwelling and causes cool deep water to expand further west across the central Pacific.

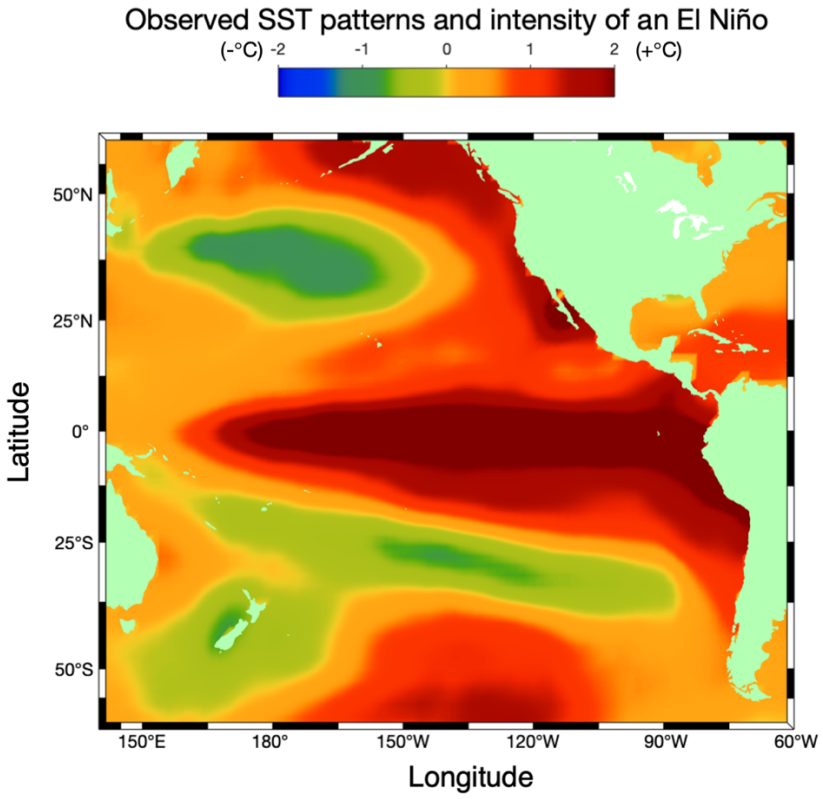

Figure 1.4: El Niño-Southern Oscillation Sea Surface Temperature (SST) Patterns. El Niño SST patterns calculated from EOFs 1 and 2. Red areas indicate warm SST anomalies; green areas indicate cool SST anomalies. SST EOFs are calculated from AVHRR OISSTv2 over the 1991-2018 interval following procedures in Messié et al. (2011).

Changes in the trade winds (and therefore the Walker Circulation) are related to the strength and position of the SPA (Figures 1.2 & 1.4). The SPA migrates south during an El Niño

event and north during a La Niña event (Zou et al., 2018). This changes the strength and location of the surface winds at the equator, and leads to either an intensification or reduction of the equatorial currents associated with 'normal' SPG circulation patterns (Zou et al., 2018). An intensification of the trade winds (and therefore Walker Circulation) is a result from the northward SPA migration and leads to anomalously strong upwelling in the eastern Pacific (Figures 1.2 & 1.4). This reduces SSTs across the eastern and central equatorial Pacific (Figure 1.4). Conversely, a breakdown in the Walker Circulation results from a southern migration of the SPA. This reduces the equatorial trade winds and forces warm waters in the western Pacific warm pool to migrate towards the eastern Pacific (Figures 1.2 & 1.4). This change in atmospheric circulation also extends to vertical convective patterns, and influences climate features (e.g. precipitation patterns) like the SPCZ.

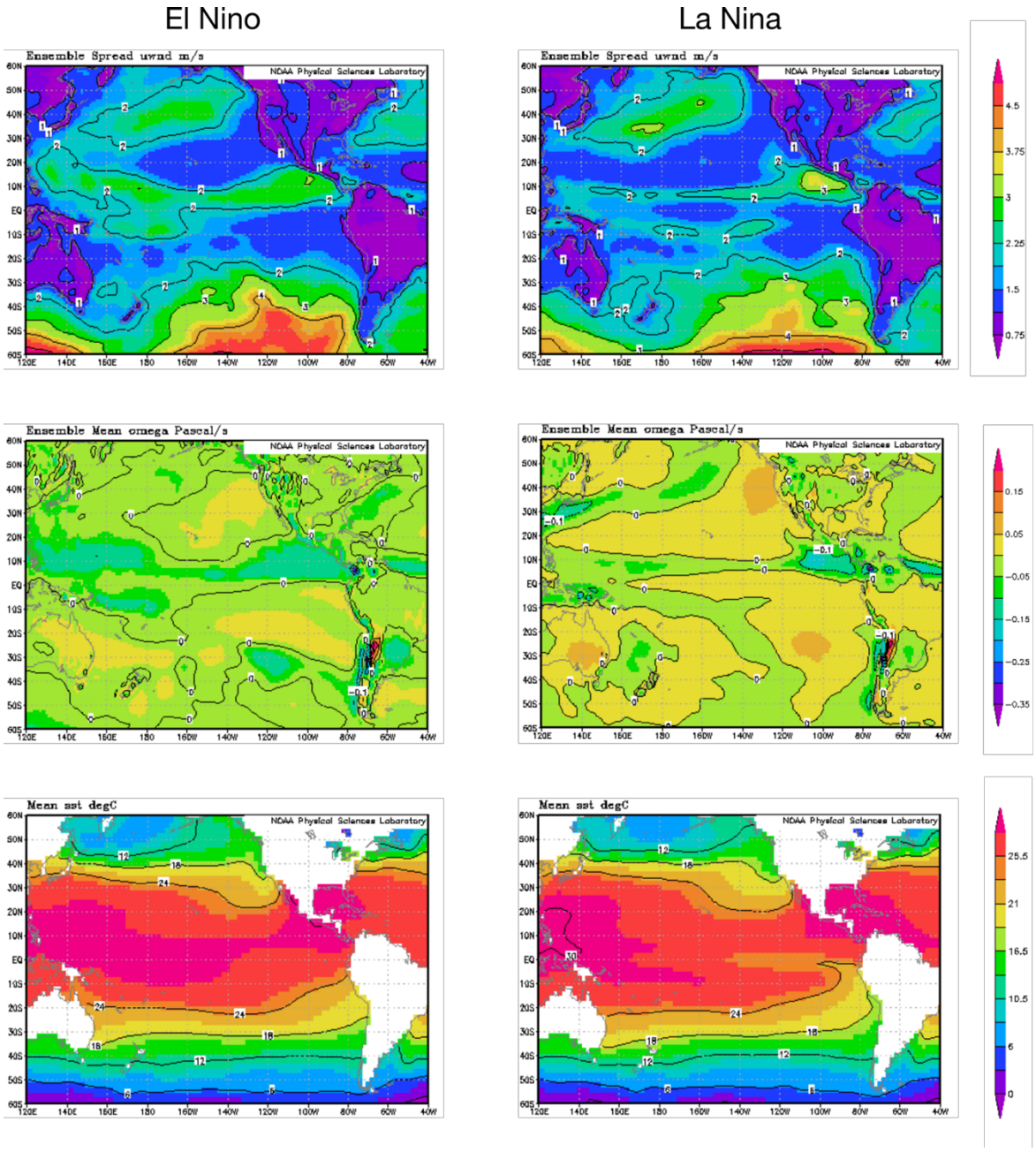

Figure 1.5: Changes in Atmospheric Circulation and Sea Surface Temperatures due to El Niño-Southern Oscillation. Top Row: El Niño (left) and La Niña (right) changes in omega (vertical velocity) at 500hPa. Data source: NCEP/NCAR Reanalysis V3Middle Row: El Niño (left) and La Niña (right) changes in u-wind (streamline function) at 1000hPa. Data source: NCEP/NCAR Reanalysis V3. Bottom Row: El Niño (left) and La Niña (right) changes in sea surface temperatures (streamline function) at 1000hPa. Data source: ERSSTv5.

ENSO variability is the largest source of variability on the SPCZ (Brown et al., 2020). During El Niño events weaker subtropical easterlies and stronger subtropical westerlies cause a northward shift in the SPCZ, while during La Niña stronger subtropical easterlies and weaker westerlies force the SPCZ to shift south (Trenberth, 1976; Brown et al., 2020). During strong El

Niño events (e.g. the 1997-1998 event) the SPCZ can shift towards the equator and rotate to an orientation more parallel to the equator (Brown et al., 2020). The opposite is true during La Niña events. These effects have considerable impacts on SPG circulation patterns and strength in two ways. The position of the SPCZ affects SPG circulation by changing the location of the WPSF (see sections 1.3.1.2 and 3.5.3 and Komugabe-Dixson et al., 2016 and references therein for details).

Some studies have suggested that ENSO events can be a response to changes in the SPA (Meinen et al., 2000; Van Oldenborgh, 2000; Zou et al., 2018). A southward migration of the SPA weakens the southeast trade winds, enhances the equatorial countercurrent (ECC) and allows for a southward intrusion of the northeast trade winds in the equatorial Pacific (see Fig. 1 in Zou et al., 2018; Y. Wang, 2019). An enhanced ECC leads to an anomalous accumulation of warm water in the central-eastern equatorial pacific brought by a reversal of the Walker circulation. Therefore, the migration of the SPA is a driver in ENSO variability and so the major climate features that drive SPG circulation (SPA, Hadley and Walker circulation) also relate to ENSO variability (Zou et al., 2018; Y. Wang, 2019). The shape of the SPG is thus subject to ENSO variability through changes in the position of the SPA.

ENSO also affects global climate patterns through atmospheric teleconnections which cause unusual weather patterns such as floods or droughts across the globe (Cane et al., 1986; Sarachik et al., 2010; Cobb et al., 2013; S. Wang et al., 2014; Sun et al., 2015). ENSO has shown variability on millennial and glacial timescales with potential connections to solar and atmospheric forcing; however, there is little consensus on what forces paleo-ENSO variability over the Holocene (Lu et al., 2018). The role that ENSO plays in major climate shifts (e.g. the Holocene Climatic Optimum; Last Glacial Maximum) is therefore unclear (Lu et al., 2018).

1.3.2 New Zealand Climatology and Oceanography

New Zealand is an ideal location for studying variations in physical and biological oceanography associated with the southwestern portion of the SPG. The landmass divides subtropical and subpolar waters, both of which have unique temperature, salinity and nutrient properties (Bradford-Grieve et al., 1999; Ellwood et al., 2013; Chiswell et al., 2015). The SPG bathes northern New Zealand in warm subtropical waters, bringing a mild climate and rainfall to that region (Ummenhofer et al., 2007; Ummenhofer et al., 2009; Chiswell et al., 2015). Conversely, southern New Zealand receives subpolar waters from the Antarctic region and is

enriched in nutrients (Orsi et al., 1995; Stramma et al., 1995; Bradford-Grieve et al., 1999; Chiswell et al., 2015). The boundary between the two is characterized by high levels of primary production and a steep gradient in ocean temperature and salinity (Figure 1.4; Murphy et al., 2001; Chiswell et al., 2013; Chiswell et al., 2015).

Winds control many of New Zealand's unique oceanographic features (e.g. nutrient upwelling and strong subtropical currents; Bradford et al., 1978; Chiswell et al., 2013; Chiswell et al., 2015; Stevens et al., 2019). The position and relative mixing of the contrasting water masses is controlled by the mid-latitude westerly wind belt and the region's ocean bathymetry (Munk, 1950; Cai et al., 2005; Chiswell et al., 2015). The strength and position of the westerlies controls the southern extent of warm, subtropical ocean currents which insulate New Zealand (Cai et al., 2005; Roemmich et al., 2007; Roemmich et al., 2016). The westerlies also drive the upwelling of deep waters along eastern New Zealand and the position of nutrient rich Antarctic waters (Bradford et al., 1978; Bradford-Grieve et al., 1999; Murphy et al., 2001; Chiswell et al., 2013; Chiswell et al., 2015; Stevens et al., 2019). Both of these support high levels of primary production and a complex biogeochemistry for the region (Bradford-Grieve et al., 1999; Murphy et al., 2001; Ellwood et al., 2013). New Zealand's complex oceanography therefore arises from multi-faceted interactions between the ocean, the atmosphere, marine life and biogeochemistry.

1.3.2.1 Ocean Currents from the New Zealand Region

North and west of New Zealand, warm waters are derived from the East Australian Current (EAC) and its branches, the EAC extension, Tasman Front (TF) and East Auckland Current (EAuC) (Figure 1.4A; Chiswell et al., 2015). South and east of New Zealand, cool polar waters are delineated by the Subtropical Front (STF) and Subantarctic Front (SAF). These fronts separate the warm, subtropical waters from the cold waters of the Antarctic Circumpolar Current (ACC) (Chiswell et al., 2015).

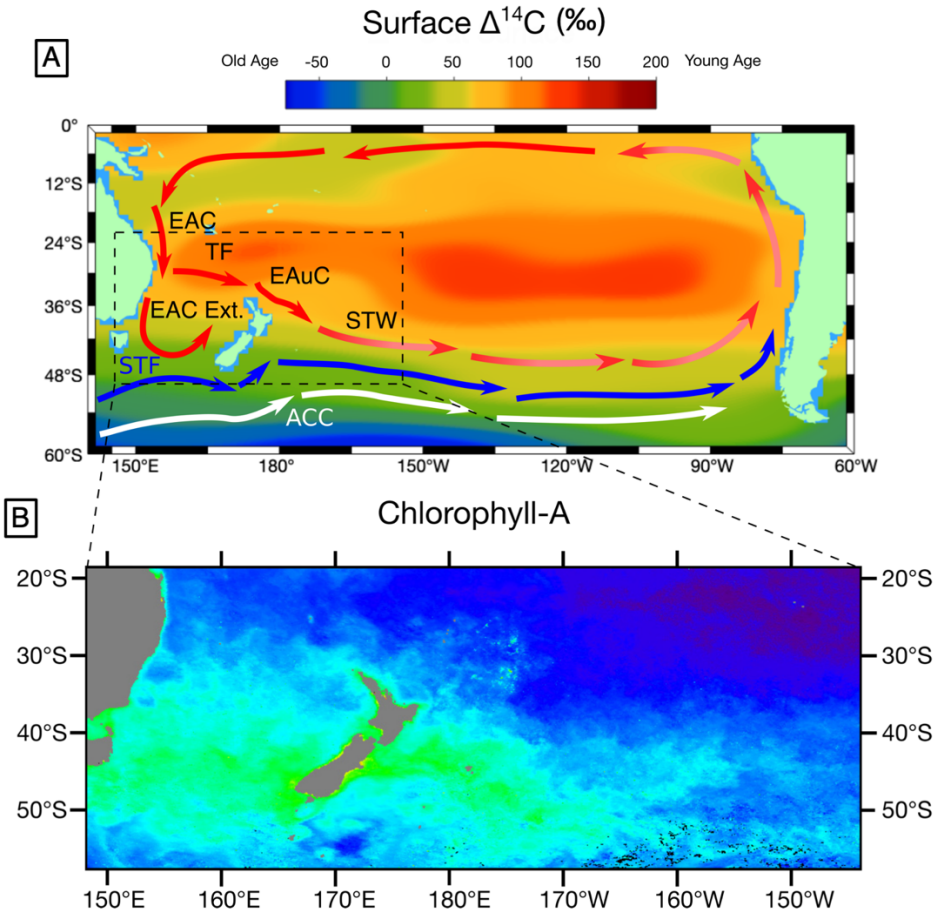

Figure 1.6: A collection of Southwest Pacific Ocean current, chlorophyll and radiocarbon information. Panel A: A schematic of South Pacific Gyre ocean currents around New Zealand overlaid on top of surface $\Delta^{14}C$ data (Key et al., 2004). Panel B: Annually averaged chl-a for the New Zealand region. Green areas indicate high levels of chl-a, while blue areas indicate regions with no chl-a. Data source: NASA MODIS.

The STF is the SPG boundary current south of Australia and southeast of New Zealand (Figure 1.1B & Figure 1.4A; Wyrtki, 1960; Stramma et al., 1995; Graham et al., 2013; Chiswell et al., 2015). East of New Zealand, the STF acts as the primary divider between subtropical gyre waters and the ACC (Figure 1.1B & Figure 1.4A; Wyrtki, 1960; Stramma et al., 1995; Graham et al., 2013; Chiswell et al., 2015). The STF is characterized by a wide spectrum of dynamical variability in time and space; it exhibits temperature, salinity, water column density, strength and position variations on seasonal to glacial/interglacial scales (Heath, 1985; De Boer et al., 2013; Smith et al., 2013; Bostock et al., 2015; Chiswell et al., 2015). East of New Zealand, the STF location is primarily constrained by the bathymetry of the shelf break east of the South Island: the Chatham Rise and Campbell Plateau (Neil et al., 2004; Kohfeld et al., 2013; Chiswell et al., 2015). East of the Chatham Islands, the STF features ocean eddies that entrain subtropical and

subantarctic waters (Graham et al., 2013). The subpolar mixing component of the east of New Zealand region promotes primary production due to high levels of nutrients from subantarctic waters (Bradford et al., 1978; Bradford-Grieve et al., 1997; Bradford-Grieve et al., 1999; DiFiore et al., 2006; DiFiore et al., 2010). High levels of productivity sequester atmospheric CO_2 into the ocean, which therefore makes the Tasman Sea, Chatham Rise, Campbell Plateau and Chatham Islands net carbon sinks (Currie et al., 1998; Sabine et al., 2004; Currie et al., 2011).

The EAC is the primary western boundary current of the SPG. It transports warm, saline waters along the east coast of Australia from 16°S to 33°S (Figure 1.4A; Godfrey et al., 1980; Cresswell, 2000; Ridgway, 2007). These oligotrophic waters release heat and moisture through evaporation which enhances atmospheric convection and rainfall in New Zealand, Tasmania and southwest Australia (Bowen et al., 2005; Ridgway, 2007; Ummenhofer et al., 2007). These waters are derived from the warm South Equatorial Current (SEC) and provide the southwest Pacific with a remarkably mild and stable climate (Edgar, 1984; Ummenhofer et al., 2007).

The tail-end of the EAC is separated into two branches in the Tasman Sea as a result of local bathymetry: the TF and EAC extension (Figure 1.4A; Godfrey et al., 1980; Tilburg et al., 2001; Chiswell et al., 2015). Each carries a different proportion of the EAC with the relative strengths of each being anti-correlated on decadal timescales (Hill et al., 2011; Ganachaud et al., 2014; Chiswell et al., 2015). Decadal variations in EAC extension and TF strength have a relationship with low-frequency changes in westerly wind location (Hill et al., 2011; Ganachaud et al., 2014). This suggests that low-frequency wind variability drives variability within the EAC system, although Hill et al. (2011) note that more data is needed to ascertain the significance of these relationships.

The EAuC is a subtropical SPG western boundary current that originates from the flow of the TF (Figure 1.4A; Chiswell et al., 2015). The EAuC is a highly variable current; it displays irregular cycles in strength on seasonal timescales but regular cycles on periods of ~100 days (Stanton et al., 2003). The northern and south eastern fringes of the EAUC hold two semi-permanent eddies, the North Cape Eddy (NCE) and the East Cape Eddy (ECE). Both eddies border the north western and eastern edges of the northern New Zealand coastline (the Bay of Plenty) (Chiswell et al., 2015). These eddies vary in size and strength; however, they likely promote moderate levels of productivity relative to the TF and STW east of New Zealand

(Bradford et al., 1982). This is due to semi-permanent eddy features that contribute to short, localized upwelling events (Chiswell et al., 2013).

1.3.2.2 Marine Productivity Around New Zealand

Marine primary productivity is the rate at which atmospheric or aqueous CO_2 is converted to organic material by photosynthetic plankton (phytoplankton; Trujillo et al., 2011). Phytoplankton require a specific suite of macronutrients (e.g. NO_3^- and PO_4^-) and micronutrients (e.g. Fe and Cd) for growth (Redfield, 1934; Trujillo et al., 2011; Martiny et al., 2014). Nutrient distributions are therefore usually the first order control on the spatial distribution of phytoplankton communities, abundance and primary production (Sarmiento et al., 2006; Trujillo et al., 2011).

In the SW Pacific, productivity reaches a maximum in the STF (Figure 1.4B). This results from the abundance of micro and macronutrients provided by the relative mixing of subtropical and subpolar waters (Bradford-Grieve et al., 1999; Boyd et al., 2000; Murphy et al., 2001; Chiswell et al., 2013; Ellwood et al., 2013). The balance of subtropical vs. subpolar waters is largely controlled by gyre circulation (Chiswell et al., 2015), which implies productivity for the entire region can be modulated by variations in ocean circulation.

Paleo proxy evidence suggests that regional productivity can respond to variations in ocean circulation on millennial timescales (Bostock et al., 2015; Bostock et al., 2019). However, it is less clear if the same mechanisms operate on shorter timescales (e.g. multi-decadal to centennial). It is possible that multi-decadal variations in primary production are related to basin-wide climate modes (e.g. Interdecadal Pacific Oscillation) through atmospheric teleconnections which change stratification, mixed-layer depth, and sea surface temperature (Karl, 1999; Corno et al., 2007; Rousseaux et al., 2014). These dynamics may act independently of (or in conjunction with) gyre circulation. However, these conclusions are drawn from data that is sparse in space and time (Henson et al., 2010; Beaulieu et al., 2013; Henson et al., 2016). Investigating whether multi-decadal to centennial productivity changes are a function of internal climate variability, gyre variability (which may be anthropogenically forced), or another anthropogenically forced change (warmer sea surface temperatures), is an important area for further study.

Several studies show a decline in primary production since 1899 (~1% per year) which may be related to a change in nutrient cycling driven by an expansion of oligotrophic subtropical gyres, stronger ocean circulation, increased surface stratification, and warmer sea surface temperatures (Polovina et al., 2008; Boyce et al., 2010; Moore et al., 2013). Most of the decline in global production has taken place in the southern hemisphere and typically in the open oceans (Gregg et al., 2003; Boyce et al., 2010). This decline may be related to the expansion of subtropical oligotrophic ocean gyres and increased vertical stratification which limits productivity (Behrenfeld et al., 2006; Polovina et al., 2008; Moore et al., 2013).

The expansion of subtropical oligotrophic gyres could be associated with the strengthening of global gyre circulation (Wu et al., 2012; Roemmich et al., 2016; Yang et al., 2020). This is often stated as a consequence of anthropogenic global warming (Roemmich et al., 2007; Polovina et al., 2008; Wu et al., 2012; Roemmich et al., 2016; Yang et al., 2020). Warming may therefore be simultaneously affecting two critical components of the ocean system: ocean currents and marine productivity (Hoegh-Guldberg et al., 2014). However, productivity observations are sparse in time and space prior to the satellite era which began around the 1980s (Boyce et al., 2010; Henson et al., 2010). The lack of *in situ* data creates considerable uncertainty in determining timescale-dependent relationships between physical and biological oceanography on multi-decadal timescales (Henson et al., 2010; Beaulieu et al., 2013; Henson et al., 2016). This also reduces the certainty in attributing recent physical and biological oceanographic changes to anthropogenic warming (Henson et al., 2010; Beaulieu et al., 2013; Henson et al., 2016).

1.3.2.3 New Zealand Natural Climate Variability

New Zealand's climate is significantly impacted by SAM and ENSO (Mullan, 1995; Kidson et al., 2002; Ummenhofer et al., 2007; Kidston et al., 2009; Ummenhofer et al., 2009). SAM explains ~47% of the natural atmospheric variability south of 20°S (Thompson et al., 2000). During positive SAM conditions the westerlies contract south and intensify, causing anomalously dry conditions for most of New Zealand and warmer sea surface temperatures (Ummenhofer et al., 2007; Kidston et al., 2009); though this is strongly variable depending on other modes of variability that are operating concurrently (Jiang et al., 2013). The shifting wind field also bathes New Zealand in more subtropical waters sourced from the EAC (Figure 1.5; Cai et al., 2005; Cai, 2006). Over recent decades SAM has been trending towards a more positive

phase (Marshall, 2003; Marshall et al., 2004; Fogt et al., 2009) reducing summer precipitation over the South Island of New Zealand and Tasmania by as much as 50% (Ummenhofer et al., 2007; Ummenhofer et al., 2009). The positive SAM trend is thought to also be responsible for the poleward shift and intensification of the EAC over the 20th century (Cai et al., 2005; Cai, 2006). However, the exact mechanism driving this positive SAM shift remains elusive; although, it is likely related to some anthropogenic activity (e.g. ozone depletion or carbon dioxide increase; Cai, 2006; Swart et al., 2012).

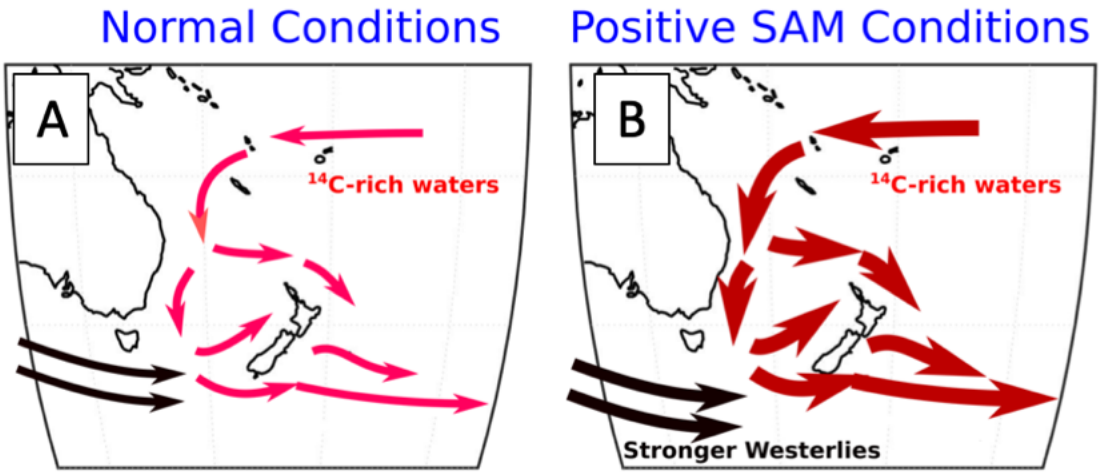

Figure 1.7: A schematic of SAM driven changes in ocean circulation around New Zealand. Panel A: Normal circulation conditions with neutral SAM. Panel B: Enhanced circulation subtropical circulation influences in the NZ region (thicker arrows) driven by a positive SAM state and stronger westerly winds displaced south of normal conditions.

The SAM has potential impacts on the physical and biological oceanography of the southwest Pacific (Hall et al., 2002; Lovenduski et al., 2005; Roemmich et al., 2007; Roemmich et al., 2016). During the positive phase of SAM surface westerlies increase over the circumpolar ocean centered around 60°S and weaken farther north. This promotes Ekman drift from 30-60°S, which intensifies the subtropical current which flow south and increases the poleward heat transport from 30-60°S. (Hall et al., 2002). The increase in subtropical current strength brings warmer waters further south during positive SAM (Hall et al., 2002; Lovenduski et al., 2005; Figure 1.6) and is characterized by higher sea surface height anomalies (Roemmich et al., 2007; Roemmich et al., 2016). Warmer than normal SSTs during positive SAM in the southwest Pacific increase vertical ocean stratification, which reduces nutrient supply and decreases primary productivity (Lovenduski et al., 2005). This has been observed in chlorophyll satellite

data, which shows an inverse correlation between SAM mean state and chlorophyll concentrations around New Zealand (Lovenduski et al., 2005; Figure 1.7).

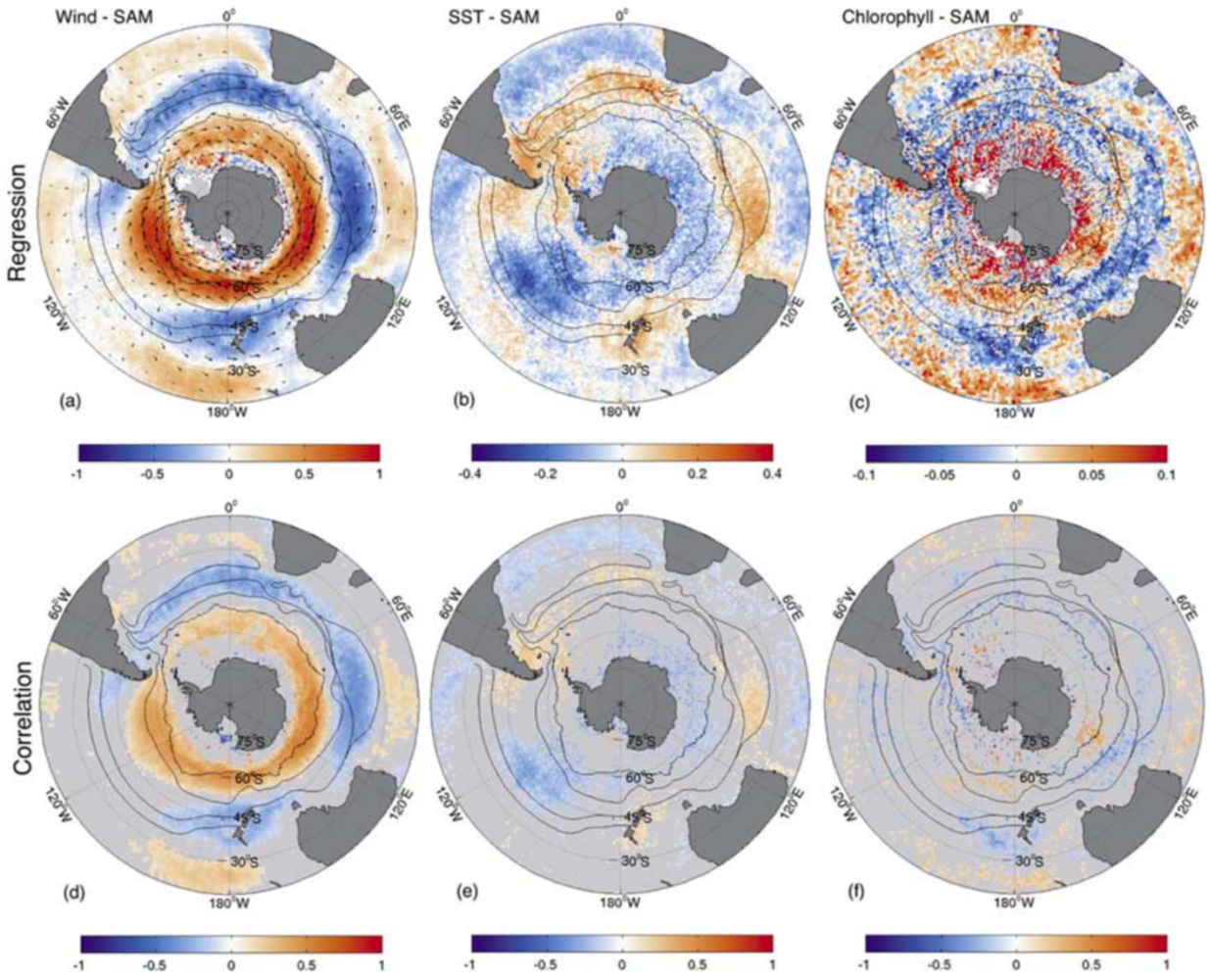

Figure 1.8: Maps of SAM driven changes in sea surface temperature and chl-a concentrations in the Southern Hemisphere. Panels A-C: Regressions between the SAM Index from 1978-2002 and wind speed (A), SST (°C) (B) and chl-a (mg m^{-3}) (C). Panels D-F: Correlations between the SAM Index from 1978-2002 and wind speed (A), SST (°C) (B) and chl-a (mg m^{-3}) (C). Black lines indicate ocean front. From equator to pole the fronts are: Antarctic Polar Front, Subantarctic Front, South Subtropical Front and North Subtropical Front. This figure is derived from Hall and Visbeck, 2002.

ENSO has the second largest impact on New Zealand climate (Ummenhofer et al., 2007; Ummenhofer et al., 2009). ENSO affects the strength and location of the westerlies (Kidson et al., 2002; Ummenhofer et al., 2007), such that during an El Niño event southwesterly wind flow increases across most of the country (Ummenhofer et al., 2007; Ummenhofer et al., 2009). El Niño conditions increase precipitation along the west coast of New Zealand but bring drought conditions to the northern and eastern regions of New Zealand (Ummenhofer et al., 2007; Jiang

et al., 2013). El Niño typically results in cooler temperatures over much of New Zealand due to the influence of increased cool, westerly and southwesterly airflow across most of the country (Ummenhofer et al., 2007; Jiang et al., 2013).

The interplay between SAM and ENSO is complex since they can operate on markedly different timescales; SAM is typically observed as a seasonal to annual variation, while ENSO operates on interannual timescales (with seasonally distinct conditions). When El Niño conditions coincide with negative SAM conditions ENSO teleconnections to the southwest Pacific are typically strengthened (and vice versa when positive SAM coincides with El Niño). These teleconnections include low sea level pressures over New Zealand, weaker circumpolar westerly winds and a southern shift in storm tracks (Fogt et al., 2006; Jones et al., 2009). The spatial structure of each climate mode in the southwest Pacific is retained, such that positive sea level pressure anomalies over New Zealand are produced by positive SAM and negative sea level pressures over Australasia are produced by La Niña (Fogt et al., 2006; Jones et al., 2009). These structures appear to add linearly, and the circulation anomalies reinforce each other. This leads to a more pronounced effect of ENSO teleconnections in the southwest Pacific (Fogt et al., 2006; Jones et al., 2009).

Some paleo-ENSO/SAM work suggests that these two climate modes experience long term periods where they are 'in-phase' (negative SAM coincides with El Niño) or 'out of phase' (negative SAM coincides with La Niña) (Gomez et al., 2012). When the modes are 'in-phase', regional effects of +SAM and -ENSO are amplified and in unison, resulting in westerly wind changes and highly variable precipitation over most of the country (Fogt et al., 2006; Gomez et al., 2012). However, studies using modern instrumental records suggest the degree to which their teleconnections reinforce each other is highly variable and inconsistent across different regions (Ummenhofer et al., 2007; Jiang et al., 2013). This inconsistency may arise from the paucity of observations in time and space in the earlier part of the 20th century. The short length of instrumental records is simply not enough to fully characterize how these climate modes interact, and unfortunately paleo-records that reconstruct ENSO and SAM conditions are too sparse in space and time to evaluate their relationship over the Holocene (Olivia Truax, pers. comm.). Moreover, the situation is obfuscated by anthropogenic climate changes (greenhouse gases and ozone depletion).

1.3.3 Late Holocene Paleoceanography for the Southwest Pacific Region

Late Holocene New Zealand paleoclimate has been studied using tree-rings, glacier moraines, lake sediment cores, and speleothems (Cook et al., 2002; Lorrey et al., 2008; Fowler et al., 2012; Gomez et al., 2012; Lorrey et al., 2012; Lorrey et al., 2014a; Lorrey et al., 2014b; Roop, 2015; Lorrey et al., 2020). These studies reveal highly variable atmospheric circulation and temperature variations on multi-centennial to millennial timescales over the Holocene (Cook et al., 2002; Lorrey et al., 2008; Fowler et al., 2012; Gomez et al., 2012; Lorrey et al., 2012; Lorrey et al., 2014a; Lorrey et al., 2014b; Roop, 2015). These records also uncovered the impact of paleo-ENSO and SAM conditions on late Holocene New Zealand paleoclimate (Fowler et al., 2012; Gomez et al., 2012). However, most Holocene paleoclimate interpretations stem from terrestrial climate proxies with little comparisons to high-resolution paleoceanographic records from the region.

Paleoceanography in the New Zealand region has primarily been studied using sediment cores (P. P. E. Weaver et al., 1998; Neil et al., 2004; Bostock et al., 2015; Bostock et al., 2019). However, these records seldom focus on the late Holocene. Low sedimentation rates and bioturbation limit the capacity of sediment cores to capture decadal to centennial ocean variability in the southwest Pacific (H. Bostock pers. comm.; Bostock et al., 2015; Bostock et al., 2019). The high-resolution Holocene paleoceanography records that do exist almost exclusively represent either the Great Barrier Reef region (McCulloch et al., 1994; Hendy et al., 2002) or the Polynesian Islands (Linsley et al., 2006; Linsley et al., 2008; DeLong et al., 2012). Thus, there is a gap in high-resolution ocean proxy records for the New Zealand region. The only high-resolution paleoceanographic record in close proximity to New Zealand is that of Komugabe-Dixson et al. (2016), which reconstructs paleocean circulation from the south Tasman Sea.

Komugabe-Dixson et al. (2016) produced a 4500 year record of marine radiocarbon reservoir age (ΔR) from the nearby Tasman Sea using black corals (Figure 1.6). ΔR reflects the balance between polar and equatorial waters, making it a useful tool for studying ocean circulation systems like the SPG (Komugabe et al., 2014; see Section 1.3.4.1 and 3.3.2 for more detail). Tropical surface waters move slowly giving them more time to take up ‘young’ atmospheric radiocarbon. In contrast, subpolar waters include a greater proportion of radiocarbon-depleted deep water since they are isolated from the atmosphere.

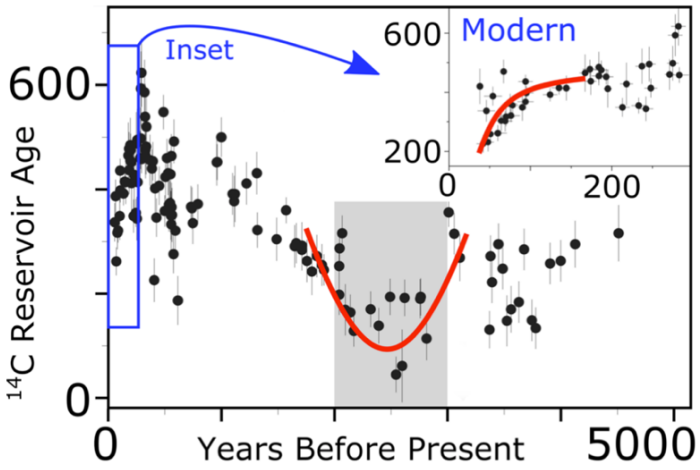

Figure 1.9: South Tasman Sea Reservoir Age Record. A 4500 year record of black coral radiocarbon reservoir ages from the south Tasman sea (Komugabe et al., 2014; Komugabe-Dixson et al., 2016). Red lines indicate the depression in reservoir age related to a strengthening of the South Pacific Gyre. Figure provided by Dan Sinclair.

The Tasman Sea ΔR record of Komugabe-Dixson et al. (2016) shows a large depression reservoir age extending from 2000-3000BP. This depression could represent a wind-driven strengthening of the entire SPG system. However, it is also possible that this just represents a strengthening of the (local) EAC extension Recent observations show that there may be an anti-phasing between the EAC extension and the Tasman Front with no net SPG change (Hill et al., 2011). The possibility of an intensified SPG between 2000-3000BP therefore remains unresolved.

1.3.4 Deep-Sea Black Coral Paleoceanographic Proxy

Black corals are one of the most promising new paleoceanographic archives of the last decade (Robinson et al., 2014; Williams, 2020). They are deep-ocean dwelling Antipatharians (phylum: Cnidaria, class: Anthozoa, subclass: Hexacorallia, order: Antipatharia); living on hard substrata over a wide depth range (0-8000m; Cairns et al., 2005). They grow semi-rigid organic skeletons made of protein and chitin bands formed around a central axis. This allows them to stand upright as solitary structures with bushy, sentinel-like forms (Figure 1.7; Goldberg, 1991; Goldberg et al., 1994; Brugler et al., 2013; Opresko et al., 2014). Black corals are thought to be one of the longest-lived skeletal-accreting marine organisms (Roark et al., 2006; Prouty et al., 2011; Carreiro-Silva et al., 2013; Prouty et al., 2015). Some species of black corals live for several millennia with extremely slow and consistent growth (~5um/yr; Komugabe-Dixson et al., 2016; Hitt et al., 2020).

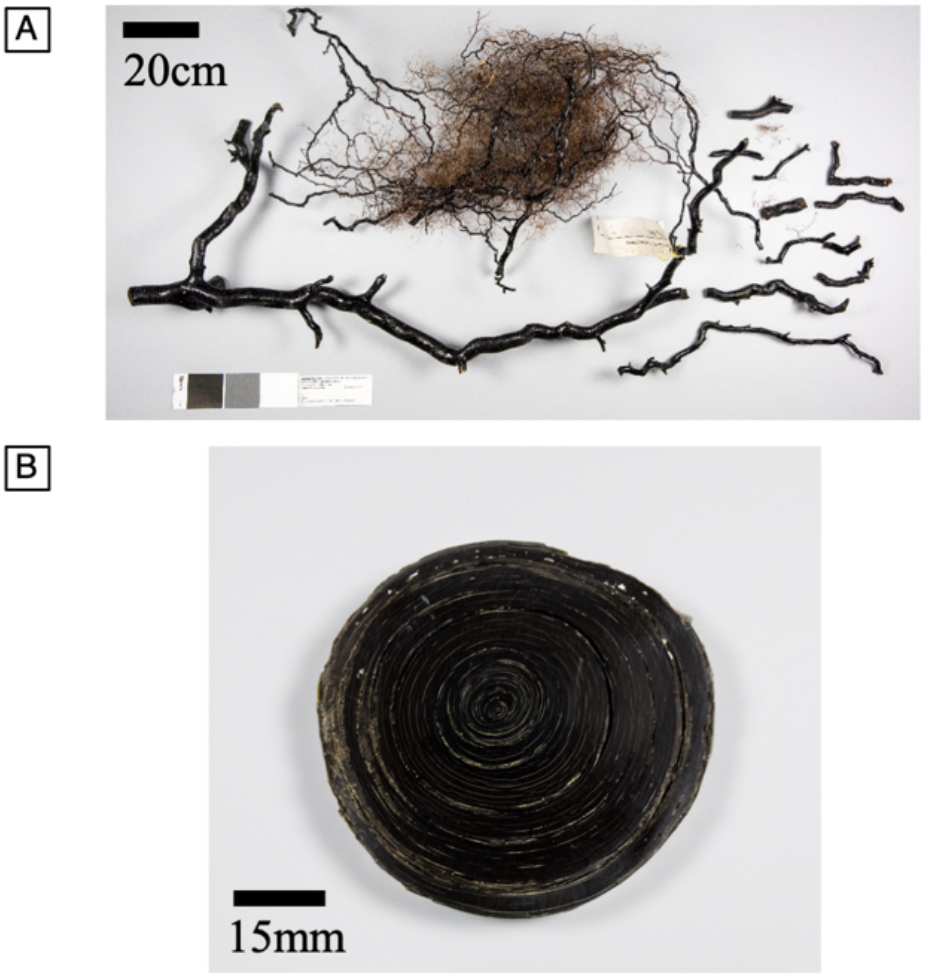

Figure 1.10: A New Zealand Black Coral Colony. Panel A: A photograph of a black coral colony collected from New Zealand. Panel B: A cross section of a black coral base. Note the concentric ring skeleton.

Black corals are 'living sediment traps'; they are opportunistic filter-feeders that build their skeletons from the surface exported particulate organic matter (POM) that they ingest (Goldberg, 1974; Williams et al., 2006; Strzepek et al., 2014). Isotopic analysis of their skeletons shows that the POM they feed on is recently exported from the surface (Williams, 2020). Black corals therefore record surface ocean processes in their skeletons (Sherwood et al., 2009; Komugabe et al., 2014; Prouty et al., 2015; Komugabe-Dixson et al., 2016). Specifically, they retain the radiocarbon, stable carbon ($\delta^{13}C$) and stable nitrogen ($\delta^{15}N$) signatures of phytoplankton (Sherwood et al., 2009; Prouty et al., 2011; Prouty et al., 2014; Robinson et al., 2014; Prouty et al., 2015; Komugabe-Dixson et al., 2016), allowing reconstruction of the ^{14}C, primary production, plankton community structure, and biogeochemistry of the ocean's surface.

Moreover, individual coral growth bands can be precisely dated by radiocarbon and uranium-thorium disequilibrium (Komugabe et al., 2014; Komugabe-Dixson et al., 2016).

The longevity of black corals makes them particularly attractive as paleoceanographic archives. Conventional paleoceanographic work relies on either tropical corals which grow quickly for a few centuries at most, or sediments that accumulate slowly over many millennia. Black coral records can bridge this gap, providing decadal resolution records that span millennia with a higher fidelity than sediments cores since they do not experience bioturbation (Komugabe et al., 2014; Komugabe-Dixson et al., 2016).

1.3.4.1 Radiocarbon

Radiocarbon (^{14}C) is a powerful tool for studying water mass movement (Bard, 1988; Matsumoto, 2007). ^{14}C is produced through cosmic ray bombardment of nitrogen in the upper stratosphere. The ^{14}C produced forms $^{14}CO_2$ which rapidly homogenizes through the atmosphere. ^{14}C decays with a half-life of 5370 years, and the concentration in the atmosphere represents a steady state between formation by bombardment and loss by radioactive decay (Libby, 1946; Anderson et al., 1947). Atmospheric $^{14}CO_2$ enters the biogeochemical cycle through both physical and biological pathways (e.g. primary production or ocean absorption). In the ocean, it dissolves into the surface via air-sea exchange. Once isolated from the atmosphere, ^{14}C concentrations are no longer supported by cosmic ray production and begin to decrease. This is the basis of radiocarbon dating marine material (Anderson et al., 1947).

Deep ocean waters can be isolated from the atmosphere for up to 1500 years, and therefore have a very low ^{14}C content (Bard, 1988; Matsumoto, 2007). Mixing of deep ocean waters into the surface ocean results in a ^{14}C age difference between the sea surface and the atmosphere (Heaton et al., 2020). This age difference, known as the 'Marine Radiocarbon Reservoir Age', varies spatially depending on mixing, upwelling and downwelling dynamics specific to a given region (Stuiver et al., 1983; Bard, 1988; Matsumoto, 2007).

The surface marine radiocarbon reservoir age is a function of how much time surface waters spend in contact with the atmosphere (Key et al., 2004). The longer water spends at the ocean surface, the more $^{14}CO_2$ it can absorb, reducing the reservoir age towards zero. Typically, tropical water masses and those at the center of ocean gyres are very slow moving and are well-ventilated to the atmosphere. This results in high radiocarbon values and corresponding low

reservoir ages (Figure 1.4A; Bard, 1988; Key et al., 2004). Conversely, polar waters have a greater input of upwelled water and spend less time with the surface, which results in higher reservoir ages (Figure 1.4A; Bard, 1988; Key et al., 2004). Measuring surface radiocarbon at a single location through time is therefore an effective way of tracking the changing relative input from contrasting water masses, hence ocean circulation (Komugabe et al., 2014; Komugabe-Dixson et al., 2016).

In the southwest Pacific, the reservoir age reflects the relative influence of tropical and polar waters (Figure 1.4A; Key et al., 2004; Petchey et al., 2008a; Petchey et al., 2008b; Komugabe et al., 2014; Komugabe-Dixson et al., 2016). Areas with increased tropical/subtropical currents (e.g. the EAuC) show persistently high radiocarbon concentrations (low ages) due to the heightened absorption of atmospheric CO_2 (Figure 1.4A; Key et al., 2004). Conversely, the STF and ACC south of New Zealand have persistently low radiocarbon values (old ages) due to the high proportion of subpolar waters (Figure 1.4A; Key et al., 2004).

Studying circulation changes in the past requires the reconstruction of radiocarbon *time series* at a single location. This has been done previously using black corals (Komugabe et al., 2014; Komugabe-Dixson et al., 2016). Their organic skeleton inherits the radiocarbon signature of the organic carbon from the surface layer (e.g. phytoplankton). Measuring radiocarbon in consecutive skeletal growth rings allows a history of surface ocean radiocarbon to be reconstructed (Komugabe et al., 2014; Komugabe-Dixson et al., 2016).

Measuring marine radiocarbon at a single location is typically done by calculating a local marine radiocarbon reservoir age correction, commonly known as ΔR. ΔR is the difference between the measured ^{14}C age of the surface ocean and that predicted from the global marine radiocarbon curve 'Marine20' (Komugabe-Dixson et al., 2016; Heaton et al., 2020). Marine20 is a radiocarbon calibration curve representing a time-series of whole-ocean averaged radiocarbon age for the last 55,000 years. It is constructed from a network of tropical and subtropical radiocarbon records that are have been independently dated using various techniques (e.g. U-Th dating; Heaton et al., 2020). The difference between the Marine20 age predicted by an independent dating method and the actual measured ^{14}C age of a sample (ΔR) indicates where local processes (e.g. circulation, upwelling) shift the water's age away from that of the average ocean (Petchey et al., 2008a; Petchey et al., 2008b; Reimer et al., 2013; Komugabe-Dixson et al., 2016; Heaton et al., 2020)

The dominant processes contributing to ΔR variability are ocean circulation and upwelling (Heaton et al., 2020). However, ΔR may also reflect stratification processes that influence the amount of radiocarbon absorbed into the surface layer of the ocean (Petchey et al., 2008a; Petchey et al., 2008b). Low ΔR values reflect increased ventilation, most often from higher input of tropical water; however, increased surface stratification can also increase $^{14}CO_2$ absorption into the surface (Petchey et al., 2008a; Petchey et al., 2008b). High ΔR values reflect decreased contact between the surface waters and atmosphere that is typical of increased polar water influence. Reduced stratification can also cause a reduction in air-sea surface contact by reducing the depth of the surface mixed layer. New Zealand ΔR is thought to mainly respond to changes in SPG circulation (Petchey et al., 2008a; Petchey et al., 2008b; Komugabe et al., 2014); however open ocean ΔR and radiocarbon datasets around New Zealand are scarce (Key et al., 2004) and so more spatially complete datasets are needed to validate this claim.

1.3.4.2 Stable Isotopes

Stable isotopes are a cornerstone of paleoclimate reconstructions (Hoefs, 2009). Isotopes are atoms of the same element with different numbers of neutrons and therefore different masses. This mass difference causes each isotope to behave slightly differently during phase changes. Often, one isotope will become enriched in one phase and depleted in another (e.g. the incorporation of inorganic carbon into organic material during photosynthesis; Mariotti et al., 1981; Goericke et al., 1994; Somes et al., 2010; Kendall et al., 2012; Magozzi et al., 2017). This is coined 'isotopic fractionation'.

Variations in stable isotope compositions are often described in ratios relative to a geochemical standard R_{std} (Hoefs, 2009). Since discrimination between isotopes is often very small, isotope ratios typically vary in the 3rd decimal place. For convenience, the convention is to use the delta notation (e.g. $\delta^{13}C$ and $\delta^{15}N$) which expresses the deviation in the 3rd decimal place of an isotope ratio relative to a standard (Eqs. 1 & 2).

$$\text{Eq 1: } \delta^{13}\text{C} = \left[\frac{\frac{^{13}C}{^{12}C}}{R_{std}} - 1 \right] x1000$$

$$\text{Eq. 2: } \delta^{15}\text{N} = \left[\frac{\frac{^{15}N}{^{14}N}}{R_{std}} - 1 \right] x1000$$

Isotopic fractionation in the oceans can occur during multiple physical and/or biological processes (e.g. sea surface temperature changes or photosynthesis), and are used by scientists to reconstruct these processes in the past (Cobb et al., 2013; McMahon et al., 2013; Prouty et al., 2014; Glynn et al., 2019; Grothe et al., 2019; Sayani et al., 2019).

1.3.4.2.1 Carbon Isotopes

Stable carbon isotopes ($\delta^{13}C$) in marine dissolved inorganic carbon (DIC) are primarily controlled by temperature and the degree of transfer between the atmospheric CO_2 and surface water. Areas of higher temperature and increased air-sea exchange (e.g. the tropics) result in higher $\delta^{13}C$ values (Figure 1.8A; Wong et al., 1978; Rau et al., 1989a; Goericke et al., 1994; Magozzi et al., 2017). Conversely at high latitudes, colder temperatures and reduced air-sea gas exchange results in lower $\delta^{13}C$ values (Figure 1.8A). This results in a strong spatial gradient in $\delta^{13}C$ between the tropics and the higher latitudes (Figure 1.8A; Wong et al., 1978; Rau et al., 1989a; Goericke et al., 1994; Magozzi et al., 2017).

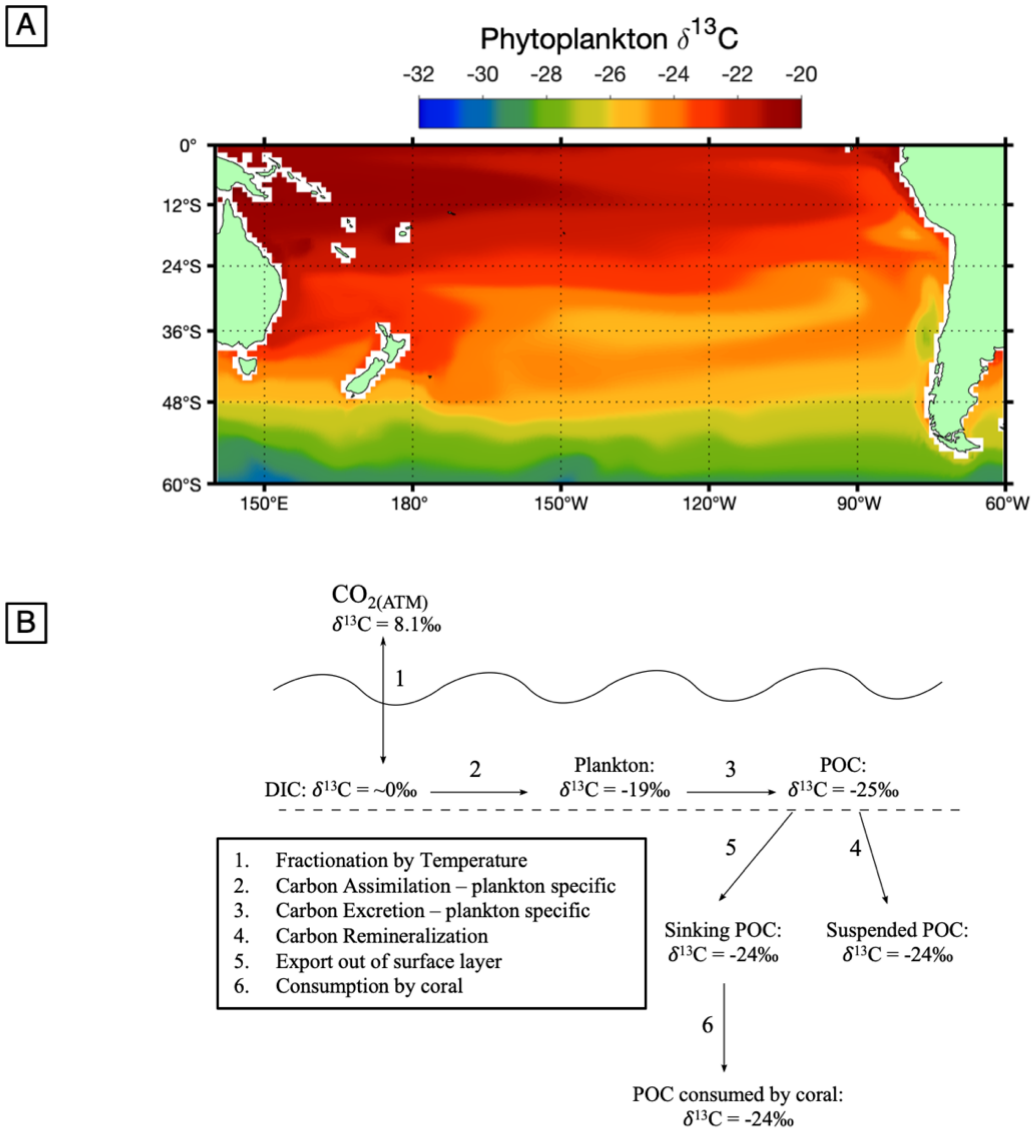

Figure 1.11: $\delta^{13}C$ in the ocean. Panel A: Spatial pattern of modelled phytoplankton $\delta^{13}C$ in the South Pacific Gyre (Magozzi et al., 2017). Panel B: $\delta^{13}C$ values from Rau et al. (1989a); Rau et al. (1989b); Nakatsuka et al. (1992); Rau et al. (1992); Keeling et al. (1995); Rau et al. (1996); Gruber et al. (1998); Druffel et al. (2003).

Marine $\delta^{13}C$ is also strongly fractionated by photosynthesis (Figure 1.8B), where ^{13}C is strongly excluded from the organic material leaving the remaining DIC enriched in ^{13}C (DeNiro et al., 1978; Wong et al., 1978; Magozzi et al., 2017). Marine organic matter therefore has a low $\delta^{13}C$. When organic matter that has sunk below the surface ocean, it is broken down by bacterial respiration and releases ^{12}C back into the DIC (Hilting et al., 2008). This process creates a vertical gradient in DIC; high at the surface and low at depth (Hilting et al., 2008).

Biological process can amplify or mute the regional $\delta^{13}C$ variations (Wong et al., 1978; Rau et al., 1992; Magozzi et al., 2017). Physiological mechanisms like cell geometry, membrane permeability, growth rate, temperature of growth and light availability all influence isotopic fractionation (Rau et al., 1989a; Nakatsuka et al., 1992; Rau et al., 1992; Popp et al., 1998). $\delta^{13}C$ can also track spatial or temporal variations in phytoplankton community structure and is an effective tool to study marine ecology (Rau et al., 1989a; Popp et al., 1998; McMahon et al., 2013; McMahon et al., 2015; McMahon et al., 2016; Glynn et al., 2019).

1.3.4.2.2 Nitrogen Isotopes

Bioavailable, or 'fixed' forms of inorganic nitrogen (e.g. NO_3^-, NO_2^-, NH_4^+) are considered by many to be the primary macronutrient limiting new production and cell growth in the ocean (Altabet, 2006; Sarmiento et al., 2006; Gruber, 2008). Bioavailable nitrogen is critical for cell growth as it is used in the construction of amino acids, proteins and DNA (Altabet, 2006; Sarmiento et al., 2006; Gruber, 2008). Nitrogen gas is a major component of our atmosphere; however, nitrogen must be in a bioavailable form to support cell growth. The triple bond in N_2 gas is difficult to break and therefore most organisms cannot utilize it for the production of organic material. Only a few organisms have the metabolic capability to 'fix nitrogen' (Postgate, 1982). This specialized process converts N_2 to NH_4^+ and is predominantly carried out by diazotroph phytoplankton (Postgate, 1982; Altabet, 2006; Sarmiento et al., 2006; Gruber, 2008). NH_4^+ then becomes oxidized to the other forms bioavailable forms (NO_3^- and NO_2^-) (Gruber, 2008).

Nitrate is the most common bioavailable nitrogen form and is the most thermodynamically favorable species for photosynthesis. Therefore, nitrate is a very important limiting nutrient for marine productivity (Altabet, 2006; Sarmiento et al., 2006; Gruber, 2008). The relative abundances of the different nitrogen species are driven by nitrogen cycle processes (Figure 1.9). These include nitrogen assimilation, nitrogen fixation, excretion, denitrification, water column nitrogen loss and benthic nitrogen loss (Figure 1.9; Altabet, 2006; Sarmiento et al., 2006; Gruber, 2008).

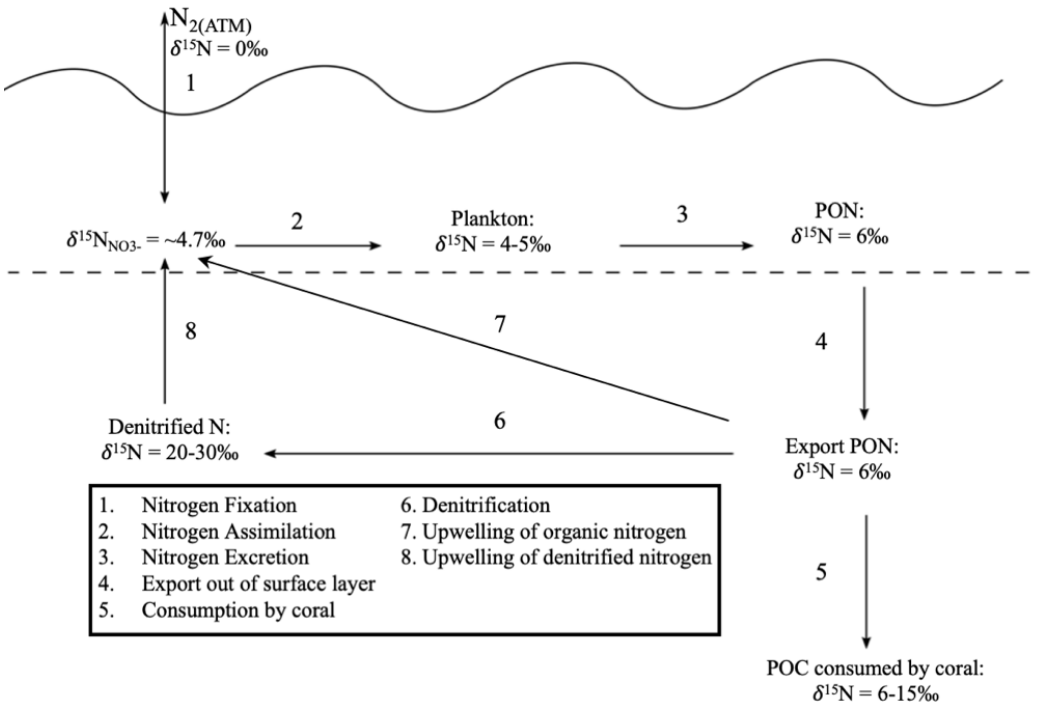

Figure 1.12: Carton of nitrogen isotope variability in the ocean. $\delta^{15}N$ values from Altabet (2006); Sarmiento et al. (2006); Somes et al. (2010).

Nitrogen cycle processes are highly sensitive to regional oceanography and large-scale climate processes (Sarmiento et al., 2006; Gruber, 2008; Somes et al., 2010). Regionally, oceanographic and climate processes set the initial distributions of the bioavailable nitrogen pool through processes such as upwelling, nitrogen fixation or advection of oligotrophic waters (Somes et al., 2010). Large climate changes, such as glacial-interglacial periods, have resulted in major changes to the nitrogen cycle and global nitrogen inventory (Galbraith et al., 2013; Schmittner et al., 2016; Somes et al., 2017). Conversely, major changes in the nitrogen cycle or nitrogen inventory control the efficiency of global primary production, and therefore the atmospheric CO_2 concentrations (Sigman et al., 2000; Gruber, 2004; Sarmiento et al., 2006). This makes the nitrogen cycle an important part of the global climate system, as it connects biology with the ocean and atmosphere. The spatial distribution of nitrogen is therefore a result of local and global processes which also control the nitrogen isotopic ratio throughout marine environments (Altabet, 2006).

Stable (i.e. not-radioactive) nitrogen isotopes in organic matter are a useful tool for studying the nitrogen cycle and its connection to the global climate system (Figure 1.9; Altabet, 2006; Somes et al., 2017). There are two stable nitrogen isotopes: ^{14}N and ^{15}N. The lighter

isotope is preferentially incorporated into the organic product during most biological processes (Figure 1.9; Nakatsuka et al., 1992; Altabet, 2006; Somes et al., 2010; Somes et al., 2013).

The nitrogen isotope composition of marine organic matter derived from photosynthesis is a function of the isotope composition of the nitrogen source available to the phytoplankton and the proportion of that nitrogen that is converted into organic material. According to the principles of Rayleigh Fractionation, organic material is most fractionated (i.e. has the lowest $\delta^{15}N$) when only a small proportion of the nitrogen is converted into organics. If all bioavailable nitrogen is converted to organic material, then mass balance dictates that the $\delta^{15}N$ of the organic material must match the $\delta^{15}N$ of the nitrate source. Therefore, increasing % utilization of bioavailable nitrogen results in organic material with a higher $\delta^{15}N$.

The variability of $\delta^{15}N$ in the surface ocean is complex due to the variety of processes in the nitrogen cycle. Different rates of nitrogen assimilation, nitrogen fixation, excretion, water column nitrogen loss, benthic nitrogen loss, trophic level fractionation, and phytoplankton specific assimilation efficiencies all alter the spatial and temporal variations in marine $\delta^{15}N$. Assimilation and production in water column increase $\delta^{15}N$ of bioavailable nitrogen in the ocean, while nitrogen fixation, excretion and remineralization add low $\delta^{15}N$ to the ocean (Figure 1.9; Altabet, 2006; Sarmiento et al., 2006; Somes et al., 2010). Many of these processes vary spatially across the ocean surface (Sarmiento et al., 2004; Sarmiento et al., 2006).

1.3.4.3 Coupling between $\delta^{15}N$ and $\delta^{13}C$

In ocean regions where macronutrients are not bio-limiting (such as the nutrient-rich, iron-deficient subpolar waters of the STF), $\delta^{15}N$ and $\delta^{13}C$ are coupled by Rayleigh Fractionation. As noted in Section 1.3.4.2, the $\delta^{15}N$ of organic material is lowest when only a small fraction of the bioavailable nitrogen is utilized. The same process causes $\delta^{13}C$ to be lightest. As the proportion of bioavailable N and C utilized increases, both $\delta^{15}N$ and $\delta^{13}C$ get higher (Burkhardt et al., 1999; DiFiore et al., 2006). This creates a latitudinal $\delta^{13}C$ and $\delta^{15}N$ isotopic gradient in the southwest Pacific, where total available carbon and nitrogen are correlated: sub-polar waters are enriched in ^{13}C and ^{15}N and subtropical waters are depleted in ^{13}C and ^{15}N (DiFiore et al., 2006; DiFiore et al., 2010).

While $\delta^{13}C$ and $\delta^{15}N$ have been widely used in studying marine ecology and geochemistry (Boecklen et al., 2011), there are a number of challenges to interpreting their variations. $\delta^{13}C$ and $\delta^{15}N$ represent an integrated signal of several competing isotopic fractionation processes at the base of the food web. These factors include i) the mix of species making up the phytoplankton community; ii) the isotopic composition of bioavailable carbon and nitrogen iii) the efficiency with which those inorganic nutrients are utilized iv) isotopic enrichments during trophic level transfers and v) bacterial degradation and nutrient recycling in the water column (Larsen et al., 2013; McMahon et al., 2013; McMahon et al., 2016). These complications contribute uncertainty to $\delta^{13}C$ and $\delta^{15}N$ data interpretations. Therefore, some constraints are needed to control for taxonomic changes at the base of the food web, location specific changes in source $\delta^{13}C$ and $\delta^{15}N$, and an assumed utilization efficacy.

In situ $\delta^{13}C$ and $\delta^{15}N$ measurements are extremely useful in studying present day marine nutrient dynamics but tell us nothing about changes in the past. $\delta^{15}N$ and $\delta^{13}C$ in marine sediment cores are often used for paleo-productivity (Rafter et al., 2012; Bostock et al., 2019). However, these cores typically cover glacial-interglacial cycles and are not usually suitable for study anthropogenically relevant variations in paleo-productivity. As with radiocarbon, $\delta^{13}C$ and $\delta^{15}N$ in proteinaceous deep-sea corals offers the potential as high-resolution productivity proxies (Prouty et al., 2014; McMahon et al., 2015; Glynn et al., 2019). These corals inherit the $\delta^{13}C$ and $\delta^{15}N$ signatures of their food source, and therefore serve as high resolution archives of surface ocean biochemistry (Williams et al., 2010b, 2010a; Prouty et al., 2014; Glynn et al., 2019). Specifically, $\delta^{13}C$ and $\delta^{15}N$ measurements in black corals have been previously used to reconstruct surface ocean conditions such as thermocline and nutricline depth, and nitrogen biogeochemistry (Williams et al., 2006, 2007; Williams et al., 2010b, 2010a; Prouty et al., 2014; Williams, 2020).

1.4 Broader Impacts

This dissertation presents the first ever decadal to centennial resolution reconstructions of New Zealand's physical and biological oceanography over the late Holocene. Much of New Zealand's high-resolution paleoclimate work is derived from terrestrial proxies. Here I provide an ocean counterpart to complete the picture of New Zealand's climate change over the last 3000

years. These results reveal a cycle in ocean circulation strength that is related to natural atmospheric variability on multi-centennial timescales. These records also provide a baseline for natural variability in physical and biological oceanography that may assist in separating natural from anthropogenic signals over the last century. Moreover, these results may assist with refining climate and ocean models which forecast future changes to southwest Pacific oceanography.

Understanding natural nutrient and productivity dynamics are critical to managing marine resources and projecting future CO_2 sequestration. Considerable international attention has therefore been focused on improving our understanding of marine biogeochemistry and physical oceanography. Several major programs are now underway which study the interplay between nutrients, productivity and physical ocean dynamics, including GEOTRACES, SOLAS and SPICE. However, these programs are all limited to the narrow window of time that instrumental records cover. These programs cannot provide information on ocean dynamics beyond the last century. Several efforts are focused on collating paleo records to provide a longer perspective against which recent ocean changes can be considered (PAGES, Oceans2K). However, high resolution records are sparse, especially in the mid latitude region of the South Pacific. This research will directly compliment existing initiatives by providing a high-resolution study of ocean circulation and productivity dynamics over the last several millennia using the combination of several powerful geochemical proxies from a new paleocean archive.

Comparing ΔR, $\delta^{13}C$ and $\delta^{15}N$ records with isotope-enabled model outputs can assist in separating local and hemispheric climate forcing and identify non-linear climate responses. Isotope-enabled global circulation models historically included only water isotopes ($\delta^{18}O$). However, new models have now been released that are equipped with radiocarbon, $\delta^{13}C$ and $\delta^{15}N$ modules (e.g. UVic Earth System Climate Model; A. J. Weaver et al., 2001; Somes et al., 2010; Somes et al., 2017). These can potentially be used to investigate climate and ocean hypotheses derived from geochemical proxy data.

Beyond just a climate perspective, the records in this thesis will be a useful tool for archaeology. The radiocarbon reservoir age record presented in this dissertation will be a particularly useful tool for marine archaeologists. The resolution of the radiocarbon record is high enough to assist in constraining radiocarbon dating curves and increase dating accuracy

over the last 3000 years. This is helpful for any studies focused on precisely dating human/ecological migrations or evolution. Conversely, the $\delta^{13}C$ and $\delta^{15}N$ records could be used to infer shifts in productivity, which may elucidate changes in the base of the food chain in the southwest Pacific. Together, the records here may help better constrain the absolute dates of species migrations and how they relate to ecological activity.

1.5 References

Abram, N. J., Mulvaney, R., Vimeux, F., Phipps, S. J., Turner, J., & England, M. H. (2014). Evolution of the Southern Annular Mode during the past millennium. *Nature Climate Change, 4*(7), 564-569. https://doi.org/10.1038/nclimate2235

Altabet, M. A. (2006). Isotopic Tracers of the Marine Nitrogen Cycle: Present and Past. In J. K. Volkman (Ed.), *Marine Organic Matter: Biomarkers, Isotopes and DNA* (pp. 251-293). Berlin, Heidelberg: Springer Berlin Heidelberg.

Ancapichún, S., & Garcés-Vargas, J. (2015). Variability of the Southeast Pacific Subtropical Anticyclone and its impact on sea surface temperature off north-central Chile. *Ciencias Marinas, 41*, 1-20.

Anderson, E., Libby, W., Weinhouse, S., Reid, A., Kirshenbaum, A., & Grosse, A. (1947). Natural radiocarbon from cosmic radiation. *Physical Review, 72*(10), 931.

Bard, E. (1988). Correction of accelerator mass spectrometry 14C ages measured in planktonic foraminifera: Paleoceanographic implications. *Paleoceanography, 3*(6), 635-645. http://dx.doi.org/10.1029/PA003i006p00635

Beaulieu, C., Henson, S. A., Sarmiento, J. L., Dunne, J. P., Doney, S. C., Rykaczewski, R., & Bopp, L. (2013). Factors challenging our ability to detect long-term trends in ocean chlorophyll. *Biogeosciences, 10*(4), 2711-2724.

Behrenfeld, M. J., O'Malley, R. T., Siegel, D. A., McClain, C. R., Sarmiento, J. L., Feldman, G. C., et al. (2006). Climate-driven trends in contemporary ocean productivity. *Nature, 444*(7120), 752-755. https://doi.org/10.1038/nature05317

Bjerknes, J. (1969). Atmospheric teleconnections from the equatorial Pacific. *Mon. Wea. Rev, 97*(3), 163-172.

Boecklen, W. J., Yarnes, C. T., Cook, B. A., & James, A. C. (2011). On the Use of Stable Isotopes in Trophic Ecology. *Annual Review of Ecology, Evolution, and Systematics, 42*(1), 411-440. https://doi.org/10.1146/annurev-ecolsys-102209-144726

Bostock, H. C., Hayward, B. W., Neil, H. L., Sabaa, A. T., & Scott, G. H. (2015). Changes in the position of the Subtropical Front south of New Zealand since the last glacial period. *Paleoceanography, 30*(7), 824-844. http://dx.doi.org/10.1002/2014PA002652

Bostock, H. C., Prebble, J. G., Cortese, G., Hayward, B., Calvo, E., Quirós-Collazos, L., et al. (2019). Paleoproductivity in the SW Pacific Ocean During the Early Holocene Climatic Optimum. *Paleoceanography and Paleoclimatology, 34*(4), 580-599. https://doi.org/10.1029/2019PA003574

Bowen, M., Wilkin, J. L., & Emery, W. J. (2005). Variability and forcing of the East Australian Current. *Journal of Geophysical Research: Oceans, 110*(C3), n/a-n/a. http://dx.doi.org/10.1029/2004JC002533

Boyce, D. G., Lewis, M. R., & Worm, B. (2010). Global phytoplankton decline over the past century. *Nature, 466*, 591. Article. https://doi.org/10.1038/nature09268

Boyd, P. W., Watson, A. J., Law, C. S., Abraham, E. R., Trull, T., Murdoch, R., et al. (2000). A mesoscale phytoplankton bloom in the polar Southern Ocean stimulated by iron fertilization. *Nature, 407*(6805), 695-702. https://doi.org/10.1038/35037500

Bradford, J. M., Heath, R. A., Chang, F. H., & Hay, C. H. (1982). The effect of warm-core eddies on oceanic productivity off northeastern New Zealand. *Deep Sea Research Part A. Oceanographic Research Papers, 29*(12), 1501-1516. http://www.sciencedirect.com/science/article/pii/0198014982900395

Bradford, J. M., & Roberts, P. E. (1978). Distribution of reactive phosphorus and plankton in relation to upwelling and surface circulation around New Zealand. *New Zealand Journal of Marine and Freshwater Research, 12*(1), 1-15. https://doi.org/10.1080/00288330.1978.9515717

Bradford-Grieve, J., Boyd, P. W., Chang, F. H., Chiswell, S. M., Hadfield, M., Hall, J., et al. (1999). Pelagic ecosystem structure and functioning in the subtropical front region east of New Zealand in austral winter and spring 1993. *Journal of Plankton Research, 21*(3), 405-428. https://doi.org/10.1093/plankt/21.3.405

Bradford-Grieve, J. M., Chang, F. H., Gall, M., Pickmere, S., & Richards, F. (1997). Size-fractionated phytoplankton standing stocks and primary production during austral winter and spring 1993 in the Subtropical Convergence region near New Zealand. *New Zealand Journal of Marine and Freshwater Research, 31*(2), 201-224. http://dx.doi.org/10.1080/00288330.1997.9516759

Brown, J. R., Lengaigne, M., Lintner, B. R., Widlansky, M. J., van der Wiel, K., Dutheil, C., et al. (2020). South Pacific Convergence Zone dynamics, variability and impacts in a changing climate. *Nature Reviews Earth & Environment, 1*(10), 530-543. https://doi.org/10.1038/s43017-020-0078-2

Brugler, M. R., Opresko, D. M., & France, S. C. (2013). The evolutionary history of the order Antipatharia (Cnidaria: Anthozoa: Hexacorallia) as inferred from mitochondrial and nuclear DNA: implications for black coral taxonomy and systematics. *Zoological Journal of the Linnean Society, 169*(2), 312-361. https://doi.org/10.1111/zoj.12060

Burkhardt, S., Riebesell, U., & Zondervan, I. (1999). Effects of growth rate, CO2 concentration, and cell size on the stable carbon isotope fractionation in marine phytoplankton. *Geochimica et Cosmochimica Acta, 63*(22), 3729-3741. http://www.sciencedirect.com/science/article/pii/S0016703799002173

Cai, W. (2006). Antarctic ozone depletion causes an intensification of the Southern Ocean super-gyre circulation. *Geophysical Research Letters, 33*(3), n/a-n/a. http://dx.doi.org/10.1029/2005GL024911

Cai, W., Shi, G., Cowan, T., Bi, D., & Ribbe, J. (2005). The response of the Southern Annular Mode, the East Australian Current, and the southern mid-latitude ocean circulation to global warming. *Geophysical Research Letters, 32*(23), n/a-n/a. http://dx.doi.org/10.1029/2005GL024701

Cairns, S. D., & Bayer, F. M. (2005). A review of the genus Primnoa (Octocorallia: Gorgonacea: Primnoidae), with the description of two new species. *Bulletin of Marine Science, 77*(2),

225-256. Review. https://www.scopus.com/inward/record.uri?eid=2-s2.0-24944554789&partnerID=40&md5=c93536a433f9a8b2fc5f22714c8dd5f9

Cane, M. A., Zebiak, S. E., & Dolan, S. C. (1986). Experimental forecasts of EL Nino. *Nature, 321*(6073), 827-832.

Carreiro-Silva, M., H Andrews, A., Braga Henriques, A., de Matos, V., Porteiro, F., & Santos, R. (2013). *Variability in growth rates of long-lived black coral Leiopathes sp. from the Azores (Northeast Atlantic)* (Vol. 473).

Cherchi, A., Ambrizzi, T., Behera, S., Freitas, A. C. V., Morioka, Y., & Zhou, T. (2018). The Response of Subtropical Highs to Climate Change. *Current Climate Change Reports, 4*(4), 371-382. https://doi.org/10.1007/s40641-018-0114-1

Chiswell, S. M., Bostock, H. C., Sutton, P. J. H., & Williams, M. J. M. (2015). Physical oceanography of the deep seas around New Zealand: a review. *New Zealand Journal of Marine and Freshwater Research, 49*(2), 286-317. https://doi.org/10.1080/00288330.2014.992918

Chiswell, S. M., Bradford-Grieve, J., Hadfield, M. G., & Kennan, S. C. (2013). Climatology of surface chlorophyll a, autumn-winter and spring blooms in the southwest Pacific Ocean. *Journal of Geophysical Research: Oceans, 118*(2), 1003-1018. https://doi.org/10.1002/jgrc.20088

Cobb, K., Westphal, N., Sayani, H., Watson, J., Di Lorenzo, E., Cheng, H., et al. (2013). Highly Variable El Nino-Southern Oscillation Throughout the Holocene. *Science, 339*, 67-70.

Cook, E. R., Palmer, J. G., & D'Arrigo, R. D. (2002). Evidence for a 'Medieval Warm Period' in a 1,100 year tree-ring reconstruction of past austral summer temperatures in New Zealand. *Geophysical Research Letters, 29*(14), 12-11-12-14. https://doi.org/10.1029/2001GL014580

Corno, G., Karl, D. M., Church, M. J., Letelier, R. M., Lukas, R., Bidigare, R. R., & Abbott, M. R. (2007). Impact of climate forcing on ecosystem processes in the North Pacific Subtropical Gyre. *Journal of Geophysical Research: Oceans, 112*(C4).

Cresswell, G. R. (2000). Currents of the continental shelf and upper slope of Tasmania. *Papers and proceedings of the Royal Society of Tasmania, 133*(3), 21-30.

Currie, K. I., & Hunter, K. A. (1998). Surface water carbon dioxide in the waters associated with the subtropical convergence, east of New Zealand. *Deep Sea Research Part I: Oceanographic Research Papers, 45*(10), 1765-1777. http://www.sciencedirect.com/science/article/pii/S0967063798000417

Currie, K. I., Reid, M. R., & Hunter, K. A. (2011). Interannual variability of carbon dioxide drawdown by subantarctic surface water near New Zealand. *Biogeochemistry, 104*(1), 23-34. https://doi.org/10.1007/s10533-009-9355-3

De Boer, A. M., Graham, R. M., Thomas, M. D., & Kohfeld, K. E. (2013). The control of the Southern Hemisphere Westerlies on the position of the Subtropical Front. *Journal of Geophysical Research: Oceans, 118*(10), 5669-5675. http://dx.doi.org/10.1002/jgrc.20407

Delcroix, T., & Hénin, C. (1991). Seasonal and interannual variations of sea surface salinity in the tropical Pacific Ocean. *Journal of Geophysical Research: Oceans, 96*(C12), 22135-22150. https://doi.org/10.1029/91JC02124

Delcroix, T., & Picaut, J. (1998). Zonal displacement of the western equatorial Pacific "fresh pool". *Journal of Geophysical Research: Oceans, 103*(C1), 1087-1098. http://dx.doi.org/10.1029/97JC01912

DeLong, K. L., Quinn, T. M., Taylor, F. W., Lin, K., & Shen, C.-C. (2012). Sea surface temperature variability in the southwest tropical Pacific since AD 1649. *Nature Climate Change, 2*(11), 799-804. https://doi.org/10.1038/nclimate1583

DeNiro, M. J., & Epstein, S. (1978). Influence of diet on the distribution of carbon isotopes in animals. *Geochimica et Cosmochimica Acta, 42*(5), 495-506. http://www.sciencedirect.com/science/article/pii/0016703778901990

Deser, C., Phillips, A. S., & Alexander, M. A. (2010). Twentieth century tropical sea surface temperature trends revisited. *Geophysical Research Letters, 37*(10), n/a-n/a. http://dx.doi.org/10.1029/2010GL043321

Di Lorenzo, E., Schneider, N., Cobb, K. M., Franks, P. J. S., Chhak, K., Miller, A. J., et al. (2008). North Pacific Gyre Oscillation links ocean climate and ecosystem change. *Geophysical Research Letters, 35*(8). https://doi.org/10.1029/2007GL032838

DiFiore, P. J., Sigman, D. M., Karsh, K. L., Trull, T. W., Dunbar, R. B., & Robinson, R. S. (2010). Poleward decrease in the isotope effect of nitrate assimilation across the Southern Ocean. *Geophysical Research Letters, 37*(17), n/a-n/a. http://dx.doi.org/10.1029/2010GL044090

DiFiore, P. J., Sigman, D. M., Trull, T. W., Lourey, M. J., Karsh, K., Cane, G., & Ho, R. (2006). Nitrogen isotope constraints on subantarctic biogeochemistry. *Journal of Geophysical Research: Oceans, 111*(C8), n/a-n/a. http://dx.doi.org/10.1029/2005JC003216

Druffel, E. R. M., Bauer, J. E., Griffin, S., & Hwang, J. (2003). Penetration of anthropogenic carbon into organic particles of the deep ocean. *Geophysical Research Letters, 30*(14). https://doi.org/10.1029/2003GL017423

Edgar, G. (1984). *General features of the ecology and biogeography of Tasmanian rocky reef communities* (Vol. 118).

Ellwood, M. J., Law, C. S., Hall, J., Woodward, E. M. S., Strzepek, R., Kuparinen, J., et al. (2013). Relationships between nutrient stocks and inventories and phytoplankton physiological status along an oligotrophic meridional transect in the Tasman Sea. *Deep Sea Research Part I: Oceanographic Research Papers, 72*, 102-120. http://www.sciencedirect.com/science/article/pii/S0967063712002087

Fairbanks, R. G., Evans, M. N., Rubenstone, J. L., Mortlock, R. A., Broad, K., Moore, M. D., & Charles, C. D. (1997). Evaluating climate indices and their geochemical proxies measured in corals. *Coral Reefs, 16*(1), S93-S100. journal article. https://doi.org/10.1007/s003380050245

Flores-Aqueveque, V., Rojas, M., Aguirre, C., Arias, P. A., & González, C. (2020). South Pacific Subtropical High from the late Holocene to the end of the 21st century: insights from

climate proxies and general circulation models. *Clim. Past, 16*(1), 79-99. https://cp.copernicus.org/articles/16/79/2020/

Fogt, R. L., & Bromwich, D. H. (2006). Decadal Variability of the ENSO Teleconnection to the High-Latitude South Pacific Governed by Coupling with the Southern Annular Mode. *Journal of Climate, 19*(6), 979-997. https://doi.org/10.1175/JCLI3671.1

Fogt, R. L., Perlwitz, J., Monaghan, A. J., Bromwich, D. H., Jones, J. M., & Marshall, G. J. (2009). Historical SAM Variability. Part II: Twentieth-Century Variability and Trends from Reconstructions, Observations, and the IPCC AR4 Models. *Journal of Climate, 22*(20), 5346-5365. https://doi.org/10.1175/2009JCLI2786.1

Fowler, A. M., Boswijk, G., Lorrey, A. M., Gergis, J., Pirie, M., McCloskey, S. P. J., et al. (2012). Multi-centennial tree-ring record of ENSO-related activity in New Zealand. *Nature Climate Change, 2*(3), 172-176. https://doi.org/10.1038/nclimate1374

Galbraith, E. D., Kienast, M., Albuquerque, A. L., Altabet, M. A., Batista, F., Bianchi, D., et al. (2013). The acceleration of oceanic denitrification during deglacial warming. *Nature Geoscience, 6*(7), 579-584.

Ganachaud, A., Cravatte, S., Melet, A., Schiller, A., Holbrook, N. J., Sloyan, B. M., et al. (2014). The Southwest Pacific Ocean circulation and climate experiment (SPICE). *Journal of Geophysical Research-Oceans, 119*(11), 7660-7686. <Go to ISI>://WOS:000346102900017

Glynn, D. S., McMahon, K. W., Guilderson, T. P., & McCarthy, M. D. (2019). Major shifts in nutrient and phytoplankton dynamics in the North Pacific Subtropical Gyre over the last 5000 years revealed by high-resolution proteinaceous deep-sea coral δ15N and δ13C records. *Earth and Planetary Science Letters, 515*, 145-153. http://www.sciencedirect.com/science/article/pii/S0012821X19301621

Godfrey, J. S., Cresswell, G. R., Golding, T. J., Pearce, A. F., & Boyd, R. (1980). The Separation of the East Australian Current. *Journal of Physical Oceanography, 10*(3), 430-440. https://journals.ametsoc.org/doi/abs/10.1175/1520-0485%281980%29010%3C0430%3ATSOTEA%3E2.0.CO%3B2

Goericke, R., & Fry, B. (1994). Variations of marine plankton δ13C with latitude, temperature, and dissolved CO2 in the world ocean. *Global Biogeochemical Cycles, 8*(1), 85-90. https://doi.org/10.1029/93GB03272

Goldberg, W. M. (1991). Chemistry and structure of skeletal growth rings in the black coral Antipathes fiordensis (Cnidaria, Antipatharia). *Hydrobiologia, 216*(1), 403-409. journal article. https://doi.org/10.1007/BF00026493

Goldberg, W. M. (1974). Evidence of a sclerotized collagen from the skeleton of a gorgonian coral. *Comparative Biochemistry and Physiology Part B: Comparative Biochemistry, 49*(3), 525-526. http://www.sciencedirect.com/science/article/pii/0305049174901886

Goldberg, W. M., Hopkins, T. L., Holl, S. M., Schaefer, J., Kramer, K. J., Morgan, T. D., & Kim, K. (1994). Chemical composition of the sclerotized black coral skeleton (Coelenterata: Antipatharia): a comparison of two species. *Comparative Biochemistry and Physiology Part B: Comparative Biochemistry, 107*(4), 633-643. http://www.sciencedirect.com/science/article/pii/030504919490197X

Gomez, B., Carter, L., Orpin, A. R., Cobb, K. M., Page, M. J., Trustrum, N. A., & Palmer, A. S. (2012). ENSO/SAM interactions during the middle and late Holocene. *The Holocene, 22*(1), 23-30. http://journals.sagepub.com/doi/abs/10.1177/0959683611405241

Graham, R. M., & De Boer, A. M. (2013). The Dynamical Subtropical Front. *Journal of Geophysical Research: Oceans, 118*(10), 5676-5685. http://dx.doi.org/10.1002/jgrc.20408

Gregg, W. W., Conkright, M. E., Ginoux, P., O'Reilly, J. E., & Casey, N. W. (2003). Ocean primary production and climate: Global decadal changes. *Geophysical Research Letters, 30*(15), n/a-n/a. http://dx.doi.org/10.1029/2003GL016889

Grothe, P. R., Cobb, K. M., Liguori, G., Di Lorenzo, E., Capotondi, A., Lu, Y., et al. (2019). Enhanced El Niño-Southern Oscillation variability in recent decades. *Geophysical Research Letters, n/a*(n/a). https://doi.org/10.1029/2019GL083906

Grotjahn, R. (2004). Remote weather associated with South Pacific subtropical sea-level high properties. *International Journal of Climatology, 24*, 823-839.

Gruber, N. (2004). The dynamics of the marine nitrogen cycle and its influence on atmospheric CO 2 variations. In *The ocean carbon cycle and climate* (pp. 97-148): Springer.

Gruber, N. (2008). The marine nitrogen cycle: overview and challenges. *Nitrogen in the marine environment, 2*, 1-50.

Gruber, N., Keeling, C. D., & Stocker, T. F. (1998). Carbon-13 constraints on the seasonal inorganic carbon budget at the BATS site in the northwestern Sargasso Sea. *Deep Sea Research Part I: Oceanographic Research Papers, 45*(4), 673-717. http://www.sciencedirect.com/science/article/pii/S0967063797000988

Hall, A., & Visbeck, M. (2002). Synchronous Variability in the Southern Hemisphere Atmosphere, Sea Ice, and Ocean Resulting from the Annular Mode. *Journal of Climate, 15*(21), 3043-3057. https://doi.org/10.1175/1520-0442(2002)015<3043:SVITSH>2.0.CO;2

Hartmann, D. L. (2015). *Global physical climatology* (Vol. 103): Newnes.

Heath, R. A. (1985). A review of the physical oceanography of the seas around New Zealand — 1982. *New Zealand Journal of Marine and Freshwater Research, 19*(1), 79-124. https://doi.org/10.1080/00288330.1985.9516077

Heaton, T. J., Köhler, P., Butzin, M., Bard, E., Reimer, R. W., Austin, W. E. N., et al. (2020). MARINE20—THE MARINE RADIOCARBON AGE CALIBRATION CURVE (0–55,000 CAL BP). *Radiocarbon*, 1-42. https://www.cambridge.org/core/article/marine20the-marine-radiocarbon-age-calibration-curve-055000-cal-bp/B3013899914A3198D4B884B7B6E5CE66

Hendy, E. J., Gagan, M. K., Alibert, C. A., McCulloch, M. T., Lough, J. M., & Isdale, P. J. (2002). Abrupt Decrease in Tropical Pacific Sea Surface Salinity at End of Little Ice Age. *Science, 295*(5559), 1511. http://science.sciencemag.org/content/295/5559/1511.abstract

Henson, S. A., Beaulieu, C., & Lampitt, R. (2016). Observing climate change trends in ocean biogeochemistry: when and where. *Global Change Biology, 22*(4), 1561-1571. https://doi.org/10.1111/gcb.13152

Henson, S. A., Sarmiento, J. L., Dunne, J. P., Bopp, L., Lima, I., Doney, S. C., et al. (2010). Detection of anthropogenic climate change in satellite records of ocean chlorophyll and productivity. *Biogeosciences, 7*(2), 621-640. https://bg.copernicus.org/articles/7/621/2010/

Hill, K. L., Rintoul, S. R., Ridgway, K. R., & Oke, P. R. (2011). Decadal changes in the South Pacific western boundary current system revealed in observations and ocean state estimates. *Journal of Geophysical Research: Oceans, 116*(C1), n/a-n/a. http://dx.doi.org/10.1029/2009JC005926

Hilting, A. K., Kump, L. R., & Bralower, T. J. (2008). Variations in the oceanic vertical carbon isotope gradient and their implications for the Paleocene-Eocene biological pump. *Paleoceanography, 23*(3). https://doi.org/10.1029/2007PA001458

Hitt, N. T., Sinclair, D. J., Fallon, S. J., Neil, H. L., Tracey, D. M., Komugabe-Dixson, A., & Marriott, P. (2020). Growth and longevity of New Zealand black corals. *Deep Sea Research Part I: Oceanographic Research Papers*, 103298. http://www.sciencedirect.com/science/article/pii/S0967063720300868

Hoefs, J. (2009). *Stable isotope geochemistry* (Vol. 285): Springer.

Hoegh-Guldberg, O., Cai, R., Poloczanska, E. S., Brewer, P. G., Sundby, S., Hilmi, K., et al. (2014). *The Ocean*. Retrieved from Cambridge, United Kingdom and New York, NY, USA:

Isoguchi, O., & Kawamura, H. (2006). Seasonal to interannual variations of the western boundary current of the subarctic North Pacific by a combination of the altimeter and tide gauge sea levels. *Journal of Geophysical Research: Oceans, 111*(C4). https://doi.org/10.1029/2005JC003080

Jiang, N., Griffiths, G., & Lorrey, A. (2013). Influence of large-scale climate modes on daily synoptic weather types over New Zealand. *International Journal of Climatology, 33*(2), 499-519. https://doi.org/10.1002/joc.3443

Johnson, C. R., Banks, S. C., Barrett, N. S., Cazassus, F., Dunstan, P. K., Edgar, G. J., et al. (2011). Climate change cascades: Shifts in oceanography, species' ranges and subtidal marine community dynamics in eastern Tasmania. *Journal of Experimental Marine Biology and Ecology, 400*(1), 17-32. http://www.sciencedirect.com/science/article/pii/S0022098111000803

Jones, J. M., Fogt, R. L., Widmann, M., Marshall, G. J., Jones, P. D., & Visbeck, M. (2009). Historical SAM Variability. Part I: Century-Length Seasonal Reconstructions. *Journal of Climate, 22*(20), 5319-5345. https://doi.org/10.1175/2009JCLI2785.1

Karl, D. M. (1999). A sea of change: biogeochemical variability in the North Pacific Subtropical Gyre. *Ecosystems, 2*(3), 181-214.

Karl, D. M., Bidigare, R., & Letelier, R. (2001a). Long-term changes in plankton community structure and productivity in the North Pacific Subtropical Gyre: The domain shift hypothesis. *Deep Sea Research Part II: Topical Studies in Oceanography, 48*(8-9), 1449-1470.

Karl, D. M., Bidigare, R. R., & Letelier, R. M. (2001b). Long-term changes in plankton community structure and productivity in the North Pacific Subtropical Gyre: The domain shift hypothesis. *Deep Sea Research Part II: Topical Studies in Oceanography, 48*(8), 1449-1470. http://www.sciencedirect.com/science/article/pii/S0967064500001491

Karl, D. M., Letelier, R., Hebel, D., Tupas, L., Dore, J., Christian, J., & Winn, C. (1995). Ecosystem changes in the North Pacific subtropical gyre attributed to the 1991–92 El Niño. *Nature, 373*(6511), 230-234. https://doi.org/10.1038/373230a0

Karl, D. M., & Lukas, R. (1996). The Hawaii Ocean Time-series (HOT) program: Background, rationale and field implementation. *Deep Sea Research Part II: Topical Studies in Oceanography, 43*(2), 129-156. http://www.sciencedirect.com/science/article/pii/0967064596000057

Keeling, C. D., Whorf, T. P., Wahlen, M., & van der Plichtt, J. (1995). Interannual extremes in the rate of rise of atmospheric carbon dioxide since 1980. *Nature, 375*(6533), 666-670. https://doi.org/10.1038/375666a0

Kendall, C., & McDonnell, J. J. (2012). *Isotope tracers in catchment hydrology*: Elsevier.

Key, R. M., Kozyr, A., Sabine, C. L., Lee, K., Wanninkhof, R., Bullister, J. L., et al. (2004). A global ocean carbon climatology: Results from Global Data Analysis Project (GLODAP). *Global Biogeochemical Cycles, 18*(4). https://doi.org/10.1029/2004GB002247

Kidson, J. W., & Renwick, J. A. (2002). Patterns of convection in the tropical pacific and their influence on New Zealand weather. *International Journal of Climatology, 22*(2), 151-174. https://doi.org/10.1002/joc.737

Kidston, J., Renwick, J., & McGregor, J. (2009). Hemispheric-scale seasonality of the Southern Annular Mode and impacts on the climate of New Zealand. *Journal of Climate, 22*(18), 4759-4770.

Kohfeld, K. E., Graham, R. M., de Boer, A. M., Sime, L. C., Wolff, E. W., Le Quéré, C., & Bopp, L. (2013). Southern Hemisphere westerly wind changes during the Last Glacial Maximum: paleo-data synthesis. *Quaternary Science Reviews, 68*, 76-95. http://www.sciencedirect.com/science/article/pii/S0277379113000267

Komugabe, A. F., Fallon, S. J., Thresher, R. E., & Eggins, S. M. (2014). Modern Tasman Sea surface reservoir ages from deep-sea black corals. *Deep Sea Research Part II: Topical Studies in Oceanography, 99*(Supplement C), 207-212. http://www.sciencedirect.com/science/article/pii/S0967064513002154

Komugabe-Dixson, A. F., Fallon, S. J., Eggins, S. M., & Thresher, R. E. (2016). Radiocarbon evidence for mid-late Holocene changes in southwest Pacific Ocean circulation. *Paleoceanography, 31*(7), 971-985. http://dx.doi.org/10.1002/2016PA002929

Kushner, P. J., Held, I. M., & Delworth, T. L. (2001). Southern Hemisphere Atmospheric Circulation Response to Global Warming. *Journal of Climate, 14*(10), 2238-2249. https://journals.ametsoc.org/doi/abs/10.1175/1520-0442%282001%29014%3C0001%3ASHACRT%3E2.0.CO%3B2

Lamy, F., Kilian, R., Arz, H. W., Francois, J.-P., Kaiser, J., Prange, M., & Steinke, T. (2010). Holocene changes in the position and intensity of the southern westerly wind belt. *Nature Geoscience, 3*, 695. http://dx.doi.org/10.1038/ngeo959

Larsen, T., Ventura, M., Andersen, N., O'Brien, D. M., Piatkowski, U., & McCarthy, M. D. (2013). Tracing Carbon Sources through Aquatic and Terrestrial Food Webs Using Amino Acid Stable Isotope Fingerprinting. *PLOS ONE, 8*(9), e73441. https://doi.org/10.1371/journal.pone.0073441

Libby, W. F. (1946). Atmospheric helium three and radiocarbon from cosmic radiation. *Physical Review, 69*(11-12), 671.

Liguori, G., & Di Lorenzo, E. (2018). Meridional Modes and Increasing Pacific Decadal Variability Under Anthropogenic Forcing. *Geophysical Research Letters, 45*(2), 983-991. https://doi.org/10.1002/2017GL076548

Linsley, B., Kaplan, A., Gouriou, Y., Salinger, J., deMenocal, P. B., Wellington, G. M., & Howe, S. S. (2006). Tracking the extent of the South Pacific Convergence Zone since the early 1600s. *Geochemistry, Geophysics, Geosystems, 7*(5), n/a-n/a. http://dx.doi.org/10.1029/2005GC001115

Linsley, B., Zhang, P., Kaplan, A., Howe, S., & M. Wellington, G. (2008). *Interdecadal-decadal climate variability from multicoral oxygen isotope records in the South Pacific Convergence Zone region since 1650 A.D* (Vol. 23).

Liu, Z., & Di Lorenzo, E. (2018). Mechanisms and Predictability of Pacific Decadal Variability. *Current Climate Change Reports, 4*(2), 128-144. https://doi.org/10.1007/s40641-018-0090-5

Lorrey, A. M., & Bostock, H. C. (2014a). Australasia: An Overview of Modern Climate and Paleoclimate during the Last Glacial Maximum. In J. Beattie, E. O'Gorman, & M. Henry (Eds.), *Climate, Science, and Colonization: Histories from Australia and New Zealand* (pp. 19-42). New York: Palgrave Macmillan US.

Lorrey, A. M., Fauchereau, N., Stanton, C., Chappell, P., Phipps, S., Mackintosh, A., et al. (2014b). The Little Ice Age climate of New Zealand reconstructed from Southern Alps cirque glaciers: a synoptic type approach. *Climate Dynamics, 42*(11), 3039-3060. https://doi.org/10.1007/s00382-013-1876-8

Lorrey, A. M., Vandergoes, M., Almond, P., Renwick, J., Stephens, T., Bostock, H., et al. (2012). Palaeocirculation across New Zealand during the last glacial maximum at ~21 ka. *Quaternary Science Reviews, 36*, 189-213. http://www.sciencedirect.com/science/article/pii/S0277379111003040

Lorrey, A. M., Williams, P., Salinger, M., Martin, T., Palmer, J., Fowler, A., et al. (2008). Speleothem stable isotope records interpreted within a multi-proxy framework and implications for New Zealand palaeoclimate reconstruction. *Quaternary International, 187*, 52-75.

Lorrey, A. M., Williams, P., Woolley, J.-M., Fauchereau, N., Hartland, A., Bostock, H., et al. (2020). Late Quaternary Climate Variability and Change from Aotearoa New Zealand Speleothems: Progress in Age Modelling, Oxygen Isotope Master Record Construction and Proxy-Model Comparisons. *Quaternary, 3*, 24.

Lovenduski, N. S., & Gruber, N. (2005). Impact of the Southern Annular Mode on Southern Ocean circulation and biology. *Geophysical Research Letters, 32*(11), n/a-n/a. http://dx.doi.org/10.1029/2005GL022727

Lu, Z., Liu, Z., Zhu, J., & Cobb, K. (2018). A Review of Paleo El Niño-Southern Oscillation. *Atmosphere, 9*, 130.

Magozzi, S., Yool, A., Vander Zanden, H. B., Wunder, M. B., & Trueman, C. N. (2017). Using ocean models to predict spatial and temporal variation in marine carbon isotopes. *Ecosphere, 8*(5), e01763. https://doi.org/10.1002/ecs2.1763

Mariotti, A., Germon, J. C., Hubert, P., Kaiser, P., Letolle, R., Tardieux, A., & Tardieux, P. (1981). Experimental determination of nitrogen kinetic isotope fractionation: Some principles; illustration for the denitrification and nitrification processes. *Plant and Soil, 62*(3), 413-430. https://doi.org/10.1007/BF02374138

Marshall, G. J. (2003). Trends in the Southern Annular Mode from Observations and Reanalyses. *Journal of Climate, 16*(24), 4134-4143. https://journals.ametsoc.org/doi/abs/10.1175/1520-0442%282003%29016%3C4134%3ATITSAM%3E2.0.CO%3B2

Marshall, G. J., Stott, P. A., Turner, J., Connolley, W. M., King, J. C., & Lachlan-Cope, T. A. (2004). Causes of exceptional atmospheric circulation changes in the Southern Hemisphere. *Geophysical Research Letters, 31*(14), n/a-n/a. http://dx.doi.org/10.1029/2004GL019952

Martiny, A., Vrugt, J., & Lomas, M. (2014). Concentrations and ratios of particulate organic carbon, nitrogen, and phosphorus in the global ocean. *Scientific Data*.

Matsumoto, K. (2007). Radiocarbon-based circulation age of the world oceans. *Journal of Geophysical Research: Oceans, 112*(C9). https://doi.org/10.1029/2007JC004095

McCulloch, M. T., Gagan, M. K., Mortimer, G. E., Chivas, A. R., & Isdale, P. J. (1994). A high-resolution Sr/Ca and δ18O coral record from the Great Barrier Reef, Australia, and the 1982–1983 El Niño. *Geochimica et Cosmochimica Acta, 58*(12), 2747-2754. http://www.sciencedirect.com/science/article/pii/0016703794901422

McMahon, K., D McCarthy, M., Sherwood, O., Larsen, T., & P Guilderson, T. (2015). *Millennial-scale plankton regime shifts in the subtropical North Pacific Ocean* (Vol. 350).

McMahon, K., Hamady, L. L., & Thorrold, S. R. (2013). A review of ecogeochemistry approaches to estimating movements of marine animals. *Limnology and Oceanography, 58*(2), 697-714. https://doi.org/10.4319/lo.2013.58.2.0697

McMahon, K., & McCarthy, M. D. (2016). Embracing variability in amino acid δ15N fractionation: mechanisms, implications, and applications for trophic ecology. *Ecosphere, 7*(12), e01511. https://doi.org/10.1002/ecs2.1511

Meinen, C. S., & McPhaden, M. J. (2000). Observations of warm water volume changes in the equatorial Pacific and their relationship to El Niño and La Niña. *Journal of Climate, 13*(20), 3551-3559.

Messié, M., & Chavez, F. (2011). Global Modes of Sea Surface Temperature Variability in Relation to Regional Climate Indices. *Journal of Climate, 24*(16), 4314-4331. www.jstor.org/stable/26191146

Moore, C. M., Mills, M. M., Arrigo, K. R., Berman-Frank, I., Bopp, L., Boyd, P. W., et al. (2013). Processes and patterns of oceanic nutrient limitation. *Nature Geoscience, 6*(9), 701-710. https://doi.org/10.1038/ngeo1765

Moreno, P. I., Francois, J. P., Moy, C. M., & Villa-Martínez, R. (2010). Covariability of the Southern Westerlies and atmospheric CO2 during the Holocene. *Geology, 38*(8), 727-730. http://dx.doi.org/10.1130/G30962.1

Moreno, P. I., François, J. P., Villa-Martínez, R. P., & Moy, C. M. (2009). Millennial-scale variability in Southern Hemisphere westerly wind activity over the last 5000 years in SW Patagonia. *Quaternary Science Reviews, 28*(1), 25-38. http://www.sciencedirect.com/science/article/pii/S0277379108002886

Moreno, P. I., Vilanova, I., Villa-Martínez, R., Dunbar, R. B., Mucciarone, D. A., Kaplan, M. R., et al. (2018). Onset and Evolution of Southern Annular Mode-Like Changes at Centennial Timescale. *Scientific Reports, 8*(1), 3458. https://doi.org/10.1038/s41598-018-21836-6

Moreno, P. I., Vilanova, I., Villa-Martínez, R., Garreaud, R. D., Rojas, M., & De Pol-Holz, R. (2014). Southern Annular Mode-like changes in southwestern Patagonia at centennial timescales over the last three millennia. *Nature Communications, 5*(1), 4375. https://doi.org/10.1038/ncomms5375

Mullan, A. (1995). On the linearity and stability of Southern Oscillation-climate relationships for New Zealand. *International Journal of Climatology, 15*(12), 1365-1386.

Munk, W. H. (1950). ON THE WIND-DRIVEN OCEAN CIRCULATION. *Journal of Meteorology, 7*(2), 80-93. http://journals.ametsoc.org/doi/abs/10.1175/1520-0469%281950%29007%3C0080%3AOTWDOC%3E2.0.CO%3B2

Murphy, R. J., Pinkerton, M. H., Richardson, K. M., Bradford-Grieve, J. M., & Boyd, P. W. (2001). Phytoplankton distributions around New Zealand derived from SeaWiFS remotely-sensed ocean colour data. *New Zealand Journal of Marine and Freshwater Research, 35*(2), 343-362. https://doi.org/10.1080/00288330.2001.9517005

Nakatsuka, T., Handa, N., Wada, E., & Wong, C. S. (1992). The dynamic changes of stable isotopic ratios of carbon and nitrogen in suspended and sedimented particulate organic matter during a phytoplankton bloom. *Journal of Marine Research, 50*(2), 267-296. https://www.ingentaconnect.com/content/jmr/jmr/1992/00000050/00000002/art00004

https://doi.org/10.1357/002224092784797692

Neil, H. L., Carter, L., & Morris, M. Y. (2004). Thermal isolation of Campbell Plateau, New Zealand, by the Antarctic Circumpolar Current over the past 130 kyr. *Paleoceanography, 19*(4), n/a-n/a. http://dx.doi.org/10.1029/2003PA000975

Newman, M., Alexander, M. A., Ault, T. R., Cobb, K. M., Deser, C., Di Lorenzo, E., et al. (2016). The Pacific Decadal Oscillation, Revisited. *Journal of Climate, 29*(12), 4399-4427. https://doi.org/10.1175/JCLI-D-15-0508.1

Oliver, E. C. J., & Holbrook, N. J. (2018). Variability and Long-Term Trends in the Shelf Circulation Off Eastern Tasmania. *Journal of Geophysical Research: Oceans, 123*(10), 7366-7381. https://doi.org/10.1029/2018JC013994

Opresko, D. M., Tracey, D. M., & Mackay, E. (2014). *Antipatharia (Black Corals) for the New Zealand Region: A Field Guide of Commonly Sampled New Zealand Black Corals Including Illustrations Highlighting Technical Terms and Black Coral Morphology*: Ministry for Primary Industries.

Orsi, A. H., Whitworth, T., & Nowlin, W. D. (1995). On the meridional extent and fronts of the Antarctic Circumpolar Current. *Deep Sea Research Part I: Oceanographic Research Papers, 42*(5), 641-673. http://www.sciencedirect.com/science/article/pii/096706379500021W

Petchey, F., Anderson, A., Hogg, A., & Zondervan, A. (2008a). The marine reservoir effect in the Southern Ocean: An evaluation of extant and new ?R values and their application to archaeological chronologies. *Journal of the Royal Society of New Zealand, 38*(4), 243-262. https://doi.org/10.1080/03014220809510559

Petchey, F., Anderson, A., Zondervan, A., Ulm, S., & Hogg, A. (2008b). New Marine ΔR Values for the South Pacific Subtropical Gyre Region. *Radiocarbon, 50*(3), 373-397. https://www.cambridge.org/core/article/new-marine-r-values-for-the-south-pacific-subtropical-gyre-region/4345B6851E825BA6A30B466D5F6F17D8

Poloczanska, E., Babcock, R., Butler, A., Hobday, A., Hoegh-Guldberg, O., J. Kunz, T., et al. (2007). *Climate Change and Australian Marine Life* (Vol. 45).

Poloczanska, E., Brown, C. J., Sydeman, W. J., Kiessling, W., Schoeman, D. S., Moore, P. J., et al. (2013). Global imprint of climate change on marine life. *Nature Clim. Change, 3*(10), 919-925. Letter. http://dx.doi.org/10.1038/nclimate1958

Poloczanska, E., Burrows, M. T., Brown, C. J., García Molinos, J., Halpern, B. S., Hoegh-Guldberg, O., et al. (2016). Responses of Marine Organisms to Climate Change across Oceans. *Frontiers in Marine Science, 3*(62). Review. https://www.frontiersin.org/article/10.3389/fmars.2016.00062

Polovina, J. J., Howell, E. A., & Abecassis, M. (2008). Ocean's least productive waters are expanding. *Geophysical Research Letters, 35*(3). https://doi.org/10.1029/2007GL031745

Popp, B. N., Laws, E. A., Bidigare, R. R., Dore, J. E., Hanson, K. L., & Wakeham, S. G. (1998). Effect of Phytoplankton Cell Geometry on Carbon Isotopic Fractionation. *Geochimica et Cosmochimica Acta, 62*(1), 69-77. http://www.sciencedirect.com/science/article/pii/S0016703797003335

Postgate, J. R. (1982). Biology Nitrogen Fixation: Fundamentals. *Philosophical transactions of the Royal Society of London. Series B, Biological sciences, 296*(1082), 375-385. www.jstor.org/stable/2395691

Prouty, N. G., Roark, E., Buster, N., & Ross, S. (2011). *Growth rate and age distribution of deep-sea black corals in the Gulf of Mexico* (Vol. 423).

Prouty, N. G., Roark, E. B., Andrews, A., Robinson, L., Hill, T., Sherwood, O., et al. (2015). *Age, growth rates, and paleoclimate studies of deep sea corals*. Retrieved from http://pubs.er.usgs.gov/publication/70103075

Prouty, N. G., Roark, E. B., Koenig, A. E., Demopoulos, A. W. J., Batista, F. C., Kocar, B. D., et al. (2014). Deep-sea coral record of human impact on watershed quality in the Mississippi River Basin. *Global Biogeochemical Cycles, 28*(1), 29-43. http://dx.doi.org/10.1002/2013GB004754

Rafter, P. A., & Charles, C. D. (2012). Pleistocene equatorial Pacific dynamics inferred from the zonal asymmetry in sedimentary nitrogen isotopes. *Paleoceanography, 27*(3). https://doi.org/10.1029/2012PA002367

Rau, G. H., Riebesell, U., & Wolf-Gladrow, D. (1996). A model of photosynthetic 13C fractionation by marine phytoplankton based on diffusive molecular CO2 uptake. *Marine Ecology Progress Series, 133*, 275-285.

Rau, G. H., Takahashi, T., & Des Marais, D. (1989a). Latitudinal variations in plankton delta C-13 - Implications for CO2 and productivity in past oceans. *341*.

Rau, G. H., Takahashi, T., Des Marais, D. J., Repeta, D. J., & Martin, J. H. (1992). The relationship between δ13C of organic matter and [CO2(aq)] in ocean surface water: Data from a JGOFS site in the northeast Atlantic Ocean and a model. *Geochimica et Cosmochimica Acta, 56*(3), 1413-1419. http://www.sciencedirect.com/science/article/pii/001670379290073R

Rau, G. H., Takahashi, T., & Marais, D. J. D. (1989b). Latitudinal variations in plankton δ13C: implications for CO2 and productivity in past oceans. *Nature, 341*(6242), 516-518. https://doi.org/10.1038/341516a0

Redfield, A. C. (1934). On the proportions of organic derivatives in sea water and their relation to the composition of plankton. *James Johnstone memorial volume*, 176-192.

Reimer, P. J., Bard, E., Bayliss, A., Beck, J. W., Blackwell, P. G., Ramsey, C. B., et al. (2013). IntCal13 and Marine13 Radiocarbon Age Calibration Curves 0–50,000 Years cal BP. *Radiocarbon, 55*(4), 1869-1887. https://www.cambridge.org/core/article/intcal13-and-marine13-radiocarbon-age-calibration-curves-050000-years-cal-bp/FB97C1341F452BD6A410C6FE4E28E090

Reynhout, S. A., Sagredo, E. A., Kaplan, M. R., Aravena, J. C., Martini, M. A., Moreno, P. I., et al. (2019). Holocene glacier fluctuations in Patagonia are modulated by summer insolation intensity and paced by Southern Annular Mode-like variability. *Quaternary Science Reviews, 220*, 178-187. http://www.sciencedirect.com/science/article/pii/S0277379119300745

Ridgway, K. R. (2007). Long-term trend and decadal variability of the southward penetration of the East Australian Current. *Geophysical Research Letters, 34*(13), n/a-n/a. http://dx.doi.org/10.1029/2007GL030393

Roark, E. B., Guilderson, T. P., Dunbar, R. B., & Ingram, B. L. (2006). Radiocarbon-based ages and growth rates of Hawaiian deep-sea corals. *Marine Ecology Progress Series, 327*, 1-14. http://www.jstor.org/stable/24870713

Robinson, L. F., Adkins, J. F., Frank, N., Gagnon, A. C., Prouty, N. G., Brendan Roark, E., & de Flierdt, T. v. (2014). The geochemistry of deep-sea coral skeletons: A review of vital effects and applications for palaeoceanography. *Deep Sea Research Part II: Topical Studies in Oceanography, 99*(Supplement C), 184-198. http://www.sciencedirect.com/science/article/pii/S096706451300235X

Rodwell, M. J., & Hoskins, B. J. (2001). Subtropical Anticyclones and Summer Monsoons. *Journal of Climate, 14*(15), 3192-3211. https://journals.ametsoc.org/view/journals/clim/14/15/1520-0442_2001_014_3192_saasm_2.0.co_2.xml

Roemmich, D., Gilson, J., Davis, R., Sutton, P., Wijffels, S., & Riser, S. (2007). Decadal Spinup of the South Pacific Subtropical Gyre. *Journal of Physical Oceanography, 37*(2), 162-173. http://journals.ametsoc.org/doi/abs/10.1175/JPO3004.1

Roemmich, D., Gilson, J., Sutton, P., & Zilberman, N. (2016). Multidecadal Change of the South Pacific Gyre Circulation. *Journal of Physical Oceanography, 46*(6), 1871-1883. https://doi.org/10.1175/JPO-D-15-0237.1

Roop, H. A. (2015). *Late-Holocene Climate Variability in Southern New Zealand: A reconstruction of regional climate from an annually laminated sediment sequence from Lake Ohau.* (Doctoral Thesis Doctoral), Victoria University of Wellington, Victoria Unversity of Wellington.

Rousseaux, C. S., & Gregg, W. W. (2014). Interannual variation in phytoplankton primary production at a global scale. *Remote sensing, 6*(1), 1-19.

Ruddiman, W. (2008). *Earth's Climate: Past and Future*: W. H. Freeman.

Ruddiman, W., & McIntyre, A. (1981). The North Atlantic Ocean during the last deglaciation. *Palaeogeography, Palaeoclimatology, Palaeoecology, 35*, 145-214. http://www.sciencedirect.com/science/article/pii/0031018281900973

Russell, J. L., Dixon, K. W., Gnanadesikan, A., Stouffer, R. J., & Toggweiler, J. R. (2006). The Southern Hemisphere Westerlies in a Warming World: Propping Open the Door to the Deep Ocean. *Journal of Climate, 19*(24), 6382-6390. https://journals.ametsoc.org/doi/abs/10.1175/JCLI3984.1

Sabine, C. L., Feely, R. A., Gruber, N., Key, R. M., Lee, K., Bullister, J. L., et al. (2004). The Oceanic Sink for Anthropogenic CO<sub>2</sub&gt. *Science, 305*(5682), 367. 10.1126/science.1097403. http://science.sciencemag.org/content/305/5682/367.abstract

Sarachik, E. S., & Cane, M. A. (2010). *The El Nino-southern oscillation phenomenon*: Cambridge University Press.

Sarmiento, J. L., & Gruber, N. (2006). *Ocean Biogeochemical Dynamics*: Princeton University Press.

Sarmiento, J. L., Gruber, N., Brzezinski, M. A., & Dunne, J. P. (2004). High-latitude controls of thermocline nutrients and low latitude biological productivity. *Nature, 427*(6969), 56-60. https://doi.org/10.1038/nature02127

Sayani, H. R., Cobb, K. M., DeLong, K., Hitt, N. T., & Druffel, E. R. M. (2019). Intercolony δ18O and Sr/Ca variability among Porites spp. corals at Palmyra Atoll: Towards more

robust coral-based estimates of climate. *Geochemistry, Geophysics, Geosystems, 0*(ja). https://doi.org/10.1029/2019GC008420

Schmittner, A., & Somes, C. J. (2016). Complementary constraints from carbon (13C) and nitrogen (15N) isotopes on the glacial ocean's soft-tissue biological pump. *Paleoceanography, 31*(6), 669-693.

Seo, I., Lee, Y., Yoo, C. M., & Hyeong, K. (2018). Migration of the Kuroshio Extension in the Northwest Pacific since the Last Glacial Maximum. *Palaeogeography, Palaeoclimatology, Palaeoecology, 496*, 323-331. http://www.sciencedirect.com/science/article/pii/S0031018217306764

Shears, N. T., & Bowen, M. M. (2017). Half a century of coastal temperature records reveal complex warming trends in western boundary currents. *Scientific Reports, 7*(1), 14527. https://doi.org/10.1038/s41598-017-14944-2

Sherwood, O., & Edinger, E. (2009). *Ages and growth rates of some deep-sea gorgonian and antipatharian corals of Newfoundland and Labrador* (Vol. 66).

Sherwood, O., Guilderson, T. P., Batista, F. C., Schiff, J. T., & McCarthy, M. D. (2013). Increasing subtropical North Pacific Ocean nitrogen fixation since the Little Ice Age. *Nature, 505*, 78. http://dx.doi.org/10.1038/nature12784

Sigman, D. M., & Boyle, E. A. (2000). Glacial/interglacial variations in atmospheric carbon dioxide. *Nature, 407*(6806), 859-869. https://doi.org/10.1038/35038000

Smith, R. O., Vennell, R., Bostock, H. C., & Williams, M. J. M. (2013). Interaction of the subtropical front with topography around southern New Zealand. *Deep Sea Research Part I: Oceanographic Research Papers, 76*, 13-26. http://www.sciencedirect.com/science/article/pii/S0967063713000551

Somes, C. J., Oschlies, A., & Schmittner, A. (2013). Isotopic constraints on the pre-industrial oceanic nitrogen budget. *Biogeosciences, 10*(9), 5889-5910. https://bg.copernicus.org/articles/10/5889/2013/

Somes, C. J., Schmittner, A., Galbraith, E. D., Lehmann, M. F., Altabet, M. A., Montoya, J. P., et al. (2010). Simulating the global distribution of nitrogen isotopes in the ocean. *Global Biogeochemical Cycles, 24*(4).

Somes, C. J., Schmittner, A., Muglia, J., & Oschlies, A. (2017). A three-dimensional model of the marine nitrogen cycle during the last glacial maximum constrained by sedimentary isotopes. *Frontiers in Marine Science, 4*, 108.

Stanton, B., & Sutton, P. (2003). Velocity measurements in the East Auckland Current north-east of North Cape, New Zealand. *New Zealand Journal of Marine and Freshwater Research, 37*(1), 195-204. https://doi.org/10.1080/00288330.2003.9517157

Stevens, C. L., O'Callaghan, J. M., Chiswell, S. M., & Hadfield, M. G. (2019). Physical oceanography of New Zealand/Aotearoa shelf seas – a review. *New Zealand Journal of Marine and Freshwater Research*, 1-40. https://doi.org/10.1080/00288330.2019.1588746

Stramma, L., Peterson, R. G., & Tomczak, M. (1995). The South Pacific Current. *Journal of Physical Oceanography, 25*(1), 77-91.

https://journals.ametsoc.org/doi/abs/10.1175/1520-0485%281995%29025%3C0077%3ATSPC%3E2.0.CO%3B2

Strzepek, K. M., Thresher, R. E., Revill, A. T., Smith, C. I., Komugabe, A. F., & Fallon, S. F. (2014). Preservation effects on the isotopic and elemental composition of skeletal structures in the deep-sea bamboo coral Lepidisis spp. (Isididae). *Deep Sea Research Part II: Topical Studies in Oceanography, 99*, 199-206. http://www.sciencedirect.com/science/article/pii/S0967064513002841

Stuiver, M., Quay, P. D., & Ostlund, H. G. (1983). Abyssal Water Carbon-14 Distribution and the Age of the World Oceans. *Science, 219*(4586), 849. http://science.sciencemag.org/content/219/4586/849.abstract

Sun, X., Renard, B., Thyer, M., Westra, S., & Lang, M. (2015). A global analysis of the asymmetric effect of ENSO on extreme precipitation. *Journal of Hydrology, 530*, 51-65. http://www.sciencedirect.com/science/article/pii/S002216941500699X

Swart, N. C., & Fyfe, J. C. (2012). Observed and simulated changes in the Southern Hemisphere surface westerly wind-stress. *Geophysical Research Letters, 39*(16). https://doi.org/10.1029/2012GL052810

Takahashi, K., & Battisti, D. S. (2007a). Processes controlling the mean tropical Pacific precipitation pattern. Part I: The Andes and the eastern Pacific ITCZ. In (Vol. 20, pp. 3434-3451).

Takahashi, K., & Battisti, D. S. (2007b). Processes Controlling the Mean Tropical Pacific Precipitation Pattern. Part II: The SPCZ and the Southeast Pacific Dry Zone. *Journal of Climate, 20*(23), 5696-5706. https://journals.ametsoc.org/view/journals/clim/20/23/2007jcli1656.1.xml

Thompson, D. W. J., & Wallace, J. M. (2000). Annular Modes in the Extratropical Circulation. Part I: Month-to-Month Variability. *Journal of Climate, 13*(5), 1000-1016. https://doi.org/10.1175/1520-0442(2000)013<1000:AMITEC>2.0.CO;2

Tilburg, C. E., Hurlburt, H. E., O'Brien, J. J., & Shriver, J. F. (2001). The Dynamics of the East Australian Current System: The Tasman Front, the East Auckland Current, and the East Cape Current. *Journal of Physical Oceanography, 31*(10), 2917-2943. https://journals.ametsoc.org/doi/abs/10.1175/1520-0485%282001%29031%3C2917%3ATDOTEA%3E2.0.CO%3B2

Toggweiler, J. R., Russell, J. L., & Carson, S. R. (2006). Midlatitude westerlies, atmospheric CO2, and climate change during the ice ages. *Paleoceanography, 21*(2), n/a-n/a. http://dx.doi.org/10.1029/2005PA001154

Trenberth, K. E. (1976). Spatial and temporal variations of the Southern Oscillation. *Quarterly Journal of the Royal Meteorological Society, 102*(433), 639-653.

Trujillo, A. P., & Thurman, H. V. (2011). *Essentials of Oceanography*: Prentice Hall.

Ummenhofer, C. C., & England, M. H. (2007). Interannual Extremes in New Zealand Precipitation Linked to Modes of Southern Hemisphere Climate Variability. *Journal of Climate, 20*(21), 5418-5440. https://journals.ametsoc.org/doi/abs/10.1175/2007JCLI1430.1

Ummenhofer, C. C., Gupta, A. S., & England, M. H. (2009). Causes of Late Twentieth-Century Trends in New Zealand Precipitation. *Journal of Climate, 22*(1), 3-19. https://journals.ametsoc.org/doi/abs/10.1175/2008JCLI2323.1

Van Oldenborgh, G. J. (2000). What caused the onset of the 1997–98 El Niño? *Monthly Weather Review, 128*(7), 2601-2607.

Wang, S., Huang, J., He, Y., & Guan, Y. (2014). Combined effects of the Pacific Decadal Oscillation and El Niño-Southern Oscillation on Global Land Dry–Wet Changes. *Scientific Reports, 4*(1), 6651. https://doi.org/10.1038/srep06651

Wang, Y. (2019). The role of Pacific subtropical high belts in the ENSO cycle. *Tellus A: Dynamic Meteorology and Oceanography, 71*(1), 1656514. https://doi.org/10.1080/16000870.2019.1656514

Weaver, A. J., Eby, M., Wiebe, E. C., Bitz, C. M., Duffy, P. B., Ewen, T. L., et al. (2001). The UVic earth system climate model: Model description, climatology, and applications to past, present and future climates. *Atmosphere-Ocean, 39*(4), 361-428. https://doi.org/10.1080/07055900.2001.9649686

Weaver, P. P. E., Carter, L., & Neil, H. L. (1998). Response of surface water masses and circulation to Late Quaternary climate change east of New Zealand. *Paleoceanography, 13*(1), 70-83. https://doi.org/10.1029/97PA02982

Williams, B. (2020). Proteinaceous corals as proxy archives of paleo-environmental change. *Earth-Science Reviews*, 103326. http://www.sciencedirect.com/science/article/pii/S001282522030372X

Williams, B., & Grottoli, A. G. (2010a). Recent shoaling of the nutricline and thermocline in the western tropical Pacific. *Geophysical Research Letters, 37*(22), n/a-n/a. http://dx.doi.org/10.1029/2010GL044867

Williams, B., & Grottoli, A. G. (2010b). Stable nitrogen and carbon isotope (δ15N and δ13C) variability in shallow tropical Pacific soft coral and black coral taxa and implications for paleoceanographic reconstructions. *Geochimica et Cosmochimica Acta, 74*(18), 5280-5288. http://www.sciencedirect.com/science/article/pii/S0016703710003674

Williams, B., Risk, M. J., Ross, S. W., & Sulak, K. J. (2006). Deep-water antipatharians: Proxies of environmental change. *Geology, 34*(9), 773-776. http://dx.doi.org/10.1130/G22685.1

Williams, B., Risk, M. J., Ross, S. W., & Sulak, K. J. (2007). Stable isotope data from deep-water antipatharians: 400-year records from the southeastern coast of the United States of America. *Bulletin of Marine Science, 81*(3), 437-447. http://www.ingentaconnect.com/content/umrsmas/bullmar/2007/00000081/00000003/art00011

Wong, W. W., & Sackett, W. M. (1978). Fractionation of stable carbon isotopes by marine phytoplankton. *Geochimica et Cosmochimica Acta, 42*(12), 1809-1815. http://www.sciencedirect.com/science/article/pii/0016703778902363

Wu, L., Cai, W., Zhang, L., Nakamura, H., Timmermann, A., Joyce, T., et al. (2012). Enhanced warming over the global subtropical western boundary currents. *Nature Clim. Change, 2*(3), 161-166. 10.1038/nclimate1353. http://dx.doi.org/10.1038/nclimate1353

Wyrtki, K. (1960). The Surface Circulation in Coral and Tasman Seas. *Division of Fisheries and Oceanography, No. 8*.

Yang, H., Lohmann, G., Krebs-Kanzow, U., Ionita, M., Shi, X., Sidorenko, D., et al. (2020). Poleward Shift of the Major Ocean Gyres Detected in a Warming Climate. *Geophysical Research Letters, 47*(5), e2019GL085868. https://doi.org/10.1029/2019GL085868

Zheng, X., Li, A., Kao, S., Gong, X., Frank, M., Kuhn, G., et al. (2016). Synchronicity of Kuroshio Current and climate system variability since the Last Glacial Maximum. *Earth and Planetary Science Letters, 452*, 247-257. http://www.sciencedirect.com/science/article/pii/S0012821X16303843

Zou, Y., & Xi, X. (2018). On the role of the south Pacific subtropical high at the onset of El Niño events. *Atmos. Chem. Phys. Discuss., 2018*, 1-22. https://acp.copernicus.org/preprints/acp-2018-82/

Chapter 2

Growth and Longevity of New Zealand Black Corals

The content in Chapter 2 was published in the peer-reviewed journal *Deep-Sea Research I: Oceanographic Research Papers*.

CITATION

Hitt, N. T., Sinclair, D. J., Fallon, S. J., Neil, H. L., Tracey, D. M., Komugabe-Dixson, A., & Marriott, P. (2020). Growth and longevity of New Zealand black corals. *Deep Sea Research Part I: Oceanographic Research Papers*, 103298. doi:https://doi.org/10.1016/j.dsr.2020.103298

Authorship contributions to this research article include the following:

Nicholas T. Hitt – Wrote manuscript, managed all co-author feedback, reviewer comments, and editing of proofs. This author prepared all samples for geochemical analysis, compiled all data, developed initial interpretations, and produced all figures.

Daniel J. Sinclair – Academic Supervisor; provided feedback on drafts and aided in the interpretation of the results. Helped to outline the Discussion section of the manuscript.

Stewart J. Fallon – Academic Supervisor; provided feedback on drafts.

Helen L. Neil – Academic Supervisor; provided feedback on drafts and aided in the interpretation of the results.

Di M. Tracey – Provided comments on the conservation section in the Discussion portion of the manuscript. Reviewed two drafts of the manuscript.

Aimée Komugabe-Dixson – Academic Supervisor; Reviewed two drafts of the manuscript.

Peter Marriot – Assisted in subsampling corals prior to micromilling

Note: The coral identifications in this chapter were published in *Deep-Sea Research I* as 'Coral Species X' (e.g. *Leiopathes* 1). Since other Chapters 2 and 3 refer to the corals by their NIWA sample codes (e.g. NIWA XXXX), I have changed the coral identifications in this chapter to their NIWA sample codes in order to be consistent across thesis chapters. The chapter also includes a section on the paleoceanographic potential that was not published in the original manuscript, a conclusions section that was not included in the original manuscript and updated references. Appendix data pertinent to this chapter are stored in 'Sheet A' in the CD-ROM at the end of the thesis.

2.1 Abstract:

Deep-sea corals are an important component of benthic ecosystems but are potentially very vulnerable to ecological disturbance due to their extreme longevity and slow growth rates. Among the slowest growing genera are the 'Black Corals' (Family Antipatharia), which can have lifespans of millennia. The waters around New Zealand contain a variety of black corals, including species that grow at shallow depths in the southern Fjords. However, while growth rates in black corals have been reported for many other parts of the world, New Zealand's black corals have received little attention. Here we present a series of high-resolution radiocarbon dates for coral colonies of the genera *Antipathella*, *Leiopathes* and *Antipathes*. Our results illustrate some corals have lifespans of up to 3000 years and slow but highly variable growth (averaging 1-140 μm/yr) for genera *Leiopathes* and *Antipathes* and fast growth (averaging 2-3cm/yr) for genera *Antipathella*, with no obvious regional variability in growth rates over time. Our results are broadly consistent with other black coral growth rate studies and reinforce that New Zealand's black corals likely have low resilience to any disturbance.

2.2 Introduction:

Deep-sea corals (DSCs), also referred to as cold water corals, are an essential component of deep-sea ecosystems. They occur in global oceans across aphotic environments in both tropical and polar regions (S. Roberts et al., 2004; J. Roberts et al., 2009). DSCs create colonies most commonly found on hard, steep continental shelves, seamounts, knolls, canyons, and ridges, where they establish themselves at depths ranging from <50m to 8000m below the surface (Tracey et al., 2007; Opresko et al., 2014). In the deep-sea environment, these corals provide habitat, refuge, and shelter for fish, structure for fishery spawning grounds, and congregation points for various marine fauna (S. Roberts et al., 2004; J. Roberts et al., 2009).

Deep-sea antipatharians (Order Antipatharia; hereafter referred to as black corals) are among the most common DSCs. Black corals are colonial cnidarians existing in all oceans in depths down to a maximum of 8000 m. They have dense populations in deep-sea biodiversity hotspots, such as seamounts and other hard substrata terrains (J. Roberts et al., 2009; Carreiro-Silva et al., 2013). Seven families of black corals have been recognized, with over 280 species

found in tropical and sub-polar aphotic environments, making them a diverse group within the global marine ecosystem (Brugler et al., 2013).

Black corals regularly appear upright and sentinel-like on the ocean floor, in clusters or as solitary structures. They are supported by a skeleton comprised of successive protein and chitin layers laid down around a central axis presenting pinnate, whip- like, bushy, and tree-like growth forms (Goldberg, 1991; Goldberg et al., 1994; Brugler et al., 2013; Opresko et al., 2014). Black corals filter-feed on organic carbon exported from the surface as either detrital matter or fresh sinking particulate organic matter, including fresh plankton cells (Roark et al., 2006; Roark et al., 2009; Sherwood et al., 2009; B. Williams et al., 2010). Generally, black corals exhibit slow radial growth (~5µm to 3mm/yr) and long lifespans of 100 years to 4500 years (Grange et al., 1993; Roark et al., 2009; Prouty et al., 2011; Carreiro-Silva et al., 2013; Prouty et al., 2015). Their growth rates contrast those of calcareous deep-sea corals, such as *Lophelia pertua* (7-25mm/yr; Freiwald et al., 1997). Much of the age and growth estimates for New Zealand's black corals are limited to those corals found in New Zealand's unique fjord environments or are on coral species known to have lifespans of centuries (*Bathypathes patula*; *Antipathella fiordensis*; Grange et al. (1993); Marriott et al. (2020)). However, New Zealand also hosts many colonies of the black coral *Leiopathes*, which exhibit slow growth (5µm/yr) over millennia in other parts of the world's oceans (Roark et al., 2009; Komugabe-Dixson et al., 2016).

The longevity and slow growth of black corals in deep-sea environments likely contributes to the vulnerability of New Zealand's deep-sea ecosystems to stressors (Clark et al., 2010a). Recent anthropogenic disturbances, such as bottom trawling, have proven to reduce ecological diversity and habitat distribution in New Zealand's DSC habitats over the last century (Clark et al., 2006; A. Williams et al., 2010; Clark et al., 2012). DSC's are also susceptible to natural disturbances, such as rapid sedimentation or tectonic activity (Hebbeln et al., 2019). Given that some of New Zealand's black corals may exhibit slow growth and extreme longevity, some corals may be particularly susceptible to any disturbance. Any life-history information that might help to evaluate how these corals recover from natural or anthropogenic impacts will further improve the efforts to conserve them.

Despite the recent awareness of the anthropogenic damage to New Zealand's deep-sea ecosystems (Clark et al., 2006; Clark et al., 2010a), the expected recovery of black coral communities to disturbances is poorly constrained due to limited estimates of New Zealand's

black coral age and growth. This study ages sub-samples of *Leiopathes*, *Antipathes* and *Antipathella Fiordensis* coral colonies collected from waters north and east of New Zealand and the southwest New Zealand fjords using a high-resolution suite of radiocarbon dates. We resolve New Zealand black coral growth rate variability at a spatial resolution an order of magnitude higher than previous studies to support the growing body of deep-sea coral life-history literature. Here we provide detailed estimates of New Zealand's black coral growth rate and longevity which may assist in evaluating the vulnerability of the black coral population to any disturbance, natural or anthropogenic.

2.3 Materials and Methods:

2.3.1 Sample Selection and Milling

Seven black coral colonies collected north, east and southwest of New Zealand were provided by the National Institute of Water (NIWA) Invertebrate Collection (Figures 2.1 & 2.2; Table 1; Supplemental Figures S2.1-7). Of the seven specimens supplied, four were identified to species level and three to genus level by Dennis Opresko (Smithsonian Museum) and Tina Molodtsova (Shirshov Institute) (Table 2.1).

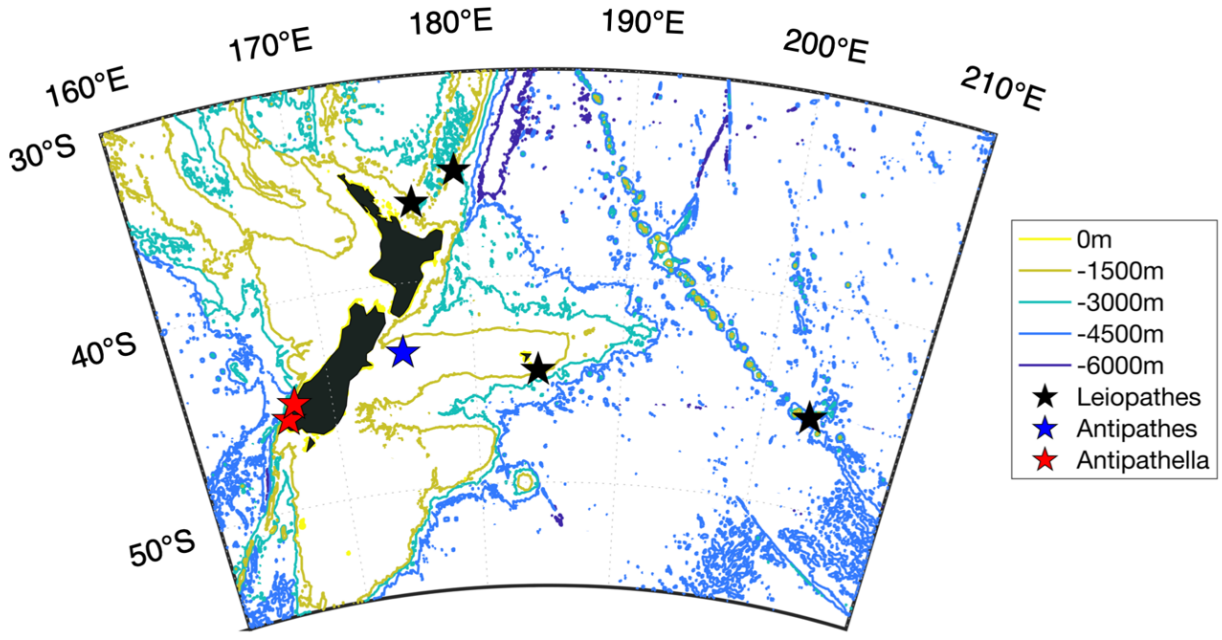

Figure 2.1: Black coral location map. A map of black coral locations (colored stars) overlaid on of bathymetry contour lines (data source: GEBCO Compilation Group 2019).

Table 2.1: Black coral information table. A table of black coral information complete with latitude, longitude, location, species, collection details, depth and diameter.

Sample ID	Latitude (°S)	Longitude (°E)	Location	Identifier	Species	Depth (m)	Diameter (mm)
NIWA35104	36.16	176.773	Bay of Plenty	Tina Molodtsova	*Leiopathes .spp*	738	55
NIWA64334	34.757	179.431	Bay of Plenty	Dennis Opresko	*Leiopathes secunda*	750	32
NIWA47966	44.563	184.316	South East Chatham Island	Dennis Opresko	*Leiopathes secunda*	758	20
NIWA15131	45.566	203.333	South Louisville Seamount Chain	Dennis Opresko	*Leiopathes .spp*	870	35
NIWA17107	45.651	166.808	Fiordland - Wet Jacket Arm, Breaksea Arm	Dennis Opresko	*Antipathella fiordensis*	35	33
NIWA17108	44.956	167.406	Fiordland - George Sound	Dennis Opresko	*Antipathella fiordensis*	34	20
NIWA80784	43.333	175.25	Mernoo Bank	Dennis Opresko	*Antipathes*	300-500	55

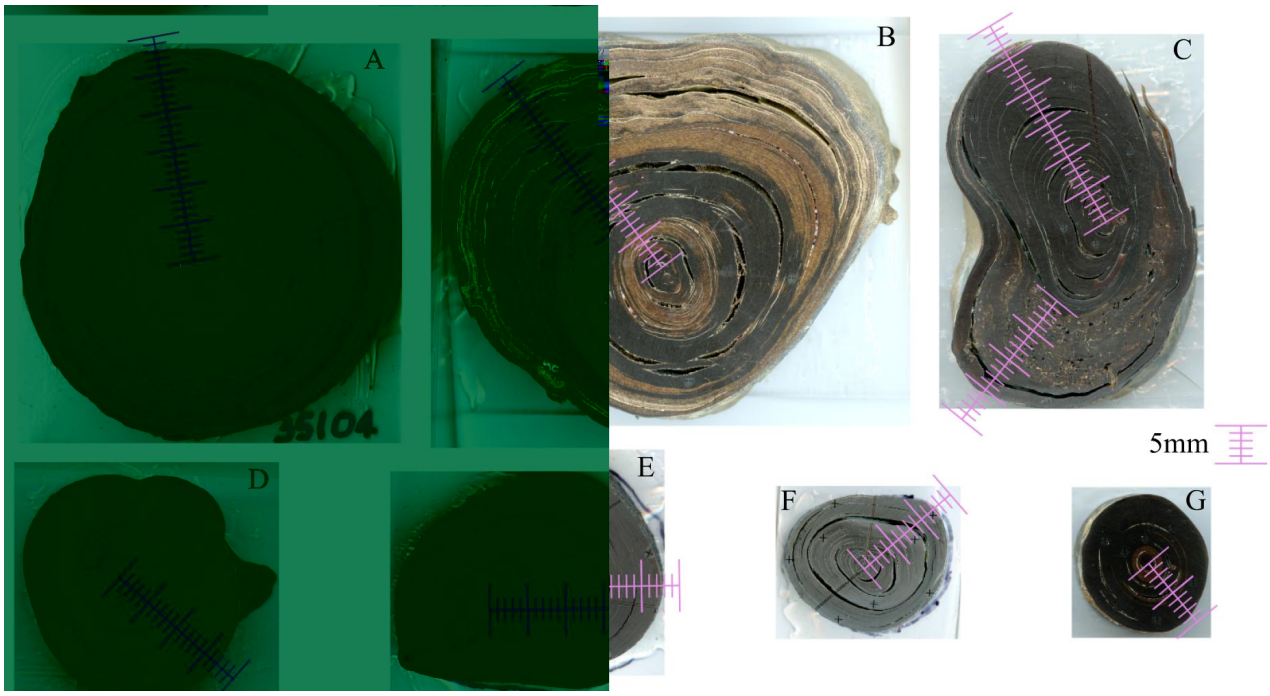

Figure 2.2: Black coral basal sections. Black coral basal sections prior to micro-milling. Reference axis are shown in purple. NIWA 35104 (Panel A), NIWA 80784 (Panel B), NIWA 15131 (Panel C), NIWA 17107 (Panel D), NIWA 64334 (Panel E), NIWA 47996 (Panel F), NIWA 17108 (Panel G)

Corals were prepared for geochemical analysis by cutting a 6-14mm thick section through the trunk near the base of each coral. Corals were sanded to a high polish using P60, P300, P1200, P2000 and P4000 grit sandpaper and coral sections were mounted on a microscope slide. Corals then had fine cross hairs ablated into the sampling surface for use as fiducial points and were scanned on a flatbed scanner at high resolution (4800 DPI) to create master images for use in plotting subsampling locations (Figure 2.2).

High-resolution coral images were loaded into the vector graphics program Inkscape and visible growth rings were digitized on the images. Multiple concentric rings were then generated by interpolation (to a nominal spacing of 50µm along a reference axis) and exported as digital

coordinates for upload to a bench-top scale Microproto Systems CNC MicroMill 2000HD-E (Chandler, Arizona, USA). The coral specimen was mounted on the mill, and milling profiles were calibrated using the fiducial points. Entire rings were then milled to a depth of 4mm, starting from the outside of the coral and working towards the center. Each milled ring generated between 0.1-25mg of powder, decreasing as milling progressed and ring circumference declined. The precision of milling profile alignment was estimated from the discrepancy between the distances measured between fidicual points on the mill compared with the scanned image and ranged from 4-34 μm. The largest sources of spatial error were found to be the accuracy with which fiducial points could be located on the mounted sample and a measurable swelling/contraction of the coral slabs, possibly resulting from changing moisture content. 17107 and 17108 were prepared in the same way as the others but were not milled on the micro mill. Instead, a smaller number of 3-4 mg subsamples were hand-drilled for radiocarbon analysis using a Dremel 3000 rotary tool (Mount Prospect, Illinois, USA).

2.3.2 Coral Dating

Radiocarbon measurements were made on ~1mg of powdered coral subsamples on a single-stage Accelerator Mass Spectrometer at the Australian National University Radiocarbon Laboratory following procedures outlined in Fallon et al. (2010) and Komugabe et al. (2014). Excess coral powders were archived for other geochemical analyses. Sub-samples from corals 35104, 47996, 64344, 15131 and 80784 were analyzed at intervals of 0.2-1mm, while inner, middle and outer samples were analyzed for corals 17107 and 17108. In areas where coral sample recovery was limited by coral geometry (i.e. small sample due to small coral circumference) two adjacent coral powder samples were combined to meet the required ~1mg of material for radiocarbon analysis. Milled powder samples were cleaned using <1ml of 0.1M HCl to remove acid-soluble contaminants (e.g. carbonate phases) that potentially hold younger contaminant ^{14}C. After cleaning, HCl was removed by pipette and samples were washed 3 times with >1ml of milliQ water. Coral samples were then frozen with dry ice and lyophilized to remove any residual moisture. Approximately 1mg of the cleaned coral sample was weighed into a 6mm OD quartz tube with ~60mg of CuO and a silver cup. Quartz tubes containing black coral samples were evacuated to <3e-3 torr and sealed with a torch. Quartz tubes were then baked at 900°C for 6 hours to generate CO_2. The resulting CO_2 was purified and converted to graphite with hydrogen and powdered Fe. The graphite was measured on the ANU single stage

accelerator mass spectrometer following standard procedures outlined in Fallon et al. (2010). Radiocarbon ages were corrected for isotopic fractionation using on-line AMS $\delta^{13}C$, normalized to Oxalic Acid I and background subtracted using ^{14}C free coal treated in the same manner as coral samples. Data are presented according to the recommendations of Stuiver et al. (1977) in the Appendix Table 1. Coral sample milling depth, $F^{14}C$, radiocarbon ages are presented for each coral sub-sample in the Appendix Table 1.

2.3.3 Post-Bomb Radiocarbon Calibration

Where the fraction of radiocarbon ($F^{14}C$) is > 1, radiocarbon ages were calibrated visually by comparing $F^{14}C$ coral data to $F^{14}C$ data from an otolith ^{14}C time series in Kalish, 1993 (Supp. Fig. S2.8). This is because calibration curves used to convert radiocarbon age to calendar age begin at 1950AD (formally defined as '0 years before present (BP)') and $F^{14}C$ values >1 indicate a calendar age after 1950AD. By comparing $F^{14}C$ with a known calendar age, such as otoliths, we can estimate unknown coral calendar ages using the similarities of two $F^{14}C$ curves (Sherwood et al., 2009). 80784 was collected live in 2012AD onboard the NIWA cruise TAN1201, and the outermost sample was assigned a calendar date of -62BP. $F^{14}C$ peaks in the Kalish, 1993 curve at 1980AD, and so the peak $F^{14}C$ value in the coral (1.0687) was assigned a calendar date of -30BP. The earliest rise in $F^{14}C$ in 80784 was assigned a calendar date of 0BP (1950AD). The calendar ages for samples in between the outermost sample, peak $F^{14}C$ sample and first bomb $F^{14}C$ sample were calculated through linear interpolation using their respective calendar ages as tie points (Supp. Fig. S2.8; Appendix Table 1). 17107 only had one radiocarbon date with an $F^{14}C$ value >1 and was not calibrated to calendar age visually using the Kalish 1993 otolith data as multiple $F^{14}C$ values >1 are needed to generate an age-depth model after 1950AD.

2.3.4 Pre-Bomb Radiocarbon Calibration

Radiocarbon ages for corals 35104, 47996, 64344, 15131, 80784 and 17108 with measured $F^{14}C$ <1 were individually calibrated to a calendar age using OxCal (v4.3; Bronk Ramsey, 2009) and the BACON Bayesian age-depth modelling program (v2.3; Blaauw et al., 2011) in conjunction with the Reimer et al. (2013) Marine13 curve (Appendix Table 1). Individual radiocarbon ages were converted to calendar age using OxCal (Figures 2.3 & 2.4) and age-depth models were generated using BACON to eliminate age reversals (Figure 2.4, Supp. Figs. S2.9-15). All BACON calculations used a thick value of 0.2, a memory strength value of 4,

a mean memory value of 0.7 and an accumulation shape of 1.5. 35104, 47996, 64344 and 15131 were calculated using an accumulation rate of 100yrs/1mm based on the assumption of lower growth rates in *Leiopathes* corals (5um/yr; Roark et al., 2009; Komugabe-Dixson et al., 2016) and 17107, 17108 and 80784 were calculated using an accumulation rate of 10yrs/1mm based on the assumption of higher growth rates in *Antipathes* and *Antipathella Fiordensis* corals (100-1000um/yr; Grange et al., 1988; Love et al., 2007). The resulting BACON calendar age vs. sampling depth curves are shown in Supp. Figures S2.9-15.

The OxCal and BACON calibrations included corrections for the known local marine radiocarbon age deviations (ΔR). The corals sampled north of New Zealand (35104 and 64344) were calibrated with ΔR values of 39 ± 31 from Sikes et al. (2000). 47996 from the Chatham Islands was calibrated with ΔR values of 69 ± 14 from Petchey et al. (2008) and 80784 from Mernoo Bank was calibrated with ΔR values of 104 ± 14 from Petchey et al. (2008). 15131 was not calibrated with any ΔR data as there are no ΔR data available in a 5ºx5º grid centered around the sample location. 17107 and 17108 were calibrated with ΔR values of 59 ± 35 from Hinojosa et al. (2015). We note that ΔR can change through time (Hinojosa et al., 2015; Komugabe-Dixson et al., 2016) and will be the subject of future publications.

2.3.5 Lifespan and Growth Rate Calculations

Black coral lifespans were determined by subtracting a coral's outermost age from its innermost age using median calibrated calendar ages from OxCal (Figure 2.3; Bronk Ramsey, 2009). Radial growth rates were calculated by dividing the age difference between samples by the linear distance between them. In this case, the calculation used the median calibrated calendar ages derived from BACON rather than the OxCal ages. This is because BACON forces a monotonic progression of ages using a gamma autoregressive Markov Chain Monte Carlo process where n=2,000 (Blaauw et al., 2011), avoiding the problem with age reversals that appear in the individually calibrated OxCal dates (Figure 2.4). Hereafter all growth rate metrics presented explicitly use BACON ages, although radial growth rates from OxCal and BACON are presented concurrently in the Appendix Table 1 for completeness.

2.4 Results:

2.4.1 Radiocarbon Ages

Coral $F^{14}C$ values ranged from the lowest concentrations in the cores to the highest concentrations at the edge (Appendix Table 1). Across all corals, the lowest $F^{14}C$ value was found in 15131 (0.6738 ± 0.0019) and was highest in 17107 (1.0814 ± 0.0021). We observe $F^{14}C$ reversals in corals with high spatial sampling. We observe fifty-one $F^{14}C$ reversals in 35104, six reversals in 47996, twenty-two reversals in 64344, six reversals in 15131 and eight reversals in 80784 (Table 2.2, Appendix Table 1). All the $F^{14}C$ reversals are outside analytical error (1σ). No $F^{14}C$ reversals were observed in 17107 and 17108 (Table 2.2). We presume these $F^{14}C$ reversals are due, in part, to the variable production of ^{14}C in the atmosphere over the last 3000 years, a variable ΔR value through time at the coral's location (Sikes et al., 2000), and the high spatial resolution of our samples in the *Leiopathes* corals (~200μm).

2.4.2 Colony Lifespans:

New Zealand black corals show a high degree of longevity. Our black coral lifespans range from 91 to 2611 years and are consistent with other studies that find black corals exhibit exceedingly long lifespans on the order of centuries to millennia (Figures 2.3 & 2.4; Table 2.2; Grange et al., 1993; Love et al., 2007; Roark et al., 2009; Carreiro-Silva et al., 2013). All four *Leiopathes* corals spanned at least one millennium and the *Antipathes* and *Antipathella fiordensis* corals spanned at least one century.

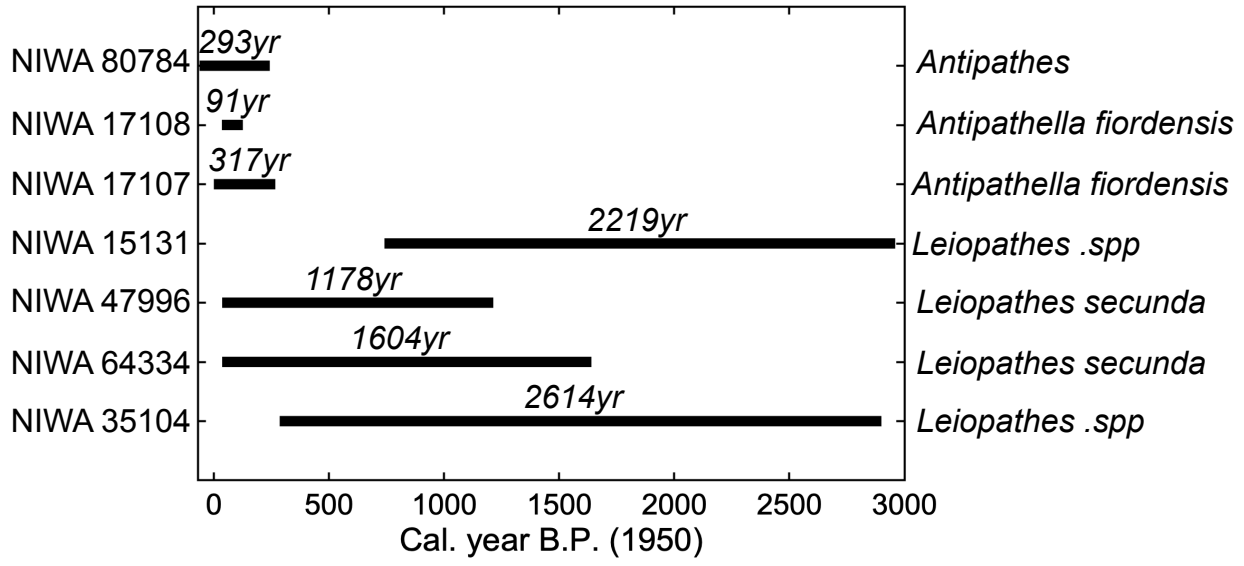

Figure 2.3: Black coral lifespans. Black coral lifespans, inner (core) and outer (edge) OxCal calibrated radiocarbon dates are used to determine the lifespan each coral (above black bars), complete with identification information.

Table 2.2: Black coral radiocarbon aging and growth rate table. A table of black coral radiocarbon dating information complete with the number of ^{14}C dates, the number of $F^{14}C$ reversals, ^{14}C age range, OxCal calibrated calendar age range and BACON radial growth rates. OxCal calibrated radiocarbon dates are shown in Years Before Present (B.P.), where B.P. is defined at 1950CE.

Sample ID	# of ^{14}C Dates	# of $F^{14}C$ Reversals	^{14}C Age	OxCal Cal. Year B.P. (1950)	BACON Radial Growth Rate (um/yr)
NIWA35104	136	51	3164-679	2900-286	1.3 - 40.0
NIWA64334	68	22	2108-11	1640-36	7.9 - 17.1
NIWA47966	42	6	1713-235	1214-36	5.5 - 14.7
NIWA15131	34	6	3172-1207	2960-741	10.8 - 32.5
NIWA17107	3	0	615-Modern	267-Modern	57
NIWA17108	3	0	505-306	126-35	50.0 - 51.3
NIWA80784	28	8	847-Modern	243-Present	90.9 - 142.9

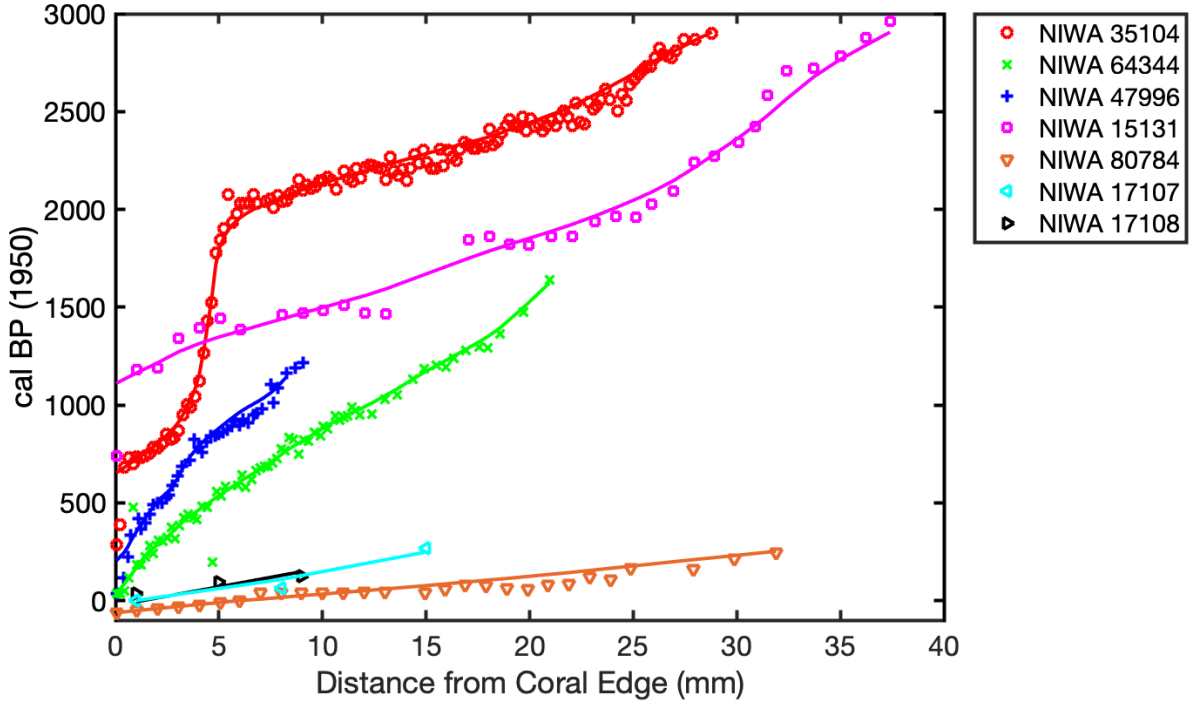

Figure 2.4: Black coral age-depth models. OxCal calibrated coral radiocarbon ages (colored markers) against distance from the coral's edge. BACON age-depth curves (smooth lines) are plotted overtop the OxCal calibrated radiocarbon ages (symbols)

2.4.3 Radial Growth Rates

Our calculated black coral growth rates show slow radial growth in *Leiopathes*, *Antipathes* and *Antipathella Fiordensis* corals. *Leiopathes* radial growth rates in samples 35104, 47996, 64344 and 15131, vary from 1.3 to 40.0 µm/yr, 7.9 to 17.1µm/yr, 5.5 to 14.7µm/yr, and

10.8 to 32.5 µm/yr, respectively (Figure 2.5, Appendix Table 1). *Antipathes* radial growth rates in 80784 ranges from 90.9-142.9µm/yr and *Antipathella fiordensis* growth rates range from 50.4-51.9µm/yr, respectively (Figure 2.5, Appendix Table 1). We note that our *Leiopathes* and *Antipathes* sampling regimen is of a significantly higher spatial resolution than most deep-sea coral aging studies allowing us to resolve growth rate variability much better than other studies (1 date/15-30 years vs. ~1 date/300yr; Roark et al., 2009; Carreiro-Silva et al., 2013).

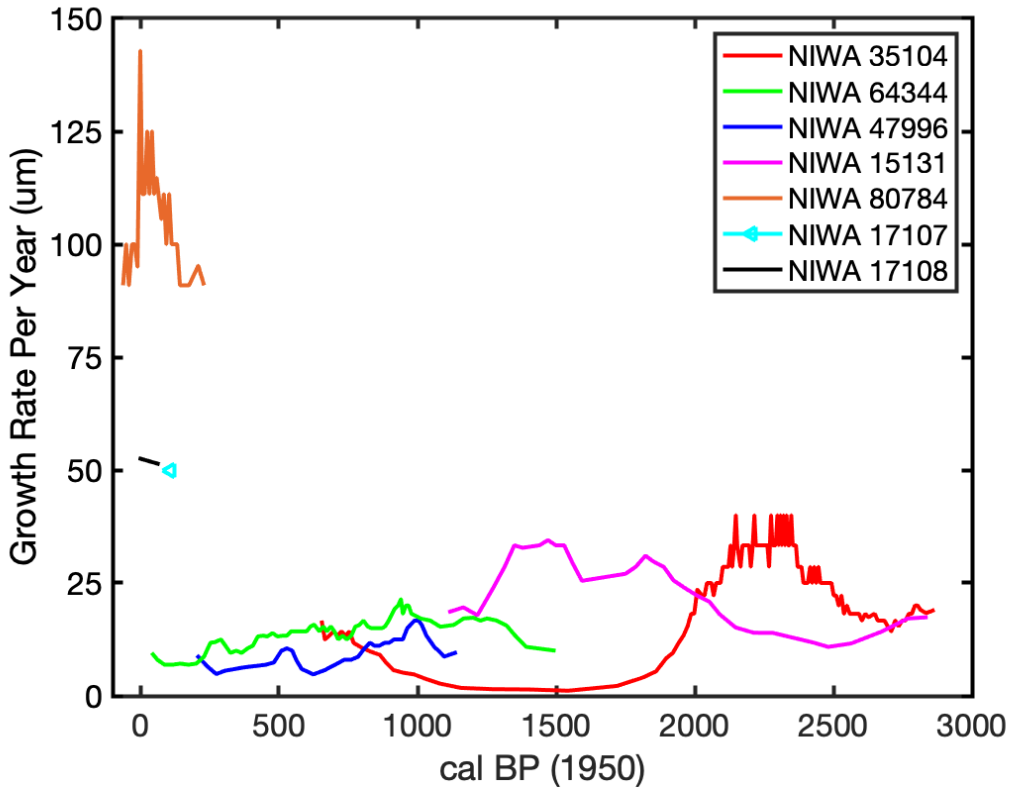

Figure 2.5: Black coral growth rates. Coral growth rates as a function of time over each coral's lifespan (multiple colors). Growth rates shown here use the BACON calibrated calendar age estimates.

2.5 Discussion

2.5.1 New Zealand Black Coral Longevity

Lifespan estimates presented here show that New Zealand's black coral colonies can live for millennia. *Leiopathes* corals exhibited millennial lifespans (1178 to 2614 years) and *Antipathes* and *Antipathella fiordensis* corals exhibited centennial lifespans (158 to 274 years) (Figures 2.3 & 2.4). Our colony ages are consistent with previous age estimates of *Leiopathes*

(Roark et al., 2009; Carreiro-Silva et al., 2013; Komugabe-Dixson et al., 2016), *Antipathes* (Love et al., 2007) and Fiordland black corals (Grange et al., 1993).

2.5.2 Black Coral Growth Rates

Long-term radial growth rates for New Zealand *Leiopathes* and *Antipathes* black corals collectively range from 1.3-40.0µm/yr and from 44-142.9µm/yr, respectively (Figure 2.5; Appendix Table 1). These results support previous work that suggests *Leiopathes* corals are the slowest growing deep-sea coral known (~5 to 22µm/yr; Roark et al. (2009); Prouty et al. (2011)) and accord with previously published *Antipathes* growth rates (100-125µm/yr - Love et al. (2007); 180-1140µm/yr - Roark et al. (2006)). Previous *Leiopathes* and *Antipathes* growth estimates are limited to the north Pacific, Gulf of Mexico and Tasman Sea (Roark et al., 2009; Prouty et al., 2011; Komugabe-Dixson et al., 2016) and our growth rates now extend those observations in the southwest Pacific Ocean. As an aside, the fact that *Antipathes* and *Leiopathes* average growth rates are quite distinct, despite being measured in a wide range of oceanographic settings, suggests that physiology may be the primary control. However, we do not have sufficient data to rule out environmental conditions (e.g. food supply) imposing an important secondary control over growth.

Our growth rate for *Antipathella fiordensis* (~50µm/yr) is about one half to one quarter the growth rates published by Grange et al. (1993) which were based on growth-band counting and cross-section autoradiography (98.4-176µm/yr). The Grange et al. (1993) growth rate estimates assumed that growth bands were deposited annually however a recent aging study on the black coral *Bathypathes patula* calls into question the accuracy of using growth bands as a universal black coral age chronometer (Marriott et al., 2020). We are not aware of any other radiometric growth-rate estimates that could corroborate our *Antipathella fiordensis* growth rate measurements. We note that radiocarbon ages are subject to uncertainties due to fluctuations in marine ^{14}C over the last several centuries (Stuiver et al., 1993; Reimer et al., 2013), and radiocarbon age ambiguities may account for the discrepancy between our results and those of Grange et al. (1993).

We note an appreciable difference in growth rate and longevity between *Leiopathes* and the other black corals in our study (*Antipathes*, and *Antipathella fiordensis*). The *Antipathella fiordensis* specimens came from the shallow and highly productive fjords of Fiordland and grew much faster than the deeper open-ocean *Leiopathes* corals (Table 2.1, Figures 2.4 & 2.5).

Although satellite Chl-a measurements are unreliable in Fiordland due to cloud cover and turbidity, Chl-a concentrations in the adjacent Tasman Sea range from 0.65-12.32 mg/m^3 (Pinkerton, 2016). In contrast, Chl-a concentrations range from 0.3-0.48 mg/m^3 in the Bay of Plenty and Chatham Islands to 0.03-0.3 mg/m^3 in the central Pacific (Pinkerton, 2016). This represents a 2-25x higher productivity (and by inference food supply) for black corals in Fiordland compared with other New Zealand coral localities. The *Antipathes sp.* specimen from the Chatham Rise (specimen 80784) grew at similar rates to the *Antipathella fiordensis* corals, despite living in much deeper but similarly productive waters as the *Leiopathes* corals.

2.5.3 Examining Specific Black Coral Growth Patterns

Growth rates in our black corals can be highly variable through their lifespans (Figure 2.5). Roark et al. (2009) suggests that a high initial growth rate in *Leiopathes* could be advantageous for a colony to establish itself. However, our results do not corroborate this, showing mixed growth rates during the early stages of *Leiopathes* life (Figures 2.4 & 2.5). 35104, 64344 and 15131 all show *slower* growth rates during their early life (Figure 2.5). 47996 is the only *Leiopathes* coral that shows fast growth early in life followed by a period of slow growth (Figure 2.5). Variability in growth may therefore be random or responding to microenvironmental factors; however, determining factors that control black coral growth rate variability is beyond the scope of this study.

2.5.3.1 Leiopathes Specimen 35104 – Bay of Plenty

35104 shows the most variable growth rate over its lifespan. From 2906-2148 BP, it grew at ~27µm/yr, peaking at 40µm/yr in 2148 BP. However; from 2148-823 BP the growth rate declined significantly, falling to 1.1µm/yr in 1548 BP before rising to 10µm/yr by 823 BP. (Figures 2.4 & 2.5; Supp. Fig. S2.9; Appendix Table 1). A change in growth of this magnitude has not been reported for any other *Leiopathes* coral, although we are not aware of any study with a comparable sampling resolution (mean date resolution is 1 date/15 years). We considered the possibility that the apparent slowing of growth was merely an artefact of imprecise sampling across a hiatus, and that the skeleton simply stopped accreting around 2148 BP (e.g. because tissue was retracted or removed at the base of the trunk). However, we rule this out because the zone of growth rate reduction spans ~5000µm which is very large compared with the precision of our sampling (±21µm, 1σ). It appears that coral grew continuously for 2100 years, but after 750 years of fast accretion, its growth suddenly declined and stayed low for another 1350 years.

We speculate that this could represent a traumatic event, such as starfish grazing or the loss of a branch, which would reduce energy availability to the coral, resulting in low skeletal accretion at the base where the coral was subsampled (Frank Parrish, Tina Molodostova, pers. comm). However, we cannot eliminate other explanations such as a sudden change in the local growth environment.

2.5.3.2 Leiopathes Specimen 15131 - Louisville Seamount Chain

15131 exhibits an unusual skeletal patterns and texture between 1mm and 15 mm from the outside edge (Figures 2.2 & 2.6B; See Supplemental Text). Rather than simple concentric rings forming a solid skeleton, the growth bands become convoluted and cryptic with many small pores of approximately 2-20 um diameter. We do not attribute this porosity and lack of laminar banding to diagenetic alteration. Proteinaceous coral skeletons and their material are thought to be resistant to diagenetic alteration of $\delta^{13}C$ and ^{14}C (Goldberg et al., 1994; Sherwood et al., 2009; Strzepek et al., 2014).

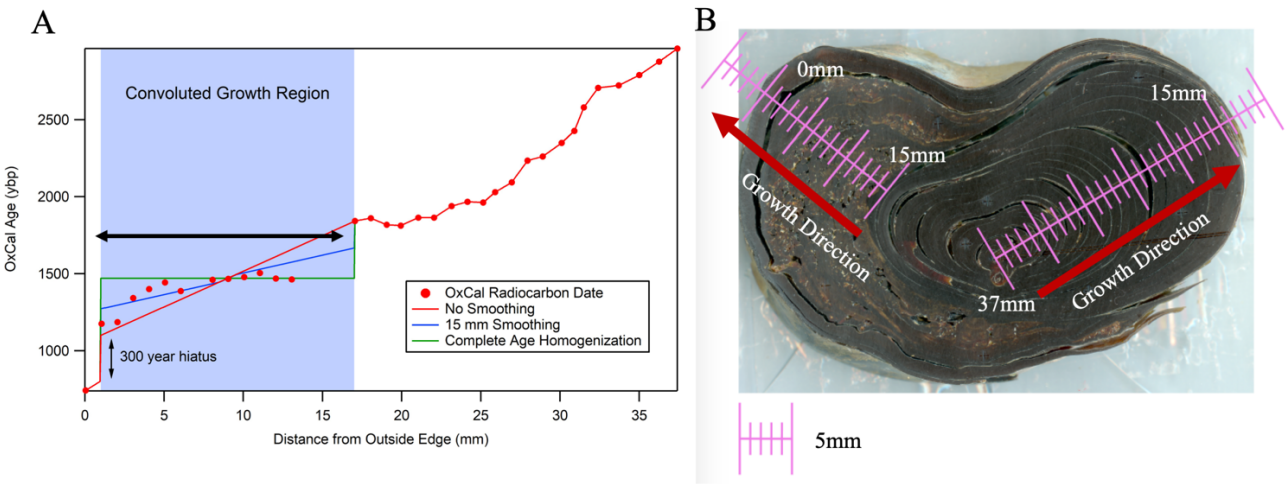

Figure 2.6: 15131 Age-Smoothing Model. (Left Panel) Models of age smoothing within the convoluted growth region of coral 15131. The measured ages are shown as red dots. The default (unsmoothed) model assumes that the coral grew continuously through the convoluted region (red line) except for a 300-year hiatus at ~ 1mm (which is needed to match models to the observed ages. The smoothed models then assume that ages within the convoluted growth region (blue box) are smoothed by a running average. The blue line represents a smoothing across 15 mm of coral (i.e. nearly the whole width of the convoluted region). The green line represents a complete breakdown of stratigraphy within the convoluted region such that the ages are completely homogenized. (Right Panel) An image of NIWA 15131 labeled with the different sampling transects and the direction of coral growth. The minimum and maximum sampling depths for each transect are shown in white.

We instead hypothesize that the convoluted growth may result from a secondary colonization of the black coral by a zoantharian (Figures 2.2 & 2.6B, Supp. Fig. S2.4). Analysis of the coral skeleton by Frederic Sinniger (University of the Ryukyus) showed Zoanthid polyps

on the outer portion of the convoluted growth. When Zoanthids first settle on a host, a period of rapid growth ensues to overwhelm the original coral, with the resulting morphology usually being a simplified form of the host (Frederic Sinniger pers. comm.; Frank Parrish pers. comm.; Carreiro-Silva et al., 2017). This is consistent with the changed growth direction, porosity and lack of laminar banding seen in 15131.

It is possible that the observed radiocarbon growth profile originates from smoothing of ages within the convoluted growth region rather than rapid growth. Where growth bands are simple concentric rings, it is possible to accurately mill along bands resulting in little or no age-smoothing. However, in the region of convoluted growth it was impossible to follow the anastomosing bands, and milling paths were crosscut across multiple bands, smoothing the ages.

To evaluate the possibility of milled age smoothing, we set up a simple simulation of smoothing across the convoluted growth (Figure 2.6A). The model reproduces the age steps and apparent faster growth rate in the convoluted region. However, to reproduce the 400-year age gaps observed, the smoothing has to be extreme: essentially a complete breakdown of stratigraphic ordering within the full 16 mm thickness of the convoluted region. This does not accord with our observations of coarse banding within the convoluted region on ~ 5mm distance scales. Band averaging over 5 mm scales would only produce age steps of ~ 100 years. We conclude that at least some of the apparent increase in growth rate across the convoluted region may be real, which is consistent with the fast-growth stage of a secondary zoantharian colonization. However, we acknowledge that coral bands were likely crosscut over this interval and so growth rates may be artificially elevated by up to 25%.

2.5.4 The Paleoceonographic Potential for New Zealand Black Corals

The millennial lifespans demonstrated by New Zealand black corals further establishes proteinaceous deep-sea corals as an archive capable of reconstructing decadal ocean changes over thousands of years (Prouty et al., 2014; Prouty et al., 2015; Komugabe-Dixson et al., 2016). Coral growth rates are fast enough (>5μm/yr) to allow decadal-scale geochemical information to be extracted from their skeletons using the micromilling techniques presented here (e.g. Prouty et al., 2014; Prouty et al., 2015; Komugabe-Dixson et al., 2016).

The long life and potential for high-resolution data make New Zealand's black corals an attractive paleoceonographic archive for the southwest Pacific. A large portion of

paleoceanographic work from around New Zealand relies on sediment cores, which are capable of elucidating changes on thousand-to-million year timescales timescales (Cortese et al., 2013; Bostock et al., 2015; Bostock et al., 2019). However, sediment cores have several limitations for studying paleoclimate at higher resolutions. They accumulate slowly and are subject to bioturbation, both of which compromise the fidelity of the records which could be extracted. This has created a critical gap in high resolution ocean proxy data from New Zealand which compromises our understanding of natural ocean change in the decades to centuries prior to instrumental records. Black corals could assist in filling this gap in the same way they have been used in other parts of the global oceans (Prouty et al., 2014; Prouty et al., 2015; Komugabe-Dixson et al., 2016).

2.5.5 Implications for Marine Conservation

Deep sea corals are key species in the deep-sea benthic ecology, providing habitats, spawning grounds and congregation points for major fisheries species and other deep-marine organisms (J. Roberts et al., 2009). These environments are characterized by their low energy and high stability compared with the surface ocean, and this quiescence has allowed the evolution of organisms like black corals with extremely slow growth and longevity. Unfortunately, these traits mean that black coral communities could take – at minimum – centuries to recover from major environmental disturbances from anthropogenic activities or natural seafloor disturbances such as abrupt sedimentation or turbidity.

The longevity and slow growth we report in this paper supports other studies cautioning that New Zealand's benthic communities have relatively low resilience to ecosystem disturbances (Clark et al., 2019). Deep-sea mining, fishing and other commercial activities have caused considerable damage to black coral communities in areas such as the Gulf of Mexico, the north Pacific and the Caribbean (Grigg, 2001; Bruckner, 2014; Gress et al., 2018). Clark et al. (2010a) estimates that in as few at 10 bottom trawls, coral cover can be reduced in an area down to 0-20% (no visible cover). Bottom trawling has already caused considerable damage to deep-sea coral communities in New Zealand (Clark et al., 2010a; Clark et al., 2019), Tasmania (Althaus et al., 2009) and the northeast Atlantic (Hall–Spencer et al., 2002; Hall-Spencer et al., 2007) among other parts of the global oceans (Clark et al., 2010b). Although New Zealand's black corals are not known to be immediately threatened with extinction, protection of these

communities from environmental stressors is important due to their high susceptibility to disturbance.

2.6 Conclusions:

The extreme longevity and growth rate estimates we present here for New Zealand black corals are consistent with other age estimates of black corals in the global ocean. Our growth estimates are of a higher resolution than other coral aging studies, allowing us to resolve rapid changes in growth rate. Our growth rate results imply that New Zealand black corals which grow faster than 10μm/yr can reconstruct decadal-scale paleoceanographic data using conventional geochemical proxies and micromilling techniques (Prouty et al., 2014; Prouty et al., 2015; Komugabe-Dixson et al., 2016). However, our growth rate and longevity estimates also imply that the New Zealand black coral community is highly susceptible to natural or anthropogenic disturbances.

2.7 Acknowledgements:

Black corals were provided by the National Institute of Water and Atmosphere Invertebrate Collection. We wish to thank Sadie Mills and Dianna Macpherson for assistance with access, providing a space to sub-sample coral sections and navigating CITES permitting. Black coral micro-milling was accommodated by the National Institute of Water and Atmosphere Stable Isotope Facility. We wish to thank Gordon Brailsford, Tony Bromley, Colin Nankivell and Sally Gray for access to laboratory space for micro-milling. Funding for this work was provided by the New Zealand Royal Society Marsden Fund Grant No. NIWA1602 awarded to HLN, DJS, SJF and AKD. Seed funding was provided by URF 210024 awarded to DJS. The authors declare no conflicts of interest.

2.8 References:

Althaus, F., Williams, A., Schlacher, T. A., Kloser, R. J., Green, M. A., Barker, B. A., et al. (2009). Impacts of bottom trawling on deep-coral ecosystems of seamounts are long-lasting. *Marine Ecology Progress Series, 397*, 279-294. https://www.int-res.com/abstracts/meps/v397/p279-294

Blaauw, M., & Christen, J. A. (2011). Flexible paleoclimate age-depth models using an autoregressive gamma process. *Bayesian Anal., 6*(3), 457-474. https://projecteuclid.org:443/euclid.ba/1339616472

Bostock, H. C., Hayward, B. W., Neil, H. L., Sabaa, A. T., & Scott, G. H. (2015). Changes in the position of the Subtropical Front south of New Zealand since the last glacial period. *Paleoceanography, 30*(7), 824-844. http://dx.doi.org/10.1002/2014PA002652

Bostock, H. C., Prebble, J. G., Cortese, G., Hayward, B., Calvo, E., Quirós-Collazos, L., et al. (2019). Paleoproductivity in the SW Pacific Ocean During the Early Holocene Climatic Optimum. *Paleoceanography and Paleoclimatology, 34*(4), 580-599. https://doi.org/10.1029/2019PA003574

Bronk Ramsey, C. (2009). Bayesian Analysis of Radiocarbon Dates. *Radiocarbon, 51*(1), 337-360. https://www.cambridge.org/core/article/bayesian-analysis-of-radiocarbon-dates/F622173B70F9C1597F2738DEFC597114

Bruckner, A. (2014). *Advances in management of precious corals in the family Corallidae: Are new measures adequate?* (Vol. 7).

Brugler, M. R., Opresko, D. M., & France, S. C. (2013). The evolutionary history of the order Antipatharia (Cnidaria: Anthozoa: Hexacorallia) as inferred from mitochondrial and nuclear DNA: implications for black coral taxonomy and systematics. *Zoological Journal of the Linnean Society, 169*(2), 312-361. https://doi.org/10.1111/zoj.12060

Carreiro-Silva, M., H Andrews, A., Braga Henriques, A., de Matos, V., Porteiro, F., & Santos, R. (2013). *Variability in growth rates of long-lived black coral Leiopathes sp. from the Azores (Northeast Atlantic)* (Vol. 473).

Carreiro-Silva, M., Ocaña, O., Stanković, D., Sampaio, Í., Porteiro, F. M., Fabri, M.-C., & Stefanni, S. (2017). Zoantharians (Hexacorallia: Zoantharia) Associated with Cold-Water Corals in the Azores Region: New Species and Associations in the Deep Sea. *Frontiers in Marine Science, 4*(88). Original Research. https://www.frontiersin.org/article/10.3389/fmars.2017.00088

Clark, M. R., Bowden, D. A., Baird, S. J., & Stewart, R. (2010a). *Effects of fishing on the benthic biodiversity of seamounts of the 'Graveyard' complex, northern Chatham Rise* (Vol. 46).

Clark, M. R., Bowden, D. A., Rowden, A. A., & Stewart, R. (2019). Little Evidence of Benthic Community Resilience to Bottom Trawling on Seamounts After 15 Years. *Frontiers in Marine Science, 6*(63). Original Research. https://www.frontiersin.org/article/10.3389/fmars.2019.00063

Clark, M. R., & Dunn, M. R. (2012). Spatial management of deep-sea seamount fisheries: balancing sustainable exploitation and habitat conservation. *Environmental Conservation,*

39(3), 204-214. https://www.cambridge.org/core/article/spatial-management-of-deepsea-seamount-fisheries-balancing-sustainable-exploitation-and-habitat-conservation/39981251A8A01633542642FCA6B90ED6

Clark, M. R., & Tittensor, D. (2010b). *An index to assess the risk to stony corals from bottom trawling on seamounts* (Vol. 31).

Clark, M. R., Tittensor, D., Rogers, A. D., Brewin, P., Schlacher, T., Rowden, A., et al. (2006). Seamounts, deep-sea corals and fisheries: vulnerability of deep-sea corals to fishing on seamounts beyond areas of national jurisdiction. In: UNEP-WCMC.

Cortese, G., Dunbar, G. B., Carter, L., Scott, G., Bostock, H., Bowen, M., et al. (2013). Southwest Pacific Ocean response to a warmer world: Insights from Marine Isotope Stage 5e. *Paleoceanography, 28*(3), 585-598. https://doi.org/10.1002/palo.20052

Fallon, S., Fifield, L., & Chappel, J. (2010). The next chapter in radiocarbon dating at the Australian National University: Status report on the single stage AMS. *Nuclear Instruments and Methods in Physics Research: Section B, 268*(7-8), 898-901.

Freiwald, A., Henrich, R., & Pätzold, J. (1997). Anatomy of a deep-water coral reef from Stjernsund, West Finmark, Northern Norway. *Cool-Water Carbonates, 56*.

Goldberg, W. M. (1991). Chemistry and structure of skeletal growth rings in the black coral Antipathes fiordensis (Cnidaria, Antipatharia). *Hydrobiologia, 216*(1), 403-409. journal article. https://doi.org/10.1007/BF00026493

Goldberg, W. M., Hopkins, T. L., Holl, S. M., Schaefer, J., Kramer, K. J., Morgan, T. D., & Kim, K. (1994). Chemical composition of the sclerotized black coral skeleton (Coelenterata: Antipatharia): a comparison of two species. *Comparative Biochemistry and Physiology Part B: Comparative Biochemistry, 107*(4), 633-643. http://www.sciencedirect.com/science/article/pii/030504919490197X

Grange, K. R., & Goldberg, W. M. (1993). Chronology of black coral growth bands: 300 years of environmental history. *Batershill CN, Schiel DR, Jones GP, Creese RG, MacDiamid AB, Proceedings of the 2nd International Temperature Reef Symposium*.

Grange, K. R., & Singleton, R. J. (1988). Population structure of black coral, Antipathes aperta, in the southern fiords of New Zealand. *New Zealand Journal of Zoology, 15*(4), 481-489. https://doi.org/10.1080/03014223.1988.10422628

Gress, E., & Andradi-Brown, D. A. (2018). Assessing population changes of historically overexploited black corals (Order: Antipatharia) in Cozumel, Mexico. *PeerJ, 6*, e5129-e5129. https://www.ncbi.nlm.nih.gov/pubmed/30013832

https://www.ncbi.nlm.nih.gov/pmc/PMC6035717/

Grigg, R. W. (2001). *Black Coral: History of a Sustainable Fishery in Hawai'i* (Vol. 55).

Hall-Spencer, J., Rogers, A., Davies, J., & Foggo, A. (2007). *Deep-sea coral distribution on seamounts, oceanic islands, and continental slopes in the Northeast Atlantic* (Vol. 81).

Hall–Spencer, J., Allain, V., & Fosså Jan, H. (2002). Trawling damage to Northeast Atlantic ancient coral reefs. *Proceedings of the Royal Society of London. Series B: Biological Sciences, 269*(1490), 507-511. https://doi.org/10.1098/rspb.2001.1910

Hebbeln, D., Portilho-Ramos, R. d. C., Wienberg, C., & Titschack, J. (2019). The Fate of Cold-Water Corals in a Changing World: A Geological Perspective. *Frontiers in Marine Science, 6*(119). Mini Review. https://www.frontiersin.org/article/10.3389/fmars.2019.00119

Hinojosa, J. L., Moy, C. M., Prior, C. A., Eglinton, T. I., McIntyre, C. P., Stirling, C. H., & Wilson, G. S. (2015). Investigating the influence of regional climate and oceanography on marine radiocarbon reservoir ages in southwest New Zealand. *Estuarine, Coastal and Shelf Science, 167*, 526-539. http://www.sciencedirect.com/science/article/pii/S027277141530127X

Komugabe, A. F., Fallon, S. J., Thresher, R. E., & Eggins, S. M. (2014). Modern Tasman Sea surface reservoir ages from deep-sea black corals. *Deep Sea Research Part II: Topical Studies in Oceanography, 99*(Supplement C), 207-212. http://www.sciencedirect.com/science/article/pii/S0967064513002154

Komugabe-Dixson, A. F., Fallon, S. J., Eggins, S. M., & Thresher, R. E. (2016). Radiocarbon evidence for mid-late Holocene changes in southwest Pacific Ocean circulation. *Paleoceanography, 31*(7), 971-985. http://dx.doi.org/10.1002/2016PA002929

Love, M., Yoklavich, M., Black, B., & Andrews, A. (2007). *Age of black coral (Antipathes dendrochristos) colonies, with notes on associated invertebrate species* (Vol. 80).

Marriott, P., Tracey, D. M., Bostock, H., Hitt, N., & Fallon, S. J. (2020). Ageing Deep-Sea Black Coral Bathypathes patula. *Frontiers in Marine Science, 7*(479). Original Research. https://www.frontiersin.org/article/10.3389/fmars.2020.00479

Opresko, D. M., Tracey, D. M., & Mackay, E. (2014). *Antipatharia (Black Corals) for the New Zealand Region: A Field Guide of Commonly Sampled New Zealand Black Corals Including Illustrations Highlighting Technical Terms and Black Coral Morphology*: Ministry for Primary Industries.

Petchey, F., Anderson, A., Hogg, A., & Zondervan, A. (2008). The marine reservoir effect in the Southern Ocean: An evaluation of extant and new ?R values and their application to archaeological chronologies. *Journal of the Royal Society of New Zealand, 38*(4), 243-262. https://doi.org/10.1080/03014220809510559

Pinkerton, M. H. (2016). Ocean colour satellite observations of phytoplankton in the New Zealand EEZ, 1997-2016. *Ministry for the Environment. Wellington: NIWA*. Report.

Prouty, N. G., Roark, E., Buster, N., & Ross, S. (2011). *Growth rate and age distribution of deep-sea black corals in the Gulf of Mexico* (Vol. 423).

Prouty, N. G., Roark, E. B., Andrews, A., Robinson, L., Hill, T., Sherwood, O., et al. (2015). *Age, growth rates, and paleoclimate studies of deep sea corals*. Retrieved from http://pubs.er.usgs.gov/publication/70103075

Prouty, N. G., Roark, E. B., Koenig, A. E., Demopoulos, A. W. J., Batista, F. C., Kocar, B. D., et al. (2014). Deep-sea coral record of human impact on watershed quality in the Mississippi River Basin. *Global Biogeochemical Cycles, 28*(1), 29-43. http://dx.doi.org/10.1002/2013GB004754

Reimer, P. J., Bard, E., Bayliss, A., Beck, J. W., Blackwell, P. G., Ramsey, C. B., et al. (2013). IntCal13 and Marine13 Radiocarbon Age Calibration Curves 0–50,000 Years cal BP. *Radiocarbon, 55*(4), 1869-1887. https://www.cambridge.org/core/article/intcal13-and-marine13-radiocarbon-age-calibration-curves-050000-years-cal-bp/FB97C1341F452BD6A410C6FE4E28E090

Roark, E. B., Guilderson, T. P., Dunbar, R. B., Fallon, S. J., & Mucciarone, D. A. (2009). Extreme longevity in proteinaceous deep-sea corals. *Proceedings of the National Academy of Sciences, 106*(13), 5204-5208. http://www.pnas.org/content/106/13/5204.abstract

Roark, E. B., Guilderson, T. P., Dunbar, R. B., & Ingram, B. L. (2006). Radiocarbon-based ages and growth rates of Hawaiian deep-sea corals. *Marine Ecology Progress Series, 327*, 1-14. http://www.jstor.org/stable/24870713

Roberts, J., Wheeler, A., Freiwald, A., & Cairns, S. (2009). *Cold Water Corals: The Biology and Geology of Deep-Sea Coral Habitats*.

Roberts, S., & Hirshfield, M. (2004). Deep-Sea Corals: Out of Sight, but No Longer out of Mind. *Frontiers in Ecology and the Environment, 2*(3), 123-130. http://www.jstor.org/stable/3868237

Sherwood, O., & Edinger, E. (2009). *Ages and growth rates of some deep-sea gorgonian and antipatharian corals of Newfoundland and Labrador* (Vol. 66).

Sikes, E. L., Samson, C. R., Guilderson, T. P., & Howard, W. R. (2000). Old radiocarbon ages in the southwest Pacific Ocean during the last glacial period and deglaciation. *Nature, 405*, 555. http://dx.doi.org/10.1038/35014581

Stuiver, M., & Braziunas, T. F. (1993). Modeling atmospheric (super 14) C influences and (super 14) C ages of marine samples to 10,000 BC. *Radiocarbon; Vol 35, No 1 (1993)*. https://journals.uair.arizona.edu/index.php/radiocarbon/article/view/1558/1562

Stuiver, M., & Polach, H. A. (1977). Discussion Reporting of 14C Data. *Radiocarbon, 19*(3), 355-363. https://www.cambridge.org/core/article/discussion-reporting-of-14c-data/D686D7894B8BAC3212589AFE418E147E

Tracey, D., Neil, H., Marriott, P., Andrews, A. H., Cailliet, G. M., & Sánchez, J. A. (2007). Age and growth of two genera of deep-sea bamboo corals (family isididae) in New Zealand waters. *Bulletin of Marine Science, 81*(3), 393-408. http://www.ingentaconnect.com/content/umrsmas/bullmar/2007/00000081/00000003/art00008

Williams, A., Schlacher, T. A., Rowden, A. A., Althaus, F., Clark, M. R., Bowden, D. A., et al. (2010). Seamount megabenthic assemblages fail to recover from trawling impacts. *Marine Ecology, 31*(s1), 183-199. https://doi.org/10.1111/j.1439-0485.2010.00385.x

Williams, B., & Grottoli, A. G. (2010). Stable nitrogen and carbon isotope (δ15N and δ13C) variability in shallow tropical Pacific soft coral and black coral taxa and implications for paleoceanographic reconstructions. *Geochimica et Cosmochimica Acta, 74*(18), 5280-5288. http://www.sciencedirect.com/science/article/pii/S0016703710003674

2.9 Supplementary Information:

2.9.1 Description of Leiopathes 4 Skeletal Texture

15131 exhibits convoluted growth only along a portion of the circumference resulting in a distinct change in the direction of preferred radial growth (Figures 2.2 and 2.6B). This convoluted growth habit is in stark contrast to growth between 15 mm and 37 mm, which follows the clean concentric banding seen in all other specimens. These two regions are separated in places by a crack suggesting skeletal discontinuity, although in places they also appear continuous.

The interval of convoluted growth is characterized by anomalies in the growth rate profile. The Age/Depth plot for the coral (Figures 2.4 & 2.6A, and see also Figure S2.12) exhibits the following features: a distinct ~400 year step in age across the onset of the convoluted growth (between 17 and 13 mm) followed by uncharacteristically rapid growth between 5 and 13 mm (a shallower slope on the Age vs Depth plot). Finally, there is another ~400 year age step across the transition from convoluted back to laminar growth at 1 mm.

2.10 Supplementary Figures:

Supp. Fig. S2.1: NIWA 35104 Images. Images of NIWA 35104. Photo Credit: Peter Marriot

Supp. Fig. S2.2: NIWA 64334 Images. Images of NIWA 64334. Photo Credit: Peter Marriot

Supp. Fig. S2.3: NIWA 47996 Images. Images of NIWA 47996. Photo Credit: Peter Marriot

Supp. Fig. S2.4: NIWA 15131 Images. Images of NIWA 15131. Photo Credit: Peter Marriot, Nicholas Hitt

Supp. Fig. S2.5: NIWA 17107 Images. Images of NIWA 17107. Photo Credit: Peter Marriot, Nicholas Hitt

Supp. Fig. S2.6: NIWA 17108 Images. Images of NIWA 17108. Photo Credit: Peter Marriot, Nicholas Hitt

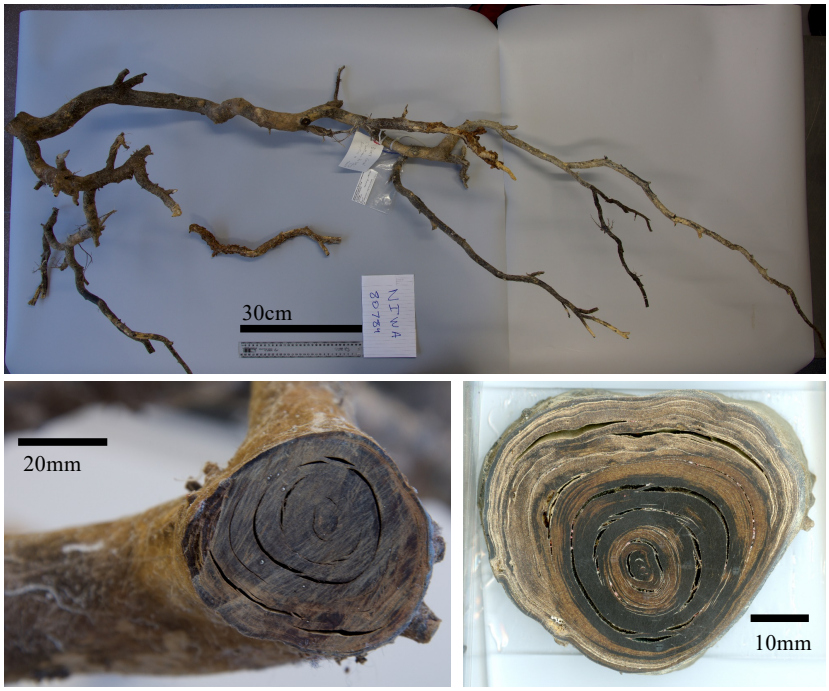

Supp. Fig. S2.7: NIWA 80784 Images. Images of NIWA 80784. Photo Credit: Peter Marriot, Nicholas Hitt

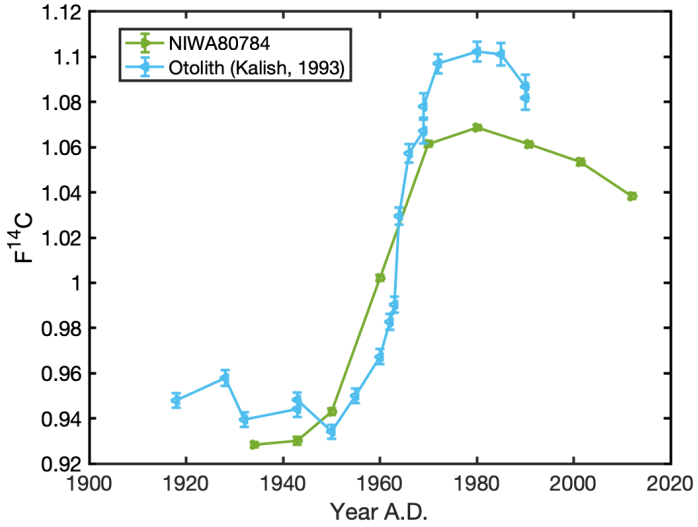

Supp. Fig. S2.8: NIWA 80784 Chronology. Age chronology for post-bomb ($F^{14}C>1$) data in NIWA80784 using otolith $F^{14}C$ data from Kalish, 1993

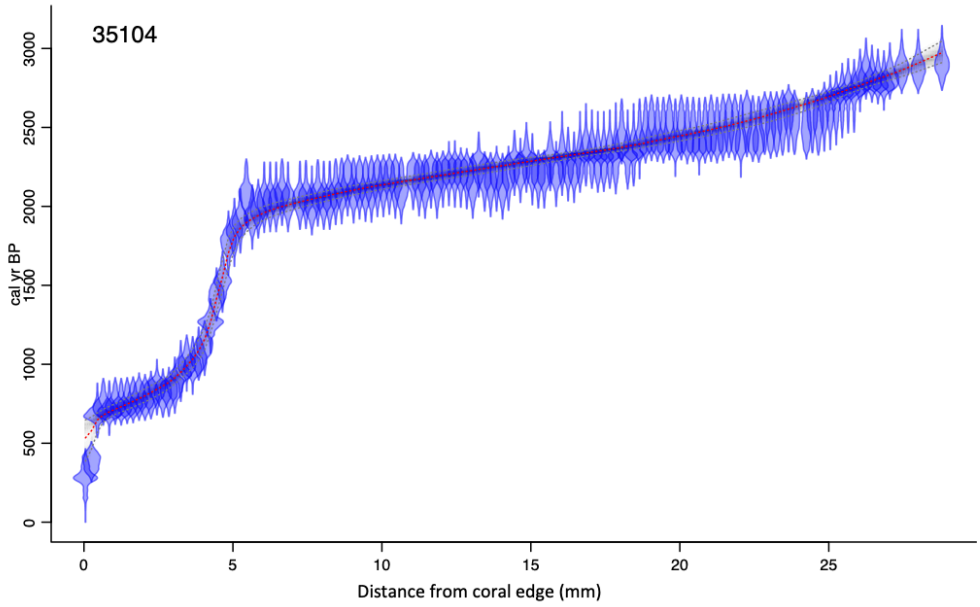

Supp. Fig. S2.9: NIWA 35104 Age Model. Age-depth model for NIWA 35104. Ages are in calendar years before present, where 'before present' is defined as 1950 CE

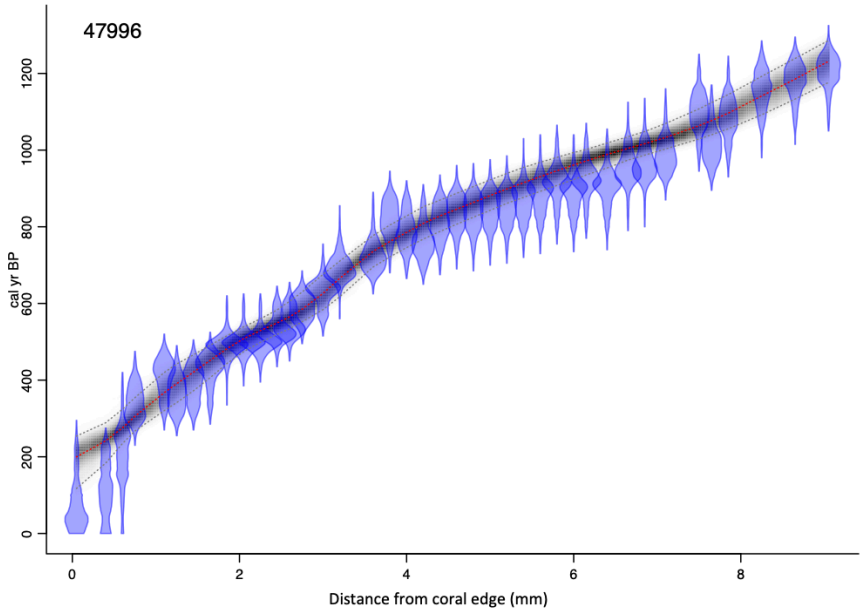

Supp. Fig. S2.10: NIWA 47996 Age Model. Age-depth model for NIWA 47996. Ages are in calendar years before present, where 'before present' is defined as 1950 CE

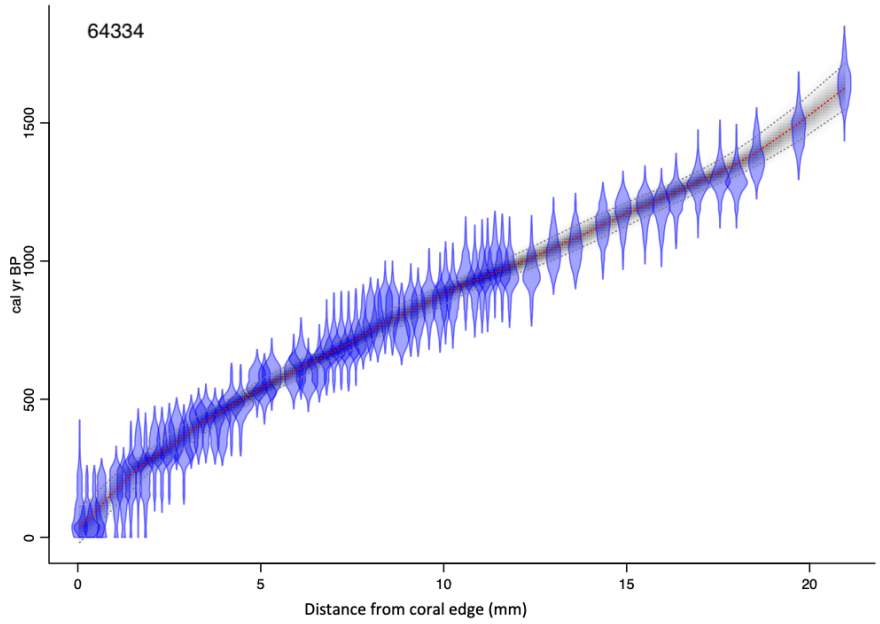

Supp. Fig. S2.11: NIWA 64334 Age Model. Age-depth model for NIWA 64334. Ages are in calendar years before present, where 'before present' is defined as 1950 CE

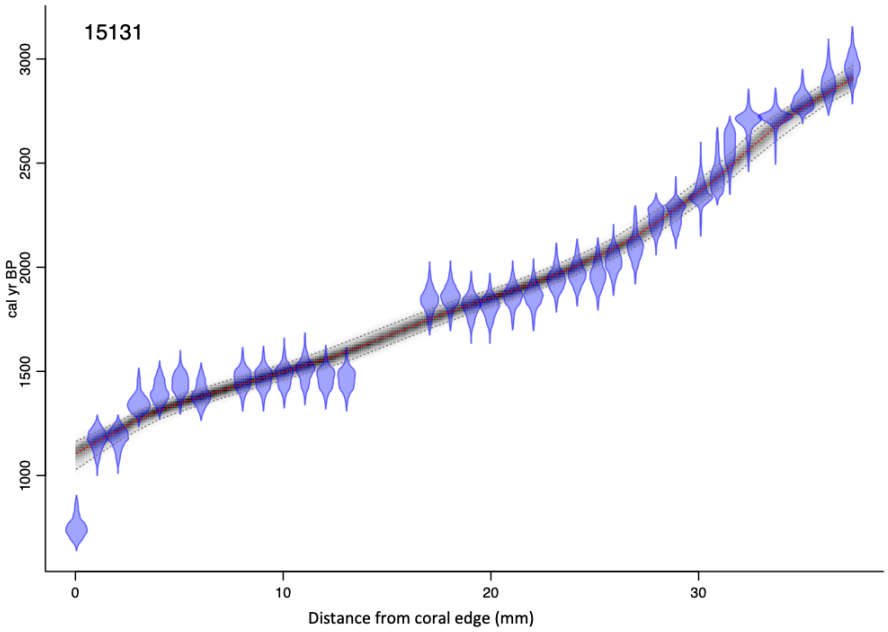

Supp. Fig. S2.12: NIWA 15131 Age Model. Age-depth model for NIWA 15131. Ages are in calendar years before present, where 'before present' is defined as 1950 CE

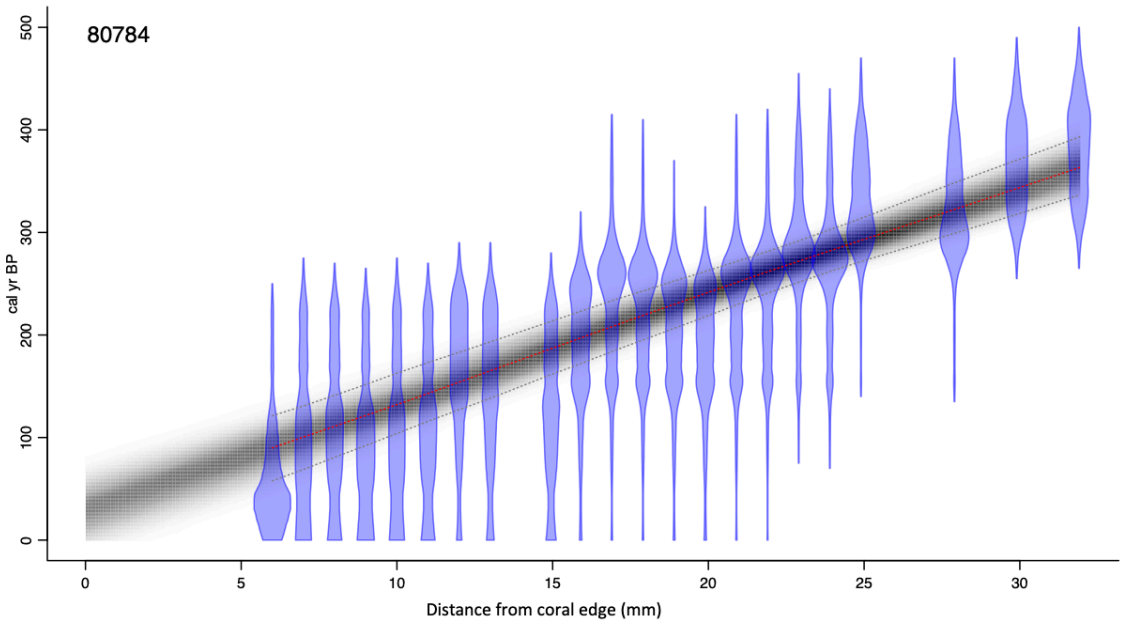

Supp. Fig. S2.13: NIWA 80784 Age Model. Age-depth model for NIWA 80784. Ages are in calendar years before present, where 'before present' is defined as 1950 CE

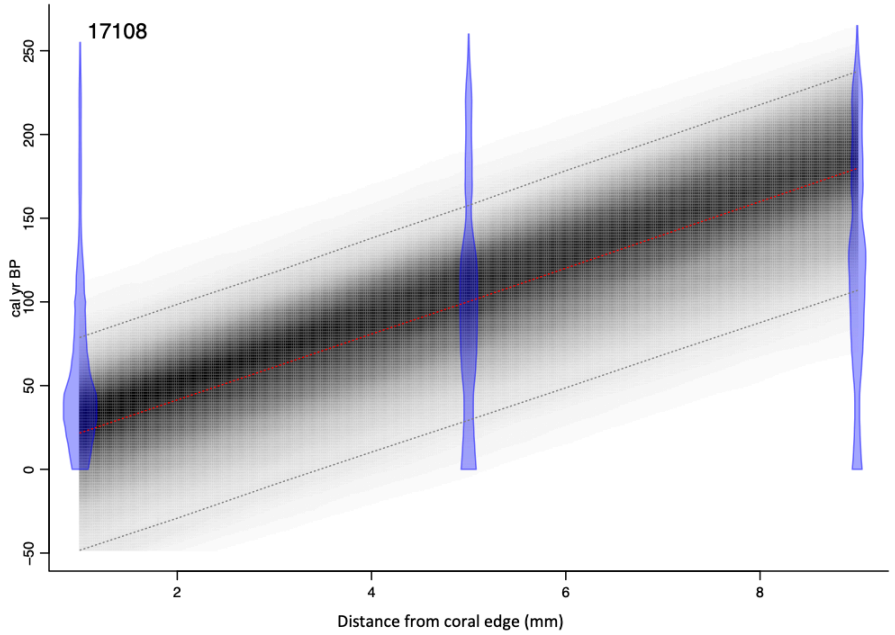

Supp. Fig. S2.14: NIWA 17108 Age Model. Age-depth model for NIWA 17108. Ages are in calendar years before present, where 'before present' is defined as 1950 CE

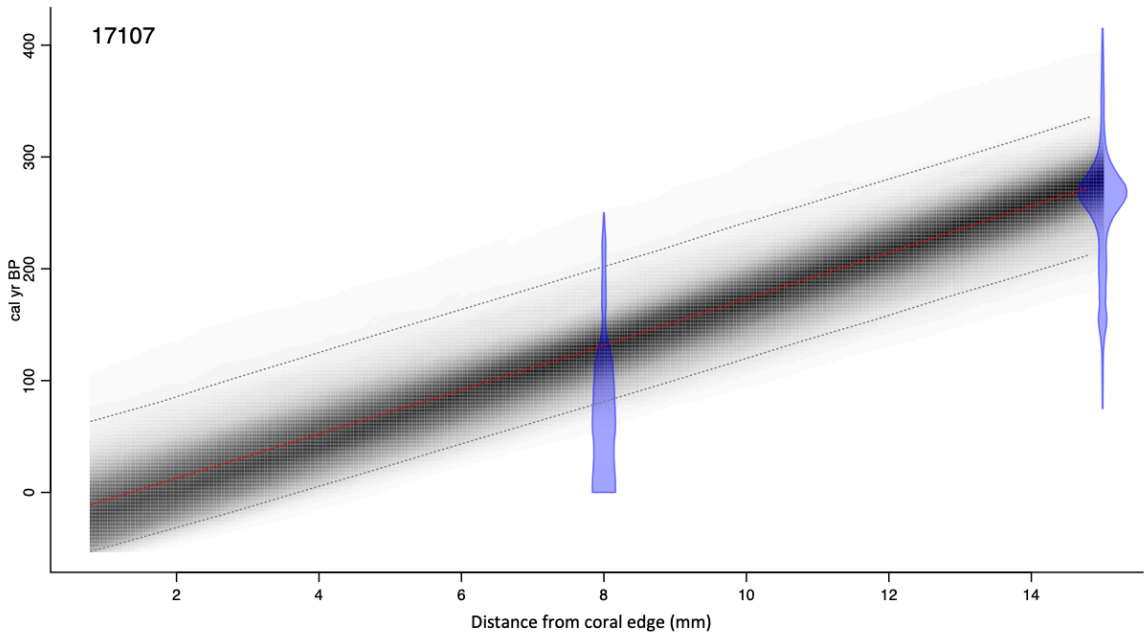

Supp. Fig. S2.15: NIWA 17107 Age Model. Age-depth model for NIWA 17107. Ages are in calendar years before present, where 'before present' is defined as 1950 CE

Chapter 3

Significant variations in late Holocene South Pacific Gyre strength reconstructed from black coral radiocarbon

The content in Chapter 3 was submitted for publication in the peer-reviewed journal *Proceeding of the National of the United States of America*.

Authorship contributions to this research article include the following:

Nicholas T. Hitt – Wrote manuscript and managed all co-author feedback, reviewer comments, and editing of proofs. This author prepared all samples for geochemical analysis, compiled all data, developed initial interpretations, and produced all figures.

Daniel J. Sinclair – Academic Supervisor; provided feedback on drafts and aided in the interpretation of the results. Helped to outline the introduction and discussion sections of the manuscript.

Helen L. Neil – Academic Supervisor; provided feedback on a draft and aided in the interpretation of the results.

Stewart J. Fallon – Academic Supervisor; analyzed ^{14}C dates; provided feedback on drafts and aided in the interpretation of the results.

Aimée Komugabe-Dixson – Academic Supervisor; Reviewed two drafts of the manuscript.

John Hellstrom – Analyzed U-Th dates for age model construction

Note: Appendix data is stored in 'Sheet B' in the CD-ROM at the end of the thesis.

3.1 Abstract:

The Pacific Ocean subtropical gyres significantly influence the Earth's climate and ecosystems. Over the last decades, an increase in subtropical South Pacific Gyre (SPG) circulation has led to warming in the southwest Pacific up to four times the global average. Are these changes anomalous or part of a natural cycle? Determining this requires long-term records of baseline ocean dynamics in the southwest Pacific. Unfortunately, SPG observations are sparse and instrumental records only span a few decades. Here we reconstruct 3000 years of SPG dynamics at decadal resolution by measuring marine radiocarbon reservoir age deviations (ΔR) in New Zealand black corals. We find that over the last millennium, century-scale ΔR variations around New Zealand are inversely correlated with reconstructions of the Southern Annular Mode (SAM) ($r = -0.48$, $p < 0.01$) from the eastern Pacific. We also observe a depression in mean ΔR between 2000-3000 year BP.

We propose that the subtropical SPG experiences influences from modes of natural variability on multi-centennial to millennial timescales. Multi-centennial ΔR oscillations may represent varying ocean circulation strength and mixed-layer depth driven by changing westerly winds. This is supported by a correspondence between ΔR/SAM variations and reconstructions of New Zealand's synoptic meteorology and temperature over the last millennium. Our record also reveals a baseline shift in subtropical SPG mean ΔR that begins ca. 1900BP. This observation mirrors a late Holocene SPG ΔR record showing a change in circulation over the 1900-3000BP interval, possibly forced by a shift in the mean state of the El Niño-Southern Oscillation (ENSO).

3.2 Introduction:

The South Pacific Gyre (SPG) is the largest ocean gyre on Earth. It modulates Pacific climate by distributing warm, subtropical waters to high latitudes along its western limb and returning cool, subpolar waters back to low latitudes along its eastern limb (Figure 3.1A). In recent decades, instrumental observations show an acceleration of the warm currents along the western SPG, leading to a rise in southwest Pacific ocean temperatures that is up to 4x the global average (Wu et al., 2012; Roemmich et al., 2016; Shears et al., 2017). While this gyre acceleration is often attributed to anthropogenic warming, little is known about long-term dynamics in the southwest Pacific region beyond the instrumental observation period (Roemmich et al., 2007).

Determining whether recent climate trends are anomalous requires records of sufficient length to resolve natural baseline ocean variability. Proxy records from marine sediment cores have traditionally been used to reconstruct SPG paleoceanography (Cortese et al., 2013; Bostock et al., 2019). Although sediments are useful for evaluating ocean dynamics on glacial timescales (Cortese et al., 2013; Bostock et al., 2015; Bostock et al., 2019), low sedimentation rates and bioturbation limit their capacity to capture decadal- to centennial-scale ocean variability. Tropical corals are sometimes employed as high-resolution ocean proxies (McCulloch et al., 1994), but are usually not available at mid-latitudes. Thus, there is a gap in high-resolution ocean proxy records for the mid-latitude South Pacific. Here we measure radiocarbon in deep-sea corals from the New Zealand region to reconstruct 3000 years of southwestern SPG circulation at sub-century resolution.

3.3 Background

3.3.1 New Zealand Ocean-Atmosphere Climatology

New Zealand sits in a complex oceanographic region (Figure 3.1A). North of New Zealand warm waters are derived from the East Australian Current (EAC) and its branches – the East Australian Current Extension (EAC extension); the Tasman Front (TF); and the East Auckland Current (EAuC) (Chiswell et al., 2015). South of New Zealand, cool subtropical/sub-polar waters are delineated by the Subtropical Front (STF), which separates the warm, saline,

subtropical waters and the cool, fresh Subantarctic waters of the Antarctic Circumpolar Current (ACC) (Chiswell et al., 2015).

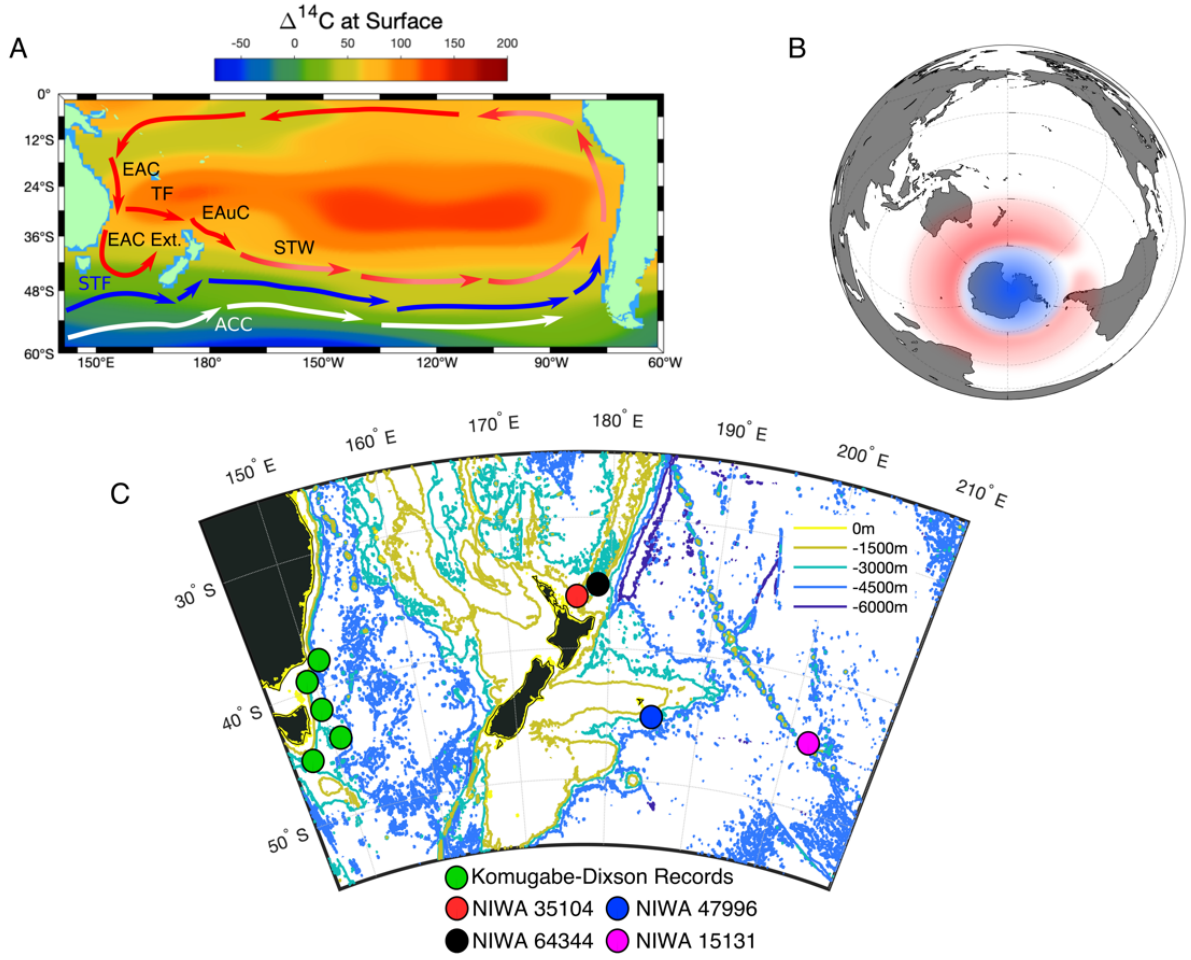

Figure 3.1: Coral Locations and Climate/Oceanographic Setting for the Southern Pacific. Panel A: A schematic of South Pacific Gyre ocean currents around New Zealand overlaid on top of gridded surface $\Delta^{14}C$ data (Key et al, 2004). Panel B: A schematic of mean sea level pressure anomalies (MSLPA) for the positive phase of the Southern Annular Mode (SAM). Red indicates positive MSLPA and blue indicates negative MSLPA. Panel C: Black coral locations overlaid on top of bathymetric contours (data source: GEBCO 2020 product). Blue, magenta, black and red circles refer to the corals presented in this study and green circles refer to those corals presented in Komugabe-Dixson et al., 2016.

Instrumental observations and paleoceanographic reconstructions show that the STF exhibits varying temperature, salinity, water column density, strength and position gradients on seasonal to glacial/interglacial timescales (De Boer et al., 2013; Graham et al., 2013; Bostock et al., 2015). East of New Zealand, the STF position is presently locked by the bathymetry of the Campbell Plateau and Chatham Rise (Figure 3.1A & C; Chiswell et al., 2015). East of the Chatham Islands, STF location is more variable, migrating up to several degrees of latitude on

seasonal to decadal timescales in the Central South Pacific (De Boer et al., 2013; Graham et al., 2013).

The East Australian Current (EAC) is the primary western boundary current of the South Pacific Ocean (Ridgway, 2007a, 2007b; Ridgway et al., 2008; Chiswell et al., 2015). It distributes heat from the tropics to the mid-latitudes and provides a mild and stable climate for southeast Australia and New Zealand (Ridgway, 2007a, 2007b; Ummenhofer et al., 2007; Ridgway et al., 2008).

Satellite altimetry observations show the EAC exhibits strength and positional variability on seasonal, interannual and decadal timescales (Ridgway, 2007a, 2007b; Ridgway et al., 2008). EAC variability is largely driven by changes in mid-latitude westerly wind strength and position, which can be modulated by the Southern Annular Mode (SAM) (Cai et al., 2005; Cai, 2006; Hill et al., 2008; Hill et al., 2011). The SAM is a low-frequency mode of climate variation characterized by nearly zonally-symmetric, synchronous sea level pressure anomalies of opposing sign between the mid-latitudes and Antarctica (Figure 3.1B). The SAM modulates the position of the westerly wind belt centered between 35°S and 65°S (Marshall, 2003; Marshall et al., 2004), with positive SAM phases manifesting as a poleward contraction and intensification of the southern Hemisphere westerly wind belt. SAM varies on seasonal to millennial timescales (Jones et al., 2009; Moreno et al., 2009; Moreno et al., 2010), and has been linked to basin-wide variability in South Pacific Ocean currents and climate (Hall et al., 2002; Cai et al., 2005; Cai, 2006). For example, the EAC has experienced a multi-decadal acceleration (Shears et al., 2017) concurrent with a shift towards the positive phase of the SAM over the late 20th century (Cai et al., 2005; Cai, 2006).

The recent SAM-induced EAC acceleration has caused the EAC to expand poleward (Cai et al., 2005; Cai, 2006). It is, however, less clear how the branches of the EAC that impinge upon New Zealand behave (the EAC extension and TF). Recent work suggests that they may not respond equally to EAC intensification (Hill et al., 2011). As the EAC intensifies, the EAC extension can be favored at the expense of the TF (and vice versa), resulting in an anticorrelation between the EAC extension and TF (Hill et al., 2011; Ganachaud et al., 2014). Constraining the response of the EAC and its branches to past SAM variability will therefore aid future efforts to forecast how local southwest Pacific climates may respond to changes in the southern westerlies.

3.3.2 Marine Radiocarbon Reconstruction

We use four long-lived organic-skeleton black corals (genus *Leiopathes*) to reconstruct local marine radiocarbon reservoir correction factors (ΔR). ΔR reflects the difference between the modelled global marine radiocarbon curve (Marine20; Heaton et al., 2020), and the radiocarbon reservoir age measured locally. ΔR variations reflect changes in local ocean circulation and upwelling that change the balance between 'old' subsurface waters, and 'young' surface waters that have equilibrated with atmospheric CO_2 (Petchey et al., 2008a; Petchey et al., 2008b; Komugabe et al., 2014; Komugabe-Dixson et al., 2016). Around New Zealand, ΔR responds to changes in the southwestern limb of the SPG, and our records provide a historical baseline for gyre variability over the late Holocene (Petchey et al., 2008a; Petchey et al., 2008b; Komugabe et al., 2014; Komugabe-Dixson et al., 2016).

3.3.3 Deep-Sea Black Corals

Deep-sea black corals are an attractive archive for reconstructing ocean dynamics on centennial to millennial timescales (Prouty et al., 2014; Komugabe-Dixson et al., 2016). These corals have a branching organic skeleton with a thick basal trunk that displays growth rings much like a tree, making it simple to establish chronological progression. These skeletons are built from the organic material that the corals consume: primarily detrital plankton matter originating in the surface ocean (Komugabe-Dixson et al., 2016; Hitt et al., 2020). Thus, growth rings inherit the radiocarbon 'age' of the surface ocean water masses. These organic skeletons are also rich in uranium (~ 20 ppm) and can therefore be precisely dated by uranium-thorium (U-Th) disequilibrium (Komugabe et al., 2014; Komugabe-Dixson et al., 2016). By pairing radiocarbon (^{14}C) and U-Th, we can reconstruct local surface ocean reservoir correction factors (ΔR) (Komugabe et al., 2014; Komugabe-Dixson et al., 2016). Since ΔR is sensitive to the balance of 'old' subsurface waters and 'young' surface waters, black coral ΔR can be used to elucidate spatial variations in ocean circulation (Komugabe et al., 2014; Komugabe-Dixson et al., 2016). Moreover, black corals can live for millennia (Komugabe-Dixson et al., 2016; Hitt et al., 2020), allowing reconstruction of ocean circulation over the late Holocene.

3.3.4 Previous Reconstructions: Tasman Sea ΔR Variability in the Late Holocene

In a recent effort to reconstruct multi-centennial EAC variability, Komugabe-Dixson et al. (2016) generated a 4500 year long record of $\Delta^{14}C$, R and ΔR using black corals collected from

the south Tasman Sea (Figures 3.1C & 3.2D). They used these records in conjunction with the $\Delta^{14}C$ pattern in the SPG (Figure 3.1A) to infer the strength and location of the EAC extension At present, subtropical waters have low ΔR values (-2±29; Petchey et al. (2008b)) and high $\Delta^{14}C$ values (>75) as these waters are better ventilated with the atmosphere (Key et al., 2004). Subpolar waters presently have higher ΔR values (136±83; Petchey et al. (2008b)) and lower $\Delta^{14}C$ values (<10) as they have spent more time beneath the surface (Figure 3.1A; Key et al., 2004). By calculating $\Delta^{14}C$ and ΔR from the subtropical and subpolar boundary, Komugabe-Dixson et al. (2016) were able to infer the relative strength and location of the EAC extension and assess EAC variability.

The Komugabe-Dixson et al. (2016) ΔR record shows a ~80 ^{14}Cyr increase from 1900-3000BP to 0-1900BP (Figure 3.2D). They attribute this to an increased flow of subtropical water into the Tasman Sea over the 1900-3000BP interval due to a stronger EAC and EAC Ext, possibly driven by a strengthening of the whole SPG. However, the EAC extension can strengthen at the expense of the TF without changing overall Gyre circulation (Hill et al., 2011), and so the Komugabe-Dixson et al. (2016) record could represent either strengthened SPG circulation *or* internal EAC variability (or some combination of both). A firm conclusion on late Holocene SPG variability cannot be made from Tasman Sea ΔR record alone; however, ΔR from the New Zealand region can help constrain spatial variability in the southwestern portion of the SPG by representing the TF.

3.4 Materials and Methods:

3.4.1 Sample Preparation and Radiocarbon Dating:

The coral radiocarbon results presented here are the same as those presented in Hitt et al. (2020). Full details of the sub-sampling and radiocarbon measurement protocols are presented in Chapter 2.3.1 and Hitt et al. (2020). Four New Zealand black coral colonies (species *Leiopathes .spp*) were provided by the National Institute of Water and Atmospheric Research Invertebrate Collection in Wellington, New Zealand (Figure 3.1C; Table 3.1). Powdered samples were generated by milling whole rings using a CNC milling machine. Radiocarbon measurements were made on cleaned splits of the powders (~1mg) on a single-stage Accelerated Mass Spectrometer (AMS) at the Australian National University Radiocarbon Laboratory following procedures outlined in Fallon et al. (2010) (Appendix Table 1).

Table 3.1: A collection of black coral information. Black coral location, species, depth, lifespan, the number of radiocarbon and U/Th dates and mean ΔR. U-Th ages are corrected for initial thorium following protocols in Hellstrom, 2006. Weighted mean ΔR is calculated according to Bevington, 1969 and the uncertainty is the standard deviation of ΔR (Bevington, 1969) scaled by the square root of the number of observations. All uncertainties are 2σ

Sample ID	Latitude (°S)	Longitude (°E)	Location	Species	Depth (m)	Lifespan (Cal. B.P.)	Number of ^{14}C Dates	Number of U/Th Dates	Avg. ^{14}C date σ	Avg. U/Th date σ	Mean ΔR (^{14}Cyr)
NIWA 64334	34.7577	179.4313	Bay of Plenty	*Leiopathes secunda*	750	100-1493	68	25	21	23	-66 ± 5
NIWA 35104	36.1600	176.7733	Bay of Plenty	*Leiopathes .spp*	738	2019-2981	108	30	23	36	-111 ± 4
NIWA 47966	44.5633	184.3167	South East Chatham Island	*Leiopathes secunda*	758	110-983	34	16	21	15	-42 ± 6
NIWA 15131	45.5667	203.3333	Central South Pacific	*Leiopathes .spp*	870	1618-2836	13	13	22	53	-54 ± 12

3.4.2 U-Th Dating:

Previous studies show that black corals have a high U concentration (10-80ppm) and exhibit closed system behavior which makes them ideal for U-Th dating (Komugabe et al., 2014; Komugabe-Dixson et al., 2016). U-Th ages were generated at 0.2-1mm intervals across all corals (Supp. Fig. S3.1, Appendix Table 2).

U-Th analyses were conducted according to the procedure of Hellstrom (2003) modified according to Drysdale et al. (2012). Black coral sub-samples up to 2mg were dissolved in ~15M HNO_3, spiked with a mixed ^{236}U-^{233}U-^{229}Th synthetic isotopic tracer and equilibrated on a hotplate overnight at ~85°C. Equilibrated samples were loaded onto 0.5 ml Eichrom TRU ion exchange columns and the black coral matrix washed off, prior to elution of U and Th as a single fraction. The purified U-Th samples were analysed using a Nu Instruments 'Plasma' MC-ICP-MS at the University of Melbourne. Samples were introduced via a Nu Instruments DSN desolvator in 5% HNO_3 and 0.5% HF using a Glass Expansion Opalmist Teflon nebulizer. All isotope ratios were determined simultaneously with the use of dual SEM ion counters for paired measurement of ^{233}U/^{234}U and ^{229}Th/^{230}Th. Most probable initial ^{230}Th/^{232}Th activity ratios were determined using the stratigraphic constraint technique of Hellstrom (2006), allowing calculation of corrected U-Th ages using the ^{234}U and ^{230}Th half-lives of Cheng et al. (2013). Th corrected U-Th dating results are provided in Supp. Fig. S3.1 and Appendix Table 2.

3.4.3 Calendar Age vs. Depth Model Construction

Age-depth models were constructed from initial-Th corrected U-Th using COPRA (Breitenbach et al., 2012), a piecewise cubic interpolation spline with a Monte Carlo simulation (n>2,000; Supp. Fig. 3.1, Appendix Tables 3-6). It was necessary to interpolate U-Th ages in

order to estimate the calendar age for each radiocarbon measurement because U-Th dates were generated at a lower frequency than ^{14}C dates (~1 in 3).

After correction for initial-Th, coral 35104 displays U-Th age reversals, possibly due to the high density of U-Th dates. A total of 5 age reversals were seen over the 2000-3000BP interval, each less than 30 years, and each occurring in intervals with a high density of surrounding U-Th dates (n>3 in an interval of 125 years). Breitenbach et al. (2012) suggests that COPRA can construct an age model from a dataset with age reversals so long as the error intervals of these age reversals overlap. However, the overlapping age reversals occur in high density U-Th dates intervals and prevent COPRA from constructing an age model in 35104 (Sebastian Breitenbach, 2019, pers. comm.). We therefore removed the five age reversals over the 2000-3000BP interval from the suite of U-Th ages (n = 30 to n = 25 over the 2000-3000BP interval) used for age model construction as per the recommendation of the COPRA authors (Sebastian Breitenbach, 2019, pers. comm.). After removing age reversals, we still maintain the same U-Th date frequency observed in corals 64344 and 47996 (~1U-Th:4^{14}C; 1U-Th:40-50yrs).

3.4.4 ΔR and $\Delta^{14}C$ Calculations

Local marine radiocarbon reservoir correction factors (ΔR) were calculated from interpolated U-Th ages and measured ^{14}C ages using the online ΔR calculation program, *deltar* (Reimer et al., 2017), with the Marine20 calibration curve (Heaton et al., 2020) (Figure 3.2A-C; Appendix Tables 3-6). We recalculate the ΔR values from Komugabe-Dixson et al. (2016) using *deltar* (Reimer et al., 2017), with the Marine20 calibration curve (Heaton et al., 2020) (Appendix Table 7; Figure 3.2D). $\Delta^{14}C$ was calculated following procedures outlined in Komugabe-Dixson et al. (2016) (Supp. Fig. S3.2; see supplementary text; Appendix Tables 3-6).

3.4.5 Exclusion of Records

The ΔR time series presented for corals 64344 and 47996 are continuous and complete. However, the ΔR time series presented for 35104 and 15131 have regions where ΔR has been omitted due to extremely slow coral growth and large uncertainties in ΔR calculations (35104) and extremely fast coral growth (15131). Coral 35104 exhibits an extreme reduction in growth rate across the interval 577-2000 BP (Supp. Figure S3.3). In this slow-growth region, the evenly-spaced U-Th dates become more separated in time. This means that U-Th dates have to be intensively interpolated to match the sampling resolution of ^{14}C dates, introducing a large

uncertainty. This is exacerbated by elevated detrital Th during the slow-growth interval which affects U-Th date precision (Supp. Fig. S3.3). Together these factors expand the error in ΔR such that measurements are not statistically distinguishable across the 577-2000B.P interval (Supp. Fig. S3.4). These data are therefore excluded from the ΔR record. A further explanation on data omission is provided in the supplementary text.

15131 exhibits a period of anomalously fast growth in its outermost layer, corresponding to the interval 700-1400BP. Banding in this interval is convoluted such that stratigraphic ordering of layers is lost and micromilling individual coral bands was impossible (Figure 2.6). Bands were crosscut during micromilling (Chapter 2.5.3.2), resulting in an artificial smoothing of ages which prevents constructing a robust U-Th age model and ΔR dataset (Figure 2.6; Supp. Fig. S3.5). These growth irregularities may also represent a secondary colonization of the coral by an unidentified colonial zoanthid (Chapter 2.5.3.2). Using a colonial zoanthid colony for reconstructing ΔR has not been previously tested before (Williams, 2020) and determining such potential is beyond the scope of this study. For these reasons, we only reconstruct ΔR and $\Delta^{14}C$ in 15131 for the 1600-2800BP interval where banding is clear and uncompromised and there is no age smoothing.

3.5 Results and Discussion:

3.5.1 Description of New Zealand ΔR

ΔR for the EAuC region shows clear multi-centennial scale fluctuations over the last 3000 years which range up to 150 ^{14}C yr (Figure 3.2A). ΔR for the Subtropical Front (STF) region exhibits some irregular variability ranging to 100 ^{14}C yr over the last millennium (Figure 3.2B). ΔR for the Central South Pacific (CSP) is too low-resolution (~1 point per 150yrs) to provide any multi-centennial interpretations (Figure 3.2C). EAuC and STF corals that overlap in time over the last millennium (64334 and 47996) exhibit a weak but significant positive correlation over the last 1000 years when resampled to an evenly spaced 50yr resolution ($r = 0.21$, $p < 0.10$, $n = 20$; Fig. 3.3B). This implies that there is likely some underlying link connecting multi-centennial ΔR variations in both regions; however, there is also likely some small-scale variability. To test correlation between the EAuC coral (351044)and CSP coral (15131), the former record was downsampled by piecewise cubic spline to match the resolution

of 15131. The two datasets were not significantly correlated ($p = 0.31$; data not shown for brevity).

3.5.2 Comparing the New Zealand ΔR and Tasman ΔR Records – Centennial Timescales

New Zealand's black coral-based ΔR records show significant multi-centennial variations up to 200 ^{14}C year in the EAuC and STF regions (Figure 3.2). On 200-year timescales, the amplitude of New Zealand ΔR variations are considerably smaller, and the records have no significant correlations with the south Tasman sea ΔR record (Figure 3.2). No significant correlations were evident even with testing phase offsets of up to 400 years. The Central South Pacific (CSP) coral (15131) ΔR record was analyzed at low-resolution (~1 point per 150yrs) and we cannot therefore study fluctuations on 200-year timescales. 15131's broader features do not correlate with the overlapping time period of coral 35104, even when the latter is down-sampled to the same temporal resolution. The lack of correlation between century-scale variations in ΔR between the EAuC, STF, CSP and south Tasman sea localities implies that site-specific processes may have a greater influence on local ΔR variation on these timescales (although longer individual ΔR records >2000 years may reveal lower frequency correlations between sites). We therefore focus our analysis of centennial ΔR variations (below) on just the New Zealand corals, and exclude the low-resolution CSP record from this analysis.

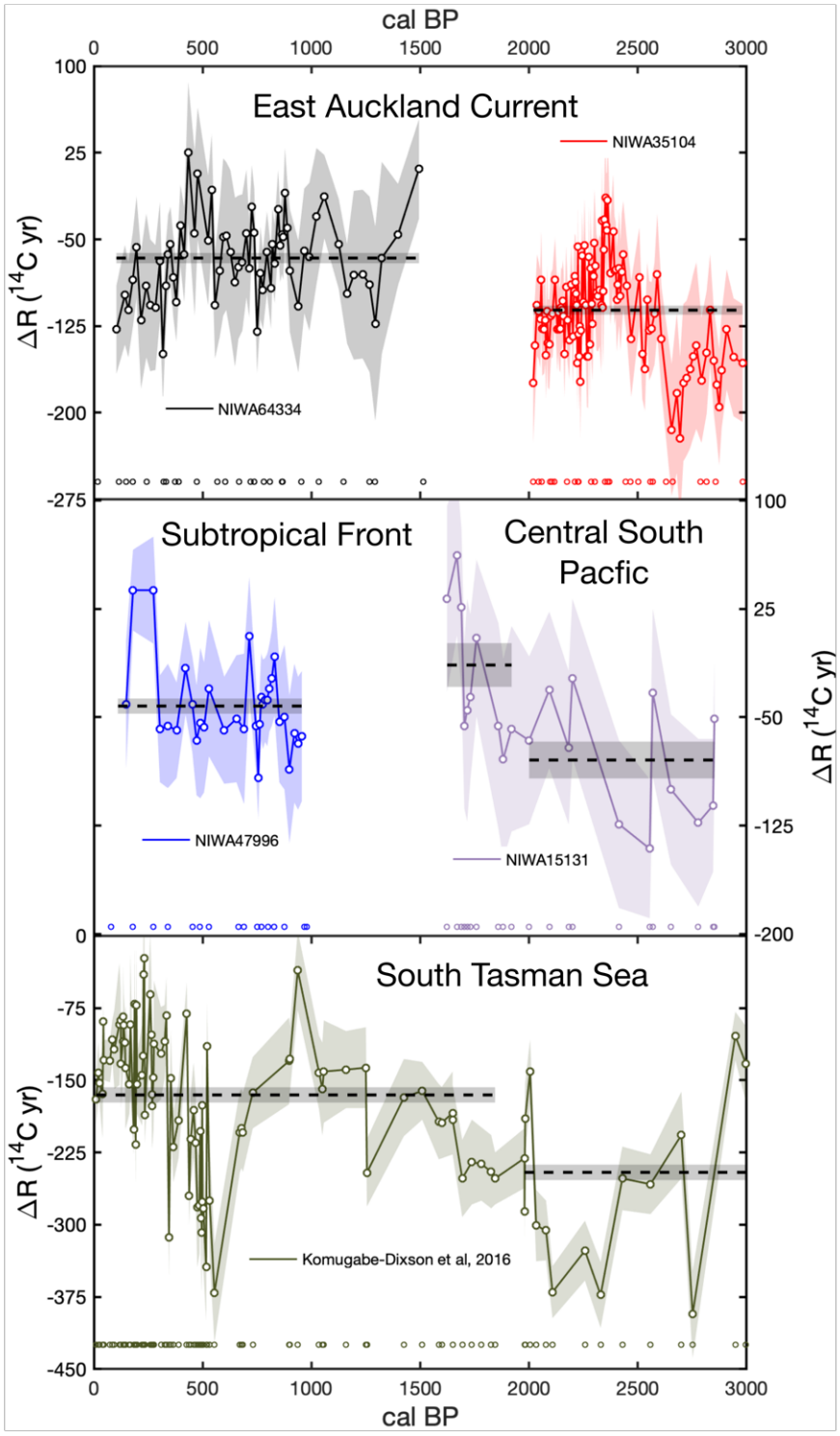

Figure 3.2: Subtropical South Pacific Gyre ΔR Reconstructions over the late Holocene. Top Panel: Black coral ΔR values for the East Auckland Current. Middle Panel: Black coral ΔR values for the Subtropical Front and central South Pacific. Bottom Panel: Black coral ΔR reconstructions for the south Tasman sea (Komugabe-Dixson et al, 2016). Open circles at the bottom of the panels show the location of U/Th dates. Weighted mean ΔR is calculated according to Bevington, 1969 and the uncertainty is the standard deviation of ΔR (Bevington, 1969) scaled by the square root of the number of observations. All uncertainties are 2σ (shaded areas).

3.5.3 Comparing the New Zealand ΔR and Tasman ΔR Records – Millennial Timescales

A major feature in the south Tasman sea record is the baseline ΔR shift towards more negative values over the 1900-3000BP interval (~ -80 ^{14}Cyr) relative to the 0-1900BP interval. The New Zealand ΔR reconstructions resolve a similar ΔR depression of -67 ^{14}Cyr and -50 ^{14}Cyr over the 1900-3000BP relative to the 0-1900BP interval (Figure 3.2). We interpret the concurrent ΔR depressions as a baseline shift in mean ΔR for the southwest Pacific region across 0-1900BP. The fact that this millennium-duration change in ΔR correlates between locations, but centennial-scale variations do not, suggests the different mechanisms may apply to these locations at these different timescales.

The 1900-3000BP ΔR suppression was previously interpreted by Komugabe-Dixson et al. (2016) as a period of stronger SPG circulation driven by strong and abrupt El Niño events and a change towards an El Niño-like mean climate state. The alternative possibility is that the EAC extension strengthened at the expense of the Tasman Front without overall strengthening of the SPG (Hill et al., 2011). However, our results seem to imply that there was a synchronous response in baseline ΔR between the EAC extension and EAuC between 1900-3000 BP that extended further 'downstream' to the CSP. Such a coherent shift in mean ΔR over such a wide longitude suggests that it was driven by changes to the SPG as a whole. We propose two scenarios (1) a change in late Holocene gyre strength, where stronger gyre circulation reduced mean ΔR or (2) a change in the distribution of SPG radiocarbon over the late Holocene.

Komugabe-Dixson et al. (2016) interpreted the reduction in mean ΔR as a shift towards stronger gyre circulation driven by a more El Niño-like mean state between 1900-2900 BP. This is supported by a number of proxies which indicate an increase in ENSO variability as well as a marginal shift towards a more El Niño-like mean state ca. 2000-3000BP (Supp. Fig. S3.6; e.g. Haug et al., 2001; Moy et al., 2002; Stott et al., 2004; Cobb et al., 2013; Emile-Geay et al., 2015; Chen et al., 2016; Barr et al., 2019). Komugabe-Dixson et al. (2016) hypothesized that a change in ENSO mean state would displace the western equatorial Pacific salinity front northward (Delcroix et al., 1998) and would facilitate increased tropical water transport into the southwest Pacific and reduce reservoir age. Indeed, new instrumental data supports this dynamic interaction between southwest Pacific subtropical water transport and El Niño events (Oliver et al., 2018).

El Niño events cause the thermocline to shallow in the western tropical Pacific (Druffel et al., 1993) which increases radiocarbon ventilation to the atmosphere. This results in higher than

usual $\Delta^{14}C$ levels and younger reservoir ages in surface waters across the equatorial Pacific basin; and this signature is then carried to the southwest Pacific by the gyre circulation (Guilderson et al., 1998). Recent instrumental data shows a weak increase in subtropical water transport into the southwest Pacific during El Niño events, which also corresponds to a poleward shift in the location of EAC bifurcation (Oliver et al., 2018). We therefore propose that the mean ΔR reduction from 1900-3000BP may reflect a change in the distribution of SPG surface radiocarbon and/or a change in gyre strength driven by the mean state of ENSO.

3.5.4 Last Millennium New Zealand ΔR and the Paleo-SAM Index

Recent work has shown that SAM influences the strength and position of the EAC (Cai et al., 2005; Cai, 2006) and subtropical water transport around New Zealand (Roemmich et al., 2007; Roemmich et al., 2016). To test this, we constructed a last millennium black coral ΔR composite from the EAuC and STF corals, given that they exhibit a weak but significant correlation (see section 3.5.1), and compared it to a last millennium paleo-SAM index from Abram et al. (2014) (Figure 3.3). The last millennium ΔR composite shows good inverse correspondence with the paleo-SAM index (Figure 3.3A). Persistently high ΔR values occur during multi-centennial long periods of negative SAM (Figure 3.3A). A bootstrapped (n=10,000) Pearson's and Spearmen rank order correlation on 30yr-binned ΔR and SAM data confirms a significant moderate inverse correlation over the last millennium ($r = -0.48$, $p < 0.01$; $n = 29$). The inverse correlation suggests that SPG circulation is inversely coupled to the mean state of SAM at multi-centennial timescales over the last millennium (Figure 3.3A).

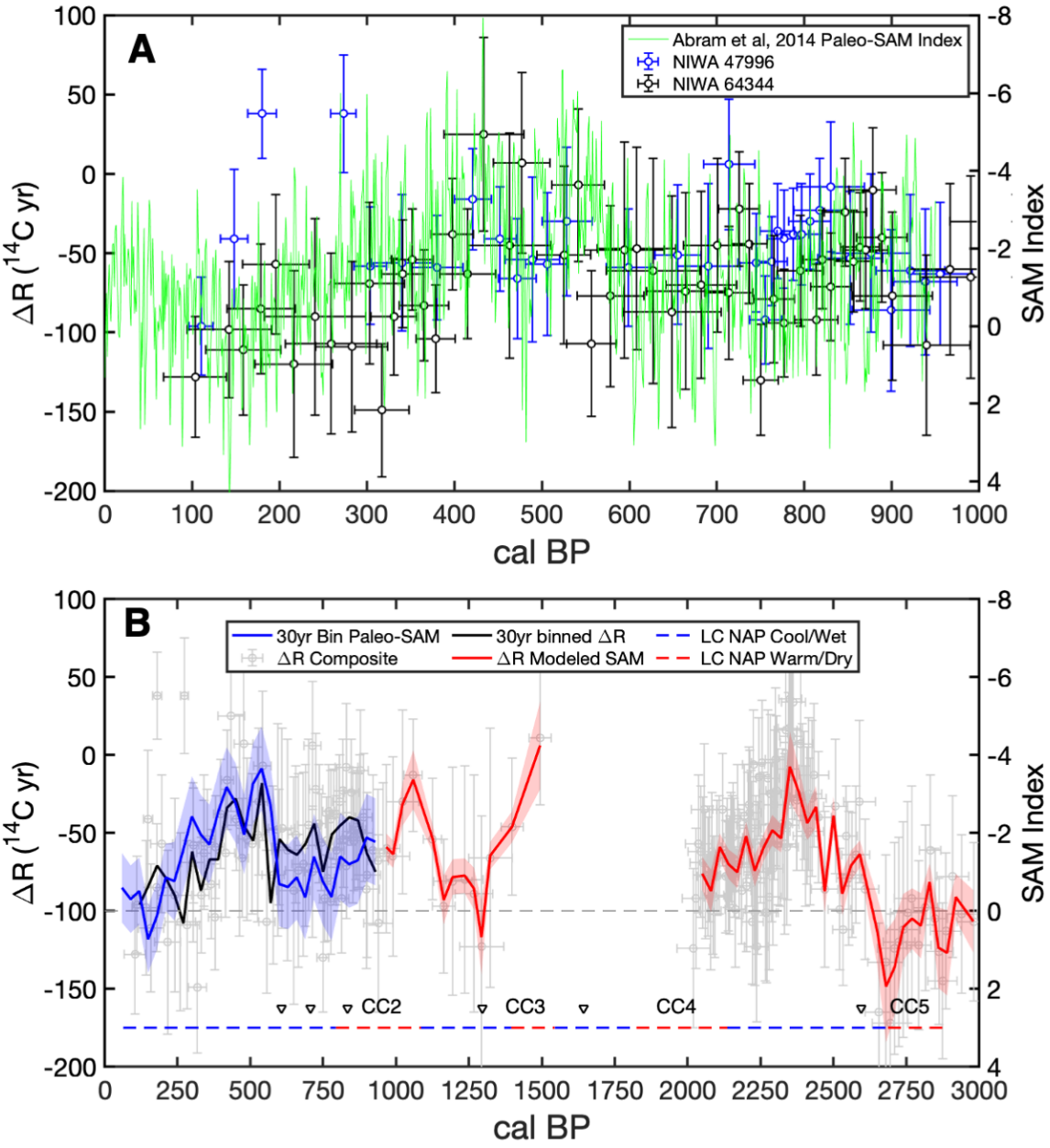

Figure 3.3: Subtropical SPG ΔR Variability and Paleo-SAM over the late Holocene. Top Panel: A comparison of black coral ΔR values for the East Auckland Current (black) and Subtropical Front (blue) with the paleo-SAM index from Abram et al, 2014 (green). Bottom Panel: A comparison of 30yr binned ΔR (black line) alongside 30yr binned Paleo-SAM (blue shaded line) overlaid on top of the ΔR composite (grey points). The linear relationship was then used to hindcast SAM conditions over the late Holocene (red shaded line). Red and blue dashed lines represent the inferred cool/wet and hot/dry periods from Ciprese Cycles (CC#) in Patagonia, South America (Moreno et al, 2014) complete with radiocarbon dates (black inverted triangles). All uncertainties shown are 2σ. The correlation between the 30yr binned paleo-SAM and ΔR records is $r = -0.48$ ($p < 0.01$; $n = 29$).

The Abram et al. (2014) Paleo-SAM index is constructed from a network of Antarctic ice cores and South American tree rings, and represents sea level pressure anomalies between 40°S

and 60°S across the Drake Passage. Although there are other climate modes at play in that region that positively/negatively interact with the SAM, namely the Zonal Wave 3 and Pacific South America Pattern (Hobbs et al., 2010; Ding et al., 2012), it is the best paleoclimate record of SAM currently available. However, the fact that records from New Zealand and the Drake Passage are in phase implies that variations in SAM have been zonally symmetric across the South Pacific Ocean over the last millennium. Previous evidence for the zonal evolution of SAM only went back as far as 550BP (using mid-latitude east and west South Pacific tree-rings; Villalba et al. (2012)). Our observations now extend that back to 950 BP.

3.5.5 Multi-Centennial ΔR-SAM Variability: Potential Mechanisms

Two different mechanisms potentially explain the relationship between these coral ΔR record and the Paleo-SAM index. These mechanisms are not mutually exclusive and may act together to produce the observed ΔR-SAM correlation.

3.5.5.1 SAM-Driven Ocean Circulation

The first mechanism is the relationship between the EAC and the SAM. The amount of subtropical water transported by the EAC is highly susceptible to the mean state of the SAM on annual to decadal timescales (Cai et al., 2005; Cai, 2006; Hill et al., 2008; Hill et al., 2011; Roemmich et al., 2016). During positive SAM phases, the westerly wind belt contracts south and allows the influx of more subtropical water into the southwest Pacific (Cai et al., 2005; Cai, 2006; Hill et al., 2008; Hill et al., 2011; Roemmich et al., 2016). This process floods the Bay of Plenty, Chatham Rise and Campbell Plateau regions with tropically-sourced waters (Roemmich et al., 2007; Roemmich et al., 2016) that are more ventilated to the atmosphere and hence have lower ΔR values (Petchey et al., 2008a; Petchey et al., 2008b; Figure 3.4A-B). Unfortunately, we cannot directly test this mechanism because 1) our data does not overlap with the instrumental era (ending at 100 BP) and 2) studying coral radiocarbon over the instrumental era (when SAM observations are most robust) is impossible because ^{14}C from atmospheric nuclear weapon testing ('bomb radiocarbon') prevents calculation of ΔR values after 1950CE (Alves et al., 2018).

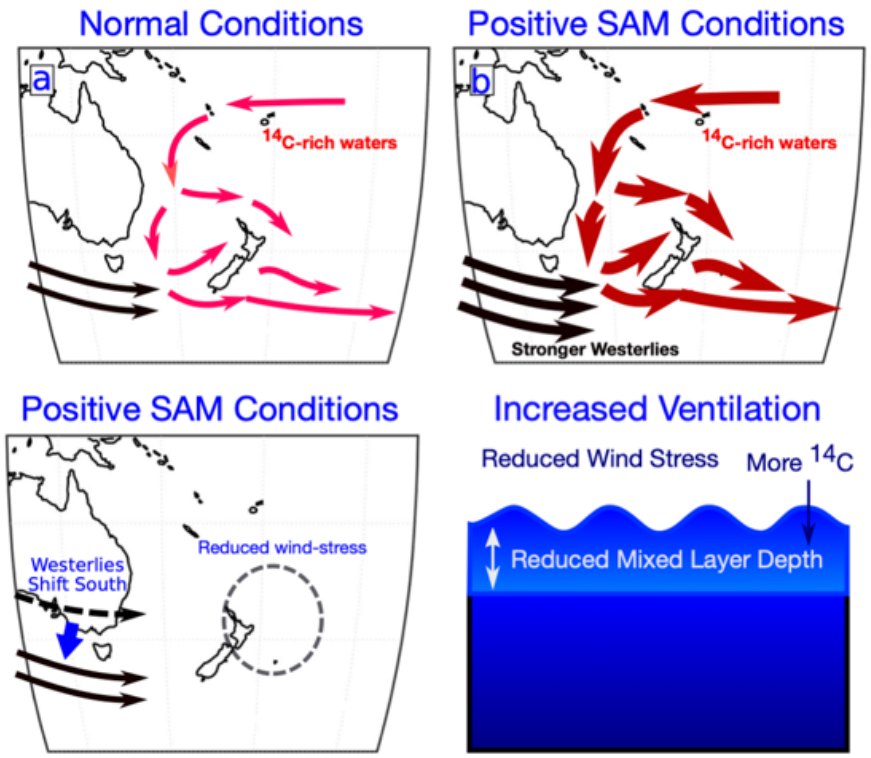

Fig. 3.4: A schematic of SAM driven changes in ocean circulation and mixed-layer depth around New Zealand. Panel A: Normal circulation conditions with neutral SAM. Panel B: Enhanced circulation (thicker arrows) driven by a positive SAM state and stronger westerly winds. Panel C: Positive SAM conditions that drive a contraction of westerly winds and reduce wind stress north and east of New Zealand. Panel D: A schematic of how positive SAM increased the air-sea gas exchange in the mixed layer.

3.5.5.2 SAM-Driven Ocean Stratification

The relationship between ΔR and SAM may also represent a change in ocean stratification driven by a decrease in wind-driven surface ocean mixing (Figure 3.4C-D). During periods of positive SAM, the mid-latitude westerlies increase in strength but contract south. This reduces surface ocean wind stress around northern and middle New Zealand and increases surface wind stress around the southern portion of New Zealand's South Island (Kidston et al., 2009; Diamond et al., 2015). The southward shift in the westerlies would effectively reduce the wind-driven surface ocean mixing north and east of New Zealand and decrease the depth of the surface mixed layer (Figure 3.4C-D). Thus, periods with positive SAM would lead to more stratified surface waters north and east of New Zealand, increasing atmospheric ventilation and decreasing ΔR. Unfortunately, we cannot evaluate this proposed mechanism over the instrumental data period for the same reasons outlined in Section 3.5.5.1.

3.5.6 Last Millennium New Zealand Climate Variability

Our ΔR record, and the variations in paleo-SAM, imply that there has been significant variability in the ocean/atmosphere system in the South Pacific over the last millennium. If so, then this would likely manifest as variations in New Zealand's terrestrial climate. We therefore compared our last-millennium ΔR composite and the Abram et al. (2014) SAM record to New Zealand records of atmospheric circulation and terrestrial temperature.

3.5.6.1 New Zealand Atmospheric Circulation

New Zealand has three synoptic weather regimes: trough, zonal, and blocking (Kidson, 2000). The trough regime is typically described as unsettled atmospheric conditions with southerly flow over New Zealand. General climate conditions resulting from this regime include are above average precipitation across the entire country, normal temperature conditions for the north and western portion of the North Island (Figure 3.5D) and below average temperatures for the southern portion of the North Island and most of the South Island (Kidson, 2000; Lorrey et al., 2007). The zonal regime results from strong westerly airflow across the country, with below average precipitation in the North Island and the north and east of coast of the South Island (Figure 3.5D) and above average precipitation along the west coast of the South Island (Kidson, 2000; Lorrey et al., 2007). Zonal regimes typically produce near normal air temperatures for all of the North Island (Figure 3.5D) and the northern portion of the South Island with above average temperatures during the middle and southern portion of the South Island (Kidson, 2000; Lorrey et al., 2007). The blocking regime is generally associated with anti-cyclonic atmospheric patterns, with warm air temperatures along the west coasts of both Islands and near normal temperatures along the east coast of both islands (Figure 3.5D). Blocking regimes generally have above average precipitation anomalies northern and eastern on the North Island regions and the north coast of the South Island, and below average precipitation in southern and western areas of both islands (Kidson, 2000; Lorrey et al., 2007).

Roop (2015) generated a paleo-atmospheric circulation index which reconstructs New Zealand synoptic weather regimes from a South Island Lake Ohau sediment core at 25yr resolution over the last 1100 years. The frequency of different New Zealand atmospheric regime types over the last millennium relate to shifts in the mean states of the ΔR and the SAM records over the last millennium (Figure 3.5B). Periods with low ΔR and positive SAM typically

correspond to periods with more blocking and zonal regimes. Conversely, periods of high ΔR and negative SAM are the only periods that include trough regimes (Figure 3.5A-B).

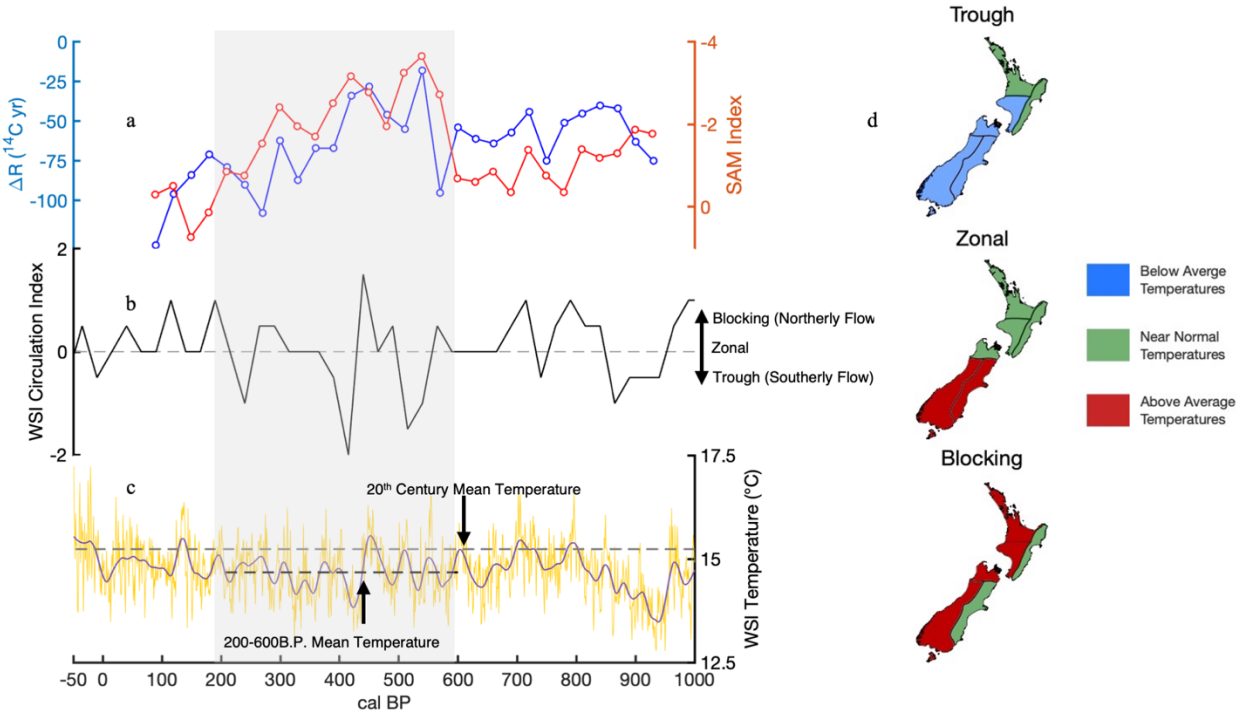

Figure 3.5: The influence of Paleo-SAM conditions on New Zealand climate and oceanography over the last millennium. Panel A: 30yr binned New Zealand ΔR and 30yr binned Paleo-SAM (Abram et al, 2014). Panel B: A circulation index representative of New Zealand's western South Island reconstructed from a Lake Ohau sediment core (Roop, 2015). Panel C: Austral summer temperatures representative of the western South Island derived from Oroko Swamp tree rings (yellow line) with a 30yr loess filter smoothing (overlaid gray line) (Cook et al, 2002). Panel D: A schematic of temperature changes driven by different atmospheric regimes (Kidson 2000; Lorrey et al, 2008).

This correspondence accords with our interpretation of the SAM-driven shift in westerly wind intensity and location over the last millennium. Periods of High ΔR and negative SAM correspond to unsettled atmospheric conditions (typical of trough regimes) as a result of the northward shift in the westerly wind belt (Figure 3.5D). Conversely, periods of low ΔR and positive SAM correspond to blocking regimes as westerlies shift southwards and are replaced by more northerly, anticyclonic airflows.

3.5.6.2 New Zealand Surface Air and Sea Surface Temperatures

Cook et al. (2002) et al. generated a terrestrial summer temperature reconstruction from the western South Island using tree-rings from the Oroko swamp (Figure 3.5A-C). Comparing this record with our ΔR record and the Abram et al. (2014) SAM record reveals that the period characterized by high ΔR/-SAM (200-600 BP; a.k.a the Little Ice Age) had temperatures up to

0.45°C cooler than present (Figure 3.5C). Conversely the two periods characterized by low ΔR/+SAM conditions (0-200 year and 600-900 year) had temperatures closer to 20th century values. The cooling during the 200-600BP interval is well documented, as other terrestrial paleoclimate records from New Zealand have shown a decrease in summer temperatures in the South Island of New Zealand up to 0.6°C (Lorrey et al., 2014). The cooling also extended to the surface ocean, as a reduction in mean SST in the southwest Pacific is documented to be cooler by up to 0.6°C around New Zealand (Lorrey et al., 2014). This suggests the long-term latitudinal positioning of the westerlies influences ocean circulation strength around New Zealand as well as mean terrestrial and sea surface temperatures on centennial timescales (Lorrey et al., 2008; Lorrey et al., 2012; Goodwin et al., 2014; Lorrey et al., 2014).

3.5.7 Late Holocene Paleo-SAM

3.5.7.1 Paleo-SAM Reconstruction Between 2000-3000BP

The Abram et al. (2014) Paleo-SAM record only dates back to 950BP. To extend this record, we use our composite ΔR record (Figure 3.3B) to reconstruct Paleo-SAM conditions for the intervals 1000-1600BP and 2000-3000BP. We calibrate this reconstruction over the 100-950BP interval by resampling the ΔR and Abram et al. SAM records to common 30 year bins and using a weighted least-squares regression (York et al., 2004) which accounts for the uncertainty in each proxy reconstruction (Supp. Fig. S3.7).

This reconstruction is presented in Figure 3.3B. We caution, however, that Abram et al. (2014) do not record a strong, long-term, positive SAM state (SAM index greater than +2). This may bias our calibration. We therefore caution against interpreting the absolute amplitude of our reconstruction. However, a good relative agreement between our reconstruction and other records (discussed below) suggests that relative changes in mean state can be interpreted with more confidence.

As noted previously, coral 35104 shows a shift in baseline ΔR towards lower values over the 1900-2900BP interval relative to the 0-1900BP interval. When converted into a paleo-SAM reconstruction using our calibration, this could be interpreted as a shift towards positive SAM conditions. However, as there is no corroborating evidence for this (Moreno et al., 2014; Moreno et al., 2018), we are hesitant to interpret millennial-timescale changes in ΔR as a shift in SAM. Instead, we focus on centennial timescale variations which are more robustly correlated in the

ΔR vs SAM calibration. To remove millennial-scale features, we therefore detrend all composite ΔR data prior to reconstructing SAM conditions (Figures 3.2 & 3.3).

3.5.7.2 Comparison with Pacific Climate Records

Our Paleo-SAM reconstruction over the 2000-3000BP interval compares favorably with climate variations on the eastern side of the South Pacific. Non-arboreal pollen (NAP) records from Lago Ciprese in Patagonia (LC NAP; Figure 3.3B; Moreno et al., 2014) capture so-called 'Ciprese Cycles' (CC) which represent periods of warm/dry conditions that serve as analogues for positive SAM-type states in Patagonia (Moreno et al., 2014). We observe a good correspondence between our SAM reconstruction and CCs over the 2000-3000BP period, with CC5 matching up with our most positive inferred Paleo-SAM conditions. We note that there is some uncertainty in the timing of CC4 based on Moreno et al. (2018) that may result from low-resolution dating constraints in the Moreno record (Figure 3.3; Appendix Tables 8-9). Nonetheless, the inferred shifts in SAM state between the CC from the Moreno et al. (2014) LC NAP record and the ΔR modeled SAM agree well over the 2000-3000BP period. These consistent shifts in SAM mean state support our assertion that variations in SAM mean state were zonally symmetric across the Pacific basin between 2000-3000BP.

3.5.7.3 Uncertainty Across the 1000-1600BP Interval

In contrast to the consistent patterns of variation seen 2000-3000BP, the relationship is less clear over the 950-1600BP interval because of some disagreement between the records. The ΔR-modeled SAM becomes inversely correlated with the LC NAP record between 900-1400BP (Figure 3.3B). In other places, the LC NAP record is contradicted by the Abram et al. (2014) SAM record, for example between 650-950BP. Here the LC NAP record shows a consistent negative SAM phase but the Abram et al. (2014) SAM index is positive. Although there is some corroborating evidence supporting the LC NAP record around the 900-1100BP interval (Goodwin et al., 2014), the exact state of paleo-SAM between 600-1600BP remains unclear. Therefore, one of the three records (ΔR, Abram et al., 2014 or the LC NAP record) may therefore not be representative of SAM over this interval.

It is possible that some of the disagreement between our ΔR-modeled SAM and the LC NAP records over the 1000-1600BP interval relates to the frequency of U-Th dates across that period. This portion of the record has a lower frequency of U-Th dates (Figure 3.2A),

necessitating larger interpolation intervals. This may add inaccuracy to the absolute chronology and therefore to ΔR variations. Additional U-Th dates may be necessary to better constrain the ΔR record over the 1000-1600BP interval.

3.5.8 Paleo-SAM and SPG Implications

We conclude that the paleo-SAM conditions inferred from our ΔR records are robust over the last millennium and 2000-3000BP period based on the relative agreement between our ΔR reconstructions, the Abram et al. (2014) Paleo-SAM index and the inferred SAM state from the Lago Cipreses record. The ΔR-SAM relationship arises from changing EAC circulation, so our reconstructions suggest the late Holocene experienced multi-centennial-long periods of enhanced gyre strength forced by more positive SAM conditions.

The co-variation between ΔR and SAM in the late Holocene appears similar to SAM-induced gyre changes over the industrial period and provides context for future projections of SAM and SPG circulation into the 21st century (Zheng et al., 2013). Modern instrumental observations reveal an increasing EAC strength over the last several decades, and a number of studies have debated an anthropogenic cause (Cai et al., 2005; Cai, 2006; Roemmich et al., 2016). However, our results suggest that modern gyre changes are not unprecedented, certainly over the last millennium.

Separating anthropogenic impacts from natural variability in SPG circulation remains a difficult task. Our study, like others (Cai et al., 2005; Cai, 2006; Moreno et al., 2014), is not able to fully constrain the external climate forcings driving coupled variations in SPG and SAM. This highlights the need to elucidate mechanisms behind natural mid-latitude ocean-atmosphere variability on centennial to multi-centennial timescales. Ultimately, evaluating southwest Pacific circulation in an anthropogenic context will require a larger set of high-resolution paleo-circulation records.

3.6 Conclusions

The coral radiocarbon records provide spatiotemporal constraints on ΔR variability in the waters around New Zealand over the last 3000 years. Over the last millennium, ΔR in New Zealand waters is significantly correlated with paleo reconstructions of SAM spanning the South America-Antarctica sector of the southern mid-to-high latitudes spanning the Drake Passage. This supports modern instrumental observations which show the SAM affects SPG strength and

wind stress in the Southwest Pacific on multi-decadal timescales (Cai et al., 2005; Cai, 2006; Roemmich et al., 2016). Both mechanisms potentially influence ΔR by altering transport of well-ventilated subtropical waters southwards in the western Pacific and changing stratification of surface waters around New Zealand. Our results suggest that these mechanisms have acted on multi-centennial timescales for at least the last 1000 years.

Over the last 1000 years, multi-centennial variations in our ΔR-SAM reconstruction correspond with changes in New Zealand's synoptic weather regimes and surface temperatures. The relationship is most evident during the extended period of negative SAM and positive ΔR between 200 and 600BP (a.k.a the Little Ice Age) where surface temperatures were up to 0.6°C cooler (Lorrey et al., 2014). This period represents a marked change in atmospheric circulation that includes several trough regimes lasting up to 100 years. These regimes typically include more unsettled atmospheric conditions that are coincident with a northern shift of the westerly wind belt during negative SAM phases.

We also observe a baseline shift in mean ΔR between 0-1900BP to 1900-3000BP that appears to match a depression in ΔR observed by Komugabe-Dixson et al. (2016) in the south Tasman Sea. We propose that this baseline shift represents a change in SPG radiocarbon distribution driven by a change in ENSO.

We infer that the SPG may be influenced by two modes of natural variability linked to large hemispheric-scale climate phenomena: 1) On multi-centennial timescales, variability in SPG strength is driven by changes in the SAM; and 2) On millennial timescales change in SPG strength is driven by changes in ENSO. Our results suggest that the strengthening of the SPG observed in the last century may not necessarily be unprecedented over the last 3000 years. While separating the influences of natural and greenhouse gas forcing on recent South Pacific Gyre variability remains a difficult task, our ΔR reconstructions provide insight into the natural variability of the SPG over the late Holocene and can be used as a benchmark for future climate projections that incorporate natural gyre variability.

3.7 Acknowledgments:

Black corals were provided by the National Institute of Water and Atmosphere Invertebrate Collection. We wish to thank Peter Marriot, Sadie Mills and Dianna Macpherson for assistance with coral access, providing a space to sub-sample coral sections and navigating

CITES permitting. Black coral micro-milling was accommodated by the National Institute of Water and Atmosphere Stable Isotope Facility. We wish to thank Gordon Brailsford, Colin Nankivell, Tony Bromley, and Sally Gray for access to laboratory space for micro-milling. This work benefited from conversations with Drew Lorrey, Di Tracey, Sebastian Breitenbach, Philip Sutton and Nicky Wright. Funding for this work was provided by the New Zealand Royal Society Marsden Fund Grant No. NIWA1602 awarded to HLN, DJS, SJF and AKD. Seed funding was provided by URF 210024 awarded to DJS. The authors declare no conflicts of interest.

3.9 References:

Abram, N. J., Mulvaney, R., Vimeux, F., Phipps, S. J., Turner, J., & England, M. H. (2014). Evolution of the Southern Annular Mode during the past millennium. *Nature Climate Change, 4*(7), 564-569. https://doi.org/10.1038/nclimate2235

Alves, E. Q., Macario, K., Ascough, P., & Bronk Ramsey, C. (2018). The Worldwide Marine Radiocarbon Reservoir Effect: Definitions, Mechanisms, and Prospects. *Reviews of Geophysics, 56*(1), 278-305. https://doi.org/10.1002/2017RG000588

Barr, C., Tibby, J., Leng, M. J., Tyler, J. J., Henderson, A. C. G., Overpeck, J. T., et al. (2019). Holocene El Niño–Southern Oscillation variability reflected in subtropical Australian precipitation. *Scientific Reports, 9*(1), 1627. https://doi.org/10.1038/s41598-019-38626-3

Bostock, H. C., Hayward, B. W., Neil, H. L., Sabaa, A. T., & Scott, G. H. (2015). Changes in the position of the Subtropical Front south of New Zealand since the last glacial period. *Paleoceanography, 30*(7), 824-844. http://dx.doi.org/10.1002/2014PA002652

Bostock, H. C., Prebble, J. G., Cortese, G., Hayward, B., Calvo, E., Quirós-Collazos, L., et al. (2019). Paleoproductivity in the SW Pacific Ocean During the Early Holocene Climatic Optimum. *Paleoceanography and Paleoclimatology, 34*(4), 580-599. https://doi.org/10.1029/2019PA003574

Breitenbach, S. F. M., Rehfeld, K., Goswami, B., Baldini, J. U. L., Ridley, H. E., Kennett, D. J., et al. (2012). COnstructing Proxy Records from Age models (COPRA). *Clim. Past, 8*(5), 1765-1779. https://www.clim-past.net/8/1765/2012/

Cai, W. (2006). Antarctic ozone depletion causes an intensification of the Southern Ocean super-gyre circulation. *Geophysical Research Letters, 33*(3), n/a-n/a. http://dx.doi.org/10.1029/2005GL024911

Cai, W., Shi, G., Cowan, T., Bi, D., & Ribbe, J. (2005). The response of the Southern Annular Mode, the East Australian Current, and the southern mid-latitude ocean circulation to global warming. *Geophysical Research Letters, 32*(23), n/a-n/a. http://dx.doi.org/10.1029/2005GL024701

Chen, S., Hoffmann, S. S., Lund, D. C., Cobb, K. M., Emile-Geay, J., & Adkins, J. F. (2016). A high-resolution speleothem record of western equatorial Pacific rainfall: Implications for Holocene ENSO evolution. *Earth and Planetary Science Letters, 442*, 61-71. http://www.sciencedirect.com/science/article/pii/S0012821X16300759

Cheng, H., Lawrence Edwards, R., Shen, C.-C., Polyak, V. J., Asmerom, Y., Woodhead, J., et al. (2013). Improvements in 230Th dating, 230Th and 234U half-life values, and U–Th isotopic measurements by multi-collector inductively coupled plasma mass spectrometry. *Earth and Planetary Science Letters, 371*(Supplement C), 82-91. http://www.sciencedirect.com/science/article/pii/S0012821X13001878

Chiswell, S. M., Bostock, H. C., Sutton, P. J. H., & Williams, M. J. M. (2015). Physical oceanography of the deep seas around New Zealand: a review. *New Zealand Journal of Marine and Freshwater Research, 49*(2), 286-317. https://doi.org/10.1080/00288330.2014.992918

Cobb, K., Westphal, N., Sayani, H., Watson, J., Di Lorenzo, E., Cheng, H., et al. (2013). Highly Variable El Nino-Southern Oscillation Throughout the Holocene. *Science, 339*, 67-70.

Cook, E. R., Palmer, J. G., & D'Arrigo, R. D. (2002). Evidence for a 'Medieval Warm Period' in a 1,100 year tree-ring reconstruction of past austral summer temperatures in New Zealand. *Geophysical Research Letters, 29*(14), 12-11-12-14. https://doi.org/10.1029/2001GL014580

Cortese, G., Dunbar, G. B., Carter, L., Scott, G., Bostock, H., Bowen, M., et al. (2013). Southwest Pacific Ocean response to a warmer world: Insights from Marine Isotope Stage 5e. *Paleoceanography, 28*(3), 585-598. https://doi.org/10.1002/palo.20052

De Boer, A. M., Graham, R. M., Thomas, M. D., & Kohfeld, K. E. (2013). The control of the Southern Hemisphere Westerlies on the position of the Subtropical Front. *Journal of Geophysical Research: Oceans, 118*(10), 5669-5675. http://dx.doi.org/10.1002/jgrc.20407

Delcroix, T., & Picaut, J. (1998). Zonal displacement of the western equatorial Pacific "fresh pool". *Journal of Geophysical Research: Oceans, 103*(C1), 1087-1098. http://dx.doi.org/10.1029/97JC01912

Diamond, H., & Renwick, J. (2015). The climatological relationship between tropical cyclones in the southwest Pacific and the southern annular mode. *International Journal of Climatology, 35*(4), 613-623.

Ding, Q., Steig, E. J., Battisti, D. S., & Wallace, J. M. (2012). Influence of the tropics on the Southern Annular Mode. *Journal of Climate, 25*(18), 6330-6348.

Druffel, E. R. M., & Griffin, S. (1993). Large variations of surface ocean radiocarbon: Evidence of circulation changes in the southwestern Pacific. *Journal of Geophysical Research: Oceans, 98*(C11), 20249-20259. http://dx.doi.org/10.1029/93JC02113

Drysdale, R. N., Spötl, C., Hellstrom, J. C., & Richards, D. A. (2012). New advances in the dating of speleothems. *Quaternary Geochronology, 14*(Complete), 1-4.

Emile-Geay, J., Cobb, K., Carré, M., Braconnot, P., Leloup, J., Zhou, Y., et al. (2015). Links between tropical Pacific seasonal, interannual and orbital variability during the Holocene. *Nature Geoscience, 9*.

Fallon, S., Fifield, L., & Chappel, J. (2010). The next chapter in radiocarbon dating at the Australian National University: Status report on the single stage AMS. *Nuclear Instruments and Methods in Physics Research: Section B, 268*(7-8), 898-901.

Ganachaud, A., Cravatte, S., Melet, A., Schiller, A., Holbrook, N. J., Sloyan, B. M., et al. (2014). The Southwest Pacific Ocean circulation and climate experiment (SPICE). *Journal of Geophysical Research-Oceans, 119*(11), 7660-7686. <Go to ISI>://WOS:000346102900017

Goodwin, I., Browning, S., Lorrey, A., Mayewski, P., Phipps, S., Bertler, N., et al. (2014). A reconstruction of extratropical Indo-Pacific sea-level pressure patterns during the Medieval Climate Anomaly. *Climate Dynamics, 43*, 1197-1219.

Graham, R. M., & De Boer, A. M. (2013). The Dynamical Subtropical Front. *Journal of Geophysical Research: Oceans, 118*(10), 5676-5685. http://dx.doi.org/10.1002/jgrc.20408

Guilderson, T. P., & Schrag, D. P. (1998). Abrupt Shift in Subsurface Temperatures in the Tropical Pacific Associated with Changes in El Niño. *Science, 281*(5374), 240. http://science.sciencemag.org/content/281/5374/240.abstract

Hall, A., & Visbeck, M. (2002). Synchronous Variability in the Southern Hemisphere Atmosphere, Sea Ice, and Ocean Resulting from the Annular Mode. *Journal of Climate, 15*(21), 3043-3057. https://doi.org/10.1175/1520-0442(2002)015<3043:SVITSH>2.0.CO;2

Haug, G. H., Hughen, K. A., Sigman, D. M., Peterson, L. C., & Röhl, U. (2001). Southward Migration of the Intertropical Convergence Zone Through the Holocene. *Science, 293*(5533), 1304. http://science.sciencemag.org/content/293/5533/1304.abstract

Heaton, T. J., Köhler, P., Butzin, M., Bard, E., Reimer, R. W., Austin, W. E. N., et al. (2020). MARINE20—THE MARINE RADIOCARBON AGE CALIBRATION CURVE (0–55,000 CAL BP). *Radiocarbon*, 1-42. https://www.cambridge.org/core/article/marine20the-marine-radiocarbon-age-calibration-curve-055000-cal-bp/B3013899914A3198D4B884B7B6E5CE66

Hellstrom, J. (2003). Rapid and accurate U/Th dating using parallel ion-counting multi-collector ICP-MS. *Journal of Analytical Atomic Spectrometry, 18*(11), 1346-1351. 10.1039/B308781F. http://dx.doi.org/10.1039/B308781F

Hellstrom, J. (2006). U-Th dating of speleothems with high initial 230Th using stratigraphical constraint. *Quaternary Geochronology, 1*, 289-295.

Hill, K. L., Rintoul, S. R., Coleman, R., & Ridgway, K. R. (2008). Wind forced low frequency variability of the East Australia Current. *Geophysical Research Letters, 35*(8), n/a-n/a. http://dx.doi.org/10.1029/2007GL032912

Hill, K. L., Rintoul, S. R., Ridgway, K. R., & Oke, P. R. (2011). Decadal changes in the South Pacific western boundary current system revealed in observations and ocean state estimates. *Journal of Geophysical Research: Oceans, 116*(C1), n/a-n/a. http://dx.doi.org/10.1029/2009JC005926

Hitt, N. T., Sinclair, D. J., Fallon, S. J., Neil, H. L., Tracey, D. M., Komugabe-Dixson, A., & Marriott, P. (2020). Growth and longevity of New Zealand black corals. *Deep Sea Research Part I: Oceanographic Research Papers*, 103298. http://www.sciencedirect.com/science/article/pii/S0967063720300868

Hobbs, W. R., & Raphael, M. N. (2010). Characterizing the zonally asymmetric component of the SH circulation. *Climate Dynamics, 35*(5), 859-873. https://doi.org/10.1007/s00382-009-0663-z

Jones, J. M., Fogt, R. L., Widmann, M., Marshall, G. J., Jones, P. D., & Visbeck, M. (2009). Historical SAM Variability. Part I: Century-Length Seasonal Reconstructions. *Journal of Climate, 22*(20), 5319-5345. https://doi.org/10.1175/2009JCLI2785.1

Key, R. M., Kozyr, A., Sabine, C. L., Lee, K., Wanninkhof, R., Bullister, J. L., et al. (2004). A global ocean carbon climatology: Results from Global Data Analysis Project (GLODAP). *Global Biogeochemical Cycles, 18*(4). https://doi.org/10.1029/2004GB002247

Kidson, J. (2000). An analysis of New Zealand synoptic types and their use in defining weather regimes. *International Journal of Climatology, 20*, 299-316.

Kidston, J., Renwick, J., & McGregor, J. (2009). Hemispheric-scale seasonality of the Southern Annular Mode and impacts on the climate of New Zealand. *Journal of Climate, 22*(18), 4759-4770.

Komugabe, A. F., Fallon, S. J., Thresher, R. E., & Eggins, S. M. (2014). Modern Tasman Sea surface reservoir ages from deep-sea black corals. *Deep Sea Research Part II: Topical Studies in Oceanography, 99*(Supplement C), 207-212. http://www.sciencedirect.com/science/article/pii/S0967064513002154

Komugabe-Dixson, A. F., Fallon, S. J., Eggins, S. M., & Thresher, R. E. (2016). Radiocarbon evidence for mid-late Holocene changes in southwest Pacific Ocean circulation. *Paleoceanography, 31*(7), 971-985. http://dx.doi.org/10.1002/2016PA002929

Lorrey, A. M., Fauchereau, N., Stanton, C., Chappell, P., Phipps, S., Mackintosh, A., et al. (2014). The Little Ice Age climate of New Zealand reconstructed from Southern Alps cirque glaciers: a synoptic type approach. *Climate Dynamics, 42*(11), 3039-3060. https://doi.org/10.1007/s00382-013-1876-8

Lorrey, A. M., Fowler, A., & Salinger, M. (2007). Regional climate regime classification as a qualitative tool for interpreting multi-proxy palaeoclimate data spatial patterns: A New Zealand case study. *Palaeogeography, Palaeoclimatology, Palaeoecology, 253*, 407–433.

Lorrey, A. M., Vandergoes, M., Almond, P., Renwick, J., Stephens, T., Bostock, H., et al. (2012). Palaeocirculation across New Zealand during the last glacial maximum at ~21 ka. *Quaternary Science Reviews, 36*, 189-213. http://www.sciencedirect.com/science/article/pii/S0277379111003040

Lorrey, A. M., Williams, P., Salinger, M., Martin, T., Palmer, J., Fowler, A., et al. (2008). Speleothem stable isotope records interpreted within a multi-proxy framework and implications for New Zealand palaeoclimate reconstruction. *Quaternary International, 187*, 52-75.

Marshall, G. J. (2003). Trends in the Southern Annular Mode from Observations and Reanalyses. *Journal of Climate, 16*(24), 4134-4143. https://journals.ametsoc.org/doi/abs/10.1175/1520-0442%282003%29016%3C4134%3ATITSAM%3E2.0.CO%3B2

Marshall, G. J., Stott, P. A., Turner, J., Connolley, W. M., King, J. C., & Lachlan-Cope, T. A. (2004). Causes of exceptional atmospheric circulation changes in the Southern Hemisphere. *Geophysical Research Letters, 31*(14), n/a-n/a. http://dx.doi.org/10.1029/2004GL019952

McCulloch, M. T., Gagan, M. K., Mortimer, G. E., Chivas, A. R., & Isdale, P. J. (1994). A high-resolution Sr/Ca and δ18O coral record from the Great Barrier Reef, Australia, and the 1982–1983 El Niño. *Geochimica et Cosmochimica Acta, 58*(12), 2747-2754. http://www.sciencedirect.com/science/article/pii/0016703794901422

Moreno, P. I., Francois, J. P., Moy, C. M., & Villa-Martínez, R. (2010). Covariability of the Southern Westerlies and atmospheric CO2 during the Holocene. *Geology, 38*(8), 727-730. http://dx.doi.org/10.1130/G30962.1

Moreno, P. I., François, J. P., Villa-Martínez, R. P., & Moy, C. M. (2009). Millennial-scale variability in Southern Hemisphere westerly wind activity over the last 5000 years in SW Patagonia. *Quaternary Science Reviews, 28*(1), 25-38. http://www.sciencedirect.com/science/article/pii/S0277379108002886

Moreno, P. I., Vilanova, I., Villa-Martínez, R., Dunbar, R. B., Mucciarone, D. A., Kaplan, M. R., et al. (2018). Onset and Evolution of Southern Annular Mode-Like Changes at Centennial Timescale. *Scientific Reports, 8*(1), 3458. https://doi.org/10.1038/s41598-018-21836-6

Moreno, P. I., Vilanova, I., Villa-Martínez, R., Garreaud, R. D., Rojas, M., & De Pol-Holz, R. (2014). Southern Annular Mode-like changes in southwestern Patagonia at centennial timescales over the last three millennia. *Nature Communications, 5*(1), 4375. https://doi.org/10.1038/ncomms5375

Moy, C. M., Seltzer, G. O., Rodbell, D. T., & Anderson, D. M. (2002). Variability of El Niño/Southern Oscillation activity at millennial timescales during the Holocene epoch. *Nature, 420*(6912), 162-165. https://doi.org/10.1038/nature01194

Oliver, E. C. J., & Holbrook, N. J. (2018). Variability and Long-Term Trends in the Shelf Circulation Off Eastern Tasmania. *Journal of Geophysical Research: Oceans, 123*(10), 7366-7381. https://doi.org/10.1029/2018JC013994

Petchey, F., Anderson, A., Hogg, A., & Zondervan, A. (2008a). The marine reservoir effect in the Southern Ocean: An evaluation of extant and new ?R values and their application to archaeological chronologies. *Journal of the Royal Society of New Zealand, 38*(4), 243-262. https://doi.org/10.1080/03014220809510559

Petchey, F., Anderson, A., Zondervan, A., Ulm, S., & Hogg, A. (2008b). New Marine ΔR Values for the South Pacific Subtropical Gyre Region. *Radiocarbon, 50*(3), 373-397. https://www.cambridge.org/core/article/new-marine-r-values-for-the-south-pacific-subtropical-gyre-region/4345B6851E825BA6A30B466D5F6F17D8

Prouty, N. G., Roark, E. B., Koenig, A. E., Demopoulos, A. W. J., Batista, F. C., Kocar, B. D., et al. (2014). Deep-sea coral record of human impact on watershed quality in the Mississippi River Basin. *Global Biogeochemical Cycles, 28*(1), 29-43. http://dx.doi.org/10.1002/2013GB004754

Reimer, R. W., & Reimer, P. J. (2017). An Online Application for ΔR Calculation. *Radiocarbon, 59*(5), 1623-1627. https://www.cambridge.org/core/article/an-online-application-for-r-calculation/4C2B1FF26FF4E7F2F7F84A707FAFBDE0

Ridgway, K. R. (2007a). Long-term trend and decadal variability of the southward penetration of the East Australian Current. *Geophysical Research Letters, 34*(13), n/a-n/a. http://dx.doi.org/10.1029/2007GL030393

Ridgway, K. R. (2007b). Seasonal circulation around Tasmania: An interface between eastern and western boundary dynamics. *Journal of Geophysical Research: Oceans, 112*(C10), n/a-n/a. http://dx.doi.org/10.1029/2006JC003898

Ridgway, K. R., Coleman, R. C., Bailey, R. J., & Sutton, P. (2008). Decadal variability of East Australian Current transport inferred from repeated high-density XBT transects, a CTD survey and satellite altimetry. *Journal of Geophysical Research: Oceans, 113*(C8), n/a-n/a. http://dx.doi.org/10.1029/2007JC004664

Roemmich, D., Gilson, J., Davis, R., Sutton, P., Wijffels, S., & Riser, S. (2007). Decadal Spinup of the South Pacific Subtropical Gyre. *Journal of Physical Oceanography, 37*(2), 162-173. http://journals.ametsoc.org/doi/abs/10.1175/JPO3004.1

Roemmich, D., Gilson, J., Sutton, P., & Zilberman, N. (2016). Multidecadal Change of the South Pacific Gyre Circulation. *Journal of Physical Oceanography, 46*(6), 1871-1883. https://doi.org/10.1175/JPO-D-15-0237.1

Roop, H. A. (2015). *Late-Holocene Climate Variability in Southern New Zealand: A reconstruction of regional climate from an annually laminated sediment sequence from Lake Ohau.* (Doctoral Thesis Doctoral), Victoria University of Wellington, Victoria Unversity of Wellington.

Shears, N. T., & Bowen, M. M. (2017). Half a century of coastal temperature records reveal complex warming trends in western boundary currents. *Scientific Reports, 7*(1), 14527. https://doi.org/10.1038/s41598-017-14944-2

Stott, L., Cannariato, K., Thunell, R., Haug, G. H., Koutavas, A., & Lund, S. (2004). Decline of surface temperature and salinity in the western tropical Pacific Ocean in the Holocene epoch. *Nature, 431*(7004), 56-59. https://doi.org/10.1038/nature02903

Ummenhofer, C. C., & England, M. H. (2007). Interannual Extremes in New Zealand Precipitation Linked to Modes of Southern Hemisphere Climate Variability. *Journal of Climate, 20*(21), 5418-5440. https://journals.ametsoc.org/doi/abs/10.1175/2007JCLI1430.1

Villalba, R., Lara, A., Masiokas, M. H., Urrutia, R., Luckman, B. H., Marshall, G. J., et al. (2012). Unusual Southern Hemisphere tree growth patterns induced by changes in the Southern Annular Mode. *Nature Geoscience, 5*(11), 793-798. https://doi.org/10.1038/ngeo1613

Williams, B. (2020). Proteinaceous corals as proxy archives of paleo-environmental change. *Earth-Science Reviews*, 103326. http://www.sciencedirect.com/science/article/pii/S001282522030372X

Wu, L., Cai, W., Zhang, L., Nakamura, H., Timmermann, A., Joyce, T., et al. (2012). Enhanced warming over the global subtropical western boundary currents. *Nature Clim. Change, 2*(3), 161-166. 10.1038/nclimate1353. http://dx.doi.org/10.1038/nclimate1353

York, D., Evensen, N. M., Martínez, M. L., & Delgado, J. D. B. (2004). Unified equations for the slope, intercept, and standard errors of the best straight line. *American Journal of Physics, 72*(3), 367-375. http://aapt.scitation.org/doi/abs/10.1119/1.1632486

Zheng, F., Li, J., Clark, R. T., & Nnamchi, H. C. (2013). Simulation and Projection of the Southern Hemisphere Annular Mode in CMIP5 Models. *Journal of Climate, 26*(24), 9860-9879. https://doi.org/10.1175/JCLI-D-13-00204.1

3.10 Supplementary Information:

3.10.1 Omission of 35104 Record Over 577-2000BP

Coral 35104 exhibits an extreme reduction in growth across the 577-2000BP interval (Supp. Fig. S3.3). Growth rapidly slows from ~35µm/yr to ~1µm/yr beginning ca. 2000BP. Growth rate is suppressed until ~1000BP, when it slowly starts to rise back to ~10µm/yr until the coral's death ~600BP. Such a rapid decline in growth rate has not been seen in other black coral studies (Roark et al., 2009; Prouty et al., 2011; Carreiro-Silva et al., 2013; Komugabe-Dixson et al., 2016). Hitt et al. (2020) speculate the change in growth may result from some traumatic event or animal grazing on the coral skeleton.

U-Th dates are sparse over the 577-2000BP (slow growth) interval. In addition, the initial $^{230/232}$Th values of these dates (54 ±11) are notably higher than the older portion of this coral (14 ± 7), and for other corals in the Southwest Pacific (1-40 for other corals studied here as well as those in Komugabe-Dixson et al. (2016)). These high initial $^{230/232}$Th values result in U-Th age uncertainties up to ten times larger between 577-2000BP compared with 2000-3000BP. In addition, the slow growth results in larger time gaps between U-Th dates, hence longer interpolations. The average 'distance' over which U-Th dates are interpolated is 20-40 years for most of our corals, but several centuries for the slow-growth interval of coral 35104. Long interpolations between more uncertain dates results in highly imprecise ΔR reconstructions and calculated ΔR values between 577-2000BP are not statistically distinguishable from each other (Supp. Fig. S3.4).

To illustrate the problem: calculating ΔR across the entire 35104 record using the full suite of the U-Th dates shows a multi-centennial ΔR cycle with an amplitude of ~500 ^{14}Cyr (Supp. Fig. S3.4). This is unrealistic: a ΔR change of ~500 ^{14}Cyr would require a major reorganization of ocean current regimes around New Zealand (Sikes et al., 2000) or a significant change to ^{14}C inventory of the global ocean (Skinner et al., 2017). Such changes only occur on glacial-interglacial timescales (Sikes et al., 2000; Skinner et al., 2017) and there is no evidence for either mechanism over the last 3000 years (Komugabe-Dixson et al., 2016).

We therefore conclude that the 577-2000BP section of 35104 is unsuitable for ΔR reconstruction with the current U-Th age datasets. We therefore remove the 35104 ΔR data over the 577-2000BP interval from all figures, calculations and data interpretations in the main text.

3.10.2 Description of $\Delta^{14}C$ Calculation

$\Delta^{14}C$ was calculated in all corals using the following equation: $\Delta^{14}\mathrm{C} = (\mathrm{F} \times e^{\lambda t} - 1) \times 1000$ where $\lambda = 1/8267$ years, based on the Cambridge (5730) half-life and *t* is the age of the sample (years before 1950 AD) (Supp. Fig. S3.2). Fraction modern is converted into a radiocarbon age using the Libby half-life of 5568 years (Stuiver et al., 1977) in the following equation:

$$\text{Radiocarbon age} = -8033 \times \ln(F_m).$$

3.11 Supplementary Figures:

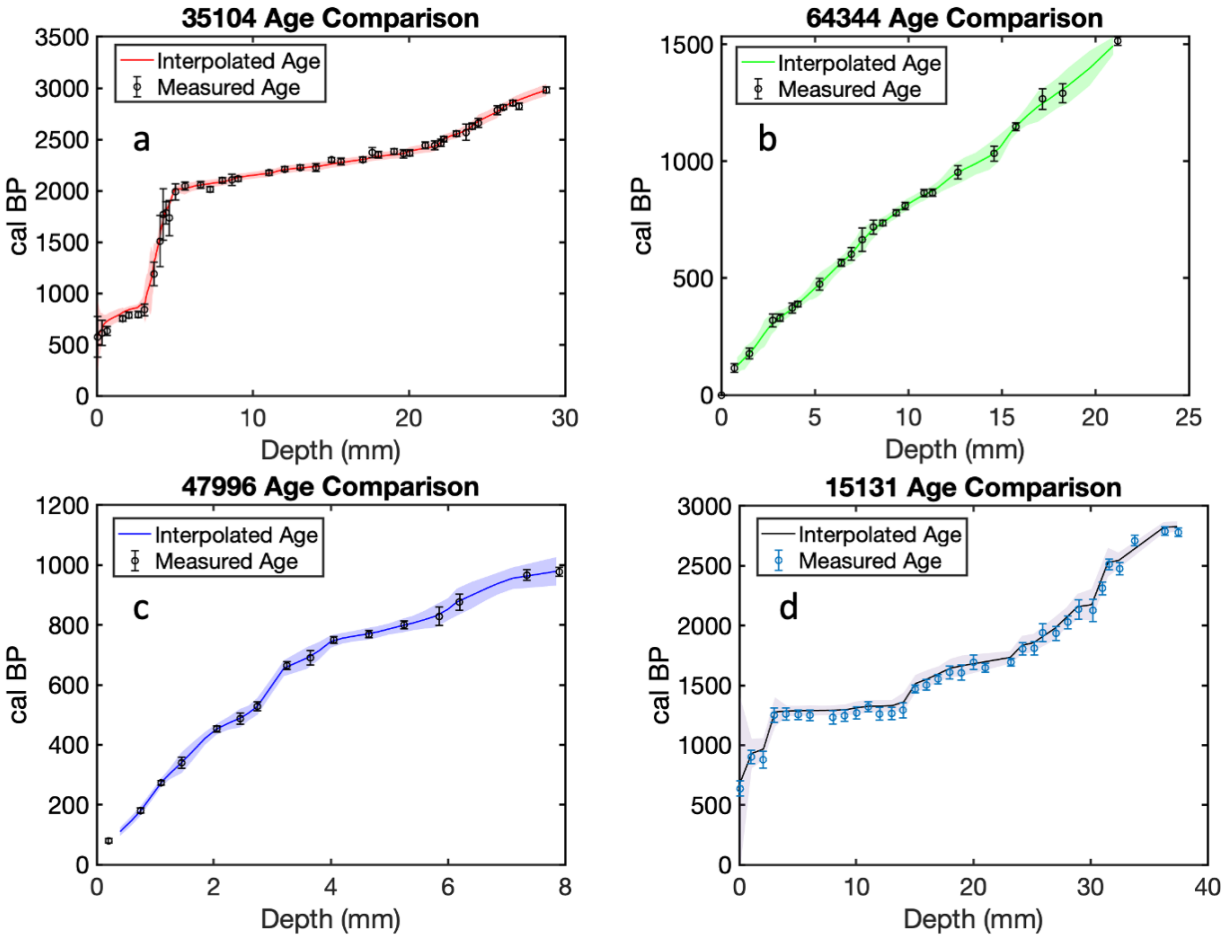

Supp. Fig. S3.1: Interpolated and initial Th corrected age comparisons. A comparison between initial Th corrected ages (symbols) and interpolated age models from COPRA (colored lines). All uncertainties shown are 2σ. Depth progresses from the outer coral (0mm) to inner coral (e.g. 20mm).

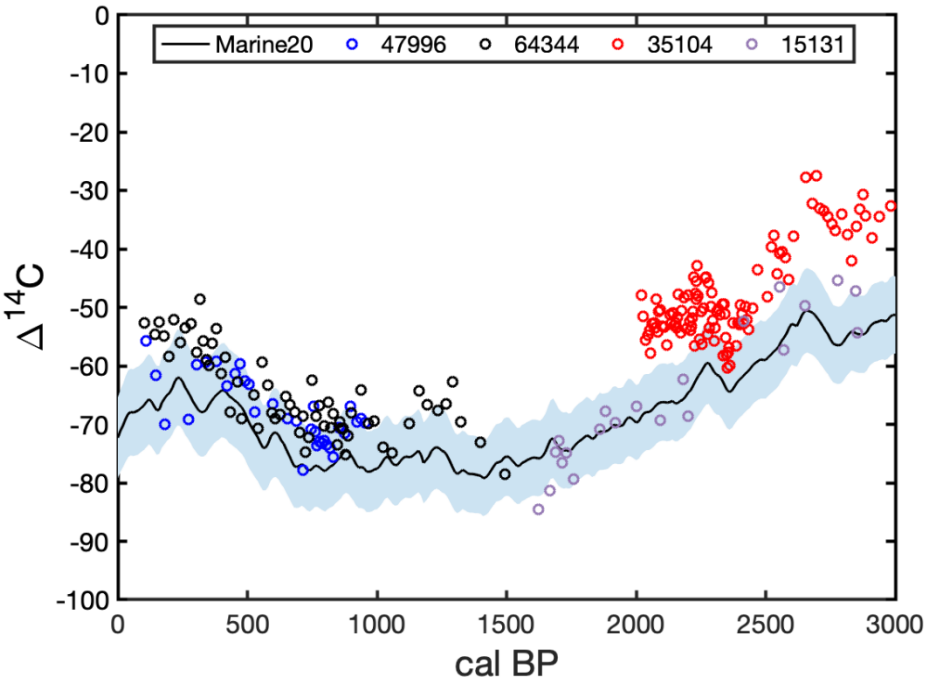

Supp. Fig. S3.2: Coral and Marine20 $\Delta^{14}C$. Coral $\Delta^{14}C$ plotted overtop $\Delta^{14}C$ from Marine13 (Heaton et al., 2020). Uncertainties shown are 1σ. Coral $\Delta^{14}C$ uncertainties are smaller than the size of individual datapoint dots.

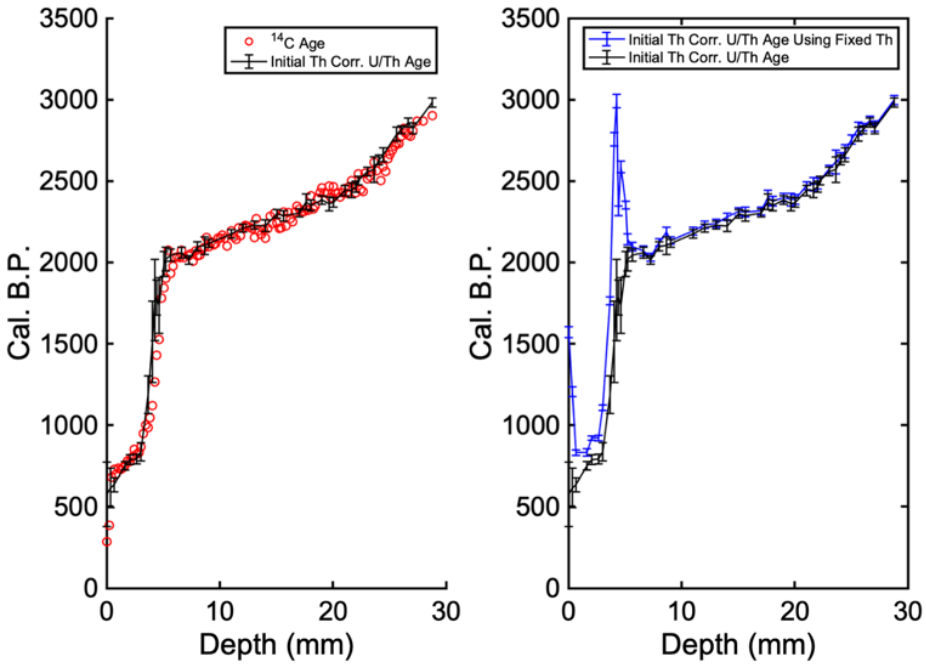

Supp. Fig. S3.3: Radiocarbon and initial Th corrected ages in coral 35104. (Left Panel) A comparison between calibrated radiocarbon ages (red circles) and initial Th corrected U-Th ages. (Right Panel) A comparison between raw U/Th ages corrected with a fixed initial Th value of 1.5 +/- 1.5 (blue line) and initial Th corrected U-Th ages following the stratigraphic constraint method of Hellstrom (2006).

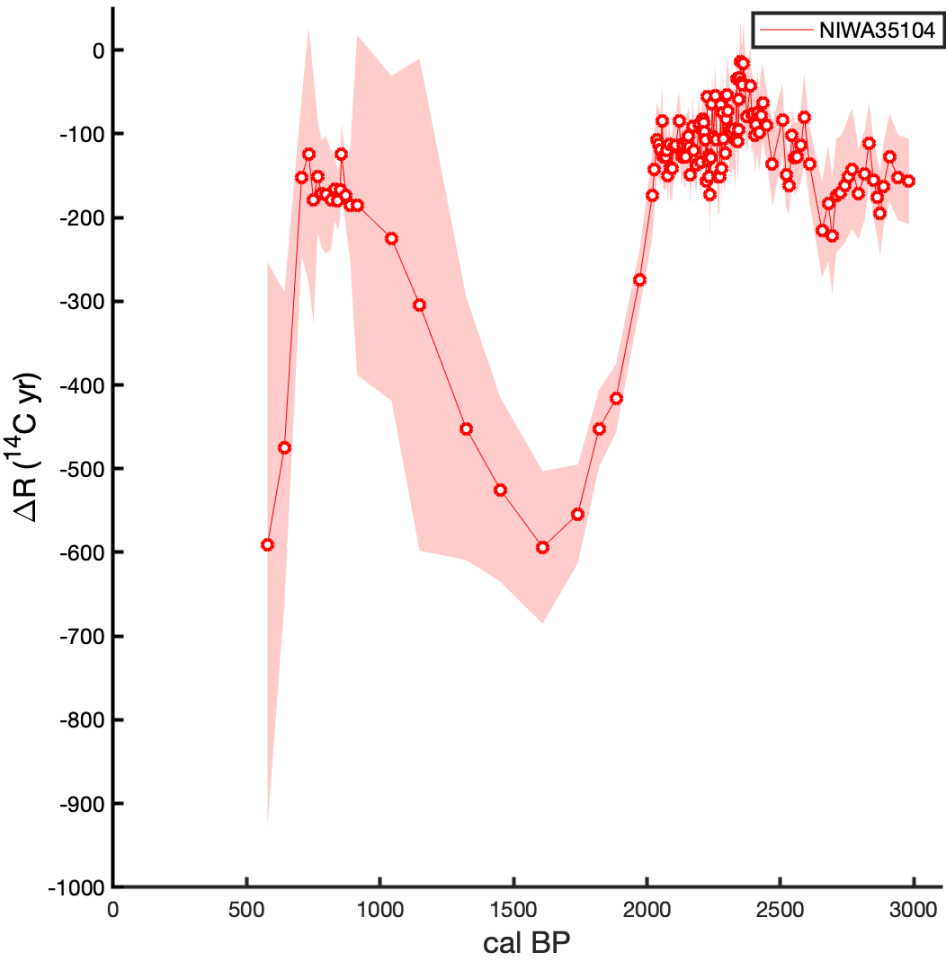

Supp. Fig. S3.4: The Complete Coral 35104 ΔR Record. ΔR in coral 35104 from 577-3000BP. ΔR shows an unrealistic oscillation with an amplitude of ~500 ^{14}Cyr over the 566-2000BP interval. This interval corresponds to unusually slow growth and high detrital Th values (Supp. Fig. S3.3). The unusually slow growth comprises accurately interpolating U-Th age to the frequency of ^{14}C dates, which contributes to the large ΔR oscillations. The high detrital Th values affect U-Th date precision which contributes to ΔR that are not significantly different from one another over this period.

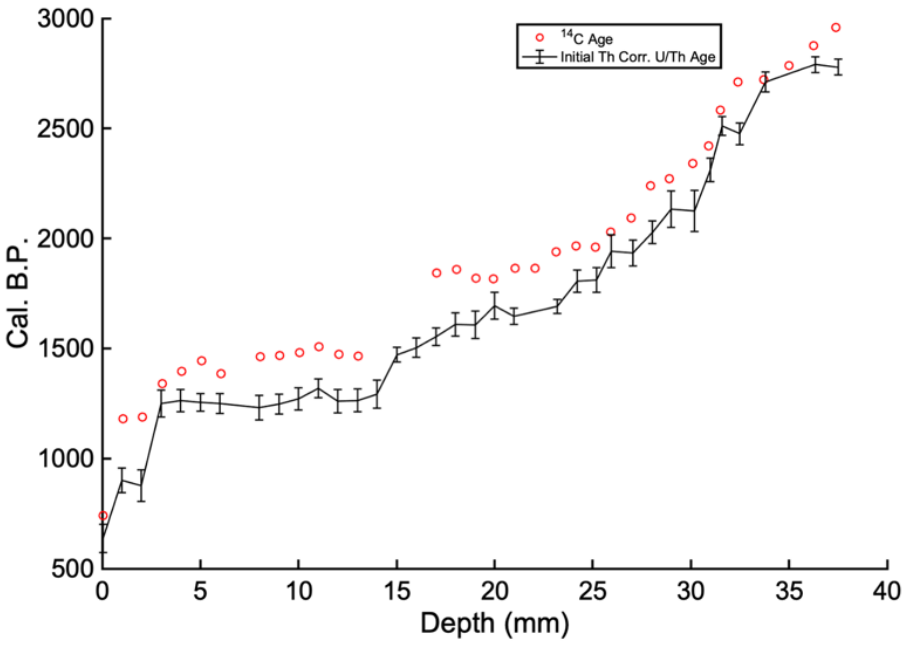

Supp. Fig. S3.5: Radiocarbon and U-Th ages in Coral 15131. A comparison of radiocarbon ages (red dots) and initial Th corrected U-Th ages following the stratigraphic constraint method of Hellstrom (2006). Both dating methods show a period of fast growth from 0-15mm followed by slower growth from 15mm-40mm. Radiocarbon uncertainties range 21-22 years (the size of the individual red dots) (Appendix A).

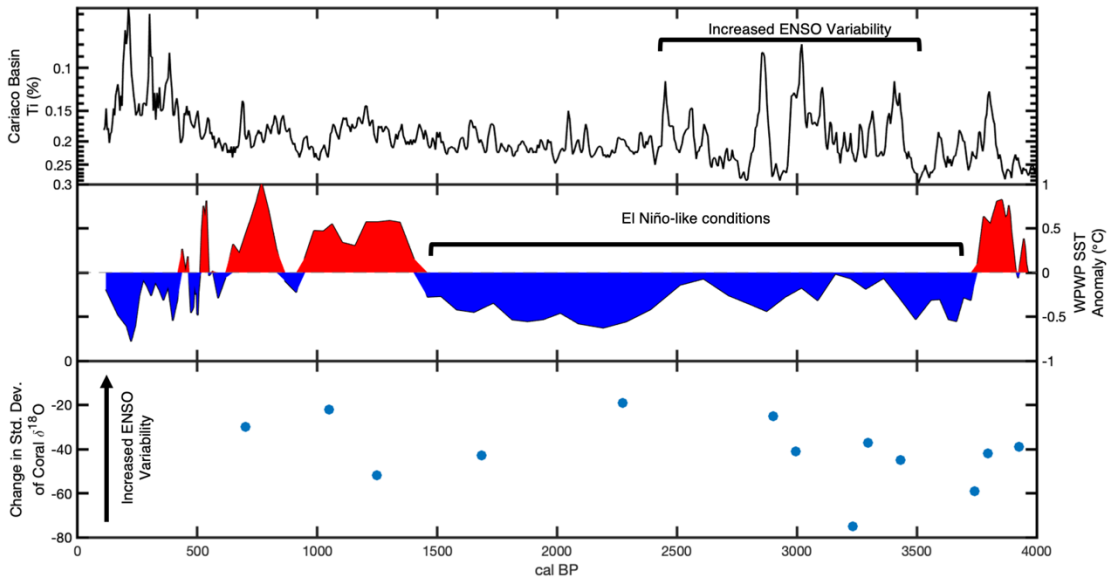

Supp. Fig. S3.6: Proxy evidence for a change in ENSO mean state and variability over the late Holocene. Top Panel: Percent of titanium in a sediment core from Cariaco Basin. The amplitude and variability of Ti % reflects ENSO variability. This record reflects activity of the ITCZ which is interpreted as being related to ENSO activity. The Cariaco Basin is also a well teleconnected region for ENSO. (Haug et al., 2001). Middle Panel: Western Pacific Warm Pool (WPWP) SST anomaly reconstructed from sediment core MD81. Cooler SST anomalies indicate a shift towards a more El Niño like mean state (Stott et al., 2004). Bottom Panel: Estimates of interannual variability from new and published coral $\delta^{18}O$ records from the northern Line Islands (Grothe et al., 2019). Relative ENSO variance changes in fossil coral $\delta^{18}O$ calculated from the standard deviation of sliding 20-year windows of monthly coral $\delta^{18}O$ data that was first 10-year high-passed, then 13-month running averaged, plotted as the average standard deviation of each coral timeseries relative to the 1987-2007CE intervals of corresponding modern spliced coral $\delta^{18}O$ timeseries from each site.

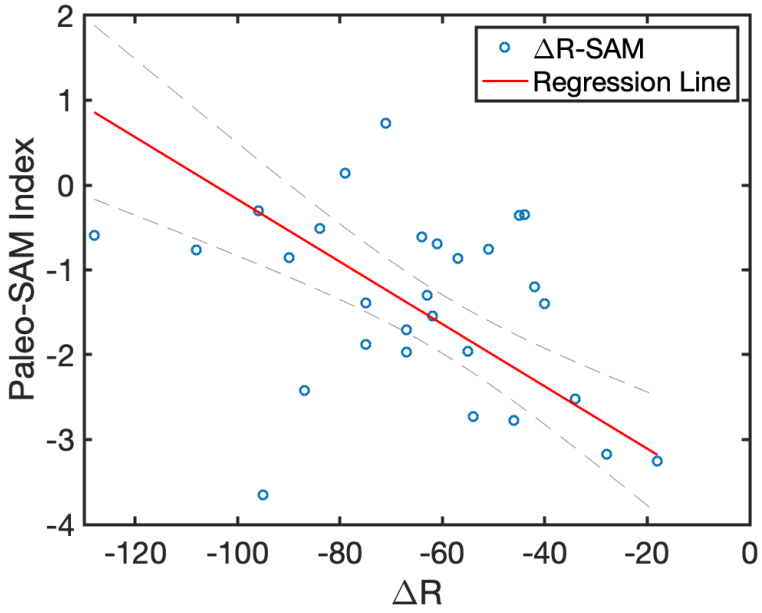

Supp. Fig. S3.7: ΔR-SAM Calibration. Coral ΔR plotted against paleo-SAM data from Abram et al. (2014). The linear regression is calculated according to the protocols in York et al. (2004), which account for uncertainty in both variables. Uncertainty bounds are 2σ. The regression equation is paleo-SAM = -0.3687(ΔR) + -3.481.

3.12 Supplemental References

Abram, N. J., Mulvaney, R., Vimeux, F., Phipps, S. J., Turner, J., & England, M. H. (2014). Evolution of the Southern Annular Mode during the past millennium. *Nature Climate Change, 4*(7), 564-569. https://doi.org/10.1038/nclimate2235

Carreiro-Silva, M., H Andrews, A., Braga Henriques, A., de Matos, V., Porteiro, F., & Santos, R. (2013). *Variability in growth rates of long-lived black coral Leiopathes sp. from the Azores (Northeast Atlantic)* (Vol. 473).

Grothe, P. R., Cobb, K. M., Liguori, G., Di Lorenzo, E., Capotondi, A., Lu, Y., et al. (2019). Enhanced El Niño-Southern Oscillation variability in recent decades. *Geophysical Research Letters, n/a*(n/a). https://doi.org/10.1029/2019GL083906

Haug, G. H., Hughen, K. A., Sigman, D. M., Peterson, L. C., & Röhl, U. (2001). Southward Migration of the Intertropical Convergence Zone Through the Holocene. *Science, 293*(5533), 1304. http://science.sciencemag.org/content/293/5533/1304.abstract

Heaton, T. J., Köhler, P., Butzin, M., Bard, E., Reimer, R. W., Austin, W. E. N., et al. (2020). MARINE20—THE MARINE RADIOCARBON AGE CALIBRATION CURVE (0–55,000 CAL BP). *Radiocarbon*, 1-42. https://www.cambridge.org/core/article/marine20the-marine-radiocarbon-age-calibration-curve-055000-cal-bp/B3013899914A3198D4B884B7B6E5CE66

Hellstrom, J. (2006). U-Th dating of speleothems with high initial 230Th using stratigraphical constraint. *Quaternary Geochronology, 1*, 289-295.

Hitt, N. T., Sinclair, D. J., Fallon, S. J., Neil, H. L., Tracey, D. M., Komugabe-Dixson, A., & Marriott, P. (2020). Growth and longevity of New Zealand black corals. *Deep Sea Research Part I: Oceanographic Research Papers*, 103298. http://www.sciencedirect.com/science/article/pii/S0967063720300868

Komugabe-Dixson, A. F., Fallon, S. J., Eggins, S. M., & Thresher, R. E. (2016). Radiocarbon evidence for mid-late Holocene changes in southwest Pacific Ocean circulation. *Paleoceanography, 31*(7), 971-985. http://dx.doi.org/10.1002/2016PA002929

Prouty, N. G., Roark, E., Buster, N., & Ross, S. (2011). *Growth rate and age distribution of deep-sea black corals in the Gulf of Mexico* (Vol. 423).

Roark, E. B., Guilderson, T. P., Dunbar, R. B., Fallon, S. J., & Mucciarone, D. A. (2009). Extreme longevity in proteinaceous deep-sea corals. *Proceedings of the National Academy of Sciences, 106*(13), 5204-5208. http://www.pnas.org/content/106/13/5204.abstract

Sikes, E. L., Samson, C. R., Guilderson, T. P., & Howard, W. R. (2000). Old radiocarbon ages in the southwest Pacific Ocean during the last glacial period and deglaciation. *Nature, 405*, 555. http://dx.doi.org/10.1038/35014581

Skinner, L. C., Primeau, F., Freeman, E., de la Fuente, M., Goodwin, P. A., Gottschalk, J., et al. (2017). Radiocarbon constraints on the glacial ocean circulation and its impact on atmospheric CO(2). *Nature Communications, 8*, 16010-16010. https://pubmed.ncbi.nlm.nih.gov/28703126

https://www.ncbi.nlm.nih.gov/pmc/articles/PMC5511348/

Stott, L., Cannariato, K., Thunell, R., Haug, G. H., Koutavas, A., & Lund, S. (2004). Decline of surface temperature and salinity in the western tropical Pacific Ocean in the Holocene epoch. *Nature, 431*(7004), 56-59. https://doi.org/10.1038/nature02903

Stuiver, M., & Polach, H. A. (1977). Discussion Reporting of 14C Data. *Radiocarbon, 19*(3), 355-363. https://www.cambridge.org/core/article/discussion-reporting-of-14c-data/D686D7894B8BAC3212589AFE418E147E

York, D., Evensen, N. M., Martínez, M. L., & Delgado, J. D. B. (2004). Unified equations for the slope, intercept, and standard errors of the best straight line. *American Journal of Physics, 72*(3), 367-375. http://aapt.scitation.org/doi/abs/10.1119/1.1632486

Chapter 4

Reconstructing Southwest Pacific Ocean Productivity and Biogeochemistry Using Black Coral $\delta^{13}C$ and $\delta^{15}N$

The content in Chapter 4 is in preparation for publication in the peer-reviewed journals *Nature Geoscience*, *Science Advances*, and *Geophysical Research Letters.*

Authorship contributions to this research article include the following:

Nicholas T. Hitt – Wrote manuscript(s) and managed all co-author feedback. This author subsampled all corals, prepared all samples for geochemical analysis, compiled all data, developed initial interpretations, and produced all figures.

Daniel J. Sinclair – Academic Supervisor; provided feedback on drafts and aided in the interpretation of the results.

Helen L. Neil – Academic Supervisor.

Stewart J. Fallon – Academic Supervisor; Analyzed black coral $\delta^{13}C$ and $\delta^{15}N$. Provided feedback on the manuscript(s).

Sarah Bury – Analyzed black coral $\delta^{13}C$ and $\delta^{15}N$ and assisted with $\delta^{13}C$ and $\delta^{15}N$ data interpretation. Provided feedback on the manuscript(s).

Amandine Sabadel - Assisted with $\delta^{13}C$ and $\delta^{15}N$ data interpretation and discussion of CSSIA-AA analysis. Provided feedback on the manuscript(s).

Julie Brown – Analyzed black coral $\delta^{13}C$ and $\delta^{15}N$

Josette Delgado – Analyzed black coral $\delta^{13}C$ and $\delta^{15}N$

Aimée Komugabe-Dixson – Academic Supervisor; Reviewed a draft of the manuscript(s).

John Hellstrom – Analyzed U-Th dates for age model construction

Note: Appendix data is stored in ‘Sheet C’ in the CD-ROM at the end of the thesis.

4.1 Abstract:

The southwest Pacific Ocean fosters high levels of primary production due to the mixing of nutrient-rich subpolar waters and micronutrient-replete subtropical waters. Phytoplankton blooms stimulated by these nutrients make the Southwest Pacific a critical carbon sink and an important component of the global climate system. However, phytoplankton abundance has been decreasing globally since the early 20th century as a result in changes to marine biogeochemistry and physical oceanography (e.g. macronutrient distributions, vertical stratification). Determining whether these changes are a part of a natural ocean cycle or a result of anthropogenic change is hindered by sparse instrumental observations prior to the instrumental era. To evaluate the significance of 20th century changes, we need high resolution productivity records spanning several centuries.

High resolution records of phytoplankton and surface ocean biogeochemistry can be reconstructed from stable carbon and nitrogen isotopes ($\delta^{13}C$ and $\delta^{15}N$) in proteinaceous deep-sea black corals which reflect $\delta^{13}C$ and $\delta^{15}N$ in particulate organic matter (POM). A number of these records now exist; however, most come from regions that exhibit low levels of primary production (e.g. the central North Pacific Gyre). Here, I aim to reconstruct records of macronutrient distributions and surface biogeochemistry for the highly productive southwest Pacific using New Zealand deep-sea black corals. I present four U-Th dated, decade-to-century resolution black coral $\delta^{13}C$ and $\delta^{15}N$ records which collectively span 100-3000BP.

My coral records show that POM $\delta^{13}C$ and $\delta^{15}N$ exhibit significant variations on multi-centennial timescales in the southwest Pacific over the last 3000 years. Multi-centennial variations in coral $\delta^{13}C$ are likely related to changes in sea surface temperatures, which may be forced by changing ocean circulation strength. Multi-centennial variations in coral $\delta^{15}N$ may be forced by variable nitrogen fixation and upwelling rates, both of which are possibly driven by basin-wide climate variability from the El Niño-Southern Oscillation.

My records also show a synchronous increase in mean $\delta^{13}C$ and $\delta^{15}N$ going from the 2000-3000BP interval to the 0-2000BP interval that corresponds to an increase in marine radiocarbon reservoir age (ΔR). This matches observations in other southwest Pacific paleoceanographic records. I interpret this as evidence for a period of an intensified and expanded South Pacific Gyre (SPG) over the 2000-3000BP interval. This paleo-SPG change is similar to the SPG

intensification observed over recent decades and may therefore serve as an analogue to modern gyre conditions.

4.3 Introduction:

Phytoplankton are a vital component of the global climate and ecosystem. They generate roughly half of the global primary production, influence the carbon cycle and support marine diversity (Boyce et al., 2010). However, phytoplankton biomass may have been declining globally since the early 20th century (Boyce et al., 2010; Rousseaux et al., 2015; Sharma et al., 2019). There are several lines of evidence suggesting this decline is driven by anthropogenically-forced oceanographic changes (Behrenfeld et al., 2006; Polovina et al., 2008; Boyce et al., 2010; Moore et al., 2013; Lewandowska et al., 2014). These changes include the expansion of oligotrophic subtropical ocean gyres, ocean warming, intensification of subtropical western boundary currents, a change in macronutrient distributions and utilization, and increased vertical ocean thermal stratification (Behrenfeld et al., 2006; Polovina et al., 2008; Boyce et al., 2010; Wu et al., 2012; Moore et al., 2013; Lewandowska et al., 2014). However, marine productivity, current velocity, macronutrient, and *in situ* temperature observations are sparse prior to the satellite era of the 1980s (Boyce et al., 2010; Deser et al., 2010; Henson et al., 2010; Henson et al., 2016). This limits our understanding of the significance of the recent decline in phytoplankton biomass, and how phytoplankton, primary production and marine biogeochemistry respond to natural and anthropogenic climate and ocean forcings (Boyce et al., 2010; Henson et al., 2010; Henson et al., 2016). It is therefore imperative that we supplement existing instrumental records with paleoceanographic reconstructions to establish the link between recent changes in phytoplankton abundance, marine biogeochemistry and physical oceanography to aid our understanding of anthropogenic climate change.

Elucidating the relationship between recent phytoplankton, primary production and climate/ocean changes requires marine observations that span several centuries (Boyce et al., 2010; Henson et al., 2010; Henson et al., 2016). Paleoceanographic records from sediment cores have traditionally provided this information across long timescales (e.g. > several centuries, Bostock et al. (2015); Bostock et al. (2019)). These records play a key role in determining the interplay between biology and climate on millennial and orbital timescales. However, sediment cores have a number of issues preventing their application to anthropogenic timescales (e.g. decades; H. Bostock pers. comm; Bostock et al. (2015); Bostock et al. (2019)). Low sedimentation rates, low microfossil availability and bioturbation all prevent sediment cores from recording sub-centennial changes in productivity and biogeochemical dynamics. Obtaining

decadal-resolution records therefore requires a new high-resolution ocean proxy. Here I aim to use $\delta^{13}C$ and $\delta^{15}N$ in the skeletons of proteinaceous black corals (Chapters 2 and 3) from around New Zealand to reconstruct decadal to centennial changes in South Pacific Gyre (SPG) paleo-nutrient distributions and biogeochemistry over the last 3000 years.

I hypothesize the southwest Pacific experienced changes in regional productivity and macronutrient distributions due to significant multi-centennial and millennial variations in SPG circulation strength over the late Holocene (Chapter 3). These circulation variations changed the balance of subtropical and subpolar waters around New Zealand (Chapter 3), which possibly altered macronutrient distributions and therefore regional productivity patterns. I evaluate this hypothesis by presenting multi-decadal $\delta^{13}C$ and $\delta^{15}N$ records measured on splits of the same samples analysed for radiocarbon and comparing them to the ΔR circulation records (Chapter 3). Thereafter, I investigate the impact of late Holocene climate variability on the distribution of macronutrients and productivity by comparing coral $\delta^{13}C$ and $\delta^{15}N$ records to the paleo-SOI index of Yan et al., 2011.

4.4 Background:

4.4.1 Southwest Pacific Primary Production and Biogeochemistry:

The southwest Pacific region is characterized by high levels of marine primary production (Figure 4.1; e.g. Chiswell et al., 2013). Elevated productivity occurs along the mid-latitudes of the South Pacific due to the mixing of micronutrient rich (e.g. Zn, Fe) subtropical waters and macronutrient rich (e.g. NO_3^-, PO_4^-) subpolar waters (See Section 1.3.2.2; Bradford et al., 1978; Levitus et al., 1993; Sarmiento et al., 2004; Sarmiento et al., 2006; Chiswell et al., 2013; Ellwood et al., 2013; Chiswell et al., 2015). The circumpolar mid-latitude band where subtropical and subpolar waters converge is the Subtropical Front (STF) (Heath, 1985; Chiswell et al., 2013; Chiswell et al., 2015). The STF is a dynamic area, characterized by steep temperature, salinity and density gradients and elevated macro/micronutrients that foster new production (Levitus et al., 1993; Stramma et al., 1995; Bradford-Grieve et al., 1999; Chiswell et al., 2013; Graham et al., 2013; Chiswell et al., 2015).

Subtropical waters are delivered into the STF from the north *via* terminal extensions of the East Australian Current (EAC), which include the EAC Extension (EAC extension), the Tasman Front (TF) and the East Auckland Current (EAuC) (Chiswell et al., 2015). These three

currents are rich in micronutrients but depleted in macronutrients (Levitus et al., 1993; Bradford-Grieve et al., 1999; Ellwood et al., 2013). Subpolar waters are brought into the STF from the south *via* the Subantarctic Front and the Polar Front that are derived from the Antarctic Circumpolar Current (Chiswell et al., 2015). Mesoscale gyres in the Subantarctic Front effectively pull macronutrient rich but micronutrient poor waters from the south to the north (Levitus et al., 1993; Bradford-Grieve et al., 1999; Ellwood et al., 2013).

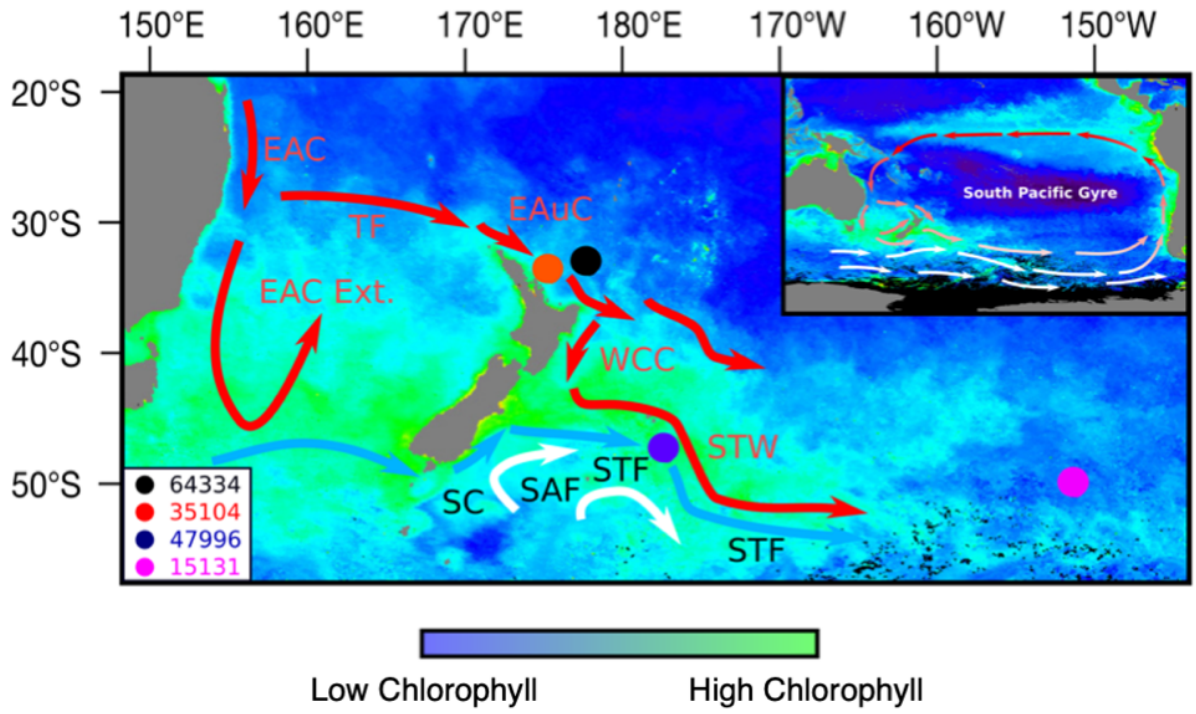

Figure 4.1: Southwest Pacific Black Coral Locations and Oceanographic Setting. Coral locations (colored circles) are overlaid on an annually averaged chlorophyll-a map (NASA MODIS). Green areas indicate high chlorophyll and blue areas indicate low chlorophyll. Arrows indicate southwest Pacific ocean currents. Red arrows indicate warm, tropical currents, pink arrows indicate temperate, subtropical currents and white arrows indicate subpolar/Antarctic currents. EAC – East Australian Current, TF – Tasman Front, EAuC – East Auckland Current, WCC – Wairarapa Coastal Current, EAC Ext. – EAC Extension, SC – Southland Current, STF – Subtropical Front, SAF – Subantarctic Front. Inset: A schematic of South Pacific gyre circulation.

Primary production in the southwest Pacific is a product of the region's complex biogeochemistry and physical oceanography (Chiswell et al., 2013; Chiswell et al., 2015). Changes in these parameters are related to variations in surface mixed-layer depth (Chiswell et al., 2013). This is shown by annual cycles in surface chlorophyll and mixed layer depth in subtropical water north of New Zealand and across the STF (Chiswell et al., 2013). In these regions, surface chlorophyll blooms occur in winter and spring as a result of higher nutrient entrainment from a deeper mixed layer driven by increased wind stress (Chiswell et al., 2013).

Winter and spring blooms also correspond to periods of reduced subtropical ocean circulation around New Zealand driven by reduced wind stress (e.g. a weaker EAC; Ridgway 1997; Chiswell 2013). This implies a link between regional ocean circulation and primary production, which could act through a number of mechanisms. Each of the southwest Pacific ocean currents has a distinct thermocline (and therefore mixed-layer) depth resulting from their unique vertical sea surface temperature gradient (Heath, 1984, 1985; Chiswell et al., 2015). A long term change in ocean circulation (e.g. a poleward expansion of oligotrophic subtropical currents) would therefore alter the north-south gradient in thermocline/mixed-layer depth (Heath, 1984, 1985; Chiswell et al., 2015), change macronutrient distributions (Ellwood et al., 2013) and likely change primary productivity patterns (Chiswell et al., 2013).

If circulation affects productivity, then productivity may in turn respond to variations in climate processes that drive circulation changes on timescales of years to centuries (e.g. the Southern Annular Mode (SAM); Komugabe-Dixson et al., 2016; Chapter 3). This has been inferred over longer timescales from Holocene and Last Interglacial sediment cores collected from the STF region (Fenner et al., 1992; Weaver et al., 1998; Bostock et al., 2015; Bostock et al., 2019). However, it is less clear if the same mechanisms operate on shorter timescales (e.g. multi-decadal to centennial) due to a paucity of reliable instrumental data prior to the satellite era of the 1980s (Henson et al., 2010; Henson et al., 2016; Sharma et al., 2019). Unfortunately, sediment cores from the southwest Pacific are too low-resolution to study centennial-timescale productivity dynamics. Investigating whether recent decadal-centennial productivity changes are a function of internal climate variability or anthropogenic change therefore requires further work.

4.4.2 Deep-Sea Coral $\delta^{13}C$ and $\delta^{15}N$ Proxy:

Carbon and nitrogen stable isotope ratios ($\delta^{13}C$ and $\delta^{15}N$) are useful geochemical tools for studying variations in phytoplankton community structure, primary productivity, marine biogeochemistry and macronutrient distributions (Davenport et al., 2002; DiFiore et al., 2010; Somes et al., 2013; Magozzi et al., 2017). Photosynthetic uptake of C and N into phytoplankton biomass strongly discriminates against the heavier isotopes (^{13}C and ^{15}N) (Somes et al., 2010; Magozzi et al., 2017). Marine $\delta^{15}N$ in surface ocean particulate organic matter is also highly sensitive to nitrogen cycle processes which can be connected to regional ocean and climate variability (Sarmiento et al., 2006; Gruber, 2008; Somes et al., 2010; Somes et al., 2017). A $\delta^{13}C$ and $\delta^{15}N$ timeseries can therefore provide information on paleo-changes in nutrient distributions,

biogeochemistry and primary productivity as they may relate to climate and ocean changes (Glynn et al. 2019).

Proteinaceous deep-sea corals can be used to reconstruct a $\delta^{13}C$ and $\delta^{15}N$ timeseries (Sherwood et al., 2013; McMahon et al., 2015; Glynn et al., 2019). These corals feed on recently exported particulate organic matter (POM) from the surface ocean, and the metabolic products of this food are used in the accretionary layers of their fibrillar organic skeletons. Studies show that the $\delta^{13}C$ and $\delta^{15}N$ 'signature' of the corals' food is inherited by the skeleton with minimal fractionation (Roark et al., 2009; Sherwood et al., 2009; Prouty et al., 2014; Glynn et al., 2019). Deep-sea coral skeletons can also be dated at a high precision using U-Th disequilibria (Komugabe et al., 2014; Komugabe-Dixson et al., 2016). Proteinaceous deep-sea corals can therefore be used to reconstruct precise histories of paleo $\delta^{13}C$ and $\delta^{15}N$ variability and study variations in marine productivity and biogeochemistry (Sherwood et al., 2013; McMahon et al., 2015; Glynn et al., 2019).

There are a number of challenges for interpreting deep-sea coral $\delta^{13}C$ and $\delta^{15}N$ data. The isotope composition of coral skeletons is an integration of several competing isotopic fractionation processes at the base of the food web as well as within the food web (Sherwood et al., 2011; Sherwood et al., 2013; Schiff et al., 2014; McMahon et al., 2015; Glynn et al., 2019). These processes are unique to each marine ecosystem and consist of either i) the specific mix of organisms making up the primary producers ii) isotopically distinct sources of bioavailable carbon and nitrogen iii) the efficiency with which those nutrients are utilized by the primary producers iv) isotopic enrichments during trophic level transfers and v) bacterial degradation and nutrient recycling in the water column (Larsen et al., 2013; McMahon et al., 2013; Sherwood et al., 2014; McMahon et al., 2015; Glynn et al., 2019). These complications contribute significant uncertainties when interpreting variability in $\delta^{13}C$ and $\delta^{15}N$ data (Larsen et al., 2013; McMahon et al., 2013; Sherwood et al., 2014; McMahon et al., 2015; Glynn et al., 2019). Evaluating any $\delta^{13}C$ and $\delta^{15}N$ data therefore requires some constraints on the specific mix of organisms making up the primary producers and their unique $\delta^{13}C$ and $\delta^{15}N$ values; an understanding of location-specific $\delta^{13}C$ and $\delta^{15}N$ sources; and the trophic level and food-web structures of a specific location.

4.4.3 Existing Southwest Pacific Paleoceanography Proxy Records:

Deep-sea corals have previously been employed as a late Holocene paleoceanographic circulation proxy in the southwest Pacific (Komugabe-Dixson et al., 2016; Chapter 3). These proxy records reconstruct the relative balance of subtropical and subpolar waters around New Zealand using marine radiocarbon reservoir ages (ΔR; see Chapters 1 and 3 for in-depth explanation). The ΔR records exhibit an inverse relationship with a paleo reconstruction of Southern Annular Mode (SAM) for the last 1000 years (Abram et al., 2014) (See Chapter 3 for in-depth explanation). This relationship between SAM and ΔR results from the effect SAM has on SPG circulation (e.g. Cai, 2006; Roemmich et al., 2016). Positive SAM represents a strengthening and southern shift of the westerly wind belt which enhances gyre circulation and suppresses ΔR values as more tropical, ventilated waters are advected south along the western Pacific Ocean boundary (Chapter 3).

Positive SAM has strengthened gyre circulation over the instrumental era (Cai et al., 2005; Roemmich et al., 2007; Roemmich et al., 2016), which is commonly interpreted as a consequence of anthropogenic climate change (Cai et al., 2005; Cai, 2006). However, the coral ΔR records imply gyre strength is highly variable on multi-decadal to centennial timescales and the recently observed SAM-driven gyre strengthening is not unique to the last 1000 years (Chapter 3). Modern observations of increasing gyre strength may therefore result from internal ocean-atmosphere variability. This raises questions about how anthropogenic change has contributed to the 20th century gyre intensification as well as how gyre intensification affects patterns of southwest Pacific marine biogeochemistry and primary production over the past.

4.5 Materials and Methods:

The four New Zealand black corals are of the genus *Leiopathes* and were sampled from the regions of the EAuC (NE of New Zealand), the STF (E of New Zealand) and the central South Pacific (Figures 4.1-5; Table 1). Procedures for preparing and sub-sampling corals are outlined in Hitt et al., (2020).

4.5.1 Stable C and N Isotope Measurement

Two laboratories were used to measure bulk $\delta^{13}C$ and $\delta^{15}N$. An interlaboratory calibration was performed by comparing mean $\delta^{15}N$ and $\delta^{13}C$ for replicated analyses at ANU of a) the NIWA primary reference standard DL-Leucine (n = 5); b) a NIWA in-house laboratory

standard comprised of squid tissue (n = 8); and c) duplicate coral samples (n = 5). For each type of standard/sample, the mean $\delta^{15}N$ and $\delta^{13}C$ measured by one lab was within 2σ of the average for both labs (Supp. Fig. S4.3). Therefore no interlaboratory offset was detected and no correction was applied to any $\delta^{15}N$ and $\delta^{13}C$ datasets.

Bulk $\delta^{13}C$ and $\delta^{15}N$ measurements were made on splits of coral powders measuring ~0.6-0.7 mg each in corals 47996, 64344 and 35104 (n = 468; see Appendix Tables 10-13). Measurements were made using a DELTA V Plus isotope ratio mass spectrometer (IRMS) equipped with a Flash 2000 Element Analyzer (Flash 2000 EA) and Mass200R Autosampler (Thermo Fisher Scientific, Bremen, German) at the NIWA Environmental and Ecological Stable Isotope Analytical Facility in Wellington, New Zealand. For samples that did not meet the mass requirement of 0.6 mg (n = 22; Appendix Tables 10-13), subsamples of 0.1-0.2 mg were analyzed for $\delta^{13}C$ and $\delta^{15}N$ using a low volume set-up for low nitrogen mass. These low volume analyses were carried out on the same EA-IRMS instrument as above using a ZeroBlank autosampler (Costech International, Milan, Italy) to minimize the blank contribution form laboratory air ingress. The Flash 2000 EA was set up for low weight samples and standards. Reference materials were used to determine isotopic values following a normalization procedure as outlined in Paul et al. (2007). All sample $\delta^{15}N$ values were normalized using isotopic data from the daily analysis of international reference materials National Institutes of Standards and Technology (NIST) 8573 USGS40 L-glutamic acid and NIST 8548 IAEA-N2 ammonium sulphate. All sample $\delta^{13}C$ values were normalized using isotopic data from the daily analysis of international reference materials NIST 8573 USG40 and NIST 8542 IAEA-CH-6 sucrose. Precision was determined by the repeat analysis of the working laboratory standard DL-Leucine (DL-2-Amino-4-methylpentanoic acid, $C_6H_{13}NO_2$, Lot 127H1084, Sigma, Australia) and L-Proline. The international standard USGS65 Glycine was used to check accuracy and precision and repeat analysis of a squid working laboratory standard provided a further check on precision. DL-Leucine and squid were chosen as standards as they have a similar matrix to the coral samples with similar isotopic values. Repeat analysis of international standards produced data accurate to within 0.2‰ for both $\delta^{15}N$ and $\delta^{13}C$, and a precision of better than 0.15‰, for $\delta^{15}N$ and 0.2‰ for $\delta^{13}C$.

Bulk $\delta^{13}C$ and $\delta^{15}N$ measurements were made on splits of coral powders measuring ~0.5-0.6mg from coral 15131 using a Sercon 20-20 equipped with an EA at the Australian National University Radiocarbon Laboratory (ANURL). All sample $\delta^{13}C$ and $\delta^{15}N$ values were normalized using a 3 point calibration using isotopic data from the daily analysis of international reference materials USGS-040, USGS-041, IAEA-600 Caffeine and ANU Sucrose ($\delta^{13}C$ only). Repeat analysis of international standards produced data accurate to within 0.15‰ for both $\delta^{15}N$ and $\delta^{13}C$, and a precision of better than 0.15‰, for $\delta^{15}N$ and 0.12‰ for $\delta^{13}C$.

Bulk $\delta^{13}C$ measurements in corals 64344 and 47996 are corrected for the Suess effect in their respective intervals that cover the industrial period (0-100BP) following protocols in McMahon et al. 2015. This involved correction of the bulk $\delta^{13}C$ data, using an estimate of the rate of $\delta^{13}C$ decrease in the atmosphere was deduced from ice cores (Francey et al., 1999). These correction factors were iteratively added and are 0.05‰ per decade from 0-100BP (Francey et al., 1999; McMahon et al., 2015).

4.5.2 Uranium-Thorium Disequilibrium Dating

All corals were dated using U-Th disequilibria at the University of Melbourne following Hellstrom (2003) with modifications according to Drysdale et al. (2012). U-Th ages were calculated using the ^{234}U and ^{230}Th half-lives from Cheng et al. (2013). Initial Th constraints and corrections were calculated using the stratigraphic constraint Monte-Carlo method of Hellstrom (2006). Age-depth models for corals 64344, 35104, 15131 and 47996 were constructed from initial-Th corrected U-Th using COPRA: a piecewise cubic hermite spline (PCHIP) with a Monte Carlo simulation (n>2,000) (Breitenbach et al., 2012). All age-depth models presented are the same as those in Chapter 3.4 and are presented in Supp. Fig. S4.1 for completeness. For a complete description of age-depth chronology construction please refer to Chapter 3.4.

4.5.3 Exclusion of records

15131 exhibits a period of anomalously fast growth in its outermost layer, corresponding to the interval 700-1400BP. Banding in this interval is convoluted such that stratigraphic ordering of layers is lost which prevents accurately micromilling individual coral bands (Figure 2.6; Sect. 2.5.3.2). Multiple coral bands were milled together and unevenly averaged (Sect. 2.5.3.2), which aliases any resulting geochemical data. This prevented constructing a robust $\delta^{13}C$ and $\delta^{15}N$ dataset and age model. Therefore, the $\delta^{13}C$ and $\delta^{15}N$ reconstruction in 15131 is

restricted to the 1450-2800BP interval where banding is clear and seemingly uncompromised and there is no smoothing of data. However, the $\delta^{13}C$ and $\delta^{15}N$ data in 15131 over the 700-1400BP interval is provided in Appendix Table 12 for completeness.

4.5.4 Determining the Contribution of Phytoplankton:Zooplankton Ratios to $\delta^{15}N$ Variability

A change in the ratio of zooplankton to phytoplankton in settling POM will alter coral $\delta^{15}N$ values because higher trophic levels produce a heavier nitrogen isotope signature in POM. I quantitatively evaluate the possible contribution of these food-web changes to the $\delta^{15}N$ variability observed in the 64344 and 47996 records using a mass balance model (Eq.1; Hayes (2004)).

$$\text{Eq. 1: } m\Sigma(\delta^{15}N_{Coral}) = m_1(\delta^{15}N_{Phyto}) + m_2(\delta^{15}N_{Zoo})$$

Equation 1: The mass balance model of Hayes (2004). *m* terms represent molar quantities of the elements of interest and the $\delta^{15}N$ terms represent fractional isotopic abundances·

This model assumes an initial 50:50 ratio of phytoplankton to zooplankton; uses a phytoplankton $\delta^{15}N$ value ($\delta^{15}N_{Phyto}$) of 4.5‰ and a zooplankton $\delta^{15}N$ value ($\delta^{15}N_{Zoo}$) of 7.5‰ (Scott Nodder, unpublished data). From this starting point, I use the total range of coral $\delta^{15}N$ observed in the 64344 and 47996 records (~1.25‰) to assess how much the phytoplankton:zooplankton ratio would have had to change to account for the full range of $\delta^{15}N$ variability observed in the 64344 and 47996 records.

4.6 Results:

4.6.1 Carbon Stable Isotopes

I present four overlapping $\delta^{13}C$ records for the EAuC (64344; 35104), STF (47996) and Central South Pacific (15131) regions that collectively span 0-3000BP (Table 1; Figure 4.2). Corals 47996 and 64344 grew into the last 150 years and their $\delta^{13}C$ records were corrected for the Suess effect following protocols in McMahon et al. (2015). Suess-corrected $\delta^{13}C$ values in 64344 show a general increase from 1500 to 100BP (0.70 ± 0.02‰/1500yr; York et al., 2004), while corrected 47996 $\delta^{13}C$ values show a series of troughs and peaks, but no overall increase or decrease over the last millennium (Appendix Table 11; Figure 4.2). Carbon isotope values in

35104 are highly variable over the 600-3000BP interval (Figure 4.2). 35104 $\delta^{13}C$ exhibits one centennial cycle ranging over 0.4‰ (600-800BP) as well as eight decadal-centennial cycles ranging between 0.25-0.5‰ superimposed on two multi-centennial cycles (2000-2400BP and 2300-2900BP) ranging up to 0.75‰ in magnitude (Appendix Table 13; Figure 4.2). Corals 47996, 35104 and 64344 each have a different mean $\delta^{13}C$ value (Figure 4.2); however, those corals reproduce $\delta^{13}C$ variability over the 0-1500BP period (Figure 4.3). Coral $\delta^{13}C$ co-variability is assessed by first resampling each record to a consistent 40yr via a piecewise cubic interpolation, linearly detrending each record using a first-order weighted least squares fit (York et al., 2004), and calculating a Pearson's correlation coefficient between the overlapping portion of the resampled and detrended records ($R = 0.44\text{-}0.66$; $p < 0.01$; $n = 11\text{-}19$).

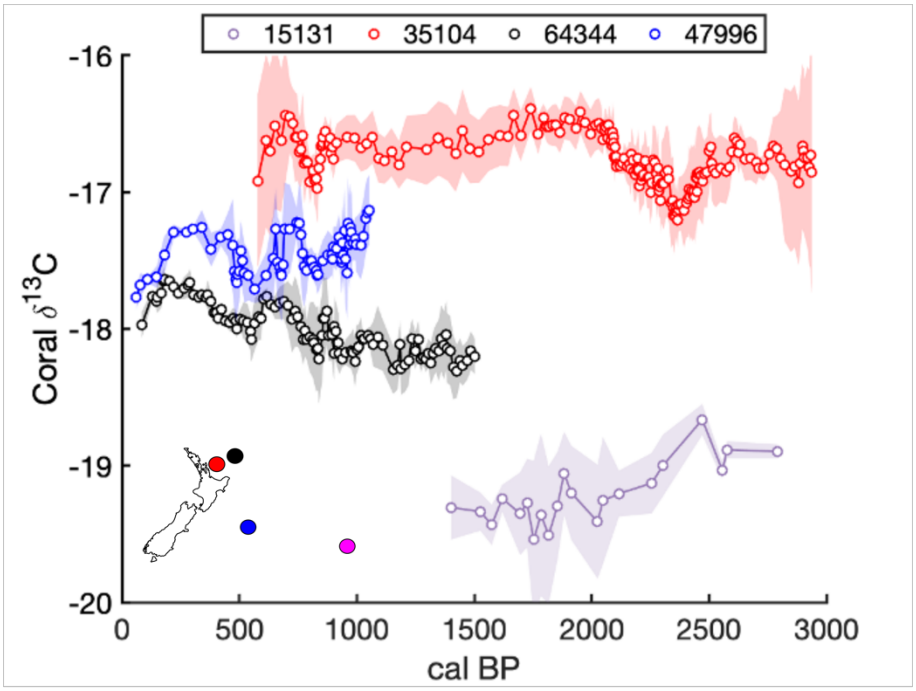

Figure 4.2: Coral $\delta^{13}C$ Over the Late Holocene. Coral $\delta^{13}C$ from the STF (47996 - blue), EAuC (64344 – black; 35104 - red) and Central South Pacific (15131 – lavender) over the last 3000 years. Shaded areas indicate the 2**σ** uncertainty range which are calculated from the U-Th uncertainties and coral $\delta^{13}C$ measurement uncertainties. Corals are corrected for Suess-effect where applicable. Corals locations are shown in the bottom left corner with corresponding colors.

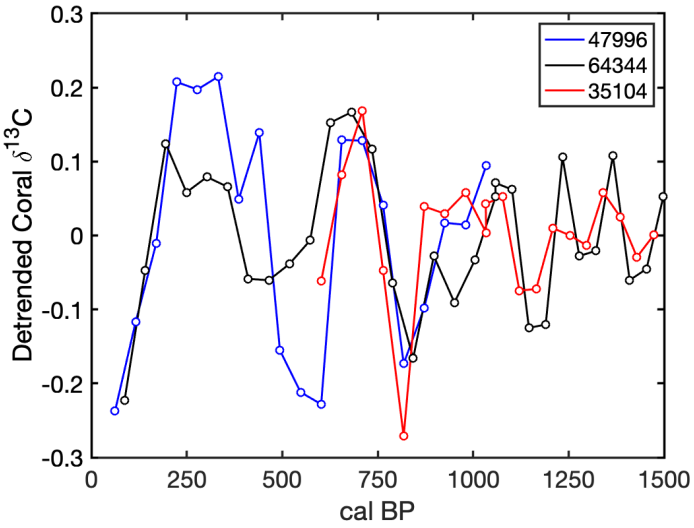

Figure 4.3: Detrended Coral δ^{13}C Over the Last Millennium. Detrended coral δ^{13}C from the STF (47996 - blue) and EAuC (64344 – black; 35104 - red) over the last 1500 years. All coral δ^{13}C records are resampled via a piecewise cubic interpolation to a consistent 40yr resolution.

Coral 15131 shows little variability in δ^{13}C values over the 1400-2900BP interval. There appear to be two discrete δ^{13}C cycles over the 1700-1900BP interval (Appendix Table 12); however, these cycles are not reproduced in any other portion of the record and are constrained by less than nine datapoints. 15131 exhibits a small, but significant, 0.4‰ baseline shift in mean δ^{13}C values between the 1400-2150BP and 2150-2900BP intervals (-18.93 ±0.08‰ vs. -19.32 ±0.04‰; Figure 4.4A). Mean δ^{13}C are calculated across these intervals using a weighted average approach (Bevington, 1969) and the timing of the baseline shift is assessed using the 'regime shift detection' methodology of Rodionov (2004).

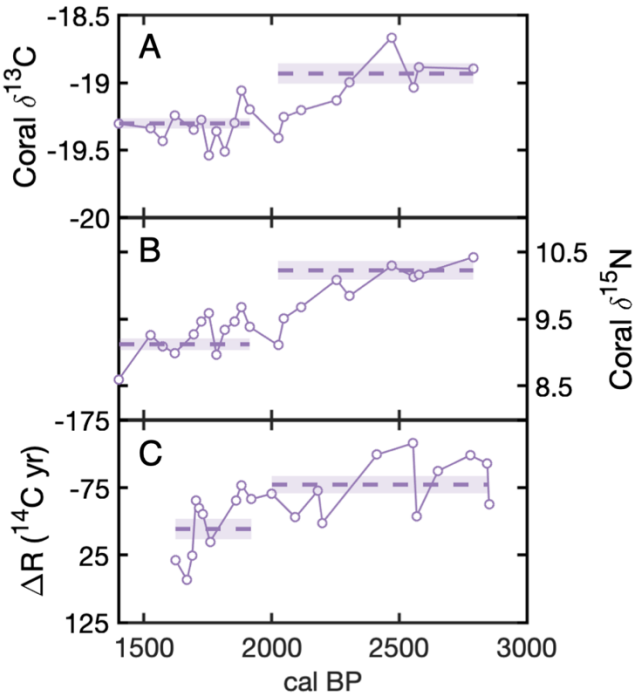

Figure 4.4: Coral 15131 δ^{15}N, δ^{13}C and ΔR. Coral 15131 δ^{15}N, δ^{13}C and ΔR from the Central South Pacific region over the 1400-2900BP period. ΔR data is from Chapter 3. Mean δ^{13}C and δ^{15}N are calculated across these intervals using a weighted average approach (Bevington, 1969).

4.6.2 Nitrogen Stable Isotopes

Coral δ^{15}N records for the EAuC (64344; 35104), STF (47996) and Central South Pacific (15131) regions overlap over the 0-3000BP interval (Figure 4.5). 64344 and 35104 δ^{15}N records both span 600-1500BP and reproduce δ^{15}N for the majority of the overlapping interval. δ^{15}N values converge over the 900-1500BP interval but diverge between 600-900BP. 35104 exhibits δ^{15}N variability up to 1.5‰ on a variety of timescales ranging from multiple decades to several centuries (Figure 4.5). A visual inspection of the data (Figure 4.5) clearly shows a shift from short-timescale oscillations (approximately 1-2 decades) in the 2000-3000 BP interval to long-timescale oscillations (approximately several centuries) in the 600-2000 BP interval.

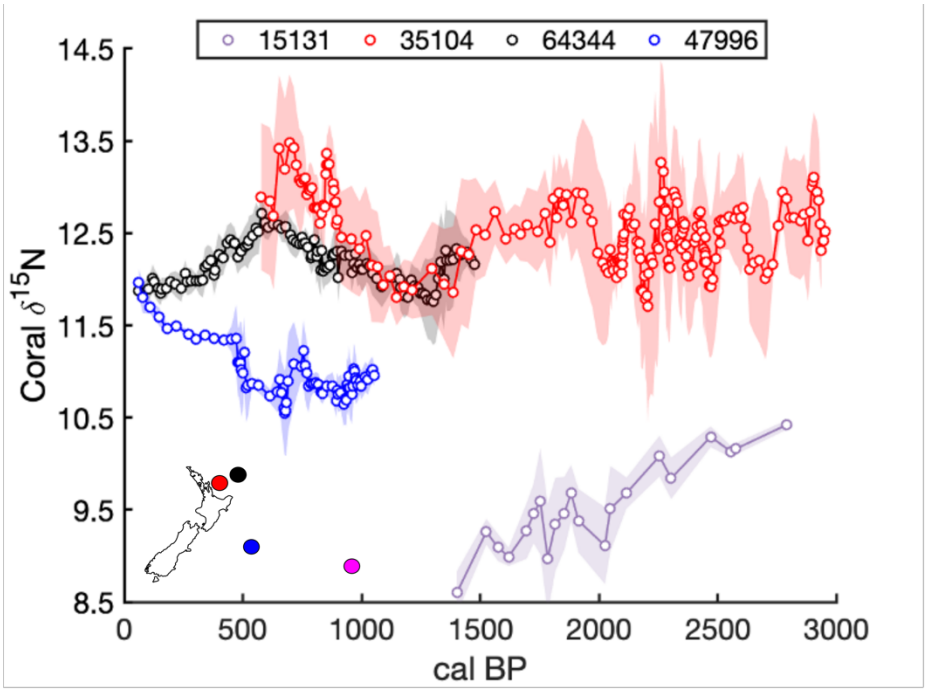

Figure 4.5: Coral δ^{15}N Over the Late Holocene. Coral δ^{15}N from the STF (47996 - blue), EAuC (64344 – black; 35104 - red) and Central South Pacific (15131 – lavender) over the last 3000 years. Shaded areas indicate the 2**σ** uncertainty range which are calculated from the U-Th uncertainties and coral δ^{15}N measurement uncertainties. Corals locations are shown in the bottom left corner with corresponding colors.

Corals 47996 and 64344 overlap from 100-900BP and show a similar range of δ^{15}N variability. 47996 δ^{15}N values vary by ~ 1.5‰ over the 100-900BP interval, with a minima of 10.56‰ at 680BP and a maximum of 11.95‰ at 100BP. 64344 δ^{15}N values vary by ~ 1‰ over the 100-900BP interval, with a maximum of 12.71‰ at 625BP and a maximum of 11.77‰ at 100BP. δ^{15}N cycles in 47996 and 64344 are nearly identical in magnitude but are *inversely* correlated over the last millennium ($R = -0.72$; $p < 0.01$).

15131 exhibits a ~1‰ drop in baseline δ^{15}N going from the 2100-2900BP interval to the 1400-2100BP interval (10.20 ± 0.14‰ vs 9.12 ± 0.09‰ respectively; Figure 4.4B). I calculate mean δ^{15}N across these intervals using the same approach as for mean δ^{13}C. I do not observe any periodic δ^{15}N variability over the entirety of the record, but this may be because 15131 has a lower temporal resolution compared to the other coral records (century scale vs. decadal scale). I therefore do not discuss δ^{15}N variability in 15131 beyond the baseline shift noted above.

4.7 Discussion:

4.7.1 Late Holocene Carbon Isotope Records

EAuC and STF $\delta^{13}C$ records (64344, 35104 and 47996) demonstrate a moderate correlation over the last 1500 years when all records are resampled to a consistent resolution and linearly detrended (Figure 4.3). These records capture similar multi-decadal to multi-centennial variations in coral $\delta^{13}C$ even though they exhibit different mean $\delta^{13}C$ values. These shared variations imply a common regional-scale centennial to multi-centennial forcing on coral $\delta^{13}C$.

4.7.1.1 Oceanic and Biological Drivers of $\delta^{13}C$ Variability

Deep-sea coral $\delta^{13}C$ data reflect the $\delta^{13}C$ values of exported POM (Schiff et al., 2014), which have their origins in planktonic $\delta^{13}C$ and source carbon at the base of the food web (McMahon et al., 2015; Glynn et al., 2019). Several factors influence these $\delta^{13}C$ values, including SST, the partial pressure of aqueous carbon dioxide (pCO_{2Aq}), $\delta^{13}C$ values in dissolved inorganic carbon ($\delta^{13}C_{DIC}$), and taxon-specific fractionation (ε_f) (Rau et al., 1989; Rau et al., 1992; McMahon et al., 2015; Magozzi et al., 2017). These factors can be coupled and may amplify or mask plankton $\delta^{13}C$ variations (Goericke et al., 1994; Magozzi et al., 2017). Disentangling the different contributing factors to phytoplankton, and ultimately coral, $\delta^{13}C$ values can therefore be challenging. In the next 3 subsections, I qualitatively assess the contribution of each individual factor to my coral $\delta^{13}C$ records.

4.7.1.1.1 Ambient CO_2/$\delta^{13}C_{DIC}$

Plankton $\delta^{13}C$ values can be influenced by atmospheric CO_2 (CO_{2Atm}) concentrations (Rau et al., 1989; Magozzi et al., 2017; Glynn et al., 2019). An increase in CO_{2Atm} usually increases surface layer DIC concentrations and lowers phytoplankton $\delta^{13}C$ values (Rau et al., 1989; Goericke et al., 1994; Magozzi et al., 2017). However, large changes in CO_{2Atm} (e.g. >100ppm) are required to significantly alter phytoplankton $\delta^{13}C$ since phytoplankton collectively have a low sensitively to CO_{2Atm} (0.0003‰/1ppm; Young et al., 2013). CO_{2Atm} has remained within a 10ppm range over the last 3000 years prior to industrialization (Figge et al., 1995; Young et al., 2013), hence I eliminate changes in CO_{2Atm} as a driver of centennial to multi-centennial $\delta^{13}C$ variability observed in my records.

4.7.1.1.2 Sea Surface Temperature

Sea surface temperature is the most important control on the spatial pattern of $\delta^{13}C$ in phytoplankton and exported POM within the SPG (Goericke et al., 1994; Magozzi et al., 2017). This is because temperature co-varies with other drivers of isotopic fractionation such as the rate of CO_2 dissolution into the surface ocean, phytoplankton growth rates, and community composition (Wiebe et al., 1940; Mook et al., 1974; Goericke et al., 1994; Magozzi et al., 2017). Values of $\delta^{13}C_{DIC}$ (and therefore $\delta^{13}C_{Plank}$ and $\delta^{13}C_{POM}$) are higher towards the equator and lower at the poles (Mook et al., 1974; Goericke et al., 1994; Magozzi et al., 2017).

Changes in $\delta^{13}C_{Plank}$ and $\delta^{13}C_{POM}$ can be related to temperature variations via several empirical transfer functions. The empirical transfer functions for $\delta^{13}C_{Plank}$ range from 0.11-0.23‰/°C, while those for $\delta^{13}C_{POM}$ can be as high as 0.41‰/°C in open ocean systems (Rau et al., 1989; Rau et al., 1992; Rau et al., 1996). Therefore, the 0.4‰ range in $\delta^{13}C$ variability observed in my coral records (Figure 4.3) would require a minimum change in SST on the order of ~1.0°C. This seems to be a plausible mechanism for the $\delta^{13}C$ variability observed in my coral records based on SST changes inferred from low resolution (sub-millennial) sediment core records that cover the last 1500 years (<1°C; Marr et al., 2013; Bostock et al., 2015). Aside from sediment core-based reconstructions, interpolated SST products (e.g. ERSSTv5) unfortunately only extend to the late 19th century (Huang et al., 2017) and the longest sub-decadally resolved paleo-SST records are limited to the 16th century in the southwest Pacific (Linsley et al., 2006; Linsley et al., 2008; DeLong et al., 2012). I therefore cannot independently verify if SST drives the multi-centennial $\delta^{13}C$ variability demonstrated in my coral records using current instrumental and decadally resolved paleoceanographic datasets.

4.7.1.1.3 Phytoplankton Community Structure

Plankton community structure is arguably the most important biological control on $\delta^{13}C_{Plank}$ (McMahon et al., 2013; McMahon et al., 2015; Glynn et al., 2019). Each phytoplankton taxon has a specific $\delta^{13}C$ fractionation factor (ε_f) which results from unique combinations of size, morphology and growth rate traits (Rau et al., 1996; Popp et al., 1998; Burkhardt et al., 1999). These traits change the degree of carbon isotopic discrimination during photosynthetic carbon fixation between different plankton taxa.

Phytoplankton $\delta^{13}C$ fractionation during photosynthesis is inversely related to size and growth; larger phytoplankton cells (e.g. picoeukaryotes) typically have more positive $\delta^{13}C$ values due to slower growth (Rau et al., 1996; Burkhardt et al., 1999). This relationship has been used in deep-sea coral records to elucidate changes in phytoplankton community structure, with shifts towards more positive $\delta^{13}C$ being interpreted as a community shift towards larger phytoplankton (Glynn et al., 2019).

The New Zealand black corals analysed here exhibit $\delta^{13}C$ changes on centennial to multi-centennial scales that are unlikely to be related to community structure. Coral $\delta^{13}C$ changes are synchronous at the two sites (EAuC and STF), which is hard to explain given that these localities have very different phytoplankton communities that respond to environmental variables unique to each site (Legendre et al., 1995; Bradford-Grieve et al., 1997; Bradford-Grieve et al., 1999; Chang et al., 2003; Pinkerton, 2011; McGregor, 2020). To elaborate:

In the EAuC, north of New Zealand, the phytoplankton community is largely a product of warm water conditions and low bioavailable nitrogen (Campbell et al., 2005; Ellwood et al., 2013). Phytoplankton communities are dominated by prokaryotic picophytoplankton (*Prochlorococcus* and *Synechoccus*), with minor stocks of diazotrophs (unicellular diazotrophs (UCYNA) and Trichodesmium; Campbell et al., 2005; Moisander et al., 2010; Sohm et al., 2011; Ellwood et al., 2013).

In the STF, east of New Zealand, plankton community structure is governed by temperature and salinity gradients across the front, and high levels of macronutrients (Legendre et al., 1995; Bradford-Grieve et al., 1999). There are 25x more picoeukaryotic plankton along the Chatham Rise compared with the community north of New Zealand (Waite et al., 2000). Diatoms and dinoflagellates comprise the majority of the macroplankton east of New Zealand (Bradford-Grieve et al., 1999; Waite et al., 2000), while diatoms are not a major contributor to plankton stocks north of New Zealand (Waite et al., 2000). Diazotrophs are not a major member of the community structure in the STF because these producers prefer warm water conditions. Indeed, SSTs in the STF east of New Zealand greatly exceed the cool threshold for the most common diazotrophs such as *Trichodesmium* and UCYNA (Campbell et al., 2005; Sohm et al., 2011).

In summary, phytoplankton community structure in the EAuC and STF are products of environmental variables (e.g. SST, macronutrients and salinity) that are unique to each location

(Legendre et al., 1995; Bradford-Grieve et al., 1999; Campbell et al., 2005; Moisander et al., 2010; Sohm et al., 2011; Ellwood et al., 2013). These variables are connected to a myriad of *local* processes (e.g. upwelling, frontal mixing), making it unlikely for both regions to experience synchronous changes.

4.7.1.2 SST-driven $\delta^{13}C$ Variability over the Late Holocene

Of the three factors controlling $\delta^{13}C_{Plank}$ listed in Section 4.7.1.1, SST is the most plausible factor coupling $\delta^{13}C$ variations in the EAuC and STF over the last 1500 years. The amplitude of the detrended coral $\delta^{13}C$ variations is ~0.4‰, which is consistent with a <1°C range in SST observed in sediment core records (Marr et al., 2013; Bostock et al., 2015), lending support to this.

I test this hypothesis by comparing the coral $\delta^{13}C$ records to the coral ΔR records in Chapter 3, which reconstructs ocean circulation around New Zealand over the last 3000 years. Ocean circulation changes may be responsible for SST variability in the region since the balance of subtropical and subpolar waters controls the north-south gradient in SST around New Zealand (Heath, 1984, 1985; Chiswell et al., 2015). While the coral ΔR records do not explicitly reconstruct SST, they have previously been used to track the balance of subtropical and subpolar waters (Chapter 3) and may therefore be applicable as a qualitative proxy for the north-south SST gradient. If this is correct, then the coral ΔR variability should correlate with the coral $\delta^{13}C$ variability.

I assessed the relationship between coral $\delta^{13}C$ and coral ΔR using four different tests: i) a correlation analysis between individual raw coral $\delta^{13}C$ sequences and corresponding ΔR sequences; ii) a correlation analysis between individual linearly detrended coral $\delta^{13}C$ sequences and corresponding ΔR sequences; iii) a correlation analysis between individual raw coral $\delta^{13}C$ sequences and the overlapping portions of the ΔR composite; and iv) a correlation analysis between individual detrended coral $\delta^{13}C$ sequences and the overlapping portions of the detrended ΔR composite. All timeseries were resampled to common data bins where the in size was set to 30 years, which is the largest data gap in both timeseries.

The coral $\delta^{13}C$ records exhibit variable relationships with the ΔR records when all records are averaged into consistent 30yr data bins (Fig. 4.6A & C). The coral $\delta^{13}C$ records have no statistically significant relationship with the ΔR reconstructions over the 0-1500BP interval

(individual sequences or the composite; trended or detrended; $p > 0.25$ for all tests) and are therefore not discussed further; however, the EAuC coral $\delta^{13}C$ record (35104) exhibits a strong correlation with trended and detrended versions of ΔR composite and individual 35104 ΔR reconstruction over the 2000-3000BP interval ($r = -0.59$-0.65; $p < 0.001$; Supp. Fig. S4.4). The consistent relationship between the EAuC coral $\delta^{13}C$ record (35104) and the corresponding ΔR record and ΔR composite is not surprising. The composite ΔR record over the 2000-3000BP interval only incorporates the ΔR data from 35104 and so the ΔR datasets used for the comparison are identical. Detrending both the $\delta^{13}C$ and ΔR data appears to slightly improve the correlations reported in the EAuC over the 2000-3000BP interval, but does not affect the significance of the relationships between coral $\delta^{13}C$ and ΔR over 0-1500BP ($p > 0.25$ for all tests). The following discussion therefore only focuses on the relationship between the detrended individual coral $\delta^{13}C$ records and the ΔR composite.

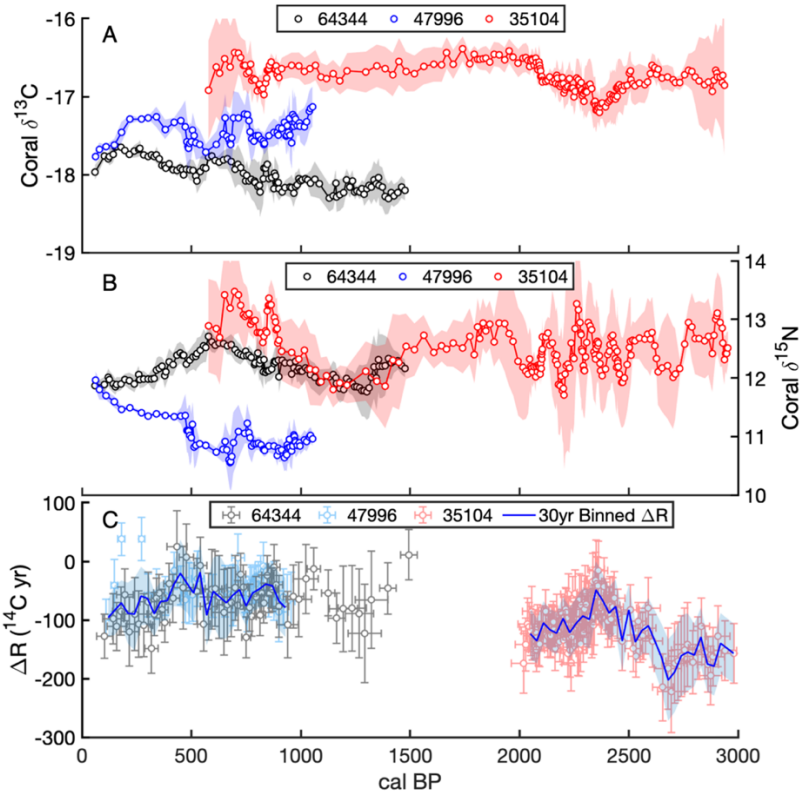

Figure 4.6: A comparison of late Holocene coral $\delta^{13}C$, $\delta^{15}N$ and ΔR. (Panel A) Trended coral $\delta^{13}C$ from the EAuC (64344 – black; 35104 - red) and STF (47996; blue) regions over the late Holocene. (Panel B) Trended coral $\delta^{15}N$ from the EAuC (64344 – black; 35104 - red) and STF (47996; blue) regions over the late Holocene. (Panel C) Trended overlapping ΔR data from the same corals over the same periods in the same colors as top panel. All ΔR data is spliced together and resampled to 30yr data bins following protocols in Chapter 3. The 600-2000BP section of the 35104 ΔR

record is omitted for reasons described in Chapter 3.4.4. All shading areas and error bars indicate the 2**σ** uncertainty range.

The disagreement between coral $\delta^{13}C$ and ΔR over 0-1500BP implies that 1) either SST does not control plankton $\delta^{13}C$ or 2) that circulation does not control SST (or both). Either way, this refutes the idea ocean circulation modulates the SST gradient over the last 1500 years and is the forcing mechanism for coral $\delta^{13}C$ co-variability. If SST is controlling coral $\delta^{13}C$ variability, then something other than gyre circulation modulates SST patterns. However, I am unable, at this time, to identify another physical mechanism responsible for changing SSTs. Therefore my hypothesis remains speculative.

That said, there is a strong correlation between detrended coral $\delta^{13}C$ and ΔR over the 2000-3000BP interval which lends some credibility to the idea that changes in ocean circulation can modulate the north-south SST gradient and therefore force coral $\delta^{13}C$ variability. The ~200 year period of weaker gyre circulation across 2230-2470BP (shown by higher ΔR) corresponds to lower coral $\delta^{13}C$ values. (Figure 4.6A & C). Weaker gyre circulation would cause warm, subtropical waters to retreat northward. This may lead to cooler SSTs and a decrease in coral $\delta^{13}C$ values based on the temperature driven gradient in phytoplankton $\delta^{13}C$ from the equator to the pole (Magozzi et al., 2017).

The fact that the coral $\delta^{13}C$ and ΔR relationship is inconsistent over the last 3000 years may simply indicate that ocean circulation and SST variability were decoupled between 0-1500BP. This nonstationary behaviour demonstrates that more work is needed to ascertain what factors potentially drive coral $\delta^{13}C$ variability.

4.7.1.3 A Trend in Coral $\delta^{13}C$ from 0-1500BP

An interesting feature of the 64344 (EAuC) $\delta^{13}C$ record is the overall increase in $\delta^{13}C$ values from 1500 to 100BP (Figure 4.2) which is not reproduced in the STF $\delta^{13}C$ record. This implies that there could be another driver of coral $\delta^{13}C$ in the EAuC. I do not attribute the overall increasing trend in $\delta^{13}C$ to a trend towards cooler SSTs, as a $\delta^{13}C$ decline of ~0.7‰ would require a SST cooling of at least ~1.75°C towards present (using a transfer function of 0.11-0.41‰/°C; Rau et al., 1992). This contradicts previous SST estimates reconstructed from a nearby sediment core (MD91-2120; Marr et al., 2013). Temperature estimates derived from Mg/Ca ratios in the foram *G. bulloides* and alkenones in MD91-2120 show a range of about 0.7°C over the last 1500 years; SSTs cool from 300-1500BP by about 0.7°C and then warm by

the same amount from 0-300BP (Marr et al., 2013). These estimates are considerably smaller than the estimate provided by the coral $\delta^{13}C$ trend.

A increase in $\delta^{13}C$ values from 1500 to 100BP could be explained by a shift towards larger and slower growing phytoplankton (e.g. picoeukaryotes; see above section or Glynn et al. (2019) for a further explanation). However, I currently have no data to independently test this hypothesis. I do note that this can be investigated by analysing $\delta^{13}C$ values of individual amino acids in my coral samples ('compound-specific stable isotope analysis' or CSSIA-AA). As mentioned above, this approach has been used to study changes in phytoplankton community structure over time (McMahon et al., 2015) and may help us to resolve whether community structure has significantly affected $\delta^{13}C$ values in my deep-sea coral records.

4.7.2 Late Holocene Nitrogen Isotope Records

Deep-sea coral $\delta^{15}N$ values may reflect a combination of three environmental signals: 1) ecological changes that alter POM $\delta^{15}N$ values within the food web (i.e. a shift in the average trophic level represented in settling POM); 2) changes to the $\delta^{15}N$ values of the source nitrogen at the base of the food web (e.g. through increased N_2 fixation or isotopically distinct NO_3^- inputs such as upwelling); and 3) the proportion of bioavailable nitrogen utilized (Altabet, 2006; Sherwood et al., 2011; McMahon et al., 2013; Sherwood et al., 2013; McMahon et al., 2016; Glynn et al., 2019). I assess these in the next section by examining common features in my overlapping coral $\delta^{15}N$ records; reviewing processes that alter the $\delta^{15}N$ of regional POM; studying the unique food webs of the EAuC and STF; and using mass balance calculations to assess the impact of trophic level scenarios on coral $\delta^{15}N$.

4.7.2.1 Assessing the Contribution of Food Web Changes to $\delta^{15}N$ Variability

The nitrogen isotope records from 64344 and 47996 are antiphased over the last millennium (Figure 4.5). This implies that there may be a single driver of coral $\delta^{15}N$ that applies in an opposite sense in the EAuC and STF. This is plausible because the spatial pattern of POM $\delta^{15}N$ in the southwest Pacific largely reflects input and removal processes that can be coupled with ocean dynamics (e.g. upwelling and the circulation of waters replete with bioavailable nitrogen fixed by diazotrophs; Somes et al., 2010; Somes et al., 2017; and see review in the following section).

Another possible explanation for the coral $\delta^{15}N$ change is a shift in the relative abundance of phytoplankton to zooplankton represented in the settling POM. Processes that could change this ratio include grazing rates (Work et al., 2003; Ducklow et al., 2006) and phytoplankton senescence (Winder et al., 2010), which can be linked to seasonal, interannual or decadal climate/ocean variability (Edwards et al., 2004; Ducklow et al., 2006; Thackeray et al., 2008; Winder et al., 2010). Unfortunately, since observations are limited to the 20th century, I have no way of testing whether these could explain the multi-centennial variability I observe over the last millennium.

However, I do not think it is likely that the antiphased $\delta^{15}N$ results from simultaneous and opposite changes to phytoplankton and zooplankton ratios at the two sites. The EAuC and STF both have different, and independent, food web structures due to different levels of nutrients, primary production and unique phytoplankton community structures (e.g. Legendre et al., 1995; Bradford-Grieve et al., 1997; Bradford-Grieve et al., 1999; Chang et al., 2003). These differences result from environmental variables unique to each site (for further details see Section 4.7.1.1.3 or Legendre et al., 1995; Bradford-Grieve et al., 1997; Bradford-Grieve et al., 1999; Chang et al., 2003; Pinkerton, 2011), making coupled changes unlikely.

Mass balance calculations (Eq. 1) further suggest that food web or trophic level dynamics are not the cause of the coupled $\delta^{15}N$ variations. The average amplitude of coral $\delta^{15}N$ variation is around 1.25‰. This would require over a *twenty-fold* shift the ratio of phytoplankton to zooplankton. While it is not impossible for a change of this magnitude to occur at a single location, a change of the same magnitude, but opposite sense, must *simultaneously* occur at the other location to explain the antiphasing I observe (Figure 4.5), which seems highly implausible (Scott Nodder, pers. comm.).

I therefore propose that the most likely explanation for the anti-phased $\delta^{15}N$ relationship in the EAuC and STF is changes to the $\delta^{15}N$ of the source (bioavailable) nitrogen at the base of the food web. However, I acknowledge that I cannot explicitly exclude a contribution from food web and trophic level changes.

4.7.2.2 Ocean Drivers of Late Holocene $\delta^{15}N$ Variability

Where only a portion of bioavailable nitrogen is taken up by phytoplankton, there exists the potential for Rayleigh Fractionation to affect the $\delta^{15}N$ of the resultant organic matter (see Section 1.3.4.2). However, in the EAuC and northern STF, nitrate is likely fully utilized

(Bradford et al., 1982; Levitus et al., 1993; Bradford-Grieve et al., 1999; Nodder et al., 2001; Ellwood et al., 2013; Bostock et al., 2019) so no net fractionation can occur. This means that phytoplankton (and hence the $\delta^{15}N$ of the coral) inherit the $\delta^{15}N$ of bioavailable nitrogen sources (Glynn et al., 2019).

Around New Zealand, bioavailable nitrogen patterns may be influenced by ocean circulation and upwelling dynamics. Ocean circulation transports subtropical waters south along northeast New Zealand *via* the EAuC (Heath, 1984, 1985; Chiswell et al., 2015). These waters carry low levels of isotopically light (0-2‰) bioavailable nitrogen produced by diazotrophs off eastern Australia (Bradford-Grieve et al., 1999; Campbell et al., 2005; Moisander et al., 2010; Somes et al., 2010; Ellwood et al., 2013; Somes et al., 2017). This bioavailable nitrogen is the limiting nutrient for new productivity (Longhurst, 2010; Ellwood et al., 2013), and is quickly utilized by primary producers as the current flows along New Zealand's northeast coastline. Variations in circulation strength may therefore modulate POM $\delta^{15}N$ in the EAuC by changing the total amount of isotopically light bioavailable nitrogen carried to northeast New Zealand.

Nitrate is the most common form of bioavailable nitrogen along eastern New Zealand and in the STF (Bradford-Grieve et al., 1999). Wind-driven upwelling along the eastern New Zealand shelf and frontal mixing with subantarctic waters supplies isotopically light nitrate (2-6‰) and other macronutrients to the surface layer of the STF (Bradford et al., 1978; Bradford-Grieve et al., 1999; Somes et al., 2017; Stevens et al., 2019). Variations in wind-driven upwelling rates or changes in ocean circulation may therefore influence POM $\delta^{15}N$ by changing the total nitrate abundance in the STF. Factors that may modulate ocean circulation or upwelling rates include changing surface stratification (Sarmiento et al., 2006) or variable wind stress (Fenner et al., 1992; Sarmiento et al., 2006; Roemmich et al., 2016).

4.7.2.2.1 Coral $\delta^{15}N$ and ΔR Comparison

The antiphased relationship between $\delta^{15}N$ in the EAuC and STF may indicate changes in the regional distribution of bioavailable nitrogen driven by variable circulation strength and upwelling rates. I therefore compare my $\delta^{15}N$ records to the ΔR reconstructions from the EAuC and STF (Figure 4.6) which have previously been used to track the balance of tropical and polar waters around New Zealand (Chapter 3).

I would expect stronger gyre circulation (lower ΔR) to produce lower $\delta^{15}N$ values in the EAuC. This is because advection of warm, subtropical waters would bring isotopically light

bioavailable nitrogen (0-2‰) further south, resulting in lower POM $\delta^{15}N$ values (Campbell et al., 2005; Moisander et al., 2010; Somes et al., 2010). East of New Zealand, stronger circulation would increase $\delta^{15}N$ values since enhanced transport of warm, subtropical water would 1) enhance thermal stratification and inhibit the upwelling of isotopically-light nitrate (3-6‰) (Altabet, 2006; Sarmiento et al., 2006) and/or 2) push subantarctic waters rich with isotopically light NO_3^- southward.

Coral $\delta^{15}N$ and ΔR, however, exhibit no significant relationship over the late Holocene (Figure 4.6B & C; p values range from 0.21 – 0.48 in all records). Instead the two proxies change over different timescales. Between 0-2000BP, Coral $\delta^{15}N$ oscillates on 600 year timescales while ΔR cycles span 400 years. Between 2000-3000BP, coral $\delta^{15}N$ cycles vary from several decades to 200 years while ΔR oscillations span ~400 years. No statistically significant correlations are found even when the records are phase shifted up to 200 years. This disagreement between $\delta^{15}N$ and ΔR implies multi-centennial circulation changes over the last 3000 years did not alter southwest Pacific bioavailable nitrogen patterns. In the next section I examine other possible drivers of antiphased $\delta^{15}N$ variability.

4.7.2.3 Climate Drivers of $\delta^{15}N$ Variability

Basin-wide climatic processes, such as ENSO, can contribute to temporal POM $\delta^{15}N$ variability. They do this by altering bioavailable nitrogen input to the surface ocean and nutrient recycling through ocean-atmosphere dynamics such as ocean circulation, surface wind stress, wind-driven upwelling, SSTs, and surface ocean stratification (Karl et al., 1995; Altabet, 2001; Rau et al., 2003; Behrenfeld et al., 2006; Lehodey et al., 2006; Sarmiento et al., 2006; Vokhshoori et al., 2014; Menkes et al., 2015). Around New Zealand, ENSO drives SST and wind direction changes such that during the positive phase (El Niño) SSTs cool and southwesterly winds prevail (Ummenhofer et al., 2007; Ummenhofer et al., 2009; Bowen et al., 2017). During the negative phase (La Niña), SSTs warm and wind flows from the northeast (Ummenhofer et al., 2007; Ummenhofer et al., 2009; Bowen et al., 2017).

These ENSO-driven SST changes may alter nitrogen fixation rates in the EAuC because diazotrophs strongly prefer warmer waters (Campbell et al., 2005; Moisander et al., 2010; Sohm et al., 2011). In addition, ENSO modulates interannual wind direction variability which may alter upwelling rates along eastern New Zealand (Sarmiento et al., 2006; Ummenhofer et al., 2007;

Ummenhofer et al., 2009). I therefore hypothesize that multi-centennial changes in paleo-ENSO may be a forcing factor on the coral $\delta^{15}N$ variability observed in the 64344 and 47996 records over the last 1500 years by altering upwelling rates east of New Zealand and nitrogen fixation north of New Zealand.

I test this hypothesis by comparing my coral $\delta^{15}N$ records to a 2,000 year long reconstruction of the paleo-Southern Oscillation Index (SOI) (Figure 4.7; Yan et al., 2011). The Yan et al. (2011) SOI reconstruction is based on a network of decadally-resolved precipitation proxies from the equatorial Indo-Pacific region. The SOI measures the pressure difference between Tahiti and Darwin, which are locations that are proximal to evaluating the patterns of atmospheric pressure that arise from the Walker Circulation that is inextricably tied to ENSO. The SOI is the atmospheric measure of the ENSO phenomenon, and can infer the manifestation of the ENSO teleconnection to the NZ region. Variations in the ENSO produce changes in mean SST and wind direction around New Zealand such that during El Niño (negative SOI) sea surface temperatures cool and northeasterly winds prevail and during La Niña (positive SOI) sea surface temperatures warm and southeasterly winds prevail (Ummenhofer et al., 2007; Ummenhofer et al., 2009; Bowen et al., 2017; see Figure 4.7).

To compare coral $\delta^{15}N$ with the paleo-SOI index I first resampled the original paleo-SOI index from Yan et al., 2011 to the same resolution as the 64344 and 47996 $\delta^{15}N$ records *via* piecewise cubic interpolation. Since I am only interested in the *variability* in the SOI and coral $\delta^{15}N$ records, I linearly detrend the resampled paleo-SOI index and coral $\delta^{15}N$ records following the same protocols used to detrend the coral $\delta^{13}C$ records (Section 4.6.1). This effectively isolates the centennial fluctuations in all timeseries.

$\delta^{15}N$ variability in 64344 is negatively correlated with the detrended and resampled paleo-SOI index ($R = -0.53$; $p < 0.001$, $n = 124$), while 47996 $\delta^{15}N$ is positively correlated ($R = 0.41$; $p < 0.001$; $n = 75$) (Figure 4.7A & B). The minima 47996 $\delta^{15}N$ record appears to coincide with the paleo-SOI minima over the last millennium (750BP). The maxima of the 64344 $\delta^{15}N$ record appears to coincide with the SOI minima over the last millennium (750BP), while the minima of the 64344 $\delta^{15}N$ record coincides with a SOI maxima at 1250BP (Figure 4.7A & B).

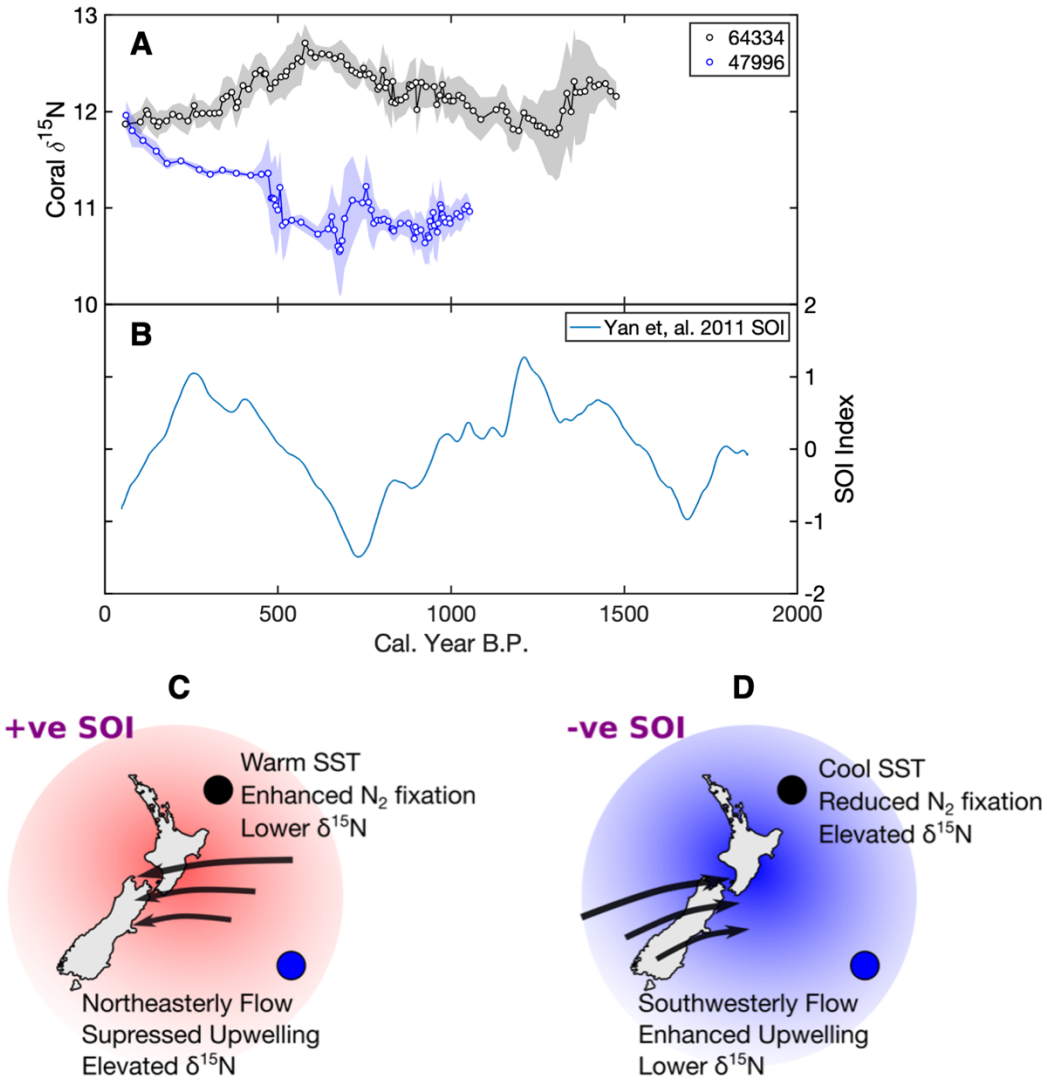

Figure 4.7: SOI-Driven $\delta^{15}N$ Variability Over The 0-1500BP Period. Panel A: Coral $\delta^{15}N$ from the EAuC (black) and STF (blue) over the 0-1500BP period. Panel B: Paleo-SOI reconstruction from the last 2,000 years (Yan et al 2011). The SOI reconstruction is resampled to a 40yr resolution using a piecewise cubic interpolation and detrended following protocols in Sect. 4. Peaks and troughs in the coral $\delta^{15}N$ from 500-1450BP correspond to peaks and troughs in the SOI reconstructions. Panels C and D: The effects of SST and wind direction changes on upwelling, nitrogen fixation and coral $\delta^{15}N$.

The correlation between the Yan et al. (2011) paleo-SOI index and my coral $\delta^{15}N$ records supports my previous idea that multi-centennial changes in the SOI may modulate upwelling and nitrogen fixation, which in turn may alter bioavailable nitrogen distributions (and hence POM/coral $\delta^{15}N$) around New Zealand (Figure 4.7). Cooler SSTs during negative SOI conditions (+ENSO; see Chapter 1 Sect 1.4.1; Figure 1.3) may inhibit rates of nitrogen fixation in the EAuC and therefore increase $\delta^{15}N$ values in coral 64344 (Figure 4.7C). Conversely, the negative SOI corresponds to southwesterly air flow across the South Island. This may enhance upwelling

along eastern New Zealand due to Ekman transport principles (see Supp. Fig. 4.2 or Sarmiento et al., 2006; Trujillo et al., 2011 for an explanation on Ekman Transport), and therefore supply more isotopically-light bioavailable nitrogen to the surface layer (Sarmiento et al., 2006). An increase in isotopically-light deep-sea nitrogen would decrease POM $\delta^{15}N$ values in 47996 (Figure 4.7D; Altabet, 2006; Sigman et al., 2009). Multi-centennial coral $\delta^{15}N$ cycles may therefore indicate a SOI-driven response in POM $\delta^{15}N$ *via* long-term SST and wind direction changes.

The mechanism above explains the inverse correlation between $\delta^{15}N$ in corals 64344 and 47996, but I caution against extrapolating this relationship to coral 35104. Although 35104 and 64344 show similar $\delta^{15}N$ trends where they overlap, 35104 exhibits a wide spectrum of $\delta^{15}N$ variability that is not observed in the other corals. This variability changes from multi-decadal cycles over the 2000-3000BP interval to multi-centennial cycles over the 0-2000BP interval (Figure 4.5). If the SOI drives these $\delta^{15}N$ cycles in coral 35104, it would imply a fundamental change in frequency somewhere around 2000BP. Unfortunately, the Yan et al. (2011) SOI reconstruction only spans the last 2000 years and so I cannot evaluate if a change in SOI periodicity is responsible for a shift in the periodicity of nitrogen fixation cycles in the EAuC.

The idea that SOI drives nitrogen fixation cycles in the EAuC assumes that $\delta^{15}N$ reflects nitrogen-source dynamics over the entirety of the last 3000 years, rather than trophic level changes or food web dynamics. This assumption may not hold, however, as some have cautioned against extrapolating source, food web or trophic control over coral $\delta^{13}C$ and $\delta^{15}N$ from one coral to another, or from one location to another (Sherwood et al., 2011; Sherwood et al., 2013; Schiff et al., 2014; McMahon et al., 2015).

4.7.3 Multi-proxy evidence for a SPG Strengthening and Expansion over the 2000-3000BP Period

Corals 35104 (EAuC) and 15131 (Central South Pacific) both grew continuously across the period 1500-2700BP. Somewhere around 2000-2100BP coral 15131 captures a shift in radiocarbon (ΔR) (Chapter 3). ΔR values are lower in both corals over the 2000-3000BP interval relative to the 0-2000BP interval, which is also seen in the south Tasman sea (Figure 4.8A & B; Komugabe-Dixson et al. (2016)). In Chapter 3, I interpret this ΔR suppression as evidence for a stronger SPG circulation during the 2000-3000BP interval.

The change in mean ΔR in these regions is synchronous with a baseline shift in Central South Pacific $\delta^{13}C$ and $\delta^{15}N$ (Figure 4.8A-E). Based on what we know about modern patterns of $\Delta^{14}C$, $\delta^{15}N_{POM}$, and $\delta^{13}C_{Plank}/\delta^{13}C_{POM}$ in the SPG, my observations can be interpreted as a *strengthening* and *poleward expansion* of the SPG over the 2000-3000BP period. Currently, $\delta^{13}C_{Plank}$ and $\delta^{13}C_{POM}$ grade from more positive in the EAuC to more negative in the Central South Pacific (Figure 4.8F; Magozzi et al., 2017). At the same time, there is a north-south gradient from high to low $\delta^{15}N$ across the STF (Figure 8G; Somes et al., 2010; Somes et al., 2017). A *strengthening* of the SPG would push high-$\delta^{13}C$ EAuC waters 'downstream' into the central south Pacific. A *poleward expansion* of the SPG would cause a southward migration of high-$\delta^{15}N$ Central Pacific waters (Figure 4.8). Combined, the effect would be to lower ΔR, and increase both $\delta^{15}N$ and $\delta^{13}C$, which is what I observe between 2000-3000BP across multiple locales (EAC extension, EAuC and Central South Pacific), supporting my hypothesis of a millennium-long period of an enhanced SPG.

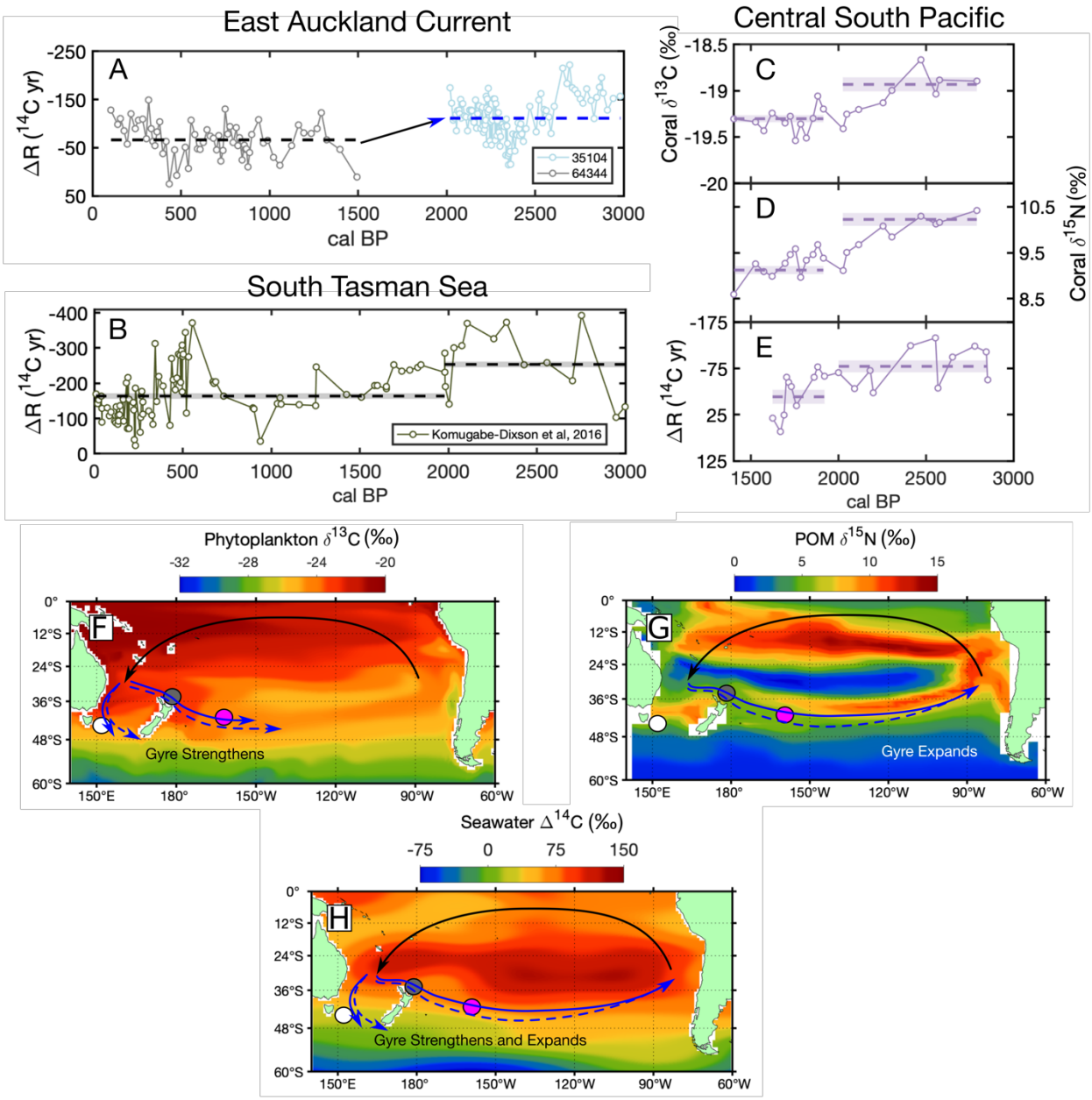

Figure 4.8: Multi-proxy Evidence for a Late Holocene South Pacific Gyre Expansion. Panels A-B: Black coral ΔR data from the EAuC and south Tasman sea regions over the last 3000 years. Panels C-E: Coral 15131 $\delta^{13}C$, $\delta^{15}N$, and ΔR from the Central South Pacific region over the 1400-2900BP period. Panels F-H: A schematic of the SPG strengthening and expansion (blue lines) overlaid on top of modelled phytoplankton $\delta^{13}C$ data (Magozzi et al., 2017), modelled POM $\delta^{15}N$ data (Somes et al., 2017), modelled surface seawater $\Delta^{14}C$ data (Key et al., 2004) and coral locations (dots; white – Komugabe-Dixson et al., 2016; grey – 35104 and 64344; magenta – 15131). Solid lines show modern circulation patterns and broken lines show the hypothesized circulation patterns during the 2000-3000BP interval.

The corroboration between the stable isotope records in coral 15131, the Komugabe-Dixson et al. (2016) ΔR records, and the Chapter 3 ΔR records suggest there may be a coupled millennium-long interplay between SPG circulation and the pattern of POM $\delta^{13}C$ and $\delta^{15}N$ over

the 2000-3000BP period. This work shows that this coupling potentially acts over millennial timescales: the SPG experienced a millennium-long period of stronger circulation which altered its biogeochemical patterns. The modern SPG intensification and expansion (Roemmich et al., 2007; Roemmich et al., 2016; Yang et al., 2020), and its effects on marine biology and biogeochemistry (e.g. Behrenfeld et al., 2006; Poloczanska et al., 2007; Polovina et al., 2008; Boyce et al., 2010; Poloczanska et al., 2013), are therefore not unique to the 20th century. My work suggests that the late Holocene held a millennium-long period in which the SPG conditions were reminiscent of those changes observed over the last several decades.

Not all of the coral data agrees with this pattern. Unlike coral 15131, coral 35104 does not show evidence for a baseline shift in either the $\delta^{15}N$ or $\delta^{13}C$ records over the 1500-3000BP interval (Figures 4.2 & 4.5). There may be several explanations for this. For example, the factors controlling coral $\delta^{15}N$ may differ between the EAuC and Central South Pacific (e.g. different source and food web contributions to coral $\delta^{15}N$). In addition, the dynamics may also change through time. However, SST (and by extension, circulation) is the dominant control on SPG $\delta^{13}C_{Plank}$ and $\delta^{13}C_{POM}$ patterns (Goericke et al., 1994; Magozzi et al., 2017). Therefore, the 35104 $\delta^{13}C$ record *should* capture a circulation-driven change in SPG $\delta^{13}C_{Plank}$ and $\delta^{13}C_{POM}$ patterns, given that I observe this change in the corresponding ΔR record (Figure 4.8). At present I cannot explain this discrepancy.

4.8 Conclusions:

The southwest Pacific coral $\delta^{13}C$ and $\delta^{15}N$ records presented here demonstrate significant variability on multi-centennial timescales. The cycles in coral $\delta^{13}C$ are likely driven by variable SSTs over the last 3000 years; however, I am unable to confirm this hypothesis with the existing paleoceanographic SST datasets. Multi-centennial cycles in coral $\delta^{15}N$ do not correlate with a late Holocene reconstruction of ocean circulation. This refutes my hypothesis that multi-centennial variations in SPG circulation altered bioavailable nitrogen distributions over the late Holocene. I propose instead that the multi-centennial cycles in coral $\delta^{15}N$ may have been modulated by variable nitrogen fixation and upwelling rates forced by the mean state of ENSO.

EAuC coral $\delta^{13}C$ exhibits a ~0.8‰ trend towards higher values over the 0-1500BP interval. This trend is too large to be driven by SST or changing $\delta^{13}C_{DIC}$ alone. I therefore

speculate this trend results from a shift in phytoplankton community structure towards larger and faster growing phytoplankton at present. Unfortunately, I cannot confirm this idea using the current coral $\delta^{13}C$ dataset; however, this will be the topic of future research using a compound-specific amino acid approach.

Over a longer timescale, my $\delta^{13}C$ and $\delta^{15}N$ coral records support my earlier hypothesis (based on radiocarbon results - see Chapter 3) that the SPG circulation was stronger over the 2000-3000BP interval. However, the coral $\delta^{13}C$ and $\delta^{15}N$ records suggest that in addition to strengthening, the SPG may have also expanded over this interval. Moreover, my results indicate that the modern strengthening of the SPG, as indicated by coral ΔR, $\delta^{13}C$ and $\delta^{15}N$ records (Roemmich et al., 2007; Roemmich et al., 2016; Yang et al., 2020), and its effects on marine life and biogeochemistry (e.g. Poloczanska et al., 2007; Polovina et al., 2008; Boyce et al., 2010; Moore et al., 2013; Poloczanska et al., 2013), are not unprecedented over the last few thousand years.

This work highlights the key role that a distributed set of deep-sea coral-based paleoceanographic reconstructions can play in elucidating the coupled interplay between physical oceanography, marine productivity and marine biogeochemistry on multi-decadal to millennial timescales. Moreover, this work has highlighted the 2000-3000BP period as a critical period of interest for studying physical and biological dynamics of a more intense SPG. This period may serve as an analogue to the modern gyre conditions and can therefore assist in untangling the effects of natural gyre variability from anthropogenic climate effects.

4.9 Acknowledgments:

Black corals were provided by the National Institute of Water and Atmosphere Invertebrate Collection. I wish to thank Peter Marriot, Sadie Mills and Dianna Macpherson for assistance with coral access, providing a space to sub-sample coral sections and navigating CITES permitting. Black coral micro-milling was accommodated by the National Institute of Water and Atmospheric Research (NIWA) Stable Isotope Facility. I wish to thank Gordon Brailsford, Colin Nankivell, Tony Bromley, and Sally Gray for access to laboratory space for micro-milling. This work benefited from conversations with Tony Wang, Christopher Somes, Di Tracey, Sebastian Breitenbach, and Philip Sutton. I wish to thank Sarah Magozzi, Clive Trueman and Christopher Somes for providing their $\delta^{13}C$ and $\delta^{15}N$ model data. Funding for this work was

provided by the New Zealand Royal Society Marsden Fund Grant No. NIWA1602 awarded to HLN, DJS, SJF and AKD. Seed funding was provided by URF 210024 awarded to DJS. The authors declare no conflicts of interest.

4.10 References:

Abram, N. J., Mulvaney, R., Vimeux, F., Phipps, S. J., Turner, J., & England, M. H. (2014). Evolution of the Southern Annular Mode during the past millennium. *Nature Climate Change, 4*(7), 564-569. https://doi.org/10.1038/nclimate2235

Altabet, M. A. (2006). Isotopic Tracers of the Marine Nitrogen Cycle: Present and Past. In J. K. Volkman (Ed.), *Marine Organic Matter: Biomarkers, Isotopes and DNA* (pp. 251-293). Berlin, Heidelberg: Springer Berlin Heidelberg.

Altabet, M. A. (2001). Nitrogen isotopic evidence for micronutrient control of fractional NO3− utilization in the equatorial Pacific. *Limnology and Oceanography, 46*(2), 368-380. https://doi.org/10.4319/lo.2001.46.2.0368

Behrenfeld, M. J., O'Malley, R. T., Siegel, D. A., McClain, C. R., Sarmiento, J. L., Feldman, G. C., et al. (2006). Climate-driven trends in contemporary ocean productivity. *Nature, 444*(7120), 752-755. https://doi.org/10.1038/nature05317

Bevington, P. R. (1969). *Data reduction and error analysis for the physical sciences*.

Bostock, H. C., Hayward, B. W., Neil, H. L., Sabaa, A. T., & Scott, G. H. (2015). Changes in the position of the Subtropical Front south of New Zealand since the last glacial period. *Paleoceanography, 30*(7), 824-844. http://dx.doi.org/10.1002/2014PA002652

Bostock, H. C., Prebble, J. G., Cortese, G., Hayward, B., Calvo, E., Quirós-Collazos, L., et al. (2019). Paleoproductivity in the SW Pacific Ocean During the Early Holocene Climatic Optimum. *Paleoceanography and Paleoclimatology, 34*(4), 580-599. https://doi.org/10.1029/2019PA003574

Bowen, M., Markham, J., Sutton, P., Zhang, X., Wu, Q., Shears, N. T., & Fernandez, D. (2017). Interannual Variability of Sea Surface Temperature in the Southwest Pacific and the Role of Ocean Dynamics. *Journal of Climate, 30*(18), 7481-7492. https://journals.ametsoc.org/doi/abs/10.1175/JCLI-D-16-0852.1

Boyce, D. G., Lewis, M. R., & Worm, B. (2010). Global phytoplankton decline over the past century. *Nature, 466*, 591. Article. https://doi.org/10.1038/nature09268

Bradford, J. M., Heath, R. A., Chang, F. H., & Hay, C. H. (1982). The effect of warm-core eddies on oceanic productivity off northeastern New Zealand. *Deep Sea Research Part A. Oceanographic Research Papers, 29*(12), 1501-1516. http://www.sciencedirect.com/science/article/pii/0198014982900395

Bradford, J. M., & Roberts, P. E. (1978). Distribution of reactive phosphorus and plankton in relation to upwelling and surface circulation around New Zealand. *New Zealand Journal of Marine and Freshwater Research, 12*(1), 1-15. https://doi.org/10.1080/00288330.1978.9515717

Bradford-Grieve, J., Boyd, P. W., Chang, F. H., Chiswell, S. M., Hadfield, M., Hall, J., et al. (1999). Pelagic ecosystem structure and functioning in the subtropical front region east of New Zealand in austral winter and spring 1993. *Journal of Plankton Research, 21*(3), 405-428. https://doi.org/10.1093/plankt/21.3.405

Bradford-Grieve, J. M., Chang, F. H., Gall, M., Pickmere, S., & Richards, F. (1997). Size-fractionated phytoplankton standing stocks and primary production during austral winter and spring 1993 in the Subtropical Convergence region near New Zealand. *New Zealand Journal of Marine and Freshwater Research, 31*(2), 201-224. http://dx.doi.org/10.1080/00288330.1997.9516759

Breitenbach, S. F. M., Rehfeld, K., Goswami, B., Baldini, J. U. L., Ridley, H. E., Kennett, D. J., et al. (2012). COnstructing Proxy Records from Age models (COPRA). *Clim. Past, 8*(5), 1765-1779. https://www.clim-past.net/8/1765/2012/

Burkhardt, S., Riebesell, U., & Zondervan, I. (1999). Effects of growth rate, CO2 concentration, and cell size on the stable carbon isotope fractionation in marine phytoplankton. *Geochimica et Cosmochimica Acta, 63*(22), 3729-3741. http://www.sciencedirect.com/science/article/pii/S0016703799002173

Cai, W. (2006). Antarctic ozone depletion causes an intensification of the Southern Ocean super-gyre circulation. *Geophysical Research Letters, 33*(3), n/a-n/a. http://dx.doi.org/10.1029/2005GL024911

Cai, W., Shi, G., Cowan, T., Bi, D., & Ribbe, J. (2005). The response of the Southern Annular Mode, the East Australian Current, and the southern mid-latitude ocean circulation to global warming. *Geophysical Research Letters, 32*(23), n/a-n/a. http://dx.doi.org/10.1029/2005GL024701

Campbell, L., Carpenter, E., Montoya, J., Kustka, A., & Capone, D. (2005). Picoplankton community structure within and outside a Trichodesmium bloom in the southwestern Pacific Ocean. *Vie et Milieu, 55*, 185-195.

Chang, F. H., Zeldis, J., Gall, M., & Hall, J. (2003). Seasonal and spatial variation of phytoplankton assemblages, biomass and cell size from spring to summer across the north-eastern New Zealand continental shelf. *Journal of Plankton Research, 25*(7), 737-758. https://doi.org/10.1093/plankt/25.7.737

Cheng, H., Lawrence Edwards, R., Shen, C.-C., Polyak, V. J., Asmerom, Y., Woodhead, J., et al. (2013). Improvements in 230Th dating, 230Th and 234U half-life values, and U–Th isotopic measurements by multi-collector inductively coupled plasma mass spectrometry. *Earth and Planetary Science Letters, 371*(Supplement C), 82-91. http://www.sciencedirect.com/science/article/pii/S0012821X13001878

Chiswell, S. M., Bostock, H. C., Sutton, P. J. H., & Williams, M. J. M. (2015). Physical oceanography of the deep seas around New Zealand: a review. *New Zealand Journal of Marine and Freshwater Research, 49*(2), 286-317. https://doi.org/10.1080/00288330.2014.992918

Chiswell, S. M., Bradford-Grieve, J., Hadfield, M. G., & Kennan, S. C. (2013). Climatology of surface chlorophyll a, autumn-winter and spring blooms in the southwest Pacific Ocean. *Journal of Geophysical Research: Oceans, 118*(2), 1003-1018. https://doi.org/10.1002/jgrc.20088

DeLong, K. L., Quinn, T. M., Taylor, F. W., Lin, K., & Shen, C.-C. (2012). Sea surface temperature variability in the southwest tropical Pacific since AD 1649. *Nature Climate Change, 2*(11), 799-804. https://doi.org/10.1038/nclimate1583

Deser, C., Phillips, A. S., & Alexander, M. A. (2010). Twentieth century tropical sea surface temperature trends revisited. *Geophysical Research Letters, 37*(10), n/a-n/a. http://dx.doi.org/10.1029/2010GL043321

Drysdale, R. N., Spötl, C., Hellstrom, J. C., & Richards, D. A. (2012). New advances in the dating of speleothems. *Quaternary Geochronology, 14*(Complete), 1-4.

Ducklow, H. W., Fraser, W., Karl, D. M., Quetin, L. B., Ross, R. M., Smith, R. C., et al. (2006). Water-column processes in the West Antarctic Peninsula and the Ross Sea: Interannual variations and foodweb structure. *Deep Sea Research Part II: Topical Studies in Oceanography, 53*(8), 834-852. http://www.sciencedirect.com/science/article/pii/S0967064506000701

Edwards, M., & Richardson, A. J. (2004). Impact of climate change on marine pelagic phenology and trophic mismatch. *Nature, 430*(7002), 881-884. https://doi.org/10.1038/nature02808

Ellwood, M. J., Law, C. S., Hall, J., Woodward, E. M. S., Strzepek, R., Kuparinen, J., et al. (2013). Relationships between nutrient stocks and inventories and phytoplankton physiological status along an oligotrophic meridional transect in the Tasman Sea. *Deep Sea Research Part I: Oceanographic Research Papers, 72*, 102-120. http://www.sciencedirect.com/science/article/pii/S0967063712002087

Fenner, J., Carter, L., & Stewart, R. (1992). Late Quaternary paleoclimatic and paleoceanographic change over northern Chatham Rise, New Zealand. *Marine Geology, 108*(3), 383-404. http://www.sciencedirect.com/science/article/pii/002532279290206W

Figge, R. A., & White, J. W. C. (1995). High-resolution holocene and late glacial atmospheric CO2 record: variability tied to changes in thermohaline circulation. *Global Biogeochemical Cycles, 9*(3), 391-403. http://dx.doi.org/10.1029/95GB01458

Francey, R., Allison, C., Etheridge, D., Trudinger, C., Enting, I., Leuenberger, M., et al. (1999). A 1000-year high precision record of δ13C in atmospheric CO2. *Tellus B, 51*(2), 170-193.

Glynn, D. S., McMahon, K. W., Guilderson, T. P., & McCarthy, M. D. (2019). Major shifts in nutrient and phytoplankton dynamics in the North Pacific Subtropical Gyre over the last 5000 years revealed by high-resolution proteinaceous deep-sea coral δ15N and δ13C records. *Earth and Planetary Science Letters, 515*, 145-153. http://www.sciencedirect.com/science/article/pii/S0012821X19301621

Goericke, R., & Fry, B. (1994). Variations of marine plankton δ13C with latitude, temperature, and dissolved CO2 in the world ocean. *Global Biogeochemical Cycles, 8*(1), 85-90. https://doi.org/10.1029/93GB03272

Graham, R. M., & De Boer, A. M. (2013). The Dynamical Subtropical Front. *Journal of Geophysical Research: Oceans, 118*(10), 5676-5685. http://dx.doi.org/10.1002/jgrc.20408

Gruber, N. (2008). The marine nitrogen cycle: overview and challenges. *Nitrogen in the marine environment, 2*, 1-50.

Hayes, J. (2004). An Introduction to Isotopic Calculations. *At. Energy*.

Heath, R. A. (1984). The depth of the mixed layer as an indicator of oceanic circulation around New Zealand. *New Zealand Journal of Marine and Freshwater Research, 18*(1), 83-92. https://doi.org/10.1080/00288330.1984.9516032

Heath, R. A. (1985). A review of the physical oceanography of the seas around New Zealand — 1982. *New Zealand Journal of Marine and Freshwater Research, 19*(1), 79-124. https://doi.org/10.1080/00288330.1985.9516077

Hellstrom, J. (2003). Rapid and accurate U/Th dating using parallel ion-counting multi-collector ICP-MS. *Journal of Analytical Atomic Spectrometry, 18*(11), 1346-1351. 10.1039/B308781F. http://dx.doi.org/10.1039/B308781F

Hellstrom, J. (2006). U-Th dating of speleothems with high initial 230Th using stratigraphical constraint. *Quaternary Geochronology, 1*, 289-295.

Henson, S. A., Beaulieu, C., & Lampitt, R. (2016). Observing climate change trends in ocean biogeochemistry: when and where. *Global Change Biology, 22*(4), 1561-1571. https://doi.org/10.1111/gcb.13152

Henson, S. A., Sarmiento, J. L., Dunne, J. P., Bopp, L., Lima, I., Doney, S. C., et al. (2010). Detection of anthropogenic climate change in satellite records of ocean chlorophyll and productivity. *Biogeosciences, 7*(2), 621-640. https://bg.copernicus.org/articles/7/621/2010/

Huang, B., Thorne, P. W., Banzon, V. F., Boyer, T., Chepurin, G., Lawrimore, J. H., et al. (2017). Extended Reconstructed Sea Surface Temperature, Version 5 (ERSSTv5): Upgrades, Validations, and Intercomparisons. *Journal of Climate, 30*(20), 8179-8205. https://doi.org/10.1175/JCLI-D-16-0836.1

Karl, D. M., Letelier, R., Hebel, D., Tupas, L., Dore, J., Christian, J., & Winn, C. (1995). Ecosystem changes in the North Pacific subtropical gyre attributed to the 1991–92 El Niño. *Nature, 373*(6511), 230-234. https://doi.org/10.1038/373230a0

Komugabe, A. F., Fallon, S. J., Thresher, R. E., & Eggins, S. M. (2014). Modern Tasman Sea surface reservoir ages from deep-sea black corals. *Deep Sea Research Part II: Topical Studies in Oceanography, 99*(Supplement C), 207-212. http://www.sciencedirect.com/science/article/pii/S0967064513002154

Komugabe-Dixson, A. F., Fallon, S. J., Eggins, S. M., & Thresher, R. E. (2016). Radiocarbon evidence for mid-late Holocene changes in southwest Pacific Ocean circulation. *Paleoceanography, 31*(7), 971-985. http://dx.doi.org/10.1002/2016PA002929

Legendre, L., & Rassoulzadegan, F. (1995). Plankton and nutrient dynamics in marine waters. *Ophelia, 41*(1), 153-172. https://doi.org/10.1080/00785236.1995.10422042

Lehodey, P., Alheit, J., Barange, M., Baumgartner, T., Beaugrand, G., Drinkwater, K., et al. (2006). Climate Variability, Fish, and Fisheries. *Journal of Climate, 19*(20), 5009-5030. https://doi.org/10.1175/JCLI3898.1

Levitus, S., Conkright, M. E., Reid, J. L., Najjar, R. G., & Mantyla, A. (1993). Distribution of nitrate, phosphate and silicate in the world oceans. *Progress in Oceanography, 31*(3), 245-273. http://www.sciencedirect.com/science/article/pii/007966119390003V

Lewandowska, A. M., Boyce, D. G., Hofmann, M., Matthiessen, B., Sommer, U., & Worm, B. (2014). Effects of sea surface warming on marine plankton. *Ecology Letters, 17*(5), 614-623. https://doi.org/10.1111/ele.12265

Linsley, B., Kaplan, A., Gouriou, Y., Salinger, J., deMenocal, P. B., Wellington, G. M., & Howe, S. S. (2006). Tracking the extent of the South Pacific Convergence Zone since the early 1600s. *Geochemistry, Geophysics, Geosystems, 7*(5), n/a-n/a. http://dx.doi.org/10.1029/2005GC001115

Linsley, B., Zhang, P., Kaplan, A., Howe, S., & M. Wellington, G. (2008). *Interdecadal-decadal climate variability from multicoral oxygen isotope records in the South Pacific Convergence Zone region since 1650 A.D* (Vol. 23).

Longhurst, A. R. (2010). *Ecological geography of the sea*: Elsevier.

Magozzi, S., Yool, A., Vander Zanden, H. B., Wunder, M. B., & Trueman, C. N. (2017). Using ocean models to predict spatial and temporal variation in marine carbon isotopes. *Ecosphere, 8*(5), e01763. https://doi.org/10.1002/ecs2.1763

Marr, J. P., Carter, L., Bostock, H. C., Bolton, A., & Smith, E. (2013). Southwest Pacific Ocean response to a warming world: Using Mg/Ca, Zn/Ca, and Mn/Ca in foraminifera to track surface ocean water masses during the last deglaciation. *Paleoceanography, 28*(2), 347-362. https://doi.org/10.1002/palo.20032

McGregor, V. (2020). *Extending process and understanding for the development of complex ecosystem models, with application to the Chatham Rise Atlantis model.* (Doctor of Philosophy), Victoria University of Wellington, Victoria University of Wellington.

McMahon, K., D McCarthy, M., Sherwood, O., Larsen, T., & P Guilderson, T. (2015). *Millennial-scale plankton regime shifts in the subtropical North Pacific Ocean* (Vol. 350).

McMahon, K., Hamady, L. L., & Thorrold, S. R. (2013). A review of ecogeochemistry approaches to estimating movements of marine animals. *Limnology and Oceanography, 58*(2), 697-714. https://doi.org/10.4319/lo.2013.58.2.0697

McMahon, K., & McCarthy, M. D. (2016). Embracing variability in amino acid δ15N fractionation: mechanisms, implications, and applications for trophic ecology. *Ecosphere, 7*(12), e01511. https://doi.org/10.1002/ecs2.1511

Menkes, C. E., Allain, V., Rodier, M., Gallois, F., Lebourges-Dhaussy, A., Hunt, B. P. V., et al. (2015). Seasonal oceanography from physics to micronekton in the south-west Pacific. *Deep Sea Research Part II: Topical Studies in Oceanography, 113*, 125-144. http://www.sciencedirect.com/science/article/pii/S0967064514003038

Moisander, P. H., Beinart, R. A., Hewson, I., White, A. E., Johnson, K. S., Carlson, C. A., et al. (2010). Unicellular Cyanobacterial Distributions Broaden the Oceanic N₂ Fixation Domain. *Science, 327*(5972), 1512. http://science.sciencemag.org/content/327/5972/1512.abstract

Mook, W. G., Bommerson, J. C., & Staverman, W. H. (1974). Carbon isotope fractionation between dissolved bicarbonate and gaseous carbon dioxide. *Earth and Planetary Science*

Letters, 22(2), 169-176. http://www.sciencedirect.com/science/article/pii/0012821X74900788

Moore, C. M., Mills, M. M., Arrigo, K. R., Berman-Frank, I., Bopp, L., Boyd, P. W., et al. (2013). Processes and patterns of oceanic nutrient limitation. *Nature Geoscience, 6*(9), 701-710. https://doi.org/10.1038/ngeo1765

Nodder, S. D., & Northcote, L. C. (2001). Episodic particulate fluxes at southern temperate mid-latitudes (42–45°S) in the Subtropical Front region, east of New Zealand. *Deep Sea Research Part I: Oceanographic Research Papers, 48*(3), 833-864. http://www.sciencedirect.com/science/article/pii/S0967063700000625

Paul, D., Skrzypek, G., & Fórizs, I. (2007). Normalization of measured stable isotopic compositions to isotope reference scales – a review. *Rapid Communications in Mass Spectrometry, 21*(18), 3006-3014. https://doi.org/10.1002/rcm.3185

Pinkerton, M. H. (2011). A balanced trophic model of the Chatham Rise, New Zealand. *Prepared for the Ministry for the Environment. Wellington: NIWA.*

Poloczanska, E., Babcock, R., Butler, A., Hobday, A., Hoegh-Guldberg, O., J. Kunz, T., et al. (2007). *Climate Change and Australian Marine Life* (Vol. 45).

Poloczanska, E., Brown, C. J., Sydeman, W. J., Kiessling, W., Schoeman, D. S., Moore, P. J., et al. (2013). Global imprint of climate change on marine life. *Nature Clim. Change, 3*(10), 919-925. Letter. http://dx.doi.org/10.1038/nclimate1958

Polovina, J. J., Howell, E. A., & Abecassis, M. (2008). Ocean's least productive waters are expanding. *Geophysical Research Letters, 35*(3). https://doi.org/10.1029/2007GL031745

Popp, B. N., Laws, E. A., Bidigare, R. R., Dore, J. E., Hanson, K. L., & Wakeham, S. G. (1998). Effect of Phytoplankton Cell Geometry on Carbon Isotopic Fractionation. *Geochimica et Cosmochimica Acta, 62*(1), 69-77. http://www.sciencedirect.com/science/article/pii/S0016703797003335

Prouty, N. G., Roark, E. B., Koenig, A. E., Demopoulos, A. W. J., Batista, F. C., Kocar, B. D., et al. (2014). Deep-sea coral record of human impact on watershed quality in the Mississippi River Basin. *Global Biogeochemical Cycles, 28*(1), 29-43. http://dx.doi.org/10.1002/2013GB004754

Rau, G. H., Ohman, M. D., & Pierrot-Bults, A. (2003). Linking nitrogen dynamics to climate variability off central California: a 51 year record based on 15N/14N in CalCOFI zooplankton. *Deep Sea Research Part II: Topical Studies in Oceanography, 50*(14), 2431-2447. http://www.sciencedirect.com/science/article/pii/S0967064503001280

Rau, G. H., Riebesell, U., & Wolf-Gladrow, D. (1996). A model of photosynthetic 13C fractionation by marine phytoplankton based on diffusive molecular CO2 uptake. *Marine Ecology Progress Series, 133*, 275-285.

Rau, G. H., Takahashi, T., & Des Marais, D. (1989). Latitudinal variations in plankton delta C-13 - Implications for CO2 and productivity in past oceans. *341*.

Rau, G. H., Takahashi, T., Des Marais, D. J., Repeta, D. J., & Martin, J. H. (1992). The relationship between δ13C of organic matter and [CO2(aq)] in ocean surface water: Data from a JGOFS site in the northeast Atlantic Ocean and a model. *Geochimica et*

Cosmochimica Acta, 56(3), 1413-1419. http://www.sciencedirect.com/science/article/pii/001670379290073R

Roark, E. B., Guilderson, T. P., Dunbar, R. B., Fallon, S. J., & Mucciarone, D. A. (2009). Extreme longevity in proteinaceous deep-sea corals. *Proceedings of the National Academy of Sciences, 106*(13), 5204-5208. http://www.pnas.org/content/106/13/5204.abstract

Rodionov, S. N. (2004). A sequential algorithm for testing climate regime shifts. *Geophysical Research Letters, 31*(9). https://doi.org/10.1029/2004GL019448

Roemmich, D., Gilson, J., Davis, R., Sutton, P., Wijffels, S., & Riser, S. (2007). Decadal Spinup of the South Pacific Subtropical Gyre. *Journal of Physical Oceanography, 37*(2), 162-173. http://journals.ametsoc.org/doi/abs/10.1175/JPO3004.1

Roemmich, D., Gilson, J., Sutton, P., & Zilberman, N. (2016). Multidecadal Change of the South Pacific Gyre Circulation. *Journal of Physical Oceanography, 46*(6), 1871-1883. https://doi.org/10.1175/JPO-D-15-0237.1

Rousseaux, C. S., & Gregg, W. W. (2015). Recent decadal trends in global phytoplankton composition. *Global Biogeochemical Cycles, 29*(10), 1674-1688. http://dx.doi.org/10.1002/2015GB005139

Sarmiento, J. L., & Gruber, N. (2006). *Ocean Biogeochemical Dynamics*: Princeton University Press.

Sarmiento, J. L., Gruber, N., Brzezinski, M. A., & Dunne, J. P. (2004). High-latitude controls of thermocline nutrients and low latitude biological productivity. *Nature, 427*(6969), 56-60. https://doi.org/10.1038/nature02127

Schiff, J. T., Batista, F. C., Sherwood, O. A., Guilderson, T. P., Hill, T. M., Ravelo, A. C., et al. (2014). Compound specific amino acid δ13C patterns in a deep-sea proteinaceous coral: Implications for reconstructing detailed δ13C records of exported primary production. *Marine Chemistry, 166*, 82-91. http://www.sciencedirect.com/science/article/pii/S030442031400156X

Sharma, P., Marinov, I., Cabre, A., Kostadinov, T., & Singh, A. (2019). Increasing Biomass in the Warm Oceans: Unexpected New Insights From SeaWiFS. *Geophysical Research Letters, 46*(7), 3900-3910. https://doi.org/10.1029/2018GL079684

Sherwood, O., & Edinger, E. (2009). *Ages and growth rates of some deep-sea gorgonian and antipatharian corals of Newfoundland and Labrador* (Vol. 66).

Sherwood, O., Guilderson, T. P., Batista, F. C., Schiff, J. T., & McCarthy, M. D. (2013). Increasing subtropical North Pacific Ocean nitrogen fixation since the Little Ice Age. *Nature, 505*, 78. http://dx.doi.org/10.1038/nature12784

Sherwood, O., Lehmann, M. F., Schubert, C. J., Scott, D. B., & McCarthy, M. D. (2011). Nutrient regime shift in the western North Atlantic indicated by compound-specific δ¹⁵N of deep-sea gorgonian corals. *Proceedings of the National Academy of Sciences, 108*(3), 1011. http://www.pnas.org/content/108/3/1011.abstract

Sigman, D. M., Karsh, K., & Casciotti, K. (2009). Ocean process tracers: nitrogen isotopes in the ocean.

Sohm, J. A., Webb, E. A., & Capone, D. G. (2011). Emerging patterns of marine nitrogen fixation. *Nature Reviews Microbiology, 9*(7), 499-508. https://doi.org/10.1038/nrmicro2594

Somes, C. J., Schmittner, A., Galbraith, E. D., Lehmann, M. F., Altabet, M. A., Montoya, J. P., et al. (2010). Simulating the global distribution of nitrogen isotopes in the ocean. *Global Biogeochemical Cycles, 24*(4).

Somes, C. J., Schmittner, A., Muglia, J., & Oschlies, A. (2017). A three-dimensional model of the marine nitrogen cycle during the last glacial maximum constrained by sedimentary isotopes. *Frontiers in Marine Science, 4*, 108.

Stevens, C. L., O'Callaghan, J. M., Chiswell, S. M., & Hadfield, M. G. (2019). Physical oceanography of New Zealand/Aotearoa shelf seas – a review. *New Zealand Journal of Marine and Freshwater Research*, 1-40. https://doi.org/10.1080/00288330.2019.1588746

Stramma, L., Peterson, R. G., & Tomczak, M. (1995). The South Pacific Current. *Journal of Physical Oceanography, 25*(1), 77-91. https://journals.ametsoc.org/doi/abs/10.1175/1520-0485%281995%29025%3C0077%3ATSPC%3E2.0.CO%3B2

Thackeray, S., Jones, I., & Maberly, S. (2008). Long-term change in the phenology of spring phytoplankton: species-specific responses to nutrient enrichment and climatic change. *Journal of Ecology, 96*(3), 523-535.

Trujillo, A. P., & Thurman, H. V. (2011). *Essentials of Oceanography*: Prentice Hall.

Ummenhofer, C. C., & England, M. H. (2007). Interannual Extremes in New Zealand Precipitation Linked to Modes of Southern Hemisphere Climate Variability. *Journal of Climate, 20*(21), 5418-5440. https://journals.ametsoc.org/doi/abs/10.1175/2007JCLI1430.1

Ummenhofer, C. C., Gupta, A. S., & England, M. H. (2009). Causes of Late Twentieth-Century Trends in New Zealand Precipitation. *Journal of Climate, 22*(1), 3-19. https://journals.ametsoc.org/doi/abs/10.1175/2008JCLI2323.1

Vokhshoori, N. L., & McCarthy, M. D. (2014). Compound-Specific δ15N Amino Acid Measurements in Littoral Mussels in the California Upwelling Ecosystem: A New Approach to Generating Baseline δ15N Isoscapes for Coastal Ecosystems. *PLOS ONE, 9*(6), e98087. https://doi.org/10.1371/journal.pone.0098087

Waite, A. M., Safi, K. A., Hall, J. A., & Nodder, S. D. (2000). Mass sedimentation of picoplankton embedded in organic aggregates. *Limnology and Oceanography, 45*(1), 87-97. https://doi.org/10.4319/lo.2000.45.1.0087

Weaver, P. P. E., Carter, L., & Neil, H. L. (1998). Response of surface water masses and circulation to Late Quaternary climate change east of New Zealand. *Paleoceanography, 13*(1), 70-83. https://doi.org/10.1029/97PA02982

Wiebe, R., & Gaddy, V. L. (1940). The Solubility of Carbon Dioxide in Water at Various Temperatures from 12 to 40° and at Pressures to 500 Atmospheres. Critical Phenomena*.

Journal of the American Chemical Society, 62(4), 815-817. https://doi.org/10.1021/ja01861a033

Winder, M., & Cloern, J. E. (2010). The annual cycles of phytoplankton biomass. *Philosophical transactions of the Royal Society of London. Series B, Biological sciences, 365*(1555), 3215-3226. https://pubmed.ncbi.nlm.nih.gov/20819814

https://www.ncbi.nlm.nih.gov/pmc/articles/PMC2981943/

Work, K. A., & Havens, K. E. (2003). Zooplankton grazing on bacteria and cyanobacteria in a eutrophic lake. *Journal of Plankton Research, 25*(10), 1301-1306. https://doi.org/10.1093/plankt/fbg092

Wu, L., Cai, W., Zhang, L., Nakamura, H., Timmermann, A., Joyce, T., et al. (2012). Enhanced warming over the global subtropical western boundary currents. *Nature Clim. Change, 2*(3), 161-166. 10.1038/nclimate1353. http://dx.doi.org/10.1038/nclimate1353

Yan, H., Sun, L., Wang, Y., Huang, W., Qiu, S., & Yang, C. (2011). A record of the Southern Oscillation Index for the past 2,000 years from precipitation proxies. *Nature Geoscience, 4*(9), 611-614. https://doi.org/10.1038/ngeo1231

Yang, H., Lohmann, G., Krebs-Kanzow, U., Ionita, M., Shi, X., Sidorenko, D., et al. (2020). Poleward Shift of the Major Ocean Gyres Detected in a Warming Climate. *Geophysical Research Letters, 47*(5), e2019GL085868. https://doi.org/10.1029/2019GL085868

York, D., Evensen, N. M., Martínez, M. L., & Delgado, J. D. B. (2004). Unified equations for the slope, intercept, and standard errors of the best straight line. *American Journal of Physics, 72*(3), 367-375. http://aapt.scitation.org/doi/abs/10.1119/1.1632486

Young, J. N., Bruggeman, J., Rickaby, R. E. M., Erez, J., & Conte, M. (2013). Evidence for changes in carbon isotopic fractionation by phytoplankton between 1960 and 2010. *Global Biogeochemical Cycles, 27*(2), 505-515. https://doi.org/10.1002/gbc.20045

4.11 Supplemental Figures:

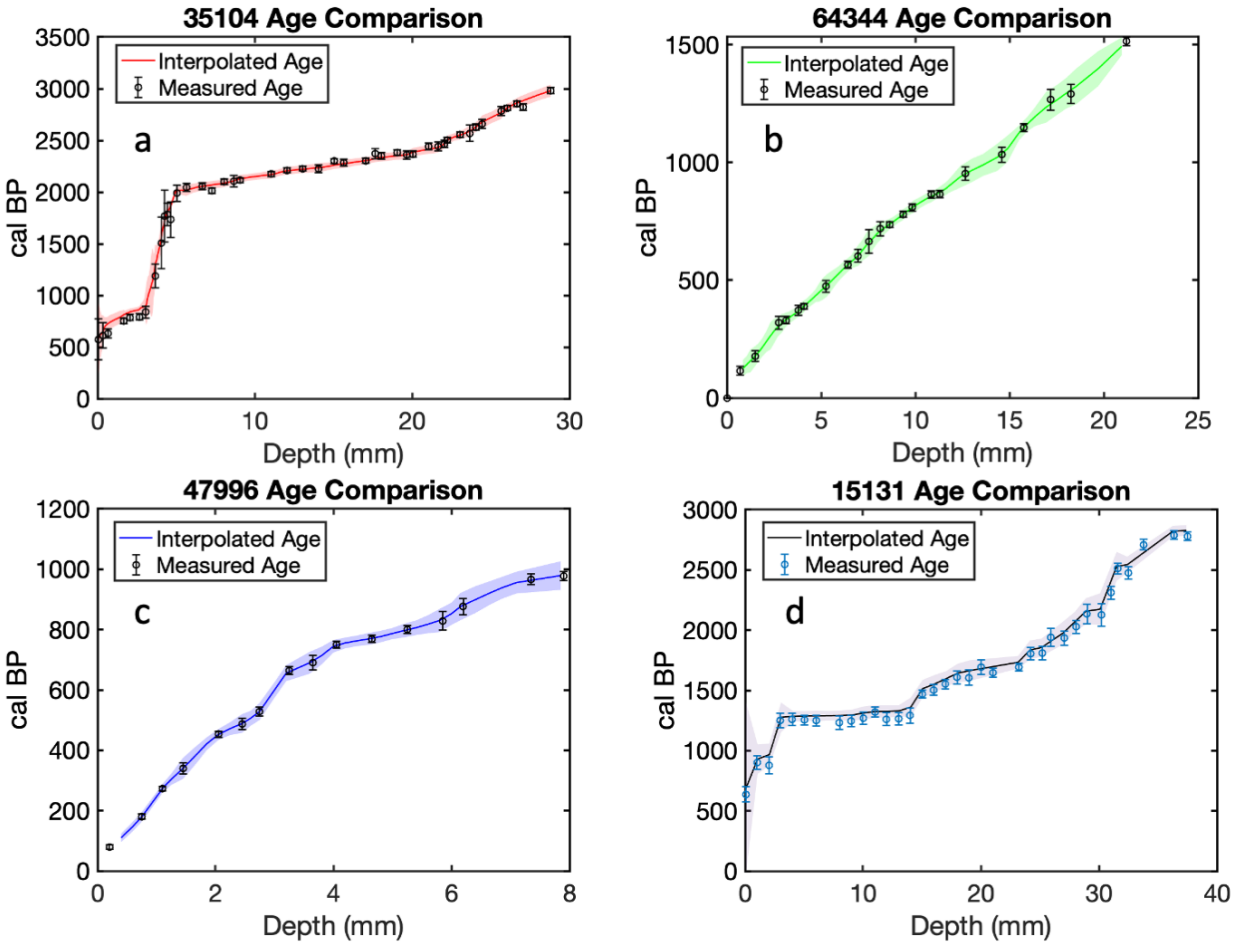

Supp. Fig. S4.1: Coral U-Th Age Models. Interpolated and initial Th corrected age comparisons. A comparison between initial Th corrected ages (symbols) and interpolated age models from COPRA (colored lines). All uncertainties shown are the 2**σ** uncertainty range. Depth progresses from the outer coral (0mm) to inner coral (e.g. 20mm).

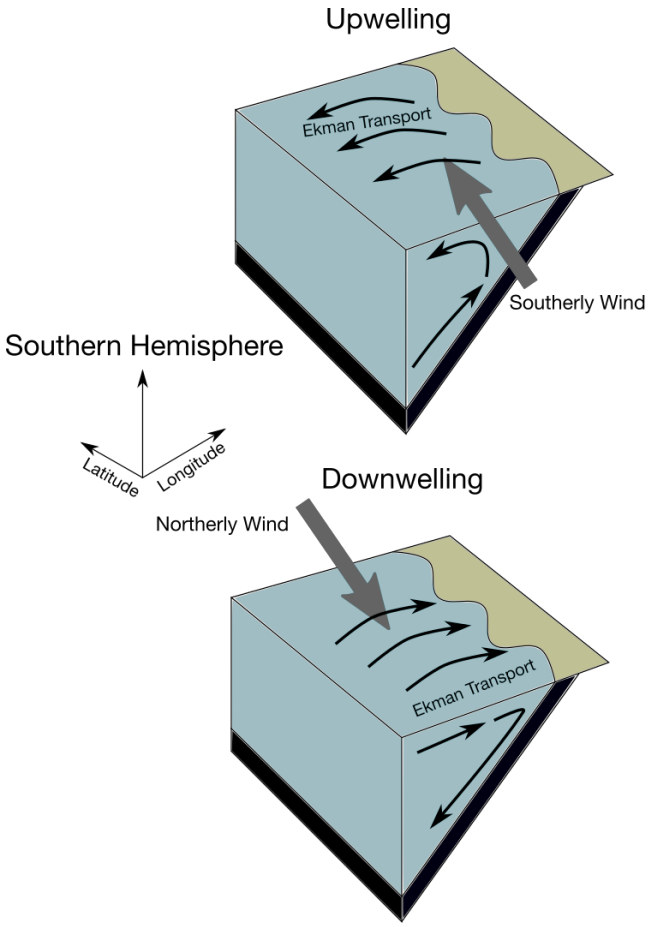

Supp. Fig. S4.2: Ekman transport and upwelling. Ekman transport an associated upwelling and downwelling from wind blown parallel to shore. Figure is modified from Sarmiento et al. (2006).

		ANU (n = 5)		NIWA (n = 54 (squid); n = 124 (Leucine))	
		$d^{13}C$	$d^{15}N$	$d^{13}C$	$d^{15}N$
Squid	Average	-17.82	13.09	-17.81	13.07
	Standard Dev.	0.17	0.32	0.18	0.12
Leucine	Average	-28.78	13.49	-28.78	13.51
	Standard Dev.	0.29	0.34	0.18	0.15

Supp. Fig. S4.3: Interlaboratory bulk $\delta^{13}C$ and $\delta^{15}N$ comparison. Bulk $\delta^{13}C$ and $\delta^{15}N$ values for the standards used at the ANU radiocarbon laboratory and the NIWA Ecological Stable Isotope Lab.

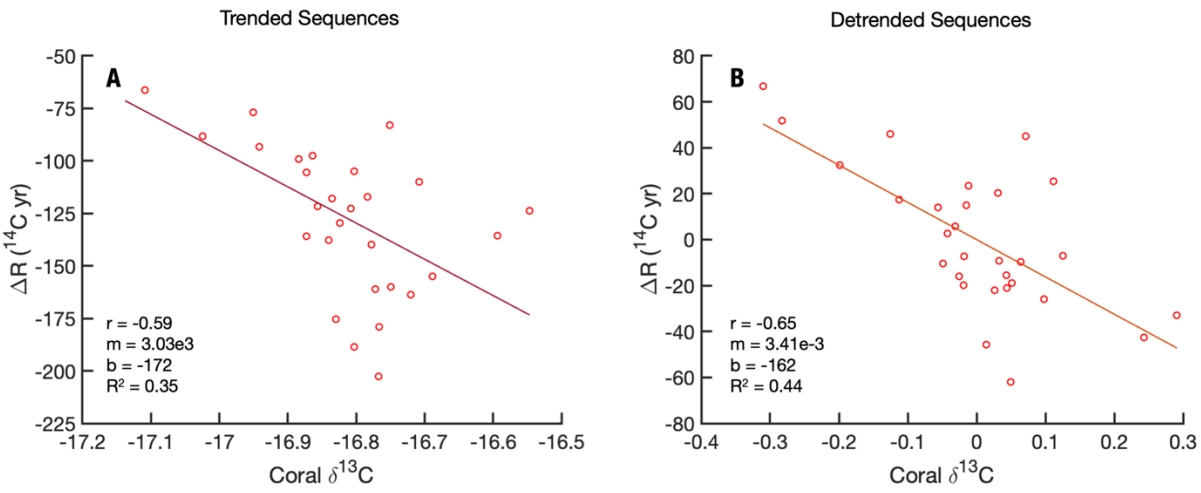

Supp. Fig. S4.4: A comparison of bulk $\delta^{13}C$ and the ΔR composite. 35104 bulk $\delta^{13}C$ and composite ΔR values. Panel A shows the trended 35104 bulk $\delta^{13}C$ and composite ΔR sequences. Panel B shows the detrended 35104 bulk $\delta^{13}C$ and composite ΔR sequences. The colored line in both panels is the least-squares linear fit, where m and b represent the slope and intercept for the equation $\Delta R = m * \delta^{13}C + b$, r indicates the correlation coefficient where $p < 0.001$ for r values reported in both panels.

Chapter 5

Conclusions, Further Research and Recommendations

5.1 Research Motivations:

The initial concept of using southwest Pacific black corals as a paleocirculation archive extends back to the pioneering work presented in Aimée Komugabe-Dixson's PhD thesis. She demonstrated for the first time that radiocarbon in black corals can precisely track ocean circulation changes. Her 4500-year long record of ocean circulation using Tasman Sea black corals provided evidence for an intensification of the South Pacific Gyre (SPG) over the 2000-3000BP period that appears to be similar to the gyre intensification observed during the late 20th century (Roemmich et al., 2007; Roemmich et al., 2016).

A thousand-year interval of stronger subtropical SPG circulation would significantly impact marine biogeochemistry and primary productivity in the southwest Pacific. In this region, ocean circulation appears to affect biogeochemical patterns by 1) changing the balance of macronutrient-rich subpolar and macronutrient-depleted subtropical waters and 2) altering vertical ocean stratification and nutrient recycling (See Chapter 1.3.2.2; Chapter 4.4.1; Sarmiento et al., 2004; Sarmiento et al., 2006; Chiswell et al., 2013; Ellwood et al., 2013; Moore et al., 2013; Chiswell et al., 2015; Sieber et al., 2019). If correct, then the 2000-3000BP interval may mirror biogeochemical changes seen over the last few decades in which ocean gyre changes (Roemmich et al., 2007; Wu et al., 2012; Hoegh-Guldberg et al., 2014; Roemmich et al., 2016) resulted in a decline in phytoplankton abundance in the mid to high latitudes (Gregg et al., 2003; Boyce et al., 2010; Rousseaux et al., 2015).

This hypothesis relies on two assumptions: 1) the Komugabe-Dixson radiocarbon record does indeed represent a strengthening of the SPG and not internal gyre variability (see Chapter 3.3.4); and 2) ocean gyre circulation is the dominant control on phytoplankton and nutrient distributions. However, as previously mentioned (See Chapter 1.3.3; Chapter 3.3.4), the Komugabe-Dixson radiocarbon record only represents one limb of the SPG - the EAC extension This region of the SPG exhibits considerable internal variability; the EAC extension can strengthen at the expense of other SPG currents (e.g. the Tasman Front) without a change to overall gyre strength (Hill et al., 2011; Ganachaud et al., 2014). The changes in the Komugabe-Dixson et al., 2016 radiocarbon record could have therefore resulted from internal gyre variability rather than a unilateral strengthening of the SPG.

Unfortunately, Komugabe-Dixson record is the only high resolution paleoceanographic record for the mid-latitude southwest Pacific over the last 3000 years and so their hypothesis remains untested. While other paleoceanographic records exist from the SW Pacific region, most are derived from sediment cores which span multiple millennia but are limited in resolution to centennial to multi-centennial timescales. More high-resolution paleoceanographic records are required to better constrain SPG dynamics over the late Holocene and ascertain if the SPG conditions over the 2000-3000BP period are analogous to those changes observed over the 20th century.

5.2 Project Summary:

The research presented in this thesis aimed to answer two overarching questions: 1) Did the SPG intensify unilaterally over the 2000-3000BP period? And if so, 2) What is the impact of a sustained gyre intensification on marine productivity, biogeochemistry and nutrient distributions in the southwest Pacific? To address these, I used a combination of radiocarbon reservoir age and stable carbon/nitrogen isotope proxies in black corals collected from the East Auckland Current, Subtropical Front and Central South Pacific Ocean. The decadal-timescale reconstructions of ocean circulation and biogeochemistry over the late Holocene are unique in the context of New Zealand's existing paleoceanographic reconstructions.

At the outset of the project, the age distribution of New Zealand's black corals was unknown. While there was no *a priori* reason to assume that these black corals would produce reconstructions of a lesser fidelity than that of the Tasman Sea corals, it was nonetheless important to establish the age and growth rates of the New Zealand specimens. This research was therefore divided into three separate, but synergistic, parts addressing the following questions:

1) What time periods could the black coral paleoceanographic reconstructions represent, and how does this influence the potential New Zealand's black corals have as a paleoceanographic proxy?
2) Was the millennium-long depression in southwest Pacific radiocarbon reservoir age observed by Komugabe-Dixson et al., 2016 driven by an acceleration of the SPG or internal gyre variability? If the radiocarbon reservoir age depression was driven by an SPG acceleration, what does this mean for the role of anthropogenic climate change in the 20th century gyre intensification?

3) What is the impact of SPG circulation variability on paleo productivity and nutrient distributions in the southwest Pacific?

These questions are addressed, respectively, in Chapters 2-4. A summary of the main conclusions of each follows in the next 3 sections:

5.2.1 Growth and Longevity of New Zealand Black Corals (Chapter 2)

New Zealand's black corals exhibit extreme longevity, with highly variable growth rates over their lifetime (Table 5.1; Chapter 2). Their lifespans typically last millennia and their radial skeletal expansions range from ~1-140um/yr. Black corals can therefore reconstruct high-frequency ocean changes over millennia since conventional computer-controlled micromilling techniques permit the extraction of decadal to multi-decadal proxy data. This is a significant advancement for New Zealand's paleoceanography community. To date, most all New Zealand paleoceonographic work has utilized sediment cores. These cores lack the resolution necessary to study decadal ocean changes due to slow accumulation and sediment bioturbation (Bostock et al., 2015; Bostock et al., 2019). Since black coral skeletons do not experience bioturbation, geochemical patterns in black coral skeletons can usually be interpreted with confidence (Chapters 2 & 3). Examples of the potential application of black corals for paleoceanography are demonstrated in Chapters 3 and 4.

Table 5.1: New Zealand's black coral lifespans and growth rates. Black coral lifespans and growth rates estimated from the radiocarbon dating results presented in Chapter 2.

Coral Genus	Lifespan (years)	Growth Rate (μm/yr)
Leiopathes .spp	2219 to 2614	1.4 to 40
Leiopathes secunda	1178 to 1604	5.5 to 17.1
Antipathella fiordensis	91 to 317	50 to 57
Antipathes	293	91 to 143

The slow growth and extreme longevity make New Zealand black coral communities highly susceptible to natural or anthropogenic disturbances (Hitt et al., 2020). Their preferred habitats are characterized by low energy and high stability compared to the surface ocean, and the corals have therefore evolved extremely slow growth and longevity (Hitt et al., 2020). Unfortunately, this means that coral communities will take a long time to recover from environmental disturbances such as deep-sea mining, commercial bottom trawling, landslides or earthquakes (Clark et al., 2006; Clark et al., 2010; M. R. Clark et al., 2019; Goode et al., 2020).

While New Zealand's black coral communities are not known to be immediately threatened with extinction, several studies demonstrate they have already experienced significant damage due to anthropogenic disturbances (Clark et al., 2006; Clark et al., 2010; M. R. Clark et al., 2019; Goode et al., 2020). If these disturbances recur on timescales that are short relative to the time it takes corals to grow to maturity, permanent degradation of the coral communities seems inevitable.

5.2.2 Highly Variable Late Holocene Southwest Pacific Gyre Strength (Chapter 3)

Analysis of marine radiocarbon reservoir ages in New Zealand's black corals revealed two distinct modes of variability in ocean circulation over the late Holocene: 1) multi-centennial gyre variations and 2) a millennium-long period of stronger gyre circulation (2000-3000BP). Both gyre modes correspond to changes in the Southern Annular Mode (SAM) and the mean state of the El Niño-Southern Oscillation (ENSO). This allows us to produce the first continuous multi-centennial to millennial record of coupled ocean-atmosphere variability for New Zealand over the late Holocene.

Multi-centennial variations in gyre strength correspond to variability in the SAM over the last 1000 years (Figure 5.1). SAM effectively modulates the strength and location of the westerly wind belt, which drives ocean circulation strength and mixed layer depth in the southwest Pacific (Cai et al., 2005; Cai, 2006; Roemmich et al., 2007; Roemmich et al., 2016). Periods when SAM is positive have stronger westerly winds that shift south. These conditions allow greater influx of subtropical waters due to diminished influences from subpolar water sources, enhance subtropical circulation around New Zealand and drive a decrease in radiocarbon reservoir age. The opposite is true for negative SAM conditions.

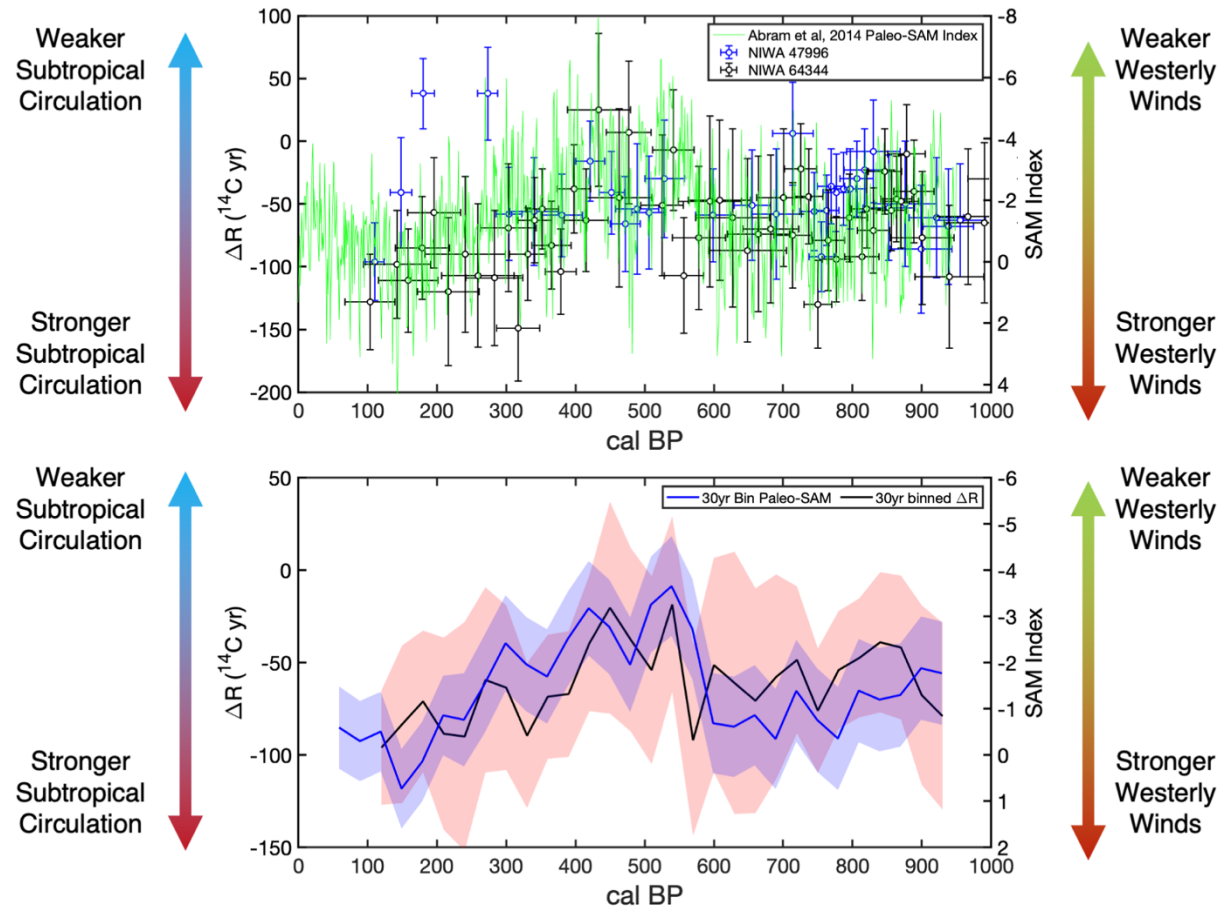

Figure 5.1: Evidence of coupled ocean-atmosphere circulation over the last millennium. Top Panel: A comparison of black coral ΔR values for the East Auckland Current (black) and Subtropical Front (blue) with the paleo-SAM index from Abram et al, 2014 (green). Bottom Panel: A comparison of 30yr binned ΔR (black line) alongside 30yr binned Paleo-SAM (blue shaded line) overlaid on top of the ΔR composite (grey points). Shaded areas are the 2**σ** uncertainty range and are calculated using the sum of squares method. The correlation between the timeseries is r = -0.48 ($p < 0.01$; n = 29).

Gyre circulation in the southwest Pacific is also affected by ENSO through its modulation of the position of the West Pacific salinity front (WPSF) (Delcroix et al., 1998). The WPSF acts as a barrier to the south equatorial current circulation in the western Pacific; however, during an El Niño event the front migrates north and facilitates stronger subtropical water flow into the southwest Pacific via the East Australian Current (Delcroix et al., 1998; Ganachaud et al., 2014; Komugabe-Dixson et al., 2016). The thousand year interval of stronger gyre circulation between 2000 and 3000BP corresponds to a period more El Niño-like conditions, with strong and abrupt ENSO events (Haug et al., 2001; Moy et al., 2002; Cobb et al., 2013; Emile-Geay et al., 2015; Chen et al., 2016; Barr et al., 2019). A change in the mean state of ENSO could change

the total flux of subtropical water into the southwest Pacific (Oliver et al., 2018) and produce a baseline shift in the radiocarbon reservoir age in the southwest Pacific.

The two modes of SPG circulation variability revealed by the reservoir age record presented in this thesis have implications for interpreting the recent 20th century acceleration of the SPG. Many studies have attributed the recent acceleration to anthropogenic climate change (Cai et al., 2005; Cai, 2006; Roemmich et al., 2007; Roemmich et al., 2016; Yang et al., 2020). However, this thesis demonstrates that the SPG exhibits natural variability on timescales that are comparable to those occurring in recent decades. This suggests that the recent gyre changes are not unprecedented over the last 3000 years, and periods of enhanced circulation can be driven by natural variability in atmospheric circulation (e.g. the SAM).

5.2.3 Reconstructing Southwest Pacific Ocean Biogeochemistry and Productivity Using Black Coral $\delta^{13}C$ and $\delta^{15}N$ (Chapter 4)

The analysis of coral $\delta^{13}C$ and $\delta^{15}N$ presented in this thesis yielded four main conclusions: 1) Multi-decadal to centennial cycles in coral $\delta^{13}C$ over the last 3000 years were likely driven by synchronous SST variations around New Zealand; 2) a millennium-long trend in coral $\delta^{13}C$ may indicate a shift towards larger and faster growing phytoplankton from 1500 to 100BP; 3) Multi-centennial cycles in the $\delta^{15}N$ of bioavailable nitrogen around New Zealand appear to be driven by similar-timescale oscillations in the atmospheric component of ENSO teleconnections to the NZ region, explained via the comparison with the paleo-Southern Oscillation Index (SOI); 4) A synchronous shift in ΔR, $\delta^{13}C$ and $\delta^{15}N$ that occurred sometime between 2000-2100BP, which implies a more intense *and* poleward-shifted SPG during the 2000-3000BP interval relative to the 0-2000BP interval.

Across the last millennium, $\delta^{13}C$ variations on decade-to-century timescales are positively correlated in corals from the EAuC and STF. This suggests that they respond to a common regional forcing. Assuming these cycles reflect changing $\delta^{13}C$ in phytoplankton, three possible mechanisms were considered: 1) changing $\delta^{13}C_{DIC}$ due to varying atmospheric CO_2; 2) SST changes; 3) changes in phytoplankton community structure (Rau et al., 1989a; Rau et al., 1992; McMahon et al., 2015; Magozzi et al., 2017; Glynn et al., 2019).

I dismiss atmospheric CO_2 changes as a driver of coral $\delta^{13}C$ variability over the last 1000 years since CO_2 variations were not large enough to elicit a significant response in phytoplankton

$\delta^{13}C$ (Rau et al., 1989b; Figge et al., 1995; Young et al., 2013; Magozzi et al., 2017). I consider phytoplankton community structure to be an unlikely driver of coral $\delta^{13}C$ variability since the EAuC and STF each have distinct and unique phytoplankton communities as a result of local environmental variables (e.g. SST, nutrient availability; see Chapter 4.7.1.1). This leaves SST variability as the most plausible explanation for the following reasons: 1) SST is the dominant control on the spatial distribution of POM $\delta^{13}C$ in the surface ocean (Goericke et al., 1994; Magozzi et al., 2017); 2) SSTs change unilaterally in both the EAuC and STF to climate forcing (Garner, 1959; Ummenhofer et al., 2007; Bowen et al., 2017); 3) the magnitude of coral $\delta^{13}C$ variations at both locations is within the range predicted from SST changes (Glynn et al., 2019); and 4) coral $\delta^{13}C$ variability is strongly correlated with the ΔR reconstruction over the 2000-3000BP interval.

EAuC coral $\delta^{13}C$ exhibits a 0.7‰ trend to higher values from 1500 to 100BP. This trend is too large to be driven by SST or changing $\delta^{13}C_{DIC}$, which therefore implies a shift in phytoplankton community structure towards larger and faster growing phytoplankton. Unfortunately, I cannot confirm this idea using the current coral $\delta^{13}C$ dataset; however, this will be the topic of future research using a compound-specific amino acid approach.

Across the last millennium, coral $\delta^{15}N$ records from the EAuC and STF appear to correlate with the mean state of the SOI as reconstructed from Yan et al. (2011). This synchronous response may be driven by SST and wind-driven upwelling changes. The SOI modulates SST patterns unilaterally around New Zealand in the EAuC and STF (Bowen et al., 2017). Circulation patterns associated with a positive SOI state cause warm SST anomalies in the EAuC, which may promote nitrogen fixation and drive EAuC coral $\delta^{15}N$ to values closer to 0‰. At the same time, atmospheric circulation patterns that are linked to both positive and negative SOI contributes to changes in wind direction across New Zealand. Positive SOI conditions provoke a more northeasterly wind flow along the eastern New Zealand coast (Ummenhofer et al., 2007; Ummenhofer et al., 2009), which may reduce coastal upwelling in the STF (Sarmiento et al., 2006; Trujillo et al., 2011). Consequently, this may reduce the supply of bioavailable nitrogen to the surface ocean and increase STF coral $\delta^{15}N$ (Sarmiento et al., 2006; see Section 4.7.2.3).

Perhaps the most novel result presented in this thesis is the identification of a period of a stronger and expanded western SPG between 2000-3000BP interval. In Chapter 4.7.3, multiple paleoceanographic proxies (ΔR, $\delta^{13}C$, and $\delta^{15}N$) are used to track the strength and latitudinal extent of the gyre. Coral ΔR values are more negative during the 2000-3000BP interval than in the 0-2000BP interval. This implies an increase in the southern advection of the ^{14}C rich waters from the equatorial western pacific due to a period of stronger western SPG circulation during the 2000-3000BP interval (Komugabe-Dixson et al., 2016). ^{14}C follows a meridional and along-gyre gradient that mirrors the gyre circulation (Fig 4.8H; Key et al., 2004). The more negative ΔR values over the 2000-3000BP could therefore indicate that the southwestern portion of the SPG either 1) experienced an expansion outward towards the pole; 2) exhibited stronger western boundary currents (e.g. the EAC) or 3) both.

Resolving the contribution of these three possible dynamics over the 2000-3000BP period requires another set of paleoceanographic proxies that vary spatially in either an along gyre or meridional gradient. POM $\delta^{13}C$ and $\delta^{15}N$ are ideal for this test as they vary in either an along-gyre or meridional fashion. POM $\delta^{13}C$ patterns in the SPG exhibit an along-gyre gradient since they primarily result from SST patterns across the gyre (Magozzi et al., 2017; Fig. 4.8F), while POM $\delta^{15}N$ patterns are primarily latitudinal and do not vary along the edge of the gyre (Fig. 4.8G) since they arise from patterns of nitrogen fixation or bioavailable nitrogen (Somes et al., 2017). Nitrogen fixation in the SPG is largely controlled by atmospheric iron deposition, and bioavailable nitrogen (e.g. NO_3^-) varies by ocean current (Somes et al., 2017). Both of these features vary latitudinally, and so POM $\delta^{15}N$ patterns vary in a north-south fashion across the SPG.

A change in western SPG circulation or current location would therefore extend to POM $\delta^{13}C$ and $\delta^{15}N$ patterns in the SPG. Central-south gyre waters are characterized by a more positive $\delta^{15}N$ (Somes et al., 2010; Somes et al., 2017), while SST gradients cause $\delta^{13}C$ to be higher in subtropical SPG currents (Goericke et al., 1994; Magozzi et al., 2017). Mean $\delta^{13}C$ were more positive during the 2000-3000BP interval than in the 0-2000BP interval, which implies stronger western subtropical currents over the 2000-3000BP interval. Mean $\delta^{15}N$ values were also more positive during the 2000-3000BP interval than in the 0-2000BP interval, which is consistent with a southward expansion of central gyre waters.

If the western SPG had *either* intensified *or* expanded then only POM mean $\delta^{13}C$ *or* $\delta^{15}N$ values would exhibit a baseline shift synchronous with the ΔR data; however, ΔR, $\delta^{13}C$ and $\delta^{15}N$ all exhibit a concurrent baseline shift ca. 1900BP. This implies a change in the shape and intensity of the western SPG over the late Holocene where the western boundary currents were stronger and expanded outwards over the 2000-3000P period.

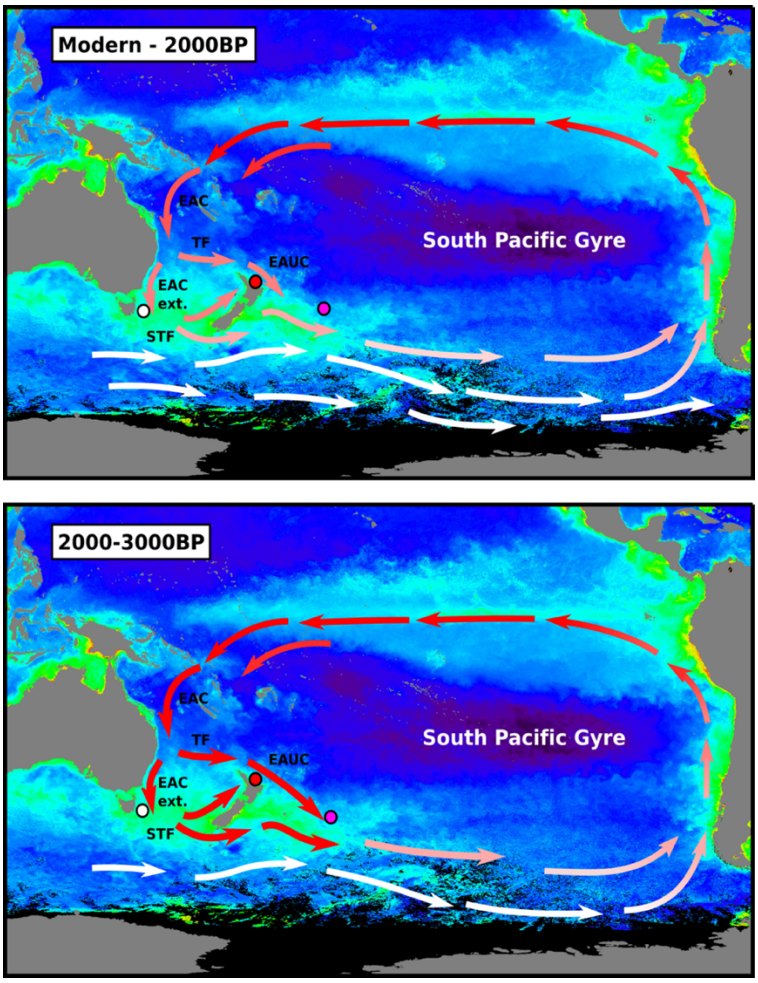

Figure 5.2: A schematic of the change in western SPG circulation and biogeochemical patterns during the late Holocene. Top Panel: The modern South Pacific Gyre circulation with subtropical currents (red), temperature currents (red-white) and polar currents (white). Curents are overlaid ontop of chl-a data (NASA MODIS). The locations of the coral locations are shown in dots (red – coral 35104; magenta – coral 15131; white – Komugabe-Dixson et al 2016 records). Bottom Panel: The hypothesized western South Pacific Gyre circulation over the 2000-3000BP interval. Subtropical currents (red), temperature currents (red-white) and polar currents (white) are overlaid ontop of chl-a data (NASA MODIS). The locations of the coral locations are shown in dots (red – coral 35104; magenta – coral 15131; white – Komugabe-Dixson et al 2016 records). Note the increase in arrow size and change in color for currents around New Zealand.

These results accord with those of Komugabe-Dixson et al., 2016, who observed a depression in ΔR between 2000-3000BP. They interpreted this as a period of stronger western

SPG circulation driven by a change in ENSO mean state and variability over this interval (Komugabe-Dixson et al., 2016; and references therein). Not only do our ΔR records accord with those data, our stable isotope data shows that the 2000-3000BP interval was also characterized by a change in POM $\delta^{13}C$ and $\delta^{15}N$ patterns. This implies that there is a coupling between SPG circulation and biogeochemistry in the Southwest Pacific on millennial timescales.

A coupling between SPG circulation and biogeochemistry has been observed on seasonal, orbital and glacial-interglacial timescales (Bostock et al., 2015; Lorrey et al., 2017; Bostock et al., 2019); however, this thesis research has shown that this coupling extends to millennial timescales as well. I have shown that synchronous changes in black coral ΔR, $\delta^{13}C$ and $\delta^{15}N$ reflect the strength of western SPG boundary currents and biogeochemical patterns in the southwest Pacific on millennial timescales. This coupling may be similar to the modern observations of increasing gyre strength, changing macronutrient distributions and declining primary productivity during the 20th century. SPG conditions between 2000-3000BP resemble those observed since the late 1980s (Cai et al., 2005; Behrenfeld et al., 2006; Cai, 2006; Polovina et al., 2008; Moore et al., 2013; Poloczanska et al., 2013; Poloczanska et al., 2016; Roemmich et al., 2016), which implies this period might be an important analogue for gyre conditions over recent and upcoming decades.

5.3 Future Contributions, Directions and Recommendations:

5.3.1 Resolving Contributions to $\delta^{13}C$ Variability

In Chapter 4, I speculate that $\delta^{13}C$ co-variations in the EAuC and STF over the last millennium are driven by changes to $\delta^{13}C$ at the base of the food web forced *via* synchronous regional variations in SST around New Zealand. I also show that EAuC coral $\delta^{13}C$ has been trending towards more positive $\delta^{13}C$ values at present, which may result from a shift towards larger, faster growing phytoplankton in the EAuC.

Both ideas will be tested in the future by measuring the carbon isotope composition of individual amino acids in the coral skeletons. This will allow us to identify the contribution of different factors to coral $\delta^{13}C$ changes (e.g. SST, $\delta^{13}C_{DIC}$, taxon-specific $\delta^{13}C$ fractionation factors; McMahon et al., 2015). It will also allow us to reconstruct the percentages of N_2-fixing

cyanobacteria, non N_2-fixing cyanobacteria and eukaryotic microalgae over the last 1500 years using a stable isotope Bayesian mixing model (McMahon et al., 2015).

5.3.2 Resolving Contributions to $\delta^{15}N$ Variability

One of the main findings of this work is that changes in the mean state of Pacific interannual variability (e.g. ENSO) may have driven nitrogen fixation and upwelling rates over the last millennium. This conclusion is drawn from the antiphased relationship between coral $\delta^{15}N$ in the EAuC and STF on multi-centennial timescales. It is assumed that these coral $\delta^{15}N$ variations are driven by changes in the isotope composition of bioavailable nitrogen at the base of the food chain (see Chapter 4.7.2). However, I cannot rule out trophic level or food web dynamics as an influence on coral $\delta^{15}N$ variability. This will be tested by measuring the nitrogen isotope composition of individual amino acids in coral skeletons which allows separation of trophic level and nitrogen-source influences on $\delta^{15}N$ variability in the corals (Sherwood et al., 2011; Sherwood et al., 2013).

The effect of ENSO and south Pacific circulation on bioavailable $\delta^{15}N$ around New Zealand will also be tested using new $\delta^{15}N$-enabled climate-ecosystem models (specifically the UVic Earth System Climate Model 2.9 equipped with the 2N2PZD ecosystem model; Weaver et al., 2001; Somes et al., 2010; Somes et al., 2017). I plan to hindcast the model over the last 30 years and isolate periods of positive and negative SOI phases and analyze the forced response on sea surface temperatures variations, upwelling rates, and bioavailable nitrogen and POM $\delta^{15}N$ patterns.

5.3.3 Interdisciplinary Contributions

The radiocarbon reservoir age records in this thesis will be a particularly useful tool for archaeology, geochronological dating techniques and paleoclimatology. The resolution of the radiocarbon record is sufficient to assist in constraining radiocarbon dating curves and increase dating accuracy over the last 3000 years. More importantly, the ΔR records demonstrate that ΔR is highly variable across the southwest Pacific across the late Holocene, which is a new and emerging field of paleo research (Komugabe-Dixson et al., 2016; Alves et al., 2018).

The ΔR records presented in this thesis are a valuable resource for several scientific disciplines, such as the Quaternary archaeological and paleoclimate research communities, which employ radiocarbon dating to develop paleoclimate chronologies and study human and

ecological migrations (Petchey et al., 2020). The paired U-Th and radiocarbon measurements can be used in future studies to assist in the development of regional marine radiocarbon calibration curves which is likely the next step in improving radiocarbon dating accuracy (Jocelyn Turnbull pers. comm.). Increasing the accuracy of radiocarbon dating has several important geographic applications, such as improving the dating of earthquake and tsunami events (K. Clark et al., 2019) and precisely tracking the Polynesian migration (Petchey et al., 2020).

From a geochemical perspective, these records may assist in developing the community understanding of regional processes of coupled ocean-atmosphere circulation and biogeochemical cycles (Alves et al., 2018; Jocelyn Turnbull pers. comm.; Erik Behrens pers. comm.). As show in this thesis, marine radiocarbon concentrations and deviations are intimately connected to local ocean-atmospheric processes and so these records can be used in conjunction with ocean-atmospheric models to elucidate physical dynamical relationships between the ocean and atmosphere (Jocelyn Turnbull pers. comm.; Erik Behrens pers. comm.). This may improve our understanding of biogeochemical cycling (e.g. the carbon cycle), a field of research which employs radiocarbon as a geochemical tracer (Alves et al., 2018).

5.3.4 A Call for Black Coral Based Paleoceanographic Records

The mid-late Holocene is widely considered the best climate analog to the present climate and is therefore a reference for future anthropogenic climate changes (McGregor et al., 2015; Neukom et al., 2019). However, to date, New Zealand's palaeoceanographic history has been mostly derived from sediment cores that are better suited to study the early Holocene, LGM and beyond (e.g. Neil et al., 2004; Bostock et al., 2015). This biases New Zealand's paleoceanographic records leaving the recent past relatively understudied. This thesis has demonstrated the great potential for New Zealand black corals to address this lack of recent records. Moreover, black corals are the only paleoceanographic archives for the region capable of reconstructing high-enough resolution climate and ocean changes over long periods (greater than a millennium) on anthropogenically-relevant timescales (e.g. decadal to multi-decadal). Other archives, such as bivalves, mollusks, and rhodoliths, can provide information on centennial to multicentennial scales; however, these reconstructions may be only span several centuries (Reynolds et al., 2018) and could be discontinuous . Black corals can provide records with a similar temporal resolution, but also span millennia and therefore better constrain ocean dyamics on similar timescales.

Black corals are found in nearly all of the water masses surrounding New Zealand and are therefore suitable for reconstructing variability in productivity and circulation in both time *and* space. They hold significant potential for reconstructing a baseline of natural decadal to millennial ocean changes. This may assist ocean modeling efforts which attempt to project future changes in ocean circulation, marine biogeochemistry and primary production. It is therefore recommended that the New Zealand paleoceanographic community consider the use of black corals, where available in existing collections, to reconstruct baselines of past ocean variability. Currently, a team of NIWA and VUW scientists are using the work presented in this thesis as a 'proof of concept' to study high-frequency baseline ocean variability over the last 300 years.

One of the most attractive characteristics of the black coral paleoceanographic archive is the ability to reconstruct two geochemical proxy records (radiocarbon and stable isotopes) from single coral samples. This affords reconstruction of past changes in ocean circulation, marine biogeochemistry, phytoplankton variability and paleo-nutrient distributions. These oceanographic properties often work in tandem; ocean circulation indirectly controls the distribution of nutrients in the ocean and therefore dominates the spatial distribution of marine productivity (Sarmiento et al., 2006; Somes et al., 2010; Trujillo et al., 2011). Combining the radiocarbon and stable isotope proxies can therefore aid in interpreting paleoceanographic data in areas where marine biogeochemistry and primary production is tied to ocean circulation. However, most reconstructions using proteinaceous corals focus on either radiocarbon (Komugabe-Dixson et al., 2016) or stable isotopes (e.g. Sherwood et al. 2011; Sherwood et al. 2013; McMahon et al. 2015; Glynn et al. 2019). To my knowledge, there are no concurrent records of coral radiocarbon and stable isotopes constructed from a single coral other than those presented in this thesis. It is therefore recommended that – where financially viable – it becomes standard practice to measure radiocarbon, U-Th and stable isotopes in single coral samples. At the very least, if only one of these proxies is measured, it might be wise to collect and archive enough sample material to run the full suite of geochemical measurements at a later date. This thesis therefore recommends a framework and methodology that is on the cutting edge of deep-sea coral paleoceanography.

5.4 References:

Alves, E. Q., Macario, K., Ascough, P., & Bronk Ramsey, C. (2018). The Worldwide Marine Radiocarbon Reservoir Effect: Definitions, Mechanisms, and Prospects. *Reviews of Geophysics, 56*(1), 278-305. https://doi.org/10.1002/2017RG000588

Barr, C., Tibby, J., Leng, M. J., Tyler, J. J., Henderson, A. C. G., Overpeck, J. T., et al. (2019). Holocene El Niño–Southern Oscillation variability reflected in subtropical Australian precipitation. *Scientific Reports, 9*(1), 1627. https://doi.org/10.1038/s41598-019-38626-3

Behrenfeld, M. J., O'Malley, R. T., Siegel, D. A., McClain, C. R., Sarmiento, J. L., Feldman, G. C., et al. (2006). Climate-driven trends in contemporary ocean productivity. *Nature, 444*(7120), 752-755. https://doi.org/10.1038/nature05317

Bostock, H. C., Hayward, B. W., Neil, H. L., Sabaa, A. T., & Scott, G. H. (2015). Changes in the position of the Subtropical Front south of New Zealand since the last glacial period. *Paleoceanography, 30*(7), 824-844. http://dx.doi.org/10.1002/2014PA002652

Bostock, H. C., Prebble, J. G., Cortese, G., Hayward, B., Calvo, E., Quirós-Collazos, L., et al. (2019). Paleoproductivity in the SW Pacific Ocean During the Early Holocene Climatic Optimum. *Paleoceanography and Paleoclimatology, 34*(4), 580-599. https://doi.org/10.1029/2019PA003574

Bowen, M., Markham, J., Sutton, P., Zhang, X., Wu, Q., Shears, N. T., & Fernandez, D. (2017). Interannual Variability of Sea Surface Temperature in the Southwest Pacific and the Role of Ocean Dynamics. *Journal of Climate, 30*(18), 7481-7492. https://journals.ametsoc.org/doi/abs/10.1175/JCLI-D-16-0852.1

Boyce, D. G., Lewis, M. R., & Worm, B. (2010). Global phytoplankton decline over the past century. *Nature, 466*, 591. Article. https://doi.org/10.1038/nature09268

Cai, W. (2006). Antarctic ozone depletion causes an intensification of the Southern Ocean super-gyre circulation. *Geophysical Research Letters, 33*(3), n/a-n/a. http://dx.doi.org/10.1029/2005GL024911

Cai, W., Shi, G., Cowan, T., Bi, D., & Ribbe, J. (2005). The response of the Southern Annular Mode, the East Australian Current, and the southern mid-latitude ocean circulation to global warming. *Geophysical Research Letters, 32*(23), n/a-n/a. http://dx.doi.org/10.1029/2005GL024701

Chen, S., Hoffmann, S. S., Lund, D. C., Cobb, K. M., Emile-Geay, J., & Adkins, J. F. (2016). A high-resolution speleothem record of western equatorial Pacific rainfall: Implications for Holocene ENSO evolution. *Earth and Planetary Science Letters, 442*, 61-71. http://www.sciencedirect.com/science/article/pii/S0012821X16300759

Chiswell, S. M., Bostock, H. C., Sutton, P. J. H., & Williams, M. J. M. (2015). Physical oceanography of the deep seas around New Zealand: a review. *New Zealand Journal of Marine and Freshwater Research, 49*(2), 286-317. https://doi.org/10.1080/00288330.2014.992918

Chiswell, S. M., Bradford-Grieve, J., Hadfield, M. G., & Kennan, S. C. (2013). Climatology of surface chlorophyll a, autumn-winter and spring blooms in the southwest Pacific Ocean.

Journal of Geophysical Research: Oceans, 118(2), 1003-1018. https://doi.org/10.1002/jgrc.20088

Clark, K., Howarth, J., Litchfield, N., Cochran, U., Turnbull, J., Dowling, L., et al. (2019). Geological evidence for past large earthquakes and tsunamis along the Hikurangi subduction margin, New Zealand. *Marine Geology, 412*, 139-172. http://www.sciencedirect.com/science/article/pii/S0025322718304511

Clark, M. R., Bowden, D. A., Baird, S. J., & Stewart, R. (2010). *Effects of fishing on the benthic biodiversity of seamounts of the 'Graveyard' complex, northern Chatham Rise* (Vol. 46).

Clark, M. R., Bowden, D. A., Rowden, A. A., & Stewart, R. (2019). Little Evidence of Benthic Community Resilience to Bottom Trawling on Seamounts After 15 Years. *Frontiers in Marine Science, 6*(63). Original Research. https://www.frontiersin.org/article/10.3389/fmars.2019.00063

Clark, M. R., Tittensor, D., Rogers, A. D., Brewin, P., Schlacher, T., Rowden, A., et al. (2006). Seamounts, deep-sea corals and fisheries: vulnerability of deep-sea corals to fishing on seamounts beyond areas of national jurisdiction. In: UNEP-WCMC.

Cobb, K., Westphal, N., Sayani, H., Watson, J., Di Lorenzo, E., Cheng, H., et al. (2013). Highly Variable El Nino-Southern Oscillation Throughout the Holocene. *Science, 339*, 67-70.

Delcroix, T., & Picaut, J. (1998). Zonal displacement of the western equatorial Pacific "fresh pool". *Journal of Geophysical Research: Oceans, 103*(C1), 1087-1098. http://dx.doi.org/10.1029/97JC01912

Ellwood, M. J., Law, C. S., Hall, J., Woodward, E. M. S., Strzepek, R., Kuparinen, J., et al. (2013). Relationships between nutrient stocks and inventories and phytoplankton physiological status along an oligotrophic meridional transect in the Tasman Sea. *Deep Sea Research Part I: Oceanographic Research Papers, 72*, 102-120. http://www.sciencedirect.com/science/article/pii/S0967063712002087

Emile-Geay, J., Cobb, K., Carré, M., Braconnot, P., Leloup, J., Zhou, Y., et al. (2015). Links between tropical Pacific seasonal, interannual and orbital variability during the Holocene. *Nature Geoscience, 9*.

Figge, R. A., & White, J. W. C. (1995). High-resolution holocene and late glacial atmospheric CO2 record: variability tied to changes in thermohaline circulation. *Global Biogeochemical Cycles, 9*(3), 391-403. http://dx.doi.org/10.1029/95GB01458

Ganachaud, A., Cravatte, S., Melet, A., Schiller, A., Holbrook, N. J., Sloyan, B. M., et al. (2014). The Southwest Pacific Ocean circulation and climate experiment (SPICE). *Journal of Geophysical Research-Oceans, 119*(11), 7660-7686. <Go to ISI>://WOS:000346102900017

Garner, D. M. (1959). The sub-tropical convergence in New Zealand surface waters. *New Zealand Journal of Geology and Geophysics, 2*(2), 315-337. https://doi.org/10.1080/00288306.1959.10417650

Glynn, D. S., McMahon, K. W., Guilderson, T. P., & McCarthy, M. D. (2019). Major shifts in nutrient and phytoplankton dynamics in the North Pacific Subtropical Gyre over the last 5000 years revealed by high-resolution proteinaceous deep-sea coral δ15N and δ13C

records. *Earth and Planetary Science Letters, 515*, 145-153. http://www.sciencedirect.com/science/article/pii/S0012821X19301621

Goericke, R., & Fry, B. (1994). Variations of marine plankton δ13C with latitude, temperature, and dissolved CO2 in the world ocean. *Global Biogeochemical Cycles, 8*(1), 85-90. https://doi.org/10.1029/93GB03272

Goode, S. L., Rowden, A. A., Bowden, D. A., & Clark, M. R. (2020). Resilience of seamount benthic communities to trawling disturbance. *Marine Environmental Research*, 105086. http://www.sciencedirect.com/science/article/pii/S0141113620303391

Gregg, W. W., Conkright, M. E., Ginoux, P., O'Reilly, J. E., & Casey, N. W. (2003). Ocean primary production and climate: Global decadal changes. *Geophysical Research Letters, 30*(15), n/a-n/a. http://dx.doi.org/10.1029/2003GL016889

Haug, G. H., Hughen, K. A., Sigman, D. M., Peterson, L. C., & Röhl, U. (2001). Southward Migration of the Intertropical Convergence Zone Through the Holocene. *Science, 293*(5533), 1304. http://science.sciencemag.org/content/293/5533/1304.abstract

Hill, K. L., Rintoul, S. R., Ridgway, K. R., & Oke, P. R. (2011). Decadal changes in the South Pacific western boundary current system revealed in observations and ocean state estimates. *Journal of Geophysical Research: Oceans, 116*(C1), n/a-n/a. http://dx.doi.org/10.1029/2009JC005926

Hitt, N. T., Sinclair, D. J., Fallon, S. J., Neil, H. L., Tracey, D. M., Komugabe-Dixson, A., & Marriott, P. (2020). Growth and longevity of New Zealand black corals. *Deep Sea Research Part I: Oceanographic Research Papers*, 103298. http://www.sciencedirect.com/science/article/pii/S0967063720300868

Hoegh-Guldberg, O., Cai, R., Poloczanska, E. S., Brewer, P. G., Sundby, S., Hilmi, K., et al. (2014). *The Ocean*. Retrieved from Cambridge, United Kingdom and New York, NY, USA:

Komugabe-Dixson, A. F., Fallon, S. J., Eggins, S. M., & Thresher, R. E. (2016). Radiocarbon evidence for mid-late Holocene changes in southwest Pacific Ocean circulation. *Paleoceanography, 31*(7), 971-985. http://dx.doi.org/10.1002/2016PA002929

Lorrey, A., & Bostock, H. (2017). The Climate of New Zealand Through the Quaternary. In (pp. 67-139).

Magozzi, S., Yool, A., Vander Zanden, H. B., Wunder, M. B., & Trueman, C. N. (2017). Using ocean models to predict spatial and temporal variation in marine carbon isotopes. *Ecosphere, 8*(5), e01763. https://doi.org/10.1002/ecs2.1763

McGregor, H. V., Evans, M. N., Goosse, H., Leduc, G., Martrat, B., Addison, J. A., et al. (2015). Robust global ocean cooling trend for the pre-industrial Common Era. *Nature Geoscience, 8*(9), 671-677. https://doi.org/10.1038/ngeo2510

McMahon, K., D McCarthy, M., Sherwood, O., Larsen, T., & P Guilderson, T. (2015). *Millennial-scale plankton regime shifts in the subtropical North Pacific Ocean* (Vol. 350).

Moore, C. M., Mills, M. M., Arrigo, K. R., Berman-Frank, I., Bopp, L., Boyd, P. W., et al. (2013). Processes and patterns of oceanic nutrient limitation. *Nature Geoscience, 6*(9), 701-710. https://doi.org/10.1038/ngeo1765

Moy, C. M., Seltzer, G. O., Rodbell, D. T., & Anderson, D. M. (2002). Variability of El Niño/Southern Oscillation activity at millennial timescales during the Holocene epoch. *Nature, 420*(6912), 162-165. https://doi.org/10.1038/nature01194

Neil, H. L., Carter, L., & Morris, M. Y. (2004). Thermal isolation of Campbell Plateau, New Zealand, by the Antarctic Circumpolar Current over the past 130 kyr. *Paleoceanography, 19*(4), n/a-n/a. http://dx.doi.org/10.1029/2003PA000975

Neukom, R., Barboza, L. A., Erb, M. P., Shi, F., Emile-Geay, J., Evans, M. N., et al. (2019). Consistent multidecadal variability in global temperature reconstructions and simulations over the Common Era. *Nature Geoscience, 12*(8), 643-649. https://doi.org/10.1038/s41561-019-0400-0

Oliver, E. C. J., & Holbrook, N. J. (2018). Variability and Long-Term Trends in the Shelf Circulation Off Eastern Tasmania. *Journal of Geophysical Research: Oceans, 123*(10), 7366-7381. https://doi.org/10.1029/2018JC013994

Petchey, F., & Schmid, M. M. E. (2020). Vital evidence: Change in the marine 14C reservoir around New Zealand (Aotearoa) and implications for the timing of Polynesian settlement. *Scientific Reports, 10*(1), 14266. https://doi.org/10.1038/s41598-020-70227-3

Poloczanska, E., Brown, C. J., Sydeman, W. J., Kiessling, W., Schoeman, D. S., Moore, P. J., et al. (2013). Global imprint of climate change on marine life. *Nature Clim. Change, 3*(10), 919-925. Letter. http://dx.doi.org/10.1038/nclimate1958

Poloczanska, E., Burrows, M. T., Brown, C. J., García Molinos, J., Halpern, B. S., Hoegh-Guldberg, O., et al. (2016). Responses of Marine Organisms to Climate Change across Oceans. *Frontiers in Marine Science, 3*(62). Review. https://www.frontiersin.org/article/10.3389/fmars.2016.00062

Polovina, J. J., Howell, E. A., & Abecassis, M. (2008). Ocean's least productive waters are expanding. *Geophysical Research Letters, 35*(3). https://doi.org/10.1029/2007GL031745

Rau, G. H., Takahashi, T., & Des Marais, D. (1989a). Latitudinal variations in plankton delta C-13 - Implications for CO2 and productivity in past oceans. *341*.

Rau, G. H., Takahashi, T., Des Marais, D. J., Repeta, D. J., & Martin, J. H. (1992). The relationship between δ13C of organic matter and [CO2(aq)] in ocean surface water: Data from a JGOFS site in the northeast Atlantic Ocean and a model. *Geochimica et Cosmochimica Acta, 56*(3), 1413-1419. http://www.sciencedirect.com/science/article/pii/001670379290073R

Rau, G. H., Takahashi, T., & Marais, D. J. D. (1989b). Latitudinal variations in plankton δ13C: implications for CO2 and productivity in past oceans. *Nature, 341*(6242), 516-518. https://doi.org/10.1038/341516a0

Reynolds, D. J., Hall, I. R., Slater, S. M., Mette, M. J., Wanamaker, A. D., Scourse, J. D., et al. (2018). Isolating and Reconstructing Key Components of North Atlantic Ocean Variability From a Sclerochronological Spatial Network. *Paleoceanography and*

Paleoclimatology, 33(10), 1086-1098. https://doi.org/10.1029/2018PA003366. https://doi.org/10.1029/2018PA003366

Roemmich, D., Gilson, J., Davis, R., Sutton, P., Wijffels, S., & Riser, S. (2007). Decadal Spinup of the South Pacific Subtropical Gyre. *Journal of Physical Oceanography, 37*(2), 162-173. http://journals.ametsoc.org/doi/abs/10.1175/JPO3004.1

Roemmich, D., Gilson, J., Sutton, P., & Zilberman, N. (2016). Multidecadal Change of the South Pacific Gyre Circulation. *Journal of Physical Oceanography, 46*(6), 1871-1883. https://doi.org/10.1175/JPO-D-15-0237.1

Rousseaux, C. S., & Gregg, W. W. (2015). Recent decadal trends in global phytoplankton composition. *Global Biogeochemical Cycles, 29*(10), 1674-1688. http://dx.doi.org/10.1002/2015GB005139

Sarmiento, J. L., & Gruber, N. (2006). *Ocean Biogeochemical Dynamics*: Princeton University Press.

Sarmiento, J. L., Gruber, N., Brzezinski, M. A., & Dunne, J. P. (2004). High-latitude controls of thermocline nutrients and low latitude biological productivity. *Nature, 427*(6969), 56-60. https://doi.org/10.1038/nature02127

Sherwood, O., Guilderson, T. P., Batista, F. C., Schiff, J. T., & McCarthy, M. D. (2013). Increasing subtropical North Pacific Ocean nitrogen fixation since the Little Ice Age. *Nature, 505*, 78. http://dx.doi.org/10.1038/nature12784

Sherwood, O., Lehmann, M. F., Schubert, C. J., Scott, D. B., & McCarthy, M. D. (2011). Nutrient regime shift in the western North Atlantic indicated by compound-specific δ¹⁵N of deep-sea gorgonian corals. *Proceedings of the National Academy of Sciences, 108*(3), 1011. http://www.pnas.org/content/108/3/1011.abstract

Sieber, M., Conway, T. M., de Souza, G. F., Obata, H., Takano, S., Sohrin, Y., & Vance, D. (2019). Physical and biogeochemical controls on the distribution of dissolved cadmium and its isotopes in the Southwest Pacific Ocean. *Chemical Geology, 511*, 494-509. http://www.sciencedirect.com/science/article/pii/S0009254118303589

Somes, C. J., Schmittner, A., Galbraith, E. D., Lehmann, M. F., Altabet, M. A., Montoya, J. P., et al. (2010). Simulating the global distribution of nitrogen isotopes in the ocean. *Global Biogeochemical Cycles, 24*(4).

Somes, C. J., Schmittner, A., Muglia, J., & Oschlies, A. (2017). A three-dimensional model of the marine nitrogen cycle during the last glacial maximum constrained by sedimentary isotopes. *Frontiers in Marine Science, 4*, 108.

Trujillo, A. P., & Thurman, H. V. (2011). *Essentials of Oceanography*: Prentice Hall.

Ummenhofer, C. C., & England, M. H. (2007). Interannual Extremes in New Zealand Precipitation Linked to Modes of Southern Hemisphere Climate Variability. *Journal of Climate, 20*(21), 5418-5440. https://journals.ametsoc.org/doi/abs/10.1175/2007JCLI1430.1

Ummenhofer, C. C., Gupta, A. S., & England, M. H. (2009). Causes of Late Twentieth-Century Trends in New Zealand Precipitation. *Journal of Climate, 22*(1), 3-19. https://journals.ametsoc.org/doi/abs/10.1175/2008JCLI2323.1

Weaver, A. J., Eby, M., Wiebe, E. C., Bitz, C. M., Duffy, P. B., Ewen, T. L., et al. (2001). The UVic earth system climate model: Model description, climatology, and applications to past, present and future climates. *Atmosphere-Ocean, 39*(4), 361-428. https://doi.org/10.1080/07055900.2001.9649686

Wu, L., Cai, W., Zhang, L., Nakamura, H., Timmermann, A., Joyce, T., et al. (2012). Enhanced warming over the global subtropical western boundary currents. *Nature Clim. Change, 2*(3), 161-166. 10.1038/nclimate1353. http://dx.doi.org/10.1038/nclimate1353

Yan, H., Sun, L., Wang, Y., Huang, W., Qiu, S., & Yang, C. (2011). A record of the Southern Oscillation Index for the past 2,000 years from precipitation proxies. *Nature Geoscience, 4*(9), 611-614. https://doi.org/10.1038/ngeo1231

Yang, H., Lohmann, G., Krebs-Kanzow, U., Ionita, M., Shi, X., Sidorenko, D., et al. (2020). Poleward Shift of the Major Ocean Gyres Detected in a Warming Climate. *Geophysical Research Letters, 47*(5), e2019GL085868. https://doi.org/10.1029/2019GL085868

Young, J. N., Bruggeman, J., Rickaby, R. E. M., Erez, J., & Conte, M. (2013). Evidence for changes in carbon isotopic fractionation by phytoplankton between 1960 and 2010. *Global Biogeochemical Cycles, 27*(2), 505-515. https://doi.org/10.1002/gbc.20045

Appendix

Appendix is available on the CD-ROM attached to the back cover. This disk contains the aging datasets used in Chapter 2 (Sheet A), the radiocarbon, U-Th, ΔR and $\Delta^{14}C$ datasets used in Chapter 3 (Sheet B), and the stable isotope datasets in Chapter 4 (Sheet C).